INTERACTIONS BETWEEN CLIMATE AND THE MARINE NITROGEN CYCLE ON GLACIAL-INTERGLACIAL TIMESCALES

by

ERIC DOUGLAS GALBRAITH

B.Sc., McGill University, 1997

A THESIS SUBMITTED IN PARTIAL FULFILMENT OF THE REQUIREMENTS FOR THE DEGREE OF

DOCTOR OF PHILOSOPHY

in

THE FACULTY OF GRADUATE STUDES

(Earth and Ocean Sciences)

THE UNIVERSITY OF BRITISH COLUMBIA

February, 2006

Abstract

Nitrogen is a principal component of living organisms and comprises the majority of the atmosphere, yet the scarcity of biologically reactive nitrogen in the ocean limits growth and appears to have varied with past changes in physical climate. This thesis takes a multi-faceted approach, including fine-scale sediment analysis, modern field observations and global numerical modeling, to contribute an integrated view of the marine nitrogen cycle and its climatic sensitivity.

Nitrogen bound in diatom frustules, extracted from laminated sediments of the Guaymas Basin, has greater seasonal $\delta^{15}N$ variability than corresponding bulk sediment. Downslope transport of frustules from the shelf contributes ^{15}N-depleted nitrogen, while pelagic diatom frustules display great sensitivity to seasonal growing conditions. Bulk sedimentary $\delta^{15}N$ represents a reliable integrated monitor of the local nitrogen substrate.

Records of bulk sedimentary $\delta^{15}N$ from the subarctic Pacific reflect the tripartite imprints of diagenesis, variable nitrate utilization and changes in $\delta^{15}N$-nitrate. Modern subsurface $\delta^{15}N$-nitrate is homogenous across the open subarctic Pacific. Diagenesis introduces ^{15}N-enrichments at core tops and there is a gradual decrease of $\delta^{15}N$ with burial. The Gulf of Alaska record does not sample HNLC waters, but records changes in $\delta^{15}N$-nitrate and diagenesis. This is used to correct for regional $\delta^{15}N$-nitrate variability, revealing rapid increases in nitrate utilization, likely due to Fe fertilization, in the western subarctic Pacific during glacial periods. The $\delta^{15}N$-nitrate record suggests denitrification may have occurred in the deep ocean during the last glacial maximum, and almost certainly in the upper water column of the deglacial subarctic Pacific.

A global compilation of $\delta^{15}N$ records evokes co-ordinated changes in denitrification throughout the global thermocline, implying large increases in aggregate denitrification rate, matched by changes in N_2 fixation, under warming conditions. A global, physically-driven modulation of subsurface oxygen concentrations is proposed as the primary relevant forcing on glacial-interglacial timescales.

Simple schemes for denitrification and N_2 fixation, based on widely accepted ecological principles, are quantified and embedded in a General Circulation Model of intermediate complexity. The model highlights the competition between diazotrophs and other phytoplankton for phosphorus as a key element of the marine biosphere. The model confirms a pronounced sensitivity of denitrification rates to the physical climate state, with more rapid rates of nitrogen cycling and expanded nitrogen limitation under warmer climates.

Table of Contents

Abstract ii

Table of Contents iii

List of Tables vii

List of Figures viii

Acknowledgements x

Co-authorship Statement xiii

Chapter I. Past changes in the marine nitrogen cycle 1

1.1 Introduction 1

1.2 Inventory changes 3

1.2.1 Marine nitrogen fixation 3

1.2.2 Sedimentary denitrification 5

1.2.3 Water column denitrification 6

1.2.4 Stabilizing N_2 feedbacks 6

1.2.5 Stabilizing sedimentary-denitrification feedbacks 7

1.2.6 Stabilizing water column denitrification feedbacks 7

1.3 Nitrate cycling and the nutrient-rich regions of the surface ocean 8

1.4 Nitrogen isotope systematics 10

1.4.1 Inputs 10

1.4.2 Outputs 13

1.4.3 Internal cycling 14

1.4.4 Deep nitrate 16

1.5 Ocean $\delta^{15}N_{nitrate}$ in the past 16

1.5.1 Local variations 17

1.5.2 Steady state mean 17

1.5.3 Application to past 18

1.6 Sedimentary N isotope records 20

1.6.1 The $\delta^{15}N$ of sinking N 20

1.6.2 The $\delta^{15}N$ of sedimentary N 21

1.7 Observations and interpretations 24

1.7.1 Glacial-interglacial inventory changes 26

1.7.2 Glacial-interglacial changes in nutrient-rich regions 29

1.8 Objectives of this thesis 31

1.9 References..... 34
Chapter II. Contrasting but complementary information recorded by $\delta^{15}N$ of diatom frustules and $\delta^{15}N$ of bulk sediment in the Guaymas Basin..... 42
2.1 Introduction..... 42
2.2 Setting..... 44
2.3 Methods..... 45
2.4 Geochemical observations..... 47
2.5 Diatom provenance: an unexpected twist..... 51
2.6 Linking frustule N to whole diatom and exported N..... 56
2.7 Low variability of bulk N isotopes..... 59
2.8 Conclusions..... 59
2.9 References..... 61
Chapter III. Nitrogen isotope dynamics of the subarctic Pacific over the past 742,000 years: influences of denitrification, iron fertilization and diagenesis..... 65
3.1 Introduction and background..... 65
3.1.1 Modern Subarctic Pacific Hydrography..... 66
3.1.2 Sediment core sites..... 67
3.1.3 General controls on $\delta^{15}N\text{-}NO_3^-$ in the N Pacific..... 72
3.2 Methods..... 73
3.2.1 $\delta^{15}N\text{-}NO_3^-$..... 73
3.2.2 Bulk sediment geochemistry methods..... 74
3.2.3 Diatom frustule-bound $\delta^{15}N$ method..... 74
3.2.4 Chronological control..... 75
3.3 Modern water column N isotope dynamics..... 75
3.3.1 Line P $\delta^{15}N\text{-}NO_3^-$..... 75
3.3.2 $\delta^{15}N\text{-}NO_3^-$ in the vicinity of the GA sediment site..... 77
3.3.3 Comparing WSG to GA and the Bering Sea..... 80
3.4 Sediment records..... 80
3.4.1 Paleoproductivity context..... 80
3.4.2 Nitrogen isotopes: Conceptual framework..... 83
3.4.3 Nitrogen isotopes: General features of the three records..... 83
3.5 Diagenesis..... 90
3.5.1 Evaluating $DIAG_{PB}$..... 90
3.5.2 Evaluating $DIAG_{WC}$..... 92

3.5.3 Potential for downcore variations in diagenesis..... 96
3.6 Changes in Relative Nitrate Utilization..... 99
3.6.1 Implications for the nutrient status of the WSG over past glacial cycles..... 100
3.7 Temporal change in δ^{15}N-nitrate..... 105
3.7.1 Implications of the GA record: a 15 ka event..... 105
3.7.2 Implications of the GA record: a 20 ka event..... 107
3.7.3 Implications: long record..... 111
3.8 Conclusions..... 111
3.9 References..... 113
Chapter IV. Glacial-interglacial modulation of the marine nitrogen cycle by high latitude O_2 supply to the global thermocline..... 121
4.1 Introduction..... 121
4.2 Materials and Methods..... 122
4.3 Past changes in sedimentary d^{15}N..... 122
4.4 Global changes in denitrification over the past 200 ky..... 124
4.5 Coupling of N_2 fixation to denitrification..... 130
4.6 Isotopic record of the fixation response..... 131
4.7 Mixed TD/Fixation d^{15}N records..... 134
4.8 Surface ocean link to global denitrification..... 135
4.9 Climatically driven changes in O_2 supply..... 138
4.10 Early Holocene d^{15}N maxima..... 142
4.11 Summary and Conclusions..... 144
4.12 References..... 144
Chapter V. Physical sensitivities and stabilizing feedbacks: Numerical simulations of the marine nitrogen cycle under present-day and glacial climates..... 151
5.1 Introduction..... 151
5.2 Model description..... 152
5.2.1 A note on Anammox..... 159
5.3 Model runs..... 160
5.3.1 Oxygen minimum zones..... 160
5.3.2 N_2 fixation..... 165
5.4 Model stability..... 167
5.5 Glacial run..... 168
5.6 Conclusions..... 173

5.7 References..... 173
Chapter VI. Concluding remarks..... 177
6.1 Perspective on progress..... 177
6.2 Contributions of this thesis..... 178
6.3 Future work..... 179
6.4 References..... 181

Appendix I. Isolating frustule-bound nitrogen from sediments: progress and pitfalls..... 182
A1.1 General protocol..... 182
A1.1.1 Physical separation..... 183
A1.1.2 Oxidation by liquid fire..... 184
A1.1.3 C and N measurements..... 185
A1.1.4 Isotopic analysis..... 185
A1.2 Oxidation tests: Liquid fire..... 186
A1.3 Oxidation tests: Peroxide..... 186
A1.4 A sticky problem: adsorption on diatom frustules..... 194
A1.6 Comparison of Combustion and PD measurements..... 196
A1.7 Summary..... 197
A1.8 References..... 199
Appendix II. Frustule-bound nitrogen in diatom cultures: detailed methodology and inconclusive results..... 201
A2.1 Methods..... 201
A2.2 Results..... 203
A2.3 Discussion..... 206
A2.4 References..... 207
Appendix III. Opal determinations for diatom-rich horizons of ODP 887B..... 209
A3.1 References..... 211
Appendix IV. Age model for Gulf of Alaska Hole ODP 887B..... 213
A4.1 References..... 218

List of Tables

3.1: Locations of sediment cores discussed in Chapter 3..... 68
4.1: Sedimentary $\delta^{15}N$ records shown in Chapter 4..... 123
5.1: Ecosystem model parameters..... 155
5.2: Model runs..... 161
A1.1: Oxidation test cleaning methods (OG) 191
A1.2: Comparison of OG analyses by Combustion and Persulphate-denitrifier..... 198
A2.1: Culture results..... 204
A4.1: Radiocarbon ages, raw and calibrated, for ODP 887B..... 214

List of Figures

1.1: Schematic view of the major sources and sinks of fixed N in the marine environment..... 4

1.2: Instantaneous nitrogen isotopic fractionation processes..... 11

1.3: Water column profiles of nitrate concentration and $\delta^{15}N_{nitrate}$..... 12

1.4: Mean ocean steady-state isotope balance..... 19

1.5: Fidelity of sedimentary $\delta^{15}N$ as a recorder of $\delta^{15}N_{nitrate}$ at coastal margins..... 22

1.6: The $\delta^{15}N$ of integrated N export versus $\delta^{15}N_{bulk}$ and $\delta^{15}N_{frustule}$..... 25

1.7: Plots of $\delta^{15}N_{bulk}$ vs. sediment age over the past 50,000 years..... 27

1.8: Paleoceanographic records from the Subantarctic and Antarctic zones of the Southern Ocean..... 30

2.1: Photograph of Guyamas Layer Cake (1) showing sample locations..... 46

2.2: Bulk geochemistry of GLC-1 samples..... 48

2.3: $\delta^{15}N_{bulk}$ measurements of GLC-1 samples..... 49

2.4: Comparison of $\delta^{15}N_{bulk}$ and $\delta^{15}N_{frustule}$ for GLC-1 samples..... 50

2.5: Comparison of $\delta^{15}N_{bulk}$ with the $\delta^{15}N$ of non-frustule N..... 52

2.6: Comparison of shelf diatom abundance with $\delta^{15}N_{bulk}$ and $\delta^{15}N_{frustule}$..... 53

2.7: Shelf diatom index vs. $\delta^{15}N_{frustule}$ for all available samples of GLC-1..... 55

2.8: Possible relationships between $\delta^{15}N_{bulk}$, $\delta^{15}N_{export}$, $\delta^{15}N_{diatom}$ and $\delta^{15}N_{frustule}$..... 57

3.1: Average July-September upper water column characteristics across the Gulf of Alaska..... 70

3.2: Water characteristics along Line P during February, 2003..... 76

3.3: Profiles of $\delta^{15}N$-NO_3 spanning the subarctic Pacific..... 78

3.4: Water chemistry at 27.10 kg m^{-3} along the western margin of North America..... 79

3.5: Variations in biogenic components of subarctic Pacific sediments over the past 150 ky..... 82

3.6: Conceptual diagram of $\delta^{15}N$ components and transformations..... 84

3.7: Three $\delta^{15}N_{bulk}$ records from the subarctic Pacific covering the past 150 ky..... 85

3.8: Parallel changes in $\delta^{15}N_{bulk}$ records throughout the Northeast Pacific..... 87

3.9: Two $\delta^{15}N_{bulk}$ records from the subarctic Pacific over the past 742 ky..... 88

3.10: GA $\delta^{15}N_{bulk}$ record with and without high opal samples..... 89

3.11: Five globally-distributed long $\delta^{15}N_{bulk}$ records..... 91

3.12: The Gulf of Alaska $\delta^{15}N$ record over successive climate cycles..... 93

3.13: Diagenetic alteration of $\delta^{15}N$ with increasing depth in the Gulf of Alaska core..... 94

3.14: The detrended Gulf of Alaska $\delta^{15}N$ record in a regional context..... 95

3.15: Bulk and frustule $\delta^{15}N$ under contrasting sedimentary conditions in the Gulf of Alaska..... 98

3.16: Difference between $\delta^{15}N$ records of the Gulf of Alaska and the Western Subarctic Gyre..... 101

3.17: Changes in nitrate utilization in the Western Subarctic Pacific during the last glacial cycle..... 104

3.18: Nitrogen isotopes and opal concentration in the subarctic and NE Pacific during the past 30 ky..... 106
3.19: Nitrogen isotopes and authigenic metals in the NE Pacific during the past 30 ky..... 108
4.1: Dissolved Oxygen on the 27.0 isopycnal..... 126
4.2: Sedimentary $\delta^{15}N$ records from areas of present and/or potential TD for the last 200 ky..... 127
4.3: Sedimentary $\delta^{15}N$ records from fixation, denitrification and well-mixed areas..... 133
4.4: Schematic illustration of high latitude surface control on denitrification and the fixation response..... 140
4.5: Schematic illustration showing expected temporal contrasts in the activity of TD..... 141
5.1: Schematic illustration of the ecosystem model..... 153
5.2: Increase of maximum growth rate vs. temperature for diazotrophs and other phytoplankton..... 157
5.3: Shallow N* distributions in the World Ocean Atlas annual climatology and model run PD..... 162
5.4: Global plot of PO_4 vs. NO_3 concentrations in model run PD and observations..... 163
5.5: Shallow subsurface O_2 in the PD run and observations..... 164
5.6: N_2 fixation rates in three model runs..... 166
5.7: Differences in net primary production due to diazotrophy..... 169
5.8: Increase of subsurface O_2 concentrations in the LGM run vs. the PD run..... 171
5.9. Decrease of ocean fertility in the LGM vs. the PD run..... 172
6.1. Modulation of marine N cycle by high latitude processes on the global thermocline..... 180
A1.1: Gulf of Alaska sediment samples before and after diatom separation and cleaning..... 187
A1.2: Silica nanospheres of an oxidized frustule..... 188
A1.3: The N isotopic composition of diatom frustules vs bulk sediment from the Gulf of Alaska..... 189
A1.4: Results of the peroxide oxidation tests..... 192
A1.5: Results of the liquid fire oxidation tests..... 195
A2.1: Cultured diatom sample following oxidative cleaning..... 205
A3.1: Sensitivity of opal measurements to aliquot size and sonication..... 210
A3.2: Relationship of Si/Al to wt. % opal..... 212
A4.1: Benthic d18O age constraint for ODP 887..... 216
A4.2: Comparison of new 887 age model with previous age model..... 217

Acknowledgments

This thesis would not have been possible without the support of a broad community including many colleagues and friends. Among these, I thank Joe Needoba for giving me a sound foundation in biology during our many extended sessions at Koerner's Pub, and for doing his best to teach me how to grow diatoms. Kristin Orians gave me an excellent introduction to marine chemistry and sparked my interest in global biogeochemical cycles. Phil Tortell and Maite Maldonado were a great source of knowledge, kindly allowed me to use their labs and culture facilities, and were excellent hosts. Susan Allen and Rich Pawlowich patiently answered many questions about physical oceanography, Max Taylor exuberantly showed me how to tell a *Coscinodiscus* from an *Asteromphalus,* and Kurt Grimm gave me a warm welcome to graduate school. Markus and Stephanie Kienast were inspirational colleagues - their intellectual rigor, efficiency and excitement gave me a great introduction to geochemistry and paleoceanography and they have continued as close collaborators and prized editors through the years. Tawnya Peterson was a great help, both with counting dead diatoms and preventing the untimely deaths of live ones. I received much support from many other grad students, including most notably Adrian Marchetti, Julie Granger, Jennifer McKay, Jonathan Mackin, Trish Amundrud, Rana El-Sabaawi, David Timothy and Tim Creyts. Kathy Gordon provided superb N isotopic measurements in a timely manner, and Bert Mueller helped me to realize just how complicated chemistry is. My gratitude to Maureen Soon, for teaching me how to do everything in the lab and taking care of my many loose ends during extended absences, cannot be fully expressed in words (I'll try chocolate instead).

Daniel Sigman, of Princeton, was a great resource throughout the course of my research and helped tremendously with many stimulating discussions; he also invited me to author a book chapter, which was an excellent experience, and guided me through the process of writing it with a fine balance of insightful criticism and encouragement. Becky Robinson and Brigitte Brunelle very kindly ran my frustule samples with their alternate technique after the problems with combustion were discovered, and without which an entire portion of my thesis would have been lost.

At IOS, Frank Whitney was tremendously generous and a font of wisdom regarding the Gulf of Alaska. Marie Robert was outstandingly helpful in providing the samples from Line P and arranging ship time in Saanich Inlet. Andrew Weaver at UVic was contagiously enthusiastic about climate and the modeling of it, Ed Weibe provided excellent technical support, and Katrin Meissner was a fantastic collaborator for my first modeling experience. Andreas Schmittner, at OSU, shared a lot of great ideas, patiently and efficiently showed me how to operate the model itself, and handed me the reins.

Thanks to the wonder of the internet, Samuel Jaccard has been a constant companion (despite the fact that he lives in Switzerland) with almost daily conversations that kept me motivated and excited throughout the otherwise isolated writing of my thesis. For their generosity with time, data and ideas I thank, in no particular order: Nele Meckler (ETH-Zurich), Gerald Haug (Potsdam), Raja Ganeshram (Edinburgh), Laetitia Pichevin (Edinburgh), Philippe Martinez (Bordeaux), Xavier Crosta (Bordeaux), Stefan Mulitza (Bremen), Christophe Voelker (Bremen), John Southon (California, Irvine), Mark Altabet (Massachusetts), Ingrid Hendy (Michigan), John Crusius (USGS) and Moritz Lehmann (Quebec, Montreal).

The members of my committee have provided invaluable insight and direction throughout the past half-decade. I am grateful to Steve Calvert for his amiable companionship, boundless curiosity, and patience with my messes all over his lab. I thank Roger Francois for his approachability and inquisitiveness, and for returning to his alma mater in time to act as my co-supervisor. Foremost, I thank Tom Pedersen for being a great role model, a generous benefactor and a rigorous critic. Tom set me off in the direction of interesting questions, encouraged me to think globally, and then gave me the time and space I needed for my ideas to gestate - I can't imagine a better supervisor or dinner guest.

I am very grateful to the EOS department for generously funding many trips to summer schools and conferences, which have been irreplaceable for developing contacts, receiving feedback and assembling a global view of the field. Also, to the Canadian people, who through their generous taxes have supported this work, and to my great luck at being born in a time and place when I can devote myself entirely to considering such esoteric questions. I thank Agnieszka for her patience with the thesis-writing troll, who spent the better part of the past year locked into the torture chamber at the end of the apartment. And most of all, I am grateful to my parents, for their unconditional support, and for teaching me to think and to wonder.

Irrationally held truths may be more harmful than reasoned errors.

Thomas Henry Huxley
Science and Culture and Other Essays (1881)

There is something fascinating about science.
One gets such wholesale returns of conjecture out of such a trifling investment of fact.

Mark Twain
Life on the Mississippi (1883)

If you really care about a serious cause or a deep subject, you may have to be prepared to be boring about it.

Christopher Hitchens
Letters to a Young Contrarian (2001)

Co-authorship statement

Chapter I: Past changes in the marine nitrogen cycle

Eric Galbraith, Daniel Sigman, Rebecca Robinson, Thomas Pedersen
In review, invited chapted in Nitrogen in the Marine Environment (2nd edition); Capone, D., Bronk, D., Mulholland, M. and Carpenter, E. (eds.).

Sigman: Principal coauthor.
Robinson: Additional input on the manuscript, contributed two figures.

I designed the structure of the book review chapter on which much of this introductory chapter is based. I independently wrote the initial draft, and incorporated all changes that arose in subsequent discussion with the coauthors. The most substantial coauthor contributions were to the sections on relative nutrient utilization in high latitude regions.

Chapter IV: Glacial-interglacial modulation of the marine nitrogen cycle by oxygen supply to intermediate waters.

Eric Galbraith, Markus Kienast, Thomas Pedersen, Stephen Calvert
Paleoceanography, 19, doi.1029/2003PA001000. October, 2004.

I developed the concept of this chapter, with substantial encouragement from Kienast and additional support from Pedersen and Calvert. The manuscript and figures were entirely prepared by me, with helpful comments from all coauthors.

Chapter I[1]

Past changes in the marine nitrogen cycle

1.1 Introduction

Many reservoirs of biologically important elements turn over so rapidly at the Earth surface that modest differences between input and output could either remove them completely or double their concentrations in the relatively short span of thousands to millions of years. Despite this precarious situation, the evidence indicates that the Earth has been remarkably stable in its habitability. The chain of multi-cellular life has been continuous for more than a half billion years. While mass extinctions have occurred, none has been demonstrated to result from the internally driven collapse of an elemental cycle. Such continuity requires a conspiracy of feedbacks within the Earth system that stabilizes the availability of life's key ingredients. Yet we know little about these feedbacks, how they develop, or the constraints that they impose on the environment and life. Beyond these fundamental scientific questions, an understanding of the regulatory mechanisms is key to predicting how the system will respond to anthropogenic climate change.

The marine nitrogen budget provides an important element of the broader effort to understand the stabilizing environmental feedbacks on the Earth surface. Most nitrogen at the Earth surface is in the form of dinitrogen gas, inaccessible to the vast majority of marine organisms. Biologically available (or "fixed") nitrogen is one of the most important nutrients to primary producers, and its residence time in the environment is among the shortest of the biologically important constituents ($\leq$ 3kyr, *[Codispoti et al., 2001]*). Because both the principal source (N_2 fixation) and sink (denitrification) of fixed nitrogen are mediated

[1] A version of this chapter will be published as a book chapter. Galbraith, E.D., Sigman, D.M., Robinson, R.S. and Pedersen, T.F. "Nitrogen in Past Marine Environments", in Nitrogen in the

entirely by microbes, the marine nitrogen cycle is particularly well-suited to the development of biological homeostasis, providing an important contrast in this regard to nutrients such as phosphorus, silicon and iron.

Although one might hope to develop a complete understanding of the ocean N budget by studying its manifestation in the modern ocean, this straightforward approach faces substantial barriers. In particular, it is exceedingly difficult to quantify the sensitivities of biogeochemical fluxes sufficiently to predict how the fluxes will interact in the future. One approach to surmount this difficulty is to look to the geological and glaciological archives, which record past events that approximate large-scale experiments in which the oceanic N budget responds to some naturally imposed forcing.

Studies with this goal have focused on the multi-millennial scale cycle of ice ages and interglacial periods that has dominated the last 2.5 million years of Earth history. Several aspects of these cycles make them well suited to this application. First, they are recent, in fact ongoing, and so are relatively well recorded in sediment and ice core records. Second, the glacial and interglacial periods are each at least a factor of three longer than the residence time of oceanic fixed N. Thus, a given glacial/interglacial transition (such as the last deglaciation) provides something akin to a discrete natural experiment, with the ocean N budget beginning at steady state, responding to the climate-driven forcing and then potentially reaching a new steady state condition. Of course, this is a simplistic view, but it provides a logical point of departure.

While the budget of fixed N is unique among the nutrients, the internal cycle of N in the ocean (i.e. as reflected in the variations in nitrate concentration) is quite representative of open ocean nutrient cycling in general. For instance, the distributions of nitrate and phosphate across the surface ocean are tightly coupled through the stoichiometry of algal uptake and subsequent remineralization. Thus, if we can come to understand the controls on the oceanic distribution of nitrate, we would in effect gain similar insight into the phosphate distribution.

One crucial question regarding the internal cycling of nutrients in the ocean is why the major nutrients nitrate and phosphate are incompletely consumed in the polar ocean.

Marine Environment (2nd edition), Capone, D., Mulholland M., Bronk, D. and Carpenter, E. (eds.) in preparation.

Again, the glacial/interglacial cycles of the late Pleistocene offer a window on this question through the relationship between climate changes and associated shifts in open ocean physical and chemical conditions. In turn, it has been posited that coupled changes in polar ocean overturning and biogeochemistry drive the observed variation in atmospheric CO_2 over glacial/interglacial cycles (see Sigman and Boyle [2000] for a review).

This chapter reviews the ongoing effort to use sediment and ice core records to understand the dynamics of oceanic fixed N. The potential changes are divided here into two broad categories, those that most directly involve changes in the ocean nitrogen inventory, that is, the total mass of fixed (non-gaseous) nitrogen in the oceans, and those that most directly involve changes in the distribution and cycling of fixed nitrogen within the ocean.

1.2. Inventory changes

Fixed nitrogen is continuously added to the ocean surface and removed from its interior by the processes depicted schematically in Figure 1.1. The emerging view of the marine nitrogen budget is largely independent of terrestrial nitrogen inputs and is dominated by the single input term of marine N_2 fixation [*Gruber*, 2005] and by the output terms of sedimentary and water column denitrification (where "denitrification" refers to the total conversion of fixed N to gaseous products by any pathway, including anaerobic ammonium oxidation, "anammox"). Given their dominance with respect to mass flux and their sensitivities, the potential for inventory changes is determined by the temporal variability of these three terms, and their self-stabilizing feedbacks. Below, the potential for variability of each is discussed, followed by an analysis of the stabilizing feedbacks that tend to resist variability.

1.2.1 Marine nitrogen fixation

It has been proposed that the availability of nitrogen in the surface ocean is currently reduced due to limitation of diazotrophs by iron or other trace metals [*Falkowski*, 1997]. If the degree of global Fe-limitation varies over geological time, then the rate of N_2 fixation might be expected to follow. It is believed that greater aridity and higher windspeeds made the glacial world dustier than the current interglacial [*Petit et al.*, 1999], which probably

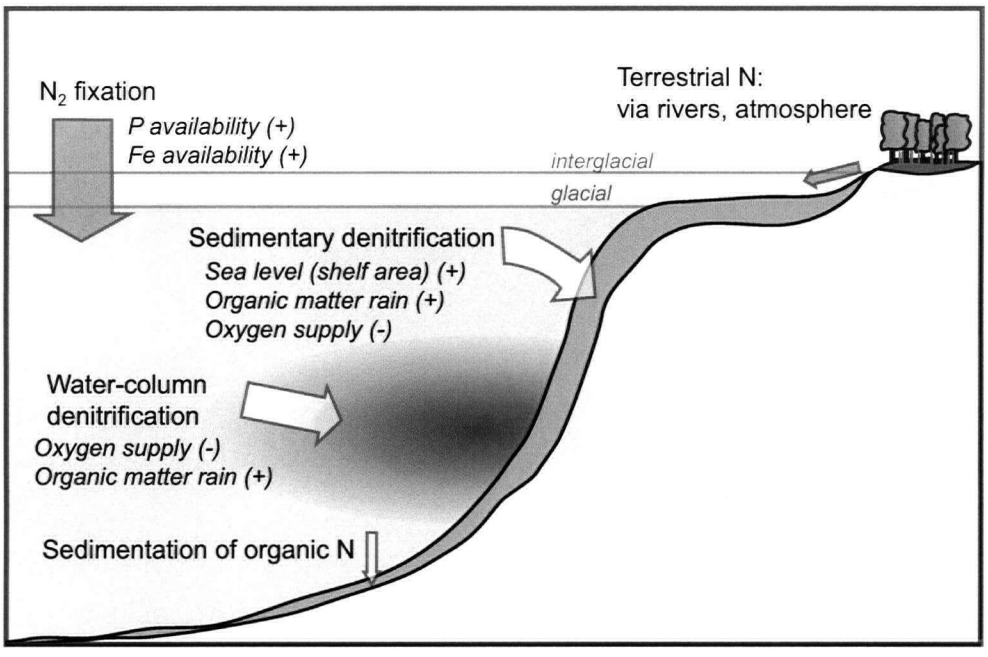

1.1. Schematic view of the major sources (green arrows) and sinks (white arrows) of fixed N in the marine environment. The most important factors for controlling the variation of each source or sink term over time are given in italics.

would have led to somewhat higher trace metal concentrations in the oceans, though it is not clear by what degree [*Parekh et al.*, 2004]. If true, this could have allowed diazotrophs to fix N at greater rates during ice ages, and the resulting increase in N_2 fixation rates could have increased the whole ocean N inventory [*Falkowski*, 1997]. Comparison of ice core records of atmospheric pCO_2 and dust led *Broecker and Henderson* [1998] to promote this idea.

1.2.2 Sedimentary denitrification

Organic matter accumulates on most continental shelves of the modern ocean, producing sediments that generally are anoxic very close to the sediment-water interface. The physical proximity of nitrate-bearing bottom waters to anoxic sediments with high concentrations of labile organic matter allows diffusion and bioturbation to effectively supply nitrate to nitrate-reducing organisms in the sediment, leading to high rates of denitrification in shelf sediments. During ice ages, sea level dropped by up to 120 m, exposing ~75 % of the global shelf area [*Hay and Southam*, 1977]. As a result, organic matter from highly productive coastal ecosystems would have been shunted to the deep sea. Because this organic matter must settle through a greater height of water column, more organic matter oxidation would have been accomplished there instead of in sediments. One would expect, therefore, that the lowering of sea level would have significantly reduced the global rate of sedimentary denitrification, as proposed by *Christensen et al.* [1987]. To obtain a rough maximal estimate of this effect, we can assume that the area-normalized rates of sedimentary denitrification on slopes and in the deep sea remained constant during glacial maxima, despite the fact that they would be the primary depositional sites for coastally produced sinking organic matter during low sea level. In this extreme case, a reduction in global shelf area to 25% of the modern value would have produced a decrease in sedimentary denitrification of 75 Tg N/yr [*Middelburg et al.*, 1996], representing a ~30 % decrease in the global rate.

Hypsometry is not the only parameter affecting global sedimentary denitrification rates. A higher flux of organic matter to the sediment strongly increases sedimentary denitrification (see 2.2.2). The oxygen content of bottom waters has a secondary and less certain effect. In some cases, higher denitrification rates would be expected under more oxygen-poor conditions [*Middelburg et al.*, 1996], though this may be reversed if nitrification becomes limited by oxygen [*Devol and Christensen*, 1993]. In general,

sedimentary denitrification seems relatively resilient to environmental change (at least when compared to water column denitrification; see below) and would be expected to have remained globally significant under most conceivable conditions throughout Earth history.

1.2.3 Water column denitrification

The other large sink of marine nitrogen at the present day is by denitrification in suboxic regions of the water column. This process becomes prominent where dissolved oxygen has been depleted through aerobic respiration, to below 2 - 5 μM O_2 [*Codispoti et al.*, 2005]. In the modern ocean, this is limited to the upper 1000 m of the Eastern Tropical Pacific [*Lipschultz et al.*, 1990] and the Arabian Sea [*Naqvi*, 1991]. These subsurface regions are driven to suboxia by the coincidence of rapid organic matter delivery with a slow re-supply of dissolved oxygen [*Olson et al.*, 1993; *Sarma*, 2002]. In theory, the extent of water column denitrification could be significantly altered by changing the export rate of organic matter to the subsurface [*Altabet et al.*, 1995; *Ganeshram et al.*, 2000], and/or by changing the oxygen supply through a physical mechanism [*Broecker and Peng*, 1982; *Galbraith et al.*, 2004]. Since nearly all subsurface respiration on the global scale is supported by oxygen, there is no *a priori* reason that water column denitrification should have been present at all times in the past; it could have varied dramatically. However, the strong sensitivities of water-column denitrification, while rendering this process susceptible to climate-driven variability, probably also make it more responsive to negative feedbacks.

1.2.4 Stabilizing N_2 fixation feedbacks

It is widely held that N_2 fixers tend to be at a competitive disadvantage to non-diazotrophs under nitrate-replete conditions: only where nitrate is nearly exhausted but phosphate remains available are N_2 fixers expected to provide substantial new nitrogen. Thus, N_2 fixation tends to be self-limiting: greater rates increase new N input to an ecosystem, reducing the degree of N limitation of non-diazotrophic competitors and, hence, the net availability of phosphate to diazotrophs [*Redfield et al.*, 1963; *Broecker*, 1982; *Tyrrell*, 1999]. This self-limiting feedback intimately ties N_2 fixers to the global aggregate rate of denitrification, which sets the global deficiency of N relative to P and, consequently, the availability of nitrate-limited environments exploitable by N_2 fixers. The sensitivity of

this feedback depends largely on the degree of disadvantage that diazotrophs suffer under nitrate-bearing replete conditions, which is poorly known (Chapter 5).

The relatively robust relationship between N and P concentrations in bulk algal stoichiometry, observed first by *Redfield* [1934], is critical when considering potential changes in the global N_2 fixation rate. This ratio reflects the nutritional requirements of the surface ocean algal community, thereby determining its ability to utilize a given phosphate supply using available nitrate, and hence, the potential for excess phosphate to be available to N_2 fixers. Although there is some degree of localized discrepancy from the canonical 'Redfield' N:P value of 16:1, the ratio holds remarkably well throughout the global ocean (see [*Gruber*, 2004] for a complete review). Broecker [1998] (section 2.1.1) invoked a much higher biomass N:P ratio during glacial periods, by on the order of 50%, to explain lower atmospheric pCO_2. This is difficult to reconcile with the low variability of N:P in the modern ocean, particularly with near-Redfield N:P in the modern Fe-replete subtropical North Atlantic [*Hansell et al.*, 2004]. Nonetheless, without a better appreciation of the mechanisms underlying this master variable, the possibility of large changes in the N:P of past oceans cannot be dismissed.

1.2.5 Stabilizing sedimentary-denitrification feedbacks

Sedimentary denitrification rates are dominantly a function of organic carbon flux to the seafloor [*Middelburg et al.*, 1996]. Hence, if a decrease in denitrification rates promotes higher export production via a relaxation of nitrate limitation, the enhanced organic carbon flux to the seafloor would reinvigorate sedimentary denitrification. Conversely, an increase in denitrification encourages nitrogen limitation and limits large increases in export production. This reflexive feedback would tend to dampen any massive swings in the N inventory. However, because sedimentary denitrification is dispersed over very large areas, many of which are not prone to significant variation in the degree of nitrate limitation in overlying surface waters, this feedback could be expected to be relatively weak.

1.2.6 Stabilizing water column denitrification feedbacks

The extent of water column suboxia is highly sensitive to organic matter flux from the surface, and would quickly respond to changes in export production. This sensitivity is

evident in the delicate balance between oxygen supply and oxidant demand in the global subsurface: the respiration history of suboxic waters (oxygen utilization plus denitrification) is almost entirely supported by oxygen, typically having consumed ~250 μM O_2 vs. 15 μM NO_3^- [*Codispoti et al.*, 2001]. Denitrification in suboxic waters is, therefore, a relatively small residual term of the difference between total respiration and oxygen supply. As a result, small changes in the total respiration, driven by export production, could have large effects on total denitrification. It follows that an increase in denitrification rates in subsurface waters will exacerbate nitrate limitation in nearby upwelling areas, restricting the organic flux back into the denitrification zone and counteracting the initial increase, both by reducing the organic matter supply to the denitrifiers within suboxic zone and by causing the suboxic zone itself to shrink [*Broecker and Peng*, 1982; *Codispoti*, 1989]. Because waters from denitrification zones supply the local upwellings that are, in turn, largely responsible for maintaining the suboxia below, this is a geographically tight coupling and would be expected to provide a strong feedback.

The sensitivity of this feedback depends on the degree to which diazotrophs near the upwelling zone are capable of eliminating N-limitation caused by a nitrate deficit in upwelled waters, thereby mitigating changes in export production. In this regard, a strong expression of the N_2 fixation-driven feedback posed above would weaken the denitrification-driven feedback described here. In fact, this is generally true for the negative feedbacks: if one of the feedbacks is particularly strong, it will dominate control of the nitrogen inventory and overwhelm the others [*Deutsch et al.*, 2004].

1.3 Nitrate cycling and the nutrient-rich regions of the surface ocean

The nutrient-rich surface waters of the equatorial upwellings and polar oceans are a particularly dynamic component of the global carbon cycle. In the Southern Ocean, for example, the nutrient-rich and CO_2-charged waters of the deep sea are exposed to the atmosphere and returned to the subsurface before the available nutrients are fully utilized by phytoplankton for carbon fixation. This incomplete utilization of upwelled nutrients allows for the leakage of biologically sequestered CO_2 back into the atmosphere, raising the atmospheric pCO_2 [*Knox and McElroy*, 1984; *Sarmiento and Toggweiler*, 1984; *Siegenthaler and Wenk*, 1984]. On this basis, increased nutrient utilization in the Southern Ocean has been

invoked as the cause of the lower pCO_2 concentrations of glacial times, through a reduced leakage of carbon into the atmosphere [*Martin and Fitzwater*, 1988; *Francois et al.*, 1997]. Nitrate is one of the principal macronutrients currently incompletely utilized in these surface regions, and therefore monitoring past changes in its relative degree of utilization has the potential to inform this facet of the climate system.

The potential changes in the polar ocean over glacial/interglacial cycles are too complex and diverse to be usefully covered here (see instead [*Sigman and Boyle*, 2000; *Sigman and Haug*, 2003]). Nevertheless, it is illustrative to consider how the nutrient status of the polar ocean would respond to a given change in ocean circulation, depending on the parameters that most strongly control algal growth in these regions (a topic of ongoing research in the modern ocean).

Consider, for example, the hypothesis that the polar ocean was more vertically stable during the last ice age than it is today [*Francois et al.*, 1997; *Toggweiler*, 1999; *Robinson et al.*, 2004; *Jaccard et al.*, 2005], focusing on the Antarctic region. Increased density stratification of the upper Antarctic water column would have reduced the rate of exchange between deep water and the euphotic zone. If algae growing in the Antarctic are most critically light limited, the increased stratification would have had little appreciable effect on productivity (ignoring additional factors such as changes in summer mixed layer depth and sea ice extent). Under this scenario, the decreased access to the deep nutrient pool would have required greater relative nutrient utilization despite an unchanged rate of export production during the ice age.

On the other hand, if Fe availability provides the overriding control on algal production in the Antarctic, the predominant route of Fe supply to the surface is the critical feature. If the Fe supply is always dominated by dissolved Fe from below, export productivity would have decreased in step with the glacial decrease in the gross supply of the macronutrients nitrate and phosphate (assuming a constant Fe : macronutrient ratio in Antarctic subsurface water). In this case, the degree of relative nitrate consumption in the glacial surface would have been unchanged relative to today. By contrast, if atmospheric Fe supply is significant (either during the last ice age or both during the last ice age and today), then glacial export production was not necessarily decreased under reduced gross macronutrient supply. Rather, it could have increased due to enhanced dust flux (or, at least,

decreased less than the gross supply of macronutrients), increasing the relative utilization of nitrate and phosphate in the glacial Antarctic surface. Details aside, it should be apparent that reconstructing the nutrient status of the polar ocean in the past and developing an understanding of the controls on algal growth in these regions go hand in hand.

1.4 Nitrogen isotope systematics

Unfortunately, there are no direct records of past nitrate concentration; one must rely instead on proxy evidence. The most specific and frequently used proxy for studying the history of the ocean N cycle is the nitrogen isotopic ratio of organic matter preserved in marine sediments.

There are two stable isotopes of N, ^{14}N (which constitutes 99.63 % of the N in the environment) and the rare isotope ^{15}N (see [*Sigman and Casciotti*, 2001] for a review). Measurements of the $\delta^{15}N$ of nitrate ($\delta^{15}N_{nitrate}$) in the deep sea have shown it to be fairly homogeneous, at about 5 ‰ relative to atmospheric N_2 [*Sigman et al.*, 2000] ($\delta^{15}N$ = $(^{15}N/^{14}N_{sample} / {}^{15}N/^{14}N_{air} - 1) * 1000$ ‰). In certain regions and depth intervals of the ocean, the $\delta^{15}N_{nitrate}$ diverges significantly from the mean deep $\delta^{15}N_{nitrate}$ because of regionally specific processes, as described below. To understand the signals that might be retrieved from sedimentary N isotopes, we first look individually at each of the key fractionating processes (Figure 1.2).

1.4.1 Inputs

Inputs of nitrogen to the marine environment are isotopically similar to atmospheric N_2. N_2 fixation occurs with little effective isotope discrimination, so that marine N_2 fixers produce reduced nitrogen with a $\delta^{15}N$ only slightly lower than that of air (0 to –2 ‰, e.g., [*Carpenter et al.*, 1997]). In regions of the subtropical ocean, thermocline $\delta^{15}N_{nitrate}$ can be as low as 2 ‰, ~3 ‰ lower than the mean deep ocean $\delta^{15}N$. This observation can be explained by N_2 fixation in the overlying surface waters and the subsequent remineralization of this low-$\delta^{15}N$ organic material in the thermocline [*Liu et al.*, 1996; *Karl et al.*, 2002; *Knapp et al.*, 2005] (Figure 1.3, North Atlantic). Fixed N is also transferred from terrestrial to marine ecosystems by riverine and atmospheric vectors, in roughly equal parts. This probably contributed no more than one quarter, and perhaps less than one eighth, of the input flux of

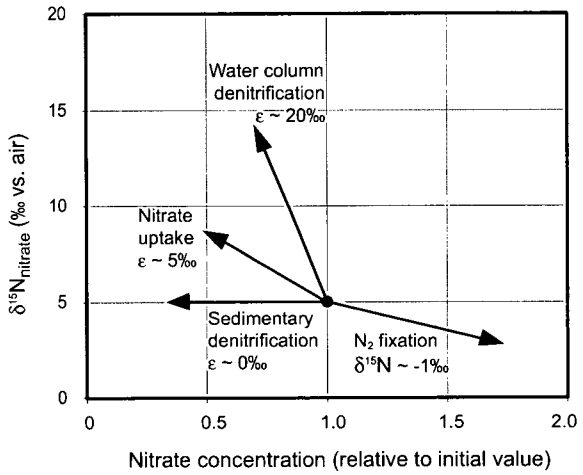

1.2. Instantaneous nitrogen isotopic fractionation processes. The vectors approximate the isotopic changes associated with the indicated addition or removal of nitrogen from an initial nitrate pool with a $\delta^{15}N$ of 5‰ (black filled circle). Note that the fractionating processes (water column denitrification and nitrate uptake) are actually nonlinear, due to the progressive enrichment of $\delta^{15}N$ in the residual pool, a feature not evident in this instantaneous view. After [Sigman and Casciotti, 2001]. The return of organic N to the nitrate pool by remineralization is not shown despite a large isotope effect associated with nitrification [Casciotti et al., 2003], since ammonium in typical open-ocean subsurface water is completely oxidized to nitrate [Thunell et al., 2004]. As a result, the nitrate produced should be similar to the organic matter being remineralized. However, remineralization can lead to significant ^{15}N enrichment in the small fraction of organic matter that has survived extensive degradation, as in the case of deep sea sediments (see Section 3.3.1).

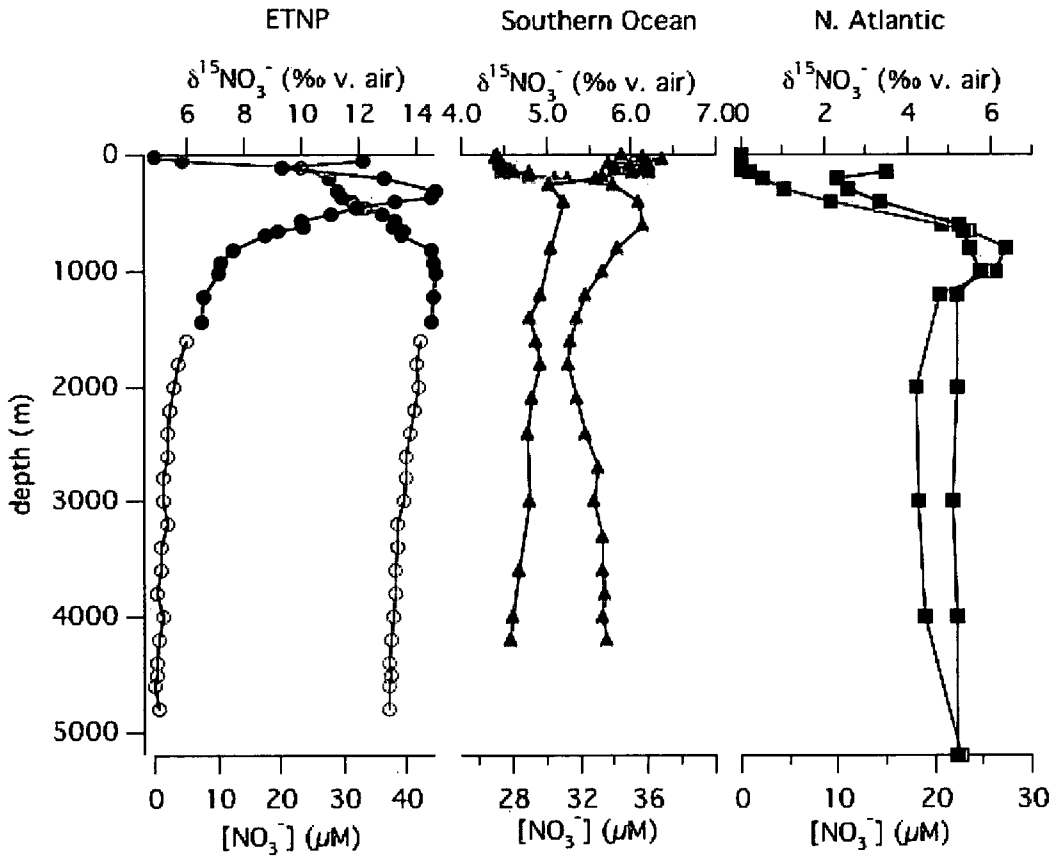

1.3. Water column profiles of nitrate concentration (grey) and $\delta^{15}N\text{-}NO_3^-$ (black) in the Eastern Tropical North Pacific (ETNP, coastal Baja California), Southern Ocean and North Atlantic (Sargasso Sea). Note that the ETNP profile includes deep measurements from near Hawaii (open circles), in order to give a sense of the strong connection between the ETNP and the deep Pacific. The ETNP shows a large increase in $\delta^{15}N\text{-}NO_3^-$ in the thermocline due to local water column denitrification. The Southern Ocean shows a homogeneous $\delta^{15}N\text{-}NO_3^-$ profile of the global deep mean value with some enrichment at the surface due to partial NO_3^- assimilation. The North Atlantic profile shows low $\delta^{15}N\text{-}NO_3^-$ in the thermocline due to the nitrification of locally fixed N. Figure courtesy of D. Sigman, pers. comm. 2005.

fixed N to the pre-industrial ocean [*Galloway et al.*, 2004]. Although it has been suggested that the $\delta^{15}N$ of terrestrial inputs sums to near 0‰ [*Brandes and Devol*, 2002], their isotopic compositions are very poorly constrained and may in fact be distinct from the N introduced by oceanic N_2 fixation. There is a great need for a systematic study of the isotopic composition of N inputs to the ocean from rivers and groundwater that takes into account the multiple chemical forms of N involved as well as the reactions that occur as rivers deposit N into the coastal ocean. Terrestrial inputs of fixed N are also a concern in paleoceanographic work given their potential to be delivered directly to ocean margin sediments, thereby contaminating the paleoceanographic signal in sediment records (see Section 1.6.2).

1.4.2 Outputs

Unlike N_2 fixation, nitrate reduction has a strong isotopic bias, favouring the light N isotope and leaving behind a residual nitrate pool that is progressively enriched in ^{15}N with increasing degree of nitrate consumption. Culture studies collectively yield a relatively broad range in the isotope effect for nitrate consumption by denitrifying bacteria, from roughly 15 to 30 ‰, with the more recent estimates falling between 20 and 30 ‰ [*Mariotti et al.*, 1981; *Barford et al.*, 1999]. By analogy with work on nitrate assimilation [*Granger et al.*, 2004; *Needoba et al.*, 2004], it would appear that isotopic discrimination primarily takes place upon reduction of nitrate to nitrite by the intracellular enzyme nitrate reductase, which has an intrinsic isotope effect of 20 – 30 ‰ [*Ledgard et al.*, 1985]. The expression of this fractionation is registered by the $\delta^{15}N$ of unconsumed nitrate that diffuses from the cells back into the ambient waters.

The resulting ^{15}N-enrichment is readily observed in water column studies, in which denitrification rates (calculated from nitrate deficits relative to phosphate) give estimates of 22-30 ‰ for the isotope effect of denitrification [*Cline and Kaplan*, 1975; *Liu and Kaplan*, 1989; *Brandes et al.*, 1998; *Altabet et al.*, 1999; *Voss et al.*, 2001; *Sigman et al.*, 2003]. Regardless of the exact value of the expressed isotope effect, water column denitrification clearly results in very high nitrate $\delta^{15}N$ in the thermocline within, and adjacent to, actively denitrifying regions of the water column (see ETNP profile, Figure 3). It is noted that, although there are no existing measurements to explicitly resolve the isotopic impact of anammox, it is implicitly included in all existing water-column (and sedimentary)

denitrification studies as part of the overall fixed N loss (although its presence would alter the gross reaction stoichiometry to some degree).

Sedimentary denitrification, in contrast, shows very little expression of the enzymatic isotope effect. Benthic flux experiments have shown that, even with high rates of sedimentary denitrification, no detectable increase of nitrate $\delta^{15}N$ is observed [*Brandes and Devol*, 1997; *Brandes and Devol*, 2002] [*Lehmann et al.*, 2004]. The common explanation is that nitrate is nearly completely consumed at the locus of sedimentary denitrification. Because no nitrate escapes the denitrification zones, there is no expression of the isotope effect. This view is supported by the observation of extreme ^{15}N enrichment of nitrate in sediment porewaters [*Sigman et al.*, 2001], which indicates that the lack of isotopic expression of denitrification in sediment cannot be explained by a lack of isotopic fractionation at the scale of the organism. Regardless of the mechanism, sedimentary denitrification is typically assumed to have a negligible isotopic effect for budgetary calculations [*Brandes and Devol*, 2002; *Sigman et al.*, 2003; *Deutsch et al.*, 2004].

These two extremes of expression of the organism-level isotope effect of denitrification – complete expression in the water column and no expression in sediments – are unlikely to apply perfectly in the ocean. Instead, we might expect some degree of under-expression of the isotope effect in the water column under some conditions [*Sigman et al.*, 2003; *Deutsch et al.*, 2004], particularly if alternate dissimilatory pathways, such as anammox, fractionate differently and are of variable importance depending on environmental conditions. An extreme case of this is provided by the Cariaco Basin, where water column denitrification appears to consume nitrate completely very near the oxic/anoxic interface, leading to minimal expression of the isotope effect of denitrification [*Thunell et al.*, 2004]. Reciprocally, isotopic discrimination by denitrification is partially expressed in some sediments, albeit to a small degree relative to water column denitrification [*Brandes and Devol*, 2002; *Lehmann et al.*, 2004]. Nevertheless, the end-member view presented above provides a useful conceptual starting point.

1.4.3 Internal cycling

Fixed nitrogen occurs in many forms in the marine environment other than nitrate, and most transformations between these nitrogen pools involve some degree of isotopic

fractionation. The most important fractionation for understanding changes in nutrient distribution (as opposed to changes in the input/output budget) occurs during nitrate assimilation. As a rule, the $\delta^{15}N$ of organic matter is lower than that of the nitrate pool on which it grew, given incomplete nitrate utilization. The $\delta^{15}N$ of both the residual nitrate and the subsequently produced organic N increase as nitrate consumption proceeds, following Rayleigh fractionation kinetics. The $\delta^{15}N$ of NO_3^- in the upper ocean suggests an isotope effect of 4-10 ‰ for NO_3^- assimilation, with most estimates closer to 5-7 ‰ [*Altabet*, 1988; *Altabet et al.*, 1999; *Sigman et al.*, 1999b; *Wu et al.*, 1999; *Altabet and Francois*, 2001]. Fractionation in cultures appears to be more variable, with isotope effects as high as 20 ‰, although many cultures yield effects of ≤6 ‰ [*Needoba et al.*, 2003].

Developing a predictive understanding of the isotope effect of nitrate assimilation has been a goal of marine N isotope studies. The isotope effect varies among species grown under similar growth conditions [*Wada and Hattori*, 1978; *Waser et al.*, 1998; *Needoba et al.*, 2003] and, for at least some species, as a function of growth conditions [*Granger et al.*, 2004; *Needoba and Harrison*, 2004]. For example, the cultured diatom *Thalassiosira weissflogii* displays a greater organism-level isotope effect under light-limitation than under iron-limitation or maximal growth rate [*Needoba and Harrison*, 2004; *Needoba et al.*, 2004]. The potential variability of the isotope effect represents an important uncertainty in paleoceanographic application of nitrogen isotopes to changes in nutrient utilization in the nitrate-replete regions of the surface ocean.

When nitrate is completely utilized, the accumulated organic matter has the same $\delta^{15}N$ as the original nitrate source. Hence, in regions where the consumption of nitrate is complete over the course of the year, isotope fractionation during nitrate assimilation has only a transitory (i.e. seasonal) effect that disappears when integrated over the seasons of growth. From the perspective of paleoceanography, the $\delta^{15}N$ of organic N exported from such an environment must be identical to that of the N supply; if subsurface nitrate is the dominant supply term, then the export should have the same $\delta^{15}N$ as the sub-euphotic zone nitrate transferred to the sunlit surface ocean. In contrast, within nutrient-rich regions of the surface ocean, where nitrate consumption is persistently incomplete, the $\delta^{15}N$ of sinking N is lower than sub-euphotic $\delta^{15}N_{nitrate}$, and the $\delta^{15}N$ of the residual surface nitrate is higher than

both the sub-euphotic zone nitrate and the sinking N (Figure 1.3, Southern Ocean) [*Sigman et al.*, 1999b; *Lourey et al.*, 2003].

1.4.4 Deep nitrate

Despite dramatic variations of $\delta^{15}N_{nitrate}$ in the surface ocean caused by incomplete nitrate uptake and remineralization, nitrate assimilation has little effect on the global distribution of N isotopes. Complete nitrate utilization in most of the surface ocean and virtually complete remineralization in the subsurface prevents the accumulation of isotopically distinct non-nitrate pools. Dissolved organic nitrogen, the only other pool of appreciable size, has a very similar isotopic composition to that of nitrate where it has been measured [*Knapp et al.*, 2005] and therefore can have limited impact in this regard. Nitrate concentrations in the deep sea are so high that the small amount of low-$\delta^{15}N$ organic matter supplied from the nutrient-rich surface has only a minimal effect on the $\delta^{15}N$ of deep ocean nitrate [*Sigman et al.*, 2000] (e.g. compare Southern Ocean deep water vs Sargasso Sea, Figure 1.3). Also, although subduction or downward mixing of surface waters with residual, high-$\delta^{15}N_{nitrate}$ occurs in nutrient-rich regions, waters that have undergone significant nitrate depletion tend to have minimal impacts on the waters with which they mix, because the ^{15}N-enriched nitrate is present only at low concentration. As a result, while there are significant variations in nitrate concentration within the ocean interior, these are not paralleled by comparable variation in $\delta^{15}N_{nitrate}$ [*Sigman et al.*, 2000].

Instead, the deep sea is remarkably homogeneous with respect to nitrate $\delta^{15}N$, so that it represents a well-integrated measure of global input and output rates. Mean deep ocean $\delta^{15}N_{nitrate}$ therefore has the potential to reflect whole-ocean inventory change. The challenge, as things stand, is to find a sedimentary archive that monitors the deep $\delta^{15}N_{nitrate}$ through time without convolution by the signal of regional thermocline and surface ocean processes.

1.5 Ocean $\delta^{15}N_{nitrate}$ in the past

Given that the rates of N_2 fixation, water column denitrification and sedimentary denitrification are much greater than those of other sources and sinks of marine nitrogen, it is fair to assume that these have been the dominant input/output terms of the marine N budget throughout the past 2.5 Myr. One can also reasonably assume that sediment records

underlying nutrient-rich regions (the equatorial upwellings and polar oceans) may contain the signal of changing degrees of nitrate consumption by algae in the surface waters, whereas it is at least a fair starting point to assume that records from the oligotrophic gyres will not. With such assumptions in place, one can begin to consider how these processes would have altered the $\delta^{15}N$ of marine nitrate, both within a given region and at the scale of the whole ocean.

1.5.1 Local variations

Because the isotope fractionating processes are not evenly distributed throughout the ocean, temporal variations at fixed points will produce predictable changes in the $\delta^{15}N$ of local nitrate pools. As examples: (1) an increase in denitrification rates within the water column on the Oman margin would increase the $\delta^{15}N_{nitrate}$ of the Arabian Sea thermocline [*Schafer and Ittekkot*, 1993; *Altabet et al.*, 1995]; (2) an increase in N_2-fixation in surface waters of the eastern Mediterranean would cause a decrease in $\delta^{15}N_{nitrate}$ in the eastern Mediterranean thermocline [*Struck et al.*, 2001]; and (3) an increase in relative nitrate consumption in Antarctic surface waters would cause an increase in local near-surface $\delta^{15}N_{nitrate}$ [*Francois et al.*, 1997]. However, it must be kept in mind that these local signals are imprinted upon any variation in the $\delta^{15}N$ baseline of mean ocean nitrate. A similar principle operates at finer scales, with changes in a N-cycle process in one region contaminating adjacent regions to various degrees, such as ^{15}N-enriched nitrate from the ETNP affecting the California Undercurrent (e.g., [*Kienast et al.*, 2002]).

1.5.2 Steady state mean

At steady state, the flux-weighted mean $\delta^{15}N$ of fixed N outputs (dominated by water column and sedimentary denitrification) equals that of the inputs (dominated by marine N_2 fixation). The $\delta^{15}N$ of nitrogen supplied by N_2 fixation is tied to the $\delta^{15}N$ of the atmosphere, which does not vary on a million year time scale. The $\delta^{15}N$ of nitrogen removed by water column and sedimentary denitrification, on the other hand, is tied to the mean $\delta^{15}N$ of oceanic nitrate, subject to the effective isotope discriminations. That the mean ocean $\delta^{15}N_{nitrate}$ is higher than the $\delta^{15}N$ of atmospheric N_2 is fundamentally due to the preferential loss of ^{14}N during denitrification.

At steady state, the mean ocean $\delta^{15}N_{nitrate}$ approaches the value at which the sum of all denitrification (including both the water column and sediment) removes nitrate with the same $\delta^{15}N$ as N added to the ocean by N_2 fixation, i.e. ~- 1 ‰. Subject to this condition, the ratio of rates of sedimentary versus water column denitrification should provide the overarching control on the mean $\delta^{15}N$ of nitrate [*Brandes and Devol*, 2002]. Roughly speaking, since water column denitrification discriminates against ^{15}N-nitrate while sedimentary denitrification does not, a higher ratio of water column to sedimentary denitrification will tend to yield a higher mean nitrate $\delta^{15}N$ (Figure 1.4). For example, if water column denitrification were homogeneously distributed throughout the oceans, an expressed isotope effect of 25 ‰ for water column denitrification would require that sedimentary denitrification be responsible for roughly 80 % of the modern loss of fixed nitrogen from the ocean in order to maintain a mean ocean nitrate $\delta^{15}N$ of 5 ‰ [*Brandes and Devol*, 2002]. The fact that water column denitrification takes place in <0.2 % of the ocean's volume, with relatively high degrees of nitrate loss (typically exceeding 40 %), means that water column denitrification causes less ^{15}N enrichment than would arise if water column denitrification were homogeneously distributed (a result of Rayleigh fractionation kinetics). The first effort to account for this "dilution effect" [*Deutsch et al.*, 2004] indicates that preindustrial water column denitrification could have accounted for ~ 30 % of the total, which is 50 % more than if the ocean were approximated as homogeneous. But such estimates remain speculative; there is more to be learned about the net isotopic effect of both water column and sedimentary denitrification and their potential to vary over time.

1.5.3 Application to the past

As mentioned above, a sediment core in a given region will simultaneously provide information on two separate quantities: changes in mean ocean nitrate $\delta^{15}N$, and changes in regional ^{15}N depletion or enrichment relative to the whole ocean change. Obviously, areas prone to large variations in water column denitrification or N_2 fixation are most likely to produce records dominated by these processes. Meanwhile, regions in which algal growth can be limited by factors other than nitrate supply (the polar ocean, the equatorial upwellings and some coastal upwelling areas) will be susceptible to significant assimilation-driven changes in surface nitrate $\delta^{15}N$.

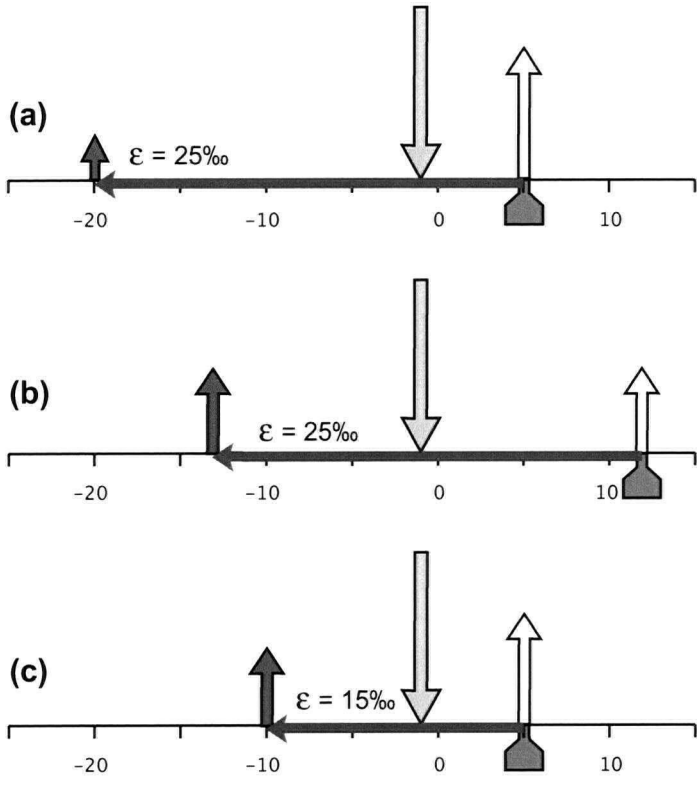

1.4. Mean ocean steady-state isotope balance associated with the budget of fixed N. Vertical arrows represent global input and output fluxes, in which the flux is proportional to the length of the arrow and the isotopic composition is shown by the position on the horizontal axis (showing $\delta^{15}N$ in ‰). The yellow downward-pointing arrow represents the N_2 fixation flux, the white arrow represents the sedimentary denitrification flux, and the blue arrow represents the water column denitrification flux. Sedimentary denitrification removes N of $\delta^{15}N$ close to that of mean ocean nitrate, and water column denitrification removes nitrogen which is depleted in ^{15}N by the expressed isotope effect, e. The green reservoir below the axis represents the $\delta^{15}N$ of mean ocean nitrate, which is determined by the ratio of sedimentary to water column denitrification. At steady state, mass and isotopic balance requires that the sum of the denitrification fluxes equal the N_2 fixation flux and that the denitrification fluxes be balanced about the N_2 fixation 'fulcrum'. Hence, a balanced isotope budget with an expressed isotope effect of 25‰ for water column denitrification requires a much larger flux of sedimentary denitrification in order to maintain a mean ocean $\delta^{15}N$ of 5‰, close to the fulcrum (the $\delta^{15}N$ of N_2 fixation, -1‰), as shown by (a). The impact of increasing the relative proportion of water column denitrification to equal that of sedimentary denitrification is shown in panel (b), which pushes the mean ocean reservoir to a higher value. If the expressed isotope effect of water column denitrification is actually less than 25‰ (c), the mean ocean nitrate is less sensitive to changes and the relative proportion of water column denitrification can be higher while maintaining a mean isotope composition of 5‰.

The mean deep $\delta^{15}N_{nitrate}$ has yet to be explicitly resolved from among the array of local changes. Sediment cores from the low and mid-latitudes contain the remains of plankton grown on N supplied from the thermocline and not directly from the deep sea. Given the regional heterogeneity of thermocline $\delta^{15}N_{nitrate}$ ($\geq$15 ‰ in the modern ocean), it is understandably difficult to extract the global mean background variability from a foreground of changes in surface and thermocline nitrate $\delta^{15}N$. Although polar ocean regions sample deep nitrate more directly, the possibility that the past degree of nitrate utilization varied means that records from these regions cannot be assumed to reflect the deep nitrate supply. Before exploring this further, however, we must discuss the development of sedimentary records of the N isotopes.

1.6 Sedimentary N isotope records

The most common paleoceanographic proxy used to reconstruct past changes in the oceanic N budget or cycle is the $\delta^{15}N$ of total combustible, or 'bulk', sedimentary nitrogen (herein $\delta^{15}N_{bulk}$). Such measurements provide a record, with a variable degree of accuracy, of the N sinking out of the surface ocean at times past [*Altabet and Francois*, 1994]. Below, we review the robustness of the connection between the organic N sinking out of the surface ocean and that preserved in paleoceanographic records as bulk sedimentary N. We also briefly discuss the ongoing development of alternatives to the bulk measurement.

1.6.1 The $\delta^{15}N$ of sinking N

Most generally, sedimentary $\delta^{15}N$ records are interpreted as providing a record of the $\delta^{15}N_{nitrate}$ in the region of study. In regions where nitrate is nearly completely consumed, the records are typically thought to reconstruct the $\delta^{15}N$ of the sub-euphotic zone nitrate that is supplied to the euphotic zone by upwelling and/or mixing. But, in some cases, the $\delta^{15}N$ of the sinking flux may not match the $\delta^{15}N$ of the nitrate supplied to the euphotic zone. For instance, in some regions, N_2 fixation may account for a significant fraction of the sinking N, such that the $\delta^{15}N$ of N sinking out of the surface ocean may be significantly lower than the subsurface $\delta^{15}N_{nitrate}$ [*Karl et al.*, 1997]. In nutrient-rich regions such as the Antarctic and Subarctic Pacific, the gross nitrate supply to the surface is only partially consumed before

being mixed or subducted back into the ocean interior or transported laterally out the system. In this case, the sinking flux $\delta^{15}N$ will be lower than the $\delta^{15}N$ of the nitrate initially supplied to that region of the surface ocean.

Beyond these upper ocean processes that are signals of interest, poorly understood processes alter the $\delta^{15}N$ of sinking nitrogen during transit through the water column and burial. It has been observed in a variety of oceanographic settings that sinking N $\delta^{15}N$ tends to decrease with depth in the water column (by up to 2‰ over several kilometers of depth [*Altabet and Francois*, 1994; *Lourey et al.*, 2003; *Nakanishi and Minagawa*, 2003]. Explanations for this observation range from the addition of low-$\delta^{15}N$ bacterial biomass to contamination of the shallower traps by zooplankton "swimmers". More recently, other deviations from expectations have been observed. The sinking N $\delta^{15}N$ in the Southern Ocean is highest during the wintertime low flux period and then decreases into the higher flux, spring bloom period as [NO_3^-] declines [*Altabet and Francois*, 2001; *Lourey et al.*, 2003]. This sense of change is the opposite of what is expected from simple isotopic fractionation during algal assimilation of surface nitrate, and may be explained by the wintertime sinking flux being dominated by very slowly sinking material that has been enriched in ^{15}N by progressive degradation, analogous to observations for the $\delta^{15}N$ of deep suspended N [*Saino and Hattori*, 1987].

1.6.2 The $\delta^{15}N$ of sedimentary N

Despite these observations, at sites where export production is high and/or organic matter preservation is good (many of which are on continental margins), an excellent correlation is found between the $\delta^{15}N$ of bulk surface sedimentary N and that of the local sub-euphotic zone nitrate (Figure 1.5) [*Thunell et al.*, 2004]. This suggests that alteration during sinking and incorporation in the sediments does not greatly confound bulk sedimentary N as a recorder of the $\delta^{15}N$ of the N sinking out of the surface ocean. It also attests to the generally tight connection between the $\delta^{15}N$ of the nitrate supply to the surface and that of the annually integrated sinking flux under conditions of complete nitrate consumption in surface waters [*Altabet et al.*, 1999] showing that, in many locations, nitrate assimilation leaves a negligible impact in sedimentary $\delta^{15}N$.

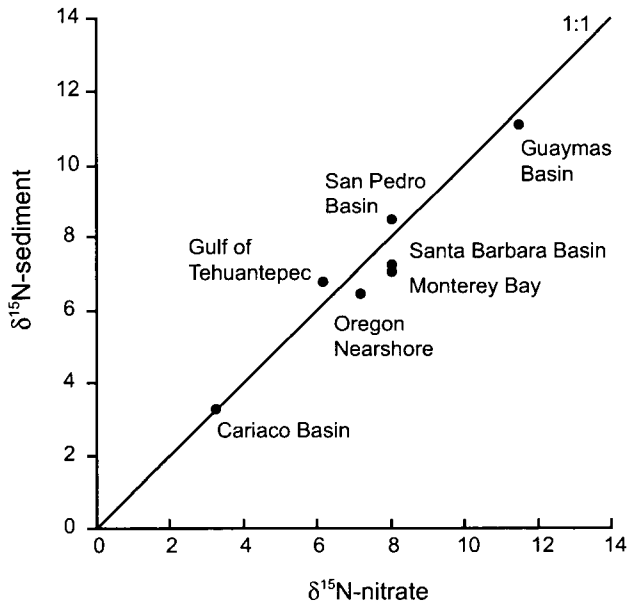

1.5. Fidelity of sedimentary $\delta^{15}N$ as a recorder of $\delta^{15}N_{nitrate}$ at coastal margins. This plot shows the $\delta^{15}N_{nitrate}$ of water at the base of the euphotic zone vs. the $\delta^{15}N$ of surface sediment at or near the same locations (data from [Altabet et al., 1999; Emmer and Thunell, 2000; Kienast et al., 2002; Liu, 1979; Pride et al., 1999; Thunell et al., 2004]. Despite the complexity of nitrogen cycling within the water column, the sediment records the $\delta^{15}N$ of thermocline nitrate with a high degree of accuracy at all of these diverse locations (modified after [Thunell et al., 2004]).

In some regions, measurements of bulk sediment $\delta^{15}N$ from the deep seafloor have uncovered patterns that qualitatively mirror expectations for assimilation-driven spatial variation in $\delta^{15}N$ [*Altabet and Francois*, 1994; *Farrell et al.*, 1995a; *Holmes et al.*, 1996]. However, in these open ocean settings, a significant ^{15}N enrichment (on the order of 3-5 ‰) is observed in bulk sedimentary N relative to sinking N [*Altabet and Francois*, 1994], and it is difficult to conclusively separate this diagenetic effect from any potential gradients of nitrate assimilation. This $\delta^{15}N$ increase is apparently due to preferential remineralization of ^{14}N during the oxidation of organic matter, and the isotopic effect of this process appears to be greatest in organic-poor deep-sea sediment, where oxidation proceeds to the greatest degree. As one might expect, there is some evidence for a continuous range in the $\delta^{15}N$ difference between sinking and sedimentary N, from no difference in the high-preservation margin environments described above to ~5 ‰ in the most organic-poor, slowly accumulating sediments of the open ocean [*Nakanishi and Minagawa*, 2003]. As a result, there is well-founded concern that extreme changes in the conditions at the sediment-water interface over time could produce a time-varying degree of diagenetic enrichment of sediment $\delta^{15}N$ [*Sachs and Repeta*, 1999].

Sedimentological processes introduce additional uncertainties that deserve mention. Two sedimentary $\delta^{15}N$ records from adjacent sites on the northern margin of the South China Sea show quite different features over the past 40 kyr despite being separated by less than 15 km [*Higginson et al.*, 2003; *Kienast*, 2005]. This is apparently due to sediment transport that redistributes the fine fraction of sediment, including the organic matter in which the N resides, over large distances [*Freudenthal et al.*, 2001; *Kienast*, 2005]. Other complicating factors can include the presence of terrestrial organic matter, which may have a distinct N isotopic composition [*Peters et al.*, 1978; *McKay et al.*, 2004], and inorganic N, which can be a significant component in the lattices of some clay minerals, particularly illite [*Schubert and Calvert*, 2001].

Because of concerns about seafloor processes affecting the $\delta^{15}N$ of bulk sedimentary N, the isotopic composition of targeted sedimentary N fractions is being pursued. Most work of this type has focused on the N bound within the silica frustules of diatoms, which should record past surface ocean processes while being protected from the isotopic effects of bacterial degradation during sinking and incorporation in the sedimentary record [*Shemesh et*

al., 1993; *Sigman et al.*, 1999a; *Crosta and Shemesh*, 2002; *Robinson et al.*, 2004]. Indeed, this work has been interpreted to indicate that open ocean bulk sediment $\delta^{15}N$ may be vulnerable to temporal changes in the amplitude of diagenetic alteration [*Robinson et al.*, 2005]. The $\delta^{15}N$ of organic matter in foraminiferal tests was briefly explored following the same rationale [*Altabet and Curry*, 1989]. Chlorophyll degradation products have also been isolated from sediments for N isotopic analysis [*Sachs and Repeta*, 1999].

The ongoing research into such specific N fractions is critical to address the fundamental issue of isotopic alteration of exported organic N in the water column and sediments. However, this work also raises a host of new questions. Consider the case of diatom frustule-bound N (Figure 1.6). The organic N of diatoms exported from the surface layer could differ from the integrated sinking N, for instance, if the isotope effect of nitrate assimilation by diatoms differs from that of the entire phytoplankton population. Moreover, the $\delta^{15}N$ of N trapped and preserved within the diatom frustule may be quite different from the bulk biomass of the diatom that produced it. Thus, diatom frustule $\delta^{15}N$ need not be a direct reflection of integrated sinking flux $\delta^{15}N$, and the relationship between the two could change over time. Nevertheless, the concerns regarding the interpretation of bulk $\delta^{15}N$ demand that approaches be developed for the analysis of specific N fractions, at least for open ocean records, as long as diagenesis remains unconstrained.

1.7 Observations and interpretations

Although questions remain regarding the fidelity of sedimentary N isotope ratios as a recorder of oceanic N dynamics, significant progress has been made by comparing multiple records from different sedimentary regimes and by using additional proxies to better constrain other environmental parameters. Indeed, many of the records generated to date show coherent variations on different spatial and temporal scales, indicating that they are undoubtedly recording something meaningful. Here we review some of the observations to date and their current interpretations, in relation to the conceptual mechanisms outlined in Section 1.2 and 1.3.

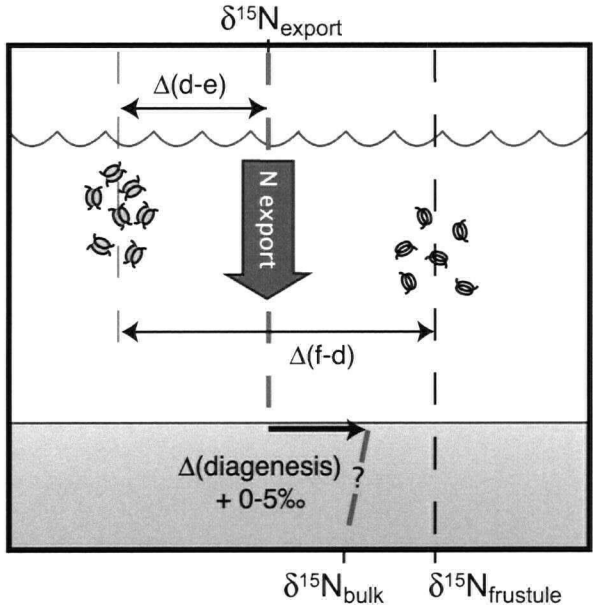

1.6. The $\delta^{15}N$ of integrated N export (represented by the downward pointing arrow, '$\delta^{15}N_{export}$') versus $\delta^{15}N_{bulk}$ and $\delta^{15}N_{frustule}$, two sedimentary measurements employed to reconstruct the $\delta^{15}N$ of N export. During sinking and burial in slowly accumulating deep-sea sediments, organic N may undergo ^{15}N enrichment due to diagenesis. The amplitude of this enrichment is environmentally variable, being absent in organic-rich ocean margins but as high as 5‰ in the less productive open ocean. The $\delta^{15}N$ of N bound within diatom frustules ($\delta^{15}N_{frustule}$) does not appear to be affected by diagenesis. However, measurements to date indicate that it is different from (higher than) '$\delta^{15}N_{export}$'. This difference may be due to (1) a $\delta^{15}N$ difference between diatom biomass sinking out of the euphotic zone and the bulk sinking N ('Δ(d-e)'), and/or (2) a $\delta^{15}N$ difference between the organic N incorporated in diatom frustules and the bulk biomass N of the diatom ('Δ(f-d)'). The amplitude of either of these $\delta^{15}N$ differences may be sensitive to changes in surface ocean conditions (e.g., because of changes in phytoplankton assemblage or in the growth conditions of diatoms). Thus, given current information, neither $\delta^{15}N_{bulk}$ nor $\delta^{15}N_{frustule}$ alone can be taken as a perfect indicator of $\delta^{15}N_{export}$.

1.7.1 Glacial-interglacial inventory changes

The most robust finding to arise from sedimentary N isotope records is of climatically-linked changes in denitrification in each of the major thermocline oxygen minimum zones of the global ocean: the Arabian Sea and the eastern tropical North and South Pacific [*Altabet et al.*, 1995; *Ganeshram et al.*, 1995; *Pride et al.*, 1999; *Ganeshram et al.*, 2000]. The success in documenting past changes in water column denitrification can be ascribed to three factors. First, the modern thermocline denitrification zones are all associated with highly productive margin environments. As described above (Section 1.6.2), the sediments from these environments have been shown to accurately record the $\delta^{15}N$ of subeuphotic zone nitrate [*Altabet et al.*, 1999; *Thunell et al.*, 2004], making many of them good monitors of nearby denitrification in the thermocline. Second, the isotope effect of water column denitrification is large, so that the isotopic signal of denitrification readily overcomes the noise of other processes (see ETNP, Fig 3). Third, a number of other sediment properties (e.g., presence of laminations, redox-sensitive metal contents) corroborate variations in water column oxygenation associated with denitrification changes.

All of the denitrification records show a general pattern of low $\delta^{15}N$ during glacials and high $\delta^{15}N$ during warm interglacial periods (Figure 1.7). These changes are accompanied by parallel evidence of water column suboxia from trace metal concentrations [*Kienast et al.*, 2002; *Nameroff et al.*, 2004], benthic foraminiferal assemblages [*Ohkushi et al.*, 2003] and sediment laminations [*Ganeshram et al.*, 2000; *Suthhof et al.*, 2001; *van Geen et al.*, 2003; *Thunell and Kepple*, 2004], confirming that thermocline suboxia was expanded during periods with high $\delta^{15}N$. There also appear to be finer-scale regional complexities superimposed on the underlying glacial-interglacial pattern, for instance in both the Arabian Sea [*Suthhof et al.*, 2001; *Altabet et al.*, 2002; *Higginson et al.*, 2004; *Ivanochko et al.*, 2005] and in the North Pacific [*Emmer and Thunell*, 2000; *Hendy et al.*, 2004], where intense millennial-scale structure is apparent in a striking resemblance to the Greenland ice core records. The Younger Dryas, a brief and largely global return to ice-age-like conditions, had less denitrification in the same regions [*Emmer and Thunell*, 2000; *Suthhof et al.*, 2001; *Altabet et al.*, 2002; *Hendy et al.*, 2004], with increased oxygen concentrations at intermediate depth corroborated by decreased sediment lamination, lower trace metal concentrations, and decreased age of intermediate waters [*Keigwin et al.*, 1992; *Behl and*

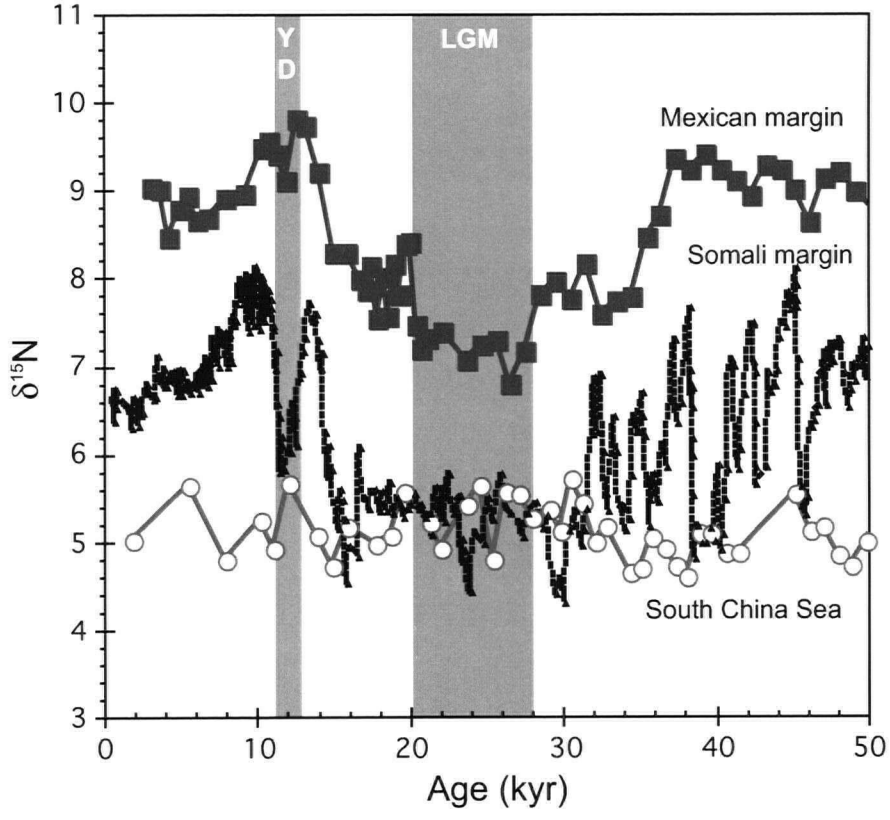

1.7. Plots of $\delta^{15}N_{bulk}$ vs. sediment age over the past 50,000 years for cores from the Mexican margin [Ganeshram et al., 1995], the Somali margin [Ivanochko et al., 2005] and the South China Sea [Kienast, 2000]. The Last Glacial Maximum and Younger Dryas cold intervals are indicated with the blue shading. The $\delta^{15}N$ offsets among the records over the Holocene (the last ~10 kyr) are consistent with the effect of modern water column denitrification, which causes high thermocline $\delta^{15}N_{nitrate}$ along the Mexican margin and in the Arabian Sea. During the last glacial maximum, this range collapsed to roughly half that of the present-day (~2‰). This appears to be due to a reduction of water column denitrification, reducing the preferential loss of ^{14}N from the oceans. The remarkable stability of the South China Sea $\delta^{15}N$ record in the face of this glacial reduction in water column denitrification suggests a compensatory global-scale reduction of N_2 fixation.

Kennett, 1996; *Pride et al.*, 1999; *Ahagon et al.*, 2003; *van Geen et al.*, 2003]. In sum, these present a general view of cold periods being typified by a better oxygenated thermocline with less denitrification.

The deglacial maximum in $\delta^{15}N$ and subsequent decrease through the Holocene observed in many sediment records is more difficult to explain. The most straightforward explanation is of a peak in water-column denitrification rates followed by a decrease during the Holocene, a sequence that could conceivably have arisen from either a circulation change or the negative feedback on water column denitrification through local nitrate limitation [*Deutsch et al.*, 2004]. However, the deglacial $\delta^{15}N$ maximum is such a pervasive signal in sediment records that it may reflect a deglacial $\delta^{15}N$ maximum in the mean ocean $\delta^{15}N_{nitrate}$ itself, caused by a maximum in the global mean ratio of water column to sedimentary denitrification [*Deutsch et al.*, 2004]. It has been argued [*Christensen et al.*, 1987] that sedimentary denitrification was also reduced during glacial periods due to the lower sea level. Thus, if both sedimentary and water column denitrification increased over the glacial-interglacial transition, but water column denitrification increased early while sedimentary denitrification increased later, a peak in $\delta^{15}N$ would have resulted when the ratio of water column to sediment denitrification was highest. Indeed, this is the pattern that would be suggested by the generally early and rapid rises in $\delta^{15}N$ (18-14 kyr) vs. the more gradual rise of sea level (18-10kyr). Nevertheless, the largest $\delta^{15}N$ maxima occur in sediments underlying the denitrification zones, suggesting that the absolute rate of thermocline denitrification has decreased to some degree since the deglacial peak, as discussed further in Chapter 4.

Despite the large reorganization of Earth's climate system and attendant changes in thermocline denitrification, it seems very unlikely that the whole ocean $\delta^{15}N$ has changed by more than ± 1‰ between the LGM and the present-day [*Altabet and Curry*, 1989; *Kienast*, 2000]). This is an important observation, given that the short residence time of marine N (~3 kyr, [*Codispoti et al.*, 2001]) requires that steady state was approached during the LGM and has been approached again since the deglaciation. Under the reigning N isotope paradigm, the ratio of water column to sedimentary denitrification during the LGM must have been very similar to the present day (Figure 1.4). Coupled with the evidence for locally higher water column denitrification rates during the interglacial, this suggests that the total (water column plus sedimentary) denitrification rate of the current interglacial is likely significantly higher

than was the total rate during the last ice age. If so, given the short residence time of oceanic fixed N, a glacial-to-interglacial increase in N_2 fixation must also have occurred. Otherwise, the $\delta^{15}N$ of nitrate in the ocean would have changed dramatically, or the ocean would have run out of nitrate, neither of which occurred.

1.7.2 Glacial-interglacial changes in nutrient-rich regions

Nutrient-rich regions of the surface ocean have undergone significant changes in export production over glacial-interglacial cycles. In the Antarctic Zone of the Southern Ocean, numerous studies have converged to show that export production was lower during the ice ages than during interglacials [*Francois et al.*, 1997; *Anderson et al.*, 1998; *Kohfeld et al.*, 2005]. In contrast, studies of the Subantarctic Zone generally indicate higher export production during ice ages, the inverse of the Antarctic climate cycle in productivity [*Mortlock et al.*, 1991; *Kumar et al.*, 1995; *Frank et al.*, 2000; *Chase et al.*, 2003]. In the Equatorial Pacific, reconstructions of glacial-interglacial export productivity are conflicting, and the picture remains equivocal [*Pedersen*, 1983; *Farrell et al.*, 1995b; *Paytan and Kastner*, 1996; *Loubere*, 1999; *Marcantonio et al.*, 2001; *Loubere et al.*, 2004]. In the subarctic Pacific, export productivity seems to have been generally lower during glacial periods [*Narita et al.*, 2002; *Kienast et al.*, 2004; *Jaccard et al.*, 2005]. The observation of variable export productivity in these nutrient-rich regions prompted sedimentary N isotope studies to explore the underlying physical mechanisms, assuming that $\delta^{15}N$ changes reflect the degree of relative nitrate consumption.

In the glacial Antarctic, evidence for reduced export production is accompanied by higher sedimentary $\delta^{15}N_{bulk}$ (Figure 1.8, [*Francois et al.*, 1997]), implying a greater degree of relative nitrate consumption despite the diminished export production. This requires that the gross rate of nitrate supply to the Antarctic euphotic zone was reduced during glacial times. Physically, this change would seem to require reduced exchange of water between the surface and deep Antarctic, as would result from year-round stratification of the upper water column (see Section 1.3). Although $\delta^{15}N_{frustule}$ records suggest that the glacial/interglacial change in environmental conditions was less homogeneous across the Antarctic zone than indicated by $\delta^{15}N_{bulk}$ [*Robinson et al.*, 2004], the coincidence of elevated $\delta^{15}N$ with lowered export productivity in the polar oceans is now consistently interpreted as a result of water

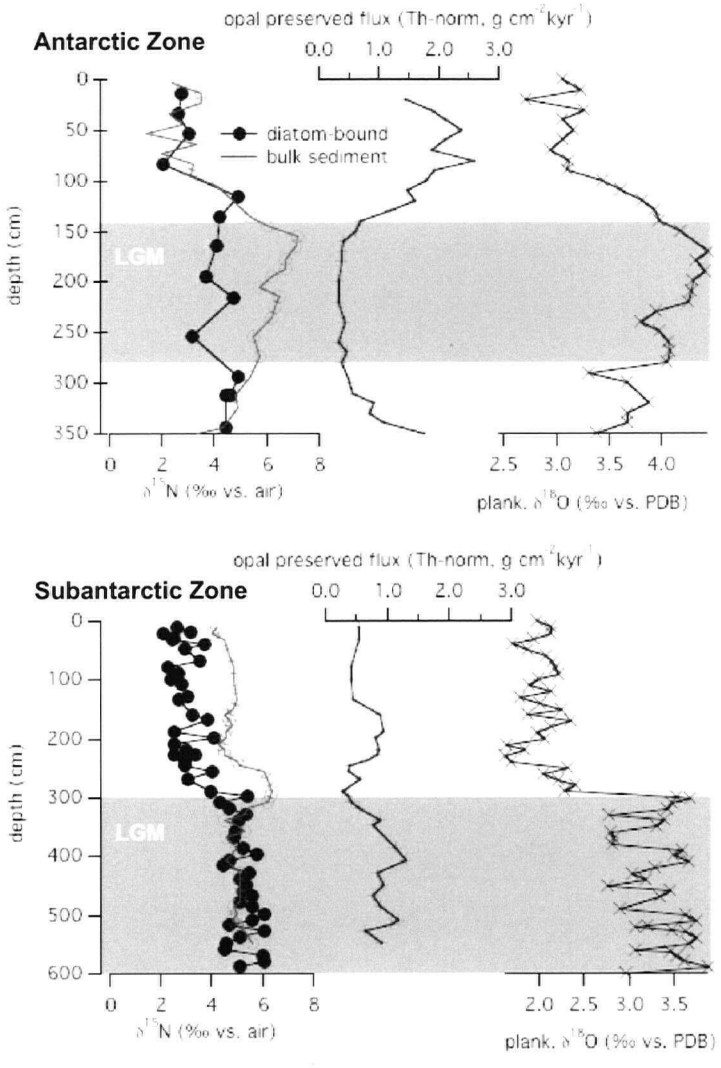

1.8. Paleoceanographic records from the Subantarctic (MD-84552) and Antarctic (E11-2) zones of the Southern Ocean. Foraminiferal $\delta^{18}O$ is shown as a proxy for global ice volume, to indicate the Last Glacial Maximum, which is shaded gray. The ^{230}Th-corrected opal flux is shown in the centre of each panel as a proxy for diatom export production, and both $\delta^{15}N_{bulk}$ and $\delta^{15}N_{frustule}$ are shown on the left (open and filled circles, respectively). During the LGM, diatom export was lower in the Antarctic Zone, and virtually unchanged in this (Indian) sector of the Subantarctic Zone. The $\delta^{15}N_{bulk}$ records appear to be compromised by diagenetic alteration in this well-oxidized, low-accumulation-rate environment. However, the $\delta^{15}N_{frustule}$ shows that the $\delta^{15}N$ of diatoms was higher in both zones during the LGM. The simplest way to reconcile these data is to invoke, during the LGM, enhanced aeolian Fe supply in the Subantarctic and decreased upward macronutrient supply throughout the surface of the Antarctic. After [Robinson et al., 2004] and [Robinson et al., 2005].

column stratification [*Haug et al.*, 1999; *Sigman et al.*, 2004; *Jaccard et al.*, 2005]. Enhanced Fe supply during the glacial may have contributed further to nitrate drawdown by supplementing the Fe from deep waters [*Lefevre and Watson*, 1999; *Archer and Johnson*, 2000; *Parekh et al.*, 2004], but this cannot be resolved from the published data.

Measurements of $\delta^{15}N_{bulk}$ from the Subantarctic show marginal glacial/interglacial patterns of change [*Francois et al.*, 1997], though $\delta^{15}N_{frustule}$ records suggest a coherent pattern of elevated $\delta^{15}N$ during glacial times (Figure 8) [*Crosta et al.*, 2005; *Robinson et al.*, 2005]. The combination of increased export production with elevated $\delta^{15}N$ is consistent with higher nutrient consumption as expected under enhanced Fe deposition. The proximity of the Subantarctic Zone to potential dust sources in Patagonia, South Africa, and Australia suggests a greater susceptibility to iron fertilization during ice ages than the higher latitudes of the Southern Ocean [*Robinson et al.*, 2005].

In the equatorial Pacific, $\delta^{15}N_{bulk}$ is low during glacial episodes and elevated during interglacials [*Farrell et al.*, 1995a]. While this may indicate lower nitrate consumption during the ice age, the equatorial Pacific exchanges water with the ETNP shadow zone (e.g. [*Higginson et al.*, 2003]), so the apparent glacial decrease in denitrification within the ETNP may have lowered the regional $\delta^{15}N_{nitrate}$ enough to impact the $\delta^{15}N$ of glacial-age sediment in the equatorial Pacific. Thus, the nutrient status of the ice-age equatorial Pacific remains enigmatic.

1.8 Objectives of this thesis

As discussed above, the application of nitrogen isotopes to the study of climatically relevant changes in the N cycle has achieved major successes. Evidence for changes in nitrate utilization in the Southern Ocean have been observed on glacial-interglacial cycles [*Francois et al.*, 1997; *Robinson et al.*, 2004], and increasingly detailed records of past changes in denitrification have accumulated [*Suthhof et al.*, 2001; *Altabet et al.*, 2002; *Ivanochko et al.*, 2005; *Liu et al.*, 2005]. Yet, there has been little attempt to draw the observations into a mechanistic framework capable of describing the nitrogen cycle at a global scale, identifying its sensitivities, or determining its potential for change. Furthermore, the interpretation of N isotope records from offshore sites has been plagued by non-unique solutions, leaving the N isotopic histories of vast regions of the ocean shrouded. Confusion

arising from diagenesis, changes in nutrient utilization and changes in the nitrogen cycle itself have left apparently intractable problems. This thesis contributes to the field by tackling some of these complexities, using a multi-faceted, multi-regional approach. It spans a seasonally-resolved sedimentary record at a single site, to a global, millennial-scale numerical model of the marine N cycle that integrates the concepts outlined in this introductory chapter to provide a new, global view.

First, an exploration of nitrogen isotope proxies is presented, involving a focused investigation of the $\delta^{15}N$ of nitrogen protected within diatom frustules. Although there are a number of published archives of past changes in this quantity, there has been little attempt to calibrate the proxy in a well-constrained setting. Chapter 2 takes a novel approach, elucidating the relationship between the $\delta^{15}N$ of diatom frustules and the coexisting bulk sediment by exploiting the laminated, diatom-rich sediments of the Guaymas Basin. The results highlight strengths, and unforeseen caveats, of this proxy, while reinforcing the tendency of the bulk sediment $\delta^{15}N$ to accurately monitor $\delta^{15}N_{nitrate}$.

Chapter 3 delves into the web of confusion entangling many nitrogen isotope records by taking a multi-proxy approach to the subarctic Pacific, a highly complex region from a nitrogen isotope perspective. First, a field study of $\delta^{15}N_{nitrate}$ is presented that elucidates the modern isotope dynamics. With this foundation, and using three different core sites, the superimposed signals of diagenesis, echoes of global changes in the nitrogen cycle, and local changes in nitrate utilization can be picked out of the summed records to provide important new information.

Chapter 4 takes a global perspective of published $\delta^{15}N_{bulk}$ records to illustrate broad trends in denitrification and N_2 fixation over past glacial-interglacial cycles. The observed coherency points toward a physical driver of denitrification in the thermocline. A novel physical mechanism is proposed as a major contributor to the observed patterns, and its implications are explored.

Finally, in Chapter 5, a conceptually simple, prognostic model of the marine nitrogen cycle is introduced to a general circulation model in order to mimic the behaviour of the marine nitrogen cycle on centennial-millennial timescales. The model illustrates sensitivities

to environmental parameters that are consistent with the large changes in denitrification rates implied by the sedimentary records.

1.9 References

Ahagon, N., K. Ohkushi, M. Uchida, and T. Mishima, Mid-depth circulation in the northwest Pacific during the last deglaciation: Evidence from foraminiferal radiocarbon ages, *Geophysical Research Letters*, 30, 2003.

Altabet, M., and W. B. Curry, Testing models of past ocean chemistry using foraminifera $^{15}N/^{14}N$, *Global Biogeochemical Cycles*, 3, 107-119, 1989.

Altabet, M. A., Variations in nitrogen isotopic composition between sinking and suspended particles: implications for nitrogen cycling and particle transformation in the deep ocean, *Deep-Sea Research*, 35, 535-554, 1988.

Altabet, M. A., and R. Francois, Sedimentary Nitrogen Isotopic Ratio As a Recorder For Surface Ocean Nitrate Utilization, *Global Biogeochemical Cycles*, 8, 103-116, 1994.

Altabet, M. A., and R. Francois, Nitrogen isotope biogeochemistry of the antarctic polar frontal zone at 170 degrees W, *Deep-Sea Research Part II-Topical Studies in Oceanography*, 48, 4247-4273, 2001.

Altabet, M. A., R. Francois, D. W. Murray, and W. L. Prell, Climate-Related Variations in Denitrification in the Arabian Sea From Sediment $^{15}N/^{14}N$ Ratios, *Nature*, 373, 506-509, 1995.

Altabet, M. A., M. J. Higginson, and D. W. Murray, The effect of millennial-scale changes in Arabian Sea denitrification on atmospheric CO_2, *Nature*, 415, 159-162, 2002.

Altabet, M. A., C. Pilskaln, R. Thunell, C. Pride, D. Sigman, F. Chavez, and R. Francois, The nitrogen isotope biogeochemistry of sinking particles from the margin of the Eastern North Pacific, *Deep-Sea Research Part I-Oceanographic Research Papers*, 46, 655-679, 1999.

Anderson, R. F., N. Kumar, R. A. Mortlock, P. N. Froelich, P. Kubik, B. Dittrich-Hannen, and M. Suter, Late-Quaternary changes in productivity of the Southern Ocean, *Journal of Marine Systems*, 17, 497-514, 1998.

Archer, D. E., and K. Johnson, A Model of the iron cycle in the ocean, *Global Biogeochemical Cycles*, 14, 269-279, 2000.

Barford, C. C., J. P. Montoya, M. A. Altabet, and R. Mitchell, Steady-state nitrogen isotope effects of N_2 and N_2O production in Paracoccus denitrificans, *Applied and Environmental Microbiology*, 65, 989-994, 1999.

Behl, R. J., and J. P. Kennett, Brief interstadial events in the Santa Barbara basin, NE Pacific, during the past 60 kyr, *Nature*, 379, 243-246, 1996.

Brandes, J. A., and A. H. Devol, Isotopic fractionation of oxygen and nitrogen in coastal marine sediments, *Geochimica Et Cosmochimica Acta*, 61, 1793-1801, 1997.

Brandes, J. A., and A. H. Devol, A global marine-fixed nitrogen isotopic budget: Implications for Holocene nitrogen cycling, *Global Biogeochemical Cycles*, 16, art. no.-1120, 2002.

Brandes, J. A., A. H. Devol, T. Yoshinari, D. A. Jayakumar, and S. W. A. Naqvi, Isotopic composition of nitrate in the central Arabian Sea and eastern tropical North Pacific: A tracer for mixing and nitrogen cycles, *Limnology and Oceanography*, 43, 1680-1689, 1998.

Broecker, W., and T. H. Peng, *Tracers in the sea*, ELDIGIO Press, New York, 1982.

Broecker, W. S., Glacial to Interglacial Changes in Ocean Chemistry, *Progress in Oceanography*, 11, 151-197, 1982.

Broecker, W. S., and G. M. Henderson, The sequence of events surrounding Termination II and their implications for the cause of glacial-interglacial CO2 changes, *Paleoceanography*, 13, 352-364, 1998.

Carpenter, E. J., H. R. Harvey, B. Fry, and D. G. Capone, Biogeochemical tracers of the marine cyanobacterium Trichodesmium, *Deep-Sea Research Part I*, 44, 27-38, 1997.

Chase, Z., R. F. Anderson, M. Q. Fleisher, and P. W. Kubik, Accumulation of biogenic and lithogenic material in the Pacific sector of the Southern Ocean during the past 40,000 years, *Deep-Sea Research Part II-Topical Studies in Oceanography*, 50, 799-832, 2003.

Christensen, J. J., J. W. Murray, A. H. Devol, and L. A. Codispoti, Denitrification in continental shelf sediments has major impact on the oceanic nitrogen budget, *Global Biogeochemical Cycles*, 1, 97-116, 1987.

Cline, J. D., and I. R. Kaplan, Isotopic fractionation of dissolved nitrate during denitrification in the eastern tropical north Pacific Ocean, *Marine Chemistry*, 3, 271-299, 1975.

Codispoti, L. A., Phosphorus vs nitrogen limitation of new and export production. in *Productivity of the ocean: Present and past*, edited by Berger, W., V. Smetacek and G. Wefer, pp. 377-394, John Wiley and Sons, Chichester, 1989.

Codispoti, L. A., J. A. Brandes, J. P. Christensen, A. H. Devol, S. W. A. Naqvi, H. W. Paerl, and T. Yoshinari, The oceanic fixed nitrogen and nitrous oxide budgets: Moving targets as we enter the anthropocene?, *Scientia Marina*, 65, 85-105, 2001.

Codispoti, L. A., T. Yoshinari, and A. H. Devol, Suboxic respiration in the oceanic water column. in *Respiration in Aquatic Ecosystems*, edited by del Giorgio, P. and P. J. LeB. Williams, pp. 328, Oxford University Press, Cambridge, UK, 2005.

Crosta, X., and A. Shemesh, Reconciling down core anticorrelation of diatom carbon and nitrogen isotopic ratios from the Southern Ocean, *Paleoceanography*, 17, 2002.

Crosta, X., A. Shemesh, J. Etourneau, R. Yam, I. Billy, and J. J. Pichon, Nutrient cycling in the Indian sector of the Southern Ocean over the last 50,000 years, *Global Biogeochemical Cycles*, 19, 10, 2005.

Deutsch, C., D. M. Sigman, R. C. Thunell, A. N. Meckler, and G. H. Haug, Isotopic constraints on glacial/interglacial changes in the oceanic nitrogen budget, *Global Biogeochemical Cycles*, 18, 2004.

Devol, A. H., and J. P. Christensen, Benthic Fluxes and Nitrogen Cycling in Sediments of the Continental-Margin of the Eastern North Pacific, *Journal of Marine Research*, 51, 345-372, 1993.

Emmer, E., and R. C. Thunell, Nitrogen isotope variations in Santa Barbara Basin sediments: Implications for denitrification in the eastern tropical North Pacific during the last 50,000 years, *Paleoceanography*, 15, 377-387, 2000.

Falkowski, P. G., Evolution of the nitrogen cycle and its influence on the biological sequestration of CO_2 in the ocean, *Nature*, 387, 272-275, 1997.

Farrell, J. W., T. F. Pedersen, S. E. Calvert, and B. Nielsen, Glacial-interglacial changes in nutrient utilization in the equatorial Pacific Ocean, *Nature*, 377, 514-517, 1995a.

Farrell, J. W., T. F. Pedersen, S. E. Calvert, and B. Nielsen, Glacial-Interglacial Changes in Nutrient Utilization in the Equatorial Pacific-Ocean, *Nature*, 377, 514-517, 1995b.

Francois, R., M. A. Altabet, E. F. Yu, D. M. Sigman, M. P. Bacon, M. Frank, G. Bohrmann, G. Bareille, and L. D. Labeyrie, Contribution of Southern Ocean surface-water stratification to low atmospheric CO_2 concentrations during the last glacial period, *Nature*, 389, 929-935, 1997.

Frank, M., R. Gersonde, M. R. van der Loeff, G. Bohrmann, C. C. Nurnberg, P. W. Kubik, M. Suter, and A. Mangini, Similar glacial and interglacial export bioproductivity in the Atlantic sector of the Southern Ocean: Multiproxy evidence and implications for glacial atmospheric CO_2, *Paleoceanography*, 15, 642-658, 2000.

Freudenthal, T., S. Neuer, H. Meggers, R. Davenport, and G. Wefer, Influence of lateral particle advection and organic matter degradation on sediment accumulation and stable nitrogen isotope ratios along a productivity gradient in the Canary Islands region, *Marine Geology*, 177, 93-109, 2001.

Galbraith, E. D., M. Kienast, T. F. Pedersen, and S. E. Calvert, Glacial-interglacial modulation of the marine nitrogen cycle by high-latitude O_2 supply to the global thermocline, *Paleoceanography*, 19, 2004.

Galloway, J. N., F. J. Dentener, D. G. Capone, E. W. Boyer, R. W. Howarth, S. P. Seitzinger, G. P. Asner, C. C. Cleveland, P. A. Green, E. A. Holland, D. M. Karl, A. F. Michaels, J. H. Porter, A. R. Townsend, and C. J. Vorosmarty, Nitrogen cycles: past, present, and future, *Biogeochemistry*, 70, 153-226, 2004.

Ganeshram, R. S., T. F. Pedersen, S. E. Calvert, G. W. McNeill, and M. R. Fontugne, Glacial-interglacial variability in denitrification in the world's oceans: Causes and consequences, *Paleoceanography*, 15, 361-376, 2000.

Ganeshram, R. S., T. F. Pedersen, S. E. Calvert, and J. W. Murray, Large changes in oceanic nutrient inventories from glacial to interglacial periods, *Nature*, 376, 755-758, 1995.

Granger, J., D. M. Sigman, J. A. Needoba, and P. J. Harrison, Coupled nitrogen and oxygen isotope fractionation of nitrate during assimilation by cultures of marine phytoplankton, *Limnology and Oceanography*, 49, 1763-1773, 2004.

Gruber, N., The dynamics of the marine nitrogen cycle and its influence on atmospheric CO_2 variations. in *Carbon-climate interactions*, edited by Follows, M. J. and T. Oguz, pp. 1-47, John Wiley & Sons, New York, 2004.

Gruber, N., Oceanography - A bigger nitrogen fix, *Nature*, 436, 786-787, 2005.

Hansell, D. A., N. R. Bates, and D. B. Olson, Excess nitrate and nitrogen fixation in the North Atlantic Ocean, *Marine Chemistry*, 84, 243-265, 2004.

Haug, G. H., D. M. Sigman, R. Tiedemann, T. F. Pedersen, and M. Sarnthein, Onset of permanent stratification in the subarctic Pacific Ocean, *Nature*, 401, 779-782, 1999.

Hay, W. W., and J. R. Southam, Modulation of marine sedimentation by the continental shelves. in *The Fate of Fossile Fuel CO_2 in the Oceans*, edited by Anderson, N. R. and A. Malahoff, pp. 569-604, Plenum, New York, 1977.

Hendy, I. L., T. F. Pedersen, J. P. Kennett, and R. Tada, Intermittent existence of a southern Californian upwelling cell during submillennial climate change of the last 60 kyr, *Paleoceanography*, 19, 2004.

Higginson, M. J., M. A. Altabet, D. W. Murray, R. W. Murray, and T. D. Herbert, Geochemical evidence for abrupt changes in relative strength of the Arabian monsoons during a stadial/interstadial climate transition, *Geochimica Et Cosmochimica Acta*, 68, 3807-3826, 2004.

Higginson, M. J., J. R. Maxwell, and M. A. Altabet, Nitrogen isotope and chlorin paleoproductivity records from the Northern South China Sea: remote vs. local forcing of millennial- and orbital-scale variability, *Marine Geology*, 201, 223-250, 2003.

Holmes, M. E., P. J. Muller, R. R. Schneider, M. Segl, J. Patzold, and G. Wefer, Stable nitrogen isotopes in Angola Basin surface sediments, *Marine Geology*, 134, 1-12, 1996.

Ivanochko, T. S., R. S. Ganeshram, G. A. Brummer, G. Ganssen, S. A. Jung, S. G. Moreton, and D. Kroon, Variations in tropical convection as an amplifier of global climate change at the millennial scale, *Earth and Planetary Science Letters*, 235, 302-314, 2005.

Jaccard, S. L., G. H. Haug, D. M. Sigman, T. F. Pedersen, H. R. Thierstein, and U. Rohl, Glacial/interglacial changes in subarctic North Pacific stratification, *Science*, 308, 1003-1006, 2005.

Karl, D., R. Letelier, L. Tupas, J. Dore, J. Christian, and D. Hebel, The role of nitrogen fixation in biogeochemical cycling in the subtropical North Pacific Ocean, *Nature*, 388, 533-538, 1997.

Karl, D., A. Michaels, B. Bergman, D. Capone, E. Carpenter, R. Letelier, F. Lipschultz, H. Paerl, D. Sigman, and L. Stal, Dinitrogen fixation in the world's oceans, *Biogeochemistry*, 57/58, 47-98, 2002.

Keigwin, L. D., G. A. Jones, and P. N. Froelich, A 15,000 Year Paleoenvironmental Record from Meiji Seamount, Far Northwestern Pacific, *Earth and Planetary Science Letters*, 111, 425-440, 1992.

Kienast, M., Unchanged nitrogen isotopic composition of organic matter in the South China Sea during the last climatic cycle: Global implications, *Paleoceanography*, 15, 244-253, 2000.

Kienast, M., On the sedimentological origin of down-core variations of bulk sedimentary nitrogen isotope ratios, *Paleoceanography*, 20, 2005.

Kienast, S. S., S. E. Calvert, and T. F. Pedersen, Nitrogen isotope and productivity variations along the northeast Pacific margin over the last 120 kyr: Surface and subsurface paleoceanography, *Paleoceanography*, 17, art. no.-1055, 2002.

Kienast, S. S., l. L. Hendy, J. Crusius, T. F. Pedersen, and S. E. Calvert, Export production in the subarctic North Pacific over the last 800 kyrs: No evidence for iron fertilization?, *Journal of Oceanography*, 60, 189-203, 2004.

Knapp, A. N., D. M. Sigman, and F. Lipschultz, N isotopic composition of dissolved organic nitrogen and nitrate at the Bermuda Atlantic time-series study site, *Global Biogeochemical Cycles*, 19, 2005.

Knox, F., and M. B. McElroy, Changes in Atmospheric CO_2 - Influence of the Marine Biota at High-Latitude, *Journal of Geophysical Research-Atmospheres*, 89, 4629-4637, 1984.

Kohfeld, K. E., C. Le Quere, S. P. Harrison, and R. F. Anderson, Role of marine biology in glacial-interglacial CO_2 cycles, *Science*, 308, 74-78, 2005.

Kumar, N., R. F. Anderson, R. A. Mortlock, P. N. Froelich, P. Kubik, B. Dittrichhannen, and M. Suter, Increased Biological Productivity and Export Production in the Glacial Southern-Ocean, *Nature*, 378, 675-680, 1995.

Ledgard, S. F., K. C. Woo, and F. J. Bergersen, Isotopic Fractionation During Reduction of Nitrate and Nitrite by Extracts of Spinach Leaves, *Australian Journal of Plant Physiology*, 12, 631-640, 1985.

Lefevre, N., and A. J. Watson, Modeling the geochemical cycle of iron in the oceans and its impact on atmospheric CO_2 concentrations, *Global Biogeochemical Cycles*, 13, 727-736, 1999.

Lehmann, M. F., D. M. Sigman, and W. M. Berelson, Coupling the $^{15}N/^{14}N$ and $^{18}O/^{16}O$ of nitrate as a constraint on benthic nitrogen cycling, *Marine Chemistry*, 88, 1-20, 2004.

Lipschultz, F., S. C. Wofsy, B. B. Ward, L. A. Codispoti, G. Friedrich, and J. W. Elkins, Bacterial Transformations of Inorganic Nitrogen in the Oxygen-Deficient Waters of the Eastern Tropical South-Pacific Ocean, *Deep-Sea Research Part a-Oceanographic Research Papers*, 37, 1513-&, 1990.

Liu, K.-K., and I. R. Kaplan, The eastern tropical Pacific as a source of ^{15}N-enriched nitrate in seawater off southern California, *Limnology and Oceanography*, 34, 820-830, 1989.

Liu, K. K., M. J. Su, C. R. Hsueh, and G. C. Gong, The nitrogen isotopic composition of nitrate in the Kuroshio Water northeast of Taiwan: Evidence for nitrogen fixation as a source of isotopically light nitrate, *Marine Chemistry*, 54, 273-292, 1996.

Liu, Z., M. Altabet, and T. Herbert, Glacial-interglacial modulation of eastern tropical North Pacific denitrification over the last 1.8-Myr, *Geophysical Research Letters*, 32, 10.1029/2005GL024439, 2005.

Loubere, P., A multiproxy reconstruction of biological productivity and oceanography in the eastern equatorial Pacific for the past 30,000 years, *Marine Micropaleontology*, 37, 173-198, 1999.

Loubere, P., F. Mekik, R. Francois, and S. Pichat, Export fluxes of calcite in the eastern equatorial Pacific from the Last Glacial Maximum to present, *Paleoceanography*, 19, 2004.

Lourey, M. J., T. W. Trull, and D. M. Sigman, Sensitivity of delta N-15 of nitrate, surface suspended and deep sinking particulate nitrogen to seasonal nitrate depletion in the Southern Ocean, *Global Biogeochemical Cycles*, 17, 2003.

Marcantonio, F., R. F. Anderson, S. Higgins, M. Stute, P. Schlosser, and P. Kubik, Sediment focusing in the central equatorial Pacific Ocean, *Paleoceanography*, 16, 260-267, 2001.

Mariotti, A., J. C. Germon, P. Hubert, P. Kaiser, R. Letolle, A. Tardieux, and P. Tardieux, Experimental-Determination of Nitrogen Kinetic Isotope Fractionation - Some Principles - Illustration for the Denitrification and Nitrification Processes, *Plant and Soil*, 62, 413-430, 1981.

Martin, J. H., and S. E. Fitzwater, Iron-Deficiency Limits Phytoplankton Growth in the Northeast Pacific Subarctic, *Nature*, 331, 341-343, 1988.

McKay, J. L., T. F. Pedersen, and S. S. Kienast, Organic carbon accumulation over the last 16 kyr off Vancouver Island, Canada: evidence for increased marine productivity during the deglacial, *Quaternary Science Reviews*, 23, 261-281, 2004.

Middelburg, J. J., K. Soetaert, P. M. J. Herman, and C. H. R. Heip, Denitrification in marine sediments: A model study, *Global Biogeochemical Cycles*, 10, 661-673, 1996.

Mortlock, R. A., C. D. Charles, P. N. Froelich, M. A. Zibello, J. Saltzman, J. D. Hays, and L. H. Burckle, Evidence for Lower Productivity in the Antarctic Ocean During the Last Glaciation, *Nature*, 351, 220-223, 1991.

Nakanishi, T., and M. Minagawa, Stable carbon and nitrogen isotopic compositions of sinking particles in the northeast Japan Sea, *Geochemical Journal*, 37, 261-275, 2003.

Nameroff, T. J., S. E. Calvert, and J. W. Murray, Glacial-interglacial variability in the eastern tropical North Pacific oxygen minimum zone recorded by redox-sensitive trace metals, *Paleoceanography*, 19, 2004.

Naqvi, S. W. A., Geographical extent of denitrification in the Arabian Sea in relation to some physical processes, *Oceanologica Acta*, 14, 281-290, 1991.

Narita, H., M. Sato, S. Tsunogai, M. Murayama, M. Ikehara, T. Nakatsuka, M. Wakatsuchi, N. Harada, and Y. Ujiie, Biogenic opal indicating less productive northwestern North Pacific during the glacial ages, *Geophysical Research Letters*, 29, 2002.

Needoba, J. A., and P. J. Harrison, Influence of low light and a light: Dark cycle on NO_3^- uptake, intracellular NO_3^-, and nitrogen isotope fractionation by marine phytoplankton, *Journal of Phycology*, 40, 505-516, 2004.

Needoba, J. A., D. M. Sigman, and P. J. Harrison, The mechanism of isotope fractionation during algal nitrate assimilation as illuminated by the $^{15}N/^{14}N$ of intracellular nitrate, *Journal of Phycology*, 40, 517-522, 2004.

Needoba, J. A., N. A. Waser, P. J. Harrison, and S. E. Calvert, Nitrogen isotope fractionation in 12 species of marine phytoplankton during growth on nitrate, *Marine Ecology-Progress Series*, 255, 81-91, 2003.

Ohkushi, K., T. Itaki, and N. Nemoto, Last Glacial-Holocene change in intermediate-water ventilation in the Northwestern Pacific, *Quaternary Science Reviews*, 22, 1477-1484, 2003.

Olson, D. B., G. L. Hitchcock, R. A. Fine, and B. A. Warren, Maintenance of the Low-Oxygen Layer in the Central Arabian Sea, *Deep-Sea Research Part Ii-Topical Studies in Oceanography*, 40, 673-685, 1993.

Parekh, P., M. J. Follows, and E. Boyle, Modeling the global ocean iron cycle, *Global Biogeochemical Cycles*, 18, 2004.

Paytan, A., and M. Kastner, Benthic Ba fluxes in the central Equatorial Pacific, implications for the oceanic Ba cycle, *Earth and Planetary Science Letters*, 142, 439-450, 1996.

Pedersen, T. F., Increased Productivity in the Eastern Equatorial Pacific During the Last Glacial Maximum (19,000 to 14,000 Yr Bp), *Geology*, 11, 16-19, 1983.

Peters, K. E., R. E. Sweeney, and I. R. Kaplan, Correlation of carbon and nitrogen stable isotope ratios in sedimentary organic matter, *Limnology and Oceanography*, 23, 598-604, 1978.

Petit, J. R., J. Jouzel, D. Raynaud, N. I. Barkov, J. M. Barnola, I. Basile, M. Bender, J. Chappellaz, M. Davis, G. Delaygue, M. Delmotte, V. M. Kotlyakov, M. Legrand, V. Y. Lipenkov, C. Lorius, L. Pepin, C. Ritz, E. Saltzman, and M. Stievenard, Climate and atmospheric history of the past 420,000 years from the Vostok ice core, Antarctica, *Nature*, 399, 429-436, 1999.

Pride, C., R. Thunell, D. Sigman, L. Keigwin, M. Altabet, and E. Tappa, Nitrogen isotopic variations in the Gulf of California since the last deglaciation: Response to global climate change, *Paleoceanography*, 14, 397-409, 1999.

Redfield, A. C., On the proportions of organic derivatives in sea water and their relation to the composition of plankton. in *James Johnstone Memorial Volume*, pp. 176-192, University of Liverpool, Liverpool, 1934.

Redfield, A. C., B. H. Ketchum, and F. A. Richards, The influence of organisms on the composition of sea-water. in *The Sea*, edited by Hill, M. N., pp. 26-77, John Wiley & Sons, New York, 1963.

Robinson, R. S., B. G. Brunelle, and D. M. Sigman, Revisiting nutrient utilization in the glacial Antarctic: Evidence from a new method for diatom-bound N isotopic analysis, *Paleoceanography*, 19, 2004.

Robinson, R. S., D. M. Sigman, P. J. DiFiore, M. M. Rohde, T. A. Mashiotta, and D. W. Lea, Diatom-bound $^{15}N/^{14}N$: New support for enhanced nutrient consumption in the ice age subantarctic, *Paleoceanography*, 20, 2005.

Sachs, J. P., and D. J. Repeta, Oligotrophy and nitrogen fixation during eastern Mediterranean sapropel events, *Science*, 286, 2485-2488, 1999.

Saino, T., and A. Hattori, Geographical variation of the water column distribution of suspended particulate organic nitrogen and its ^{15}N natural abundance in the Pacific and its marginal seas, *Deep-Sea Research*, 34, 807-827, 1987.

Sarma, V., An evaluation of physical and biogeochemical processes regulating perennial suboxic conditions in the water column of the Arabian Sea, *Global Biogeochemical Cycles*, 16, art. no.-1082, 2002.

Sarmiento, J. L., and J. R. Toggweiler, A New Model for the Role of the Oceans in Determining Atmospheric pCO_2, *Nature*, 308, 621-624, 1984.

Schafer, P., and V. Ittekkot, Seasonal Variability of $\delta^{15}N$ in Settling Particles in the Arabian Sea and Its Palaeogeochemical Significance, *Naturwissenschaften*, 80, 511-513, 1993.

Schubert, C. J., and S. E. Calvert, Nitrogen and carbon isotopic composition of marine and terrestrial organic matter in Arctic Ocean sediments: implications for nutrient utilization and organic matter composition, *Deep-Sea Research Part I-Oceanographic Research Papers*, 48, 789-810, 2001.

Shemesh, A., S. A. Macko, C. D. Charles, and G. H. Rau, Isotopic Evidence for Reduced Productivity in the Glacial Southern-Ocean, *Science*, 262, 407-410, 1993.

Siegenthaler, U., and T. Wenk, Rapid Atmospheric CO_2 Variations and Ocean Circulation, *Nature*, 308, 624-626, 1984.

Sigman, D. M., M. A. Altabet, R. Francois, D. C. McCorkle, and J.-F. Gaillard, The isotopic composition of diatom-bound nitrogen in Southern Ocean sediments, *Paleoceanography*, 14, 118-134, 1999a.

Sigman, D. M., M. A. Altabet, D. C. McCorkle, R. Francois, and G. Fischer, The $\delta^{15}N$ of nitrate in the Southern Ocean: Consumption of nitrate in surface waters, *Global Biogeochemical Cycles*, 13, 1149-1166, 1999b.

Sigman, D. M., M. A. Altabet, D. C. McCorkle, R. Francois, and G. Fischer, The $\delta^{15}N$ of nitrate in the Southern Ocean: Nitrogen cycling and circulation in the ocean interior, *Journal of Geophysical Research-Oceans*, 105, 19599-19614, 2000.

Sigman, D. M., and E. A. Boyle, Glacial/interglacial variations in atmospheric carbon dioxide, *Nature*, 407, 859-869, 2000.

Sigman, D. M., and K. L. Casciotti, Nitrogen isotopes in the ocean. in *Encyclopedia of Ocean Sciences*, edited by Steele, J. H., K. K. Turekian and S. A. Thorpe, pp. 2249, Academic Press, London, 2001.

Sigman, D. M., K. L. Casciotti, M. Andreani, C. Barford, M. Galanter, and J. K. Bohlke, A bacterial method for the nitrogen isotopic analysis of nitrate in seawater and freshwater, *Analytical Chemistry*, 73, 4145-4153, 2001.

Sigman, D. M., and G. H. Haug, The Biological Pump in the Past. in *Treatise on Geochemistry*, edited by Holland, D. and K. K. Turekian, pp. 491-528, Elsevier, Amsterdam, 2003.

Sigman, D. M., S. L. Jaccard, and G. H. Haug, Polar ocean stratification in a cold climate, *Nature*, 428, 59-63, 2004.

Sigman, D. M., R. Robinson, A. N. Knapp, A. van Geen, D. C. McCorkle, J. A. Brandes, and R. C. Thunell, Distinguishing between water column and sedimentary denitrification in the Santa Barbara Basin using the stable isotopes of nitrate, *Geochemistry Geophysics Geosystems*, 4, art. no.-1040, 2003.

Struck, U., K. C. Emeis, M. Voss, M. D. Krom, and G. H. Rau, Biological productivity during sapropel S5 formation in the Eastern Mediterranean Sea: Evidence from stable isotopes of nitrogen and carbon, *Geochimica Et Cosmochimica Acta*, 65, 3249-3266, 2001.

Suthhof, A., V. Ittekkot, and B. Gaye-Haake, Millennial-scale oscillation of denitrification intensity in the Arabian Sea during the late Quaternary and its potential influence on atmospheric N_2O and global climate, *Global Biogeochemical Cycles*, 15, 637-649, 2001.

Thunell, R. C., and A. B. Kepple, Glacial-holocene $\delta^{15}N$ record from the Gulf of Tehuantepec, Mexico: Implications for denitrification in the eastern equatorial Pacific and changes in atmospheric N_2O, *Global Biogeochemical Cycles*, 18, 2004.

Thunell, R. C., D. M. Sigman, F. Muller-Karger, Y. Astor, and R. Varela, Nitrogen isotope dynamics of the Cariaco Basin, Venezuela, *Global Biogeochemical Cycles*, 18, 2004.

Toggweiler, J. R., Variation of atmospheric CO_2 by ventilation of the ocean's deepest water, *Paleoceanography*, 14, 571-588, 1999.

Tyrrell, T., The relative influences of nitrogen and phosphorus on oceanic primary production, *Nature*, 400, 525-531, 1999.

van Geen, A., Y. Zheng, J. M. Bernhard, K. G. Cannariato, J. Carriquiry, W. E. Dean, B. W. Eakins, J. D. Ortiz, and J. Pike, On the preservation of laminated sediments along the western margin of North America, *Paleoceanography*, 18, 2003.

Voss, M., J. W. Dippner, and J. P. Montoya, Nitrogen isotope patterns in the oxygen-deficient waters of the Eastern Tropical North Pacific Ocean, *Deep-Sea Research Part I-Oceanographic Research Papers*, 48, 1905-1921, 2001.

Wada, E., and A. Hattori, Nitrogen isotope effects in the assimilation of inorganic nitrogenous compounds by marine diatoms, *Geomicrobiology Journal*, 1, 85-101, 1978.

Waser, N. A. D., P. J. Harrison, B. Nielsen, and S. E. Calvert, Nitrogen isotope fractionation during the uptake and assimilation of nitrate, nitrite, ammonium and urea by a marine diatom, *Limnology and Oceanography*, 43, 215-224, 1998.

Wu, J. P., S. E. Calvert, C. S. Wong, and F. A. Whitney, Carbon and nitrogen isotopic composition of sedimenting particulate material at Station Papa in the subarctic northeast Pacific, *Deep-Sea Research Part Ii-Topical Studies in Oceanography*, 46, 2793-2832, 1999.

Chapter II

Contrasting but complementary information recorded by $\delta^{15}N$ of diatom frustules and $\delta^{15}N$ of bulk sediment in the Guaymas Basin

2.1 Introduction

Many studies of past changes in nutrient cycling rely heavily on sedimentary records of stable N isotope ratios (e.g. [*Calvert et al.*, 1992; *Altabet et al.*, 1995; *Ganeshram et al.*, 1995; *Francois et al.*, 1997]). The most common sedimentary N isotope measurement, $\delta^{15}N_{bulk}$, is made simply by placing dried, ground sediment in a high temperature furnace and measuring the isotopic composition of N in the combustion products. This convenient and economical method is very useful for sediments in which the N present is dominantly in marine organic matter, transferred from the upper water column to the sediment with little or no alteration. However, there is some concern that additional nitrogenous constituents, such as terrestrial organic N or clay-bound N, may contribute significantly to $\delta^{15}N_{bulk}$ in some areas (e.g. [*Peters et al.*, 1978; *Schubert and Calvert*, 2001; *McKay et al.*, 2004; *Kienast*, 2005]) and, if so, might obfuscate the marine N signal. In addition, diagenetic alteration of the N isotopic composition of marine organic matter during sinking and burial has a significant impact on $\delta^{15}N_{bulk}$ in slowly accumulating, deep-sea sediments [*Altabet and Francois*, 1994; *Nakanishi and Minagawa*, 2003]. This has impeded the interpretation of $\delta^{15}N_{bulk}$ records from most of the open ocean floor, limiting application of this proxy to continental margin deposits where diagenesis is minor and downcore profiles of $\delta^{15}N_{bulk}$ can be more easily interpreted [*Altabet et al.*, 1999]. In response to such limitations, extractable, distinct marine sedimentary N components have been sought. One such component is the N bound within fossil diatoms.

Diatoms are photosynthetic protists, responsible for approximately 40 % of global marine primary productivity [*Falciatore and Bowler*, 2002]. All diatoms construct ornate silicified cell walls (frustules) that serve variously and debatably as ultraviolet filters, armour against grazing, ballast, or as proton buffers to aid carbon acquisition [*Milligan and Morel*, 2002]. Frustules are formed by rapid polymerization of silica immediately following mitosis, in as little as ten minutes [*Hazelaar et al.*, 2005]. The growth of silica nanospheres, each 10-100 nm in diameter [*Crawford et al.*, 2001] (Appendix A1.3), is directed by polycationic polypeptides and long-chain polyamines, which have been characterized following isolation from the frustules of cultured diatoms [*Kroger et al.*, 1999; *Kroger et al.*, 2000; *Sumper*, 2002]. As the solid silica lattice forms, it consumes these N-rich organic molecules, and they become intrinsically bound within the frustule. As such, the frustule-bound amino acids are extremely well protected after cell death, both from bacterial degradation and from chemical attack in laboratories thousands of years later [*Ingalls et al.*, 2003].

The extraction and measurement of the isotopic composition of frustule-bound N (here $\delta^{15}N_{frustule}$) was pioneered by *Shemesh et al.* [1993]. It has been used primarily in high-latitude sediment records in order to infer changes in past physical and ecological conditions in the upper water column over glacial-interglacial cycles (e.g. [*Sigman et al.*, 1999; *Crosta and Shemesh*, 2002; *Robinson et al.*, 2004; *Crosta et al.*, 2005; *Robinson et al.*, 2005; *Schneider-Mor et al.*, 2005]). Often, $\delta^{15}N_{frustule}$ data are interpreted as faithful recordings of surface $\delta^{15}N_{nitrate}$, itself dominantly a function of relative nitrate utilization, denitrification and N_2 fixation (Chapter 1). However, questions remain regarding the isotopic relationship between $\delta^{15}N_{frustule}$, the diatom biomass (here $\delta^{15}N_{diatom}$), and the substrate N on which the diatom community grew (here $\delta^{15}N_{nitrate}$); these cloud interpretations. The N analyzed in diatom frustules is <1 % of the total diatom biomass N and, given the large N isotopic contrasts between internal cellular pools of diatoms [*Needoba et al.*, 2004] and different amino acids in general [*Macko et al.*, 1987], $\delta^{15}N_{frustule}$ is not necessarily strictly correlated to $\delta^{15}N_{diatom}$. Conceivably, $\delta^{15}N_{frustule}$ could equal $\delta^{15}N_{diatom}$, be consistently offset from $\delta^{15}N_{diatom}$, or be offset from $\delta^{15}N_{diatom}$ by a variable amount.

This study presents sedimentary data from the unique diatom-rich, laminated deposits of the Guaymas Basin in order to provide insight into these relationships. The Guaymas Basin has been shown to have minimal diagenetic alteration of sinking marine N, and hence

$\delta^{15}N_{bulk}$ is essentially equal to $\delta^{15}N_{nitrate}$ [*Pride et al.*, 1999; *Thunell and Kepple*, 2004]. Diatoms are an abundant component of the Guaymas Basin sediments, and vary in abundance annually, providing a seasonally resolved record. As shown below, this combination of features allows the identification of surprisingly large and variable offsets between $\delta^{15}N_{bulk}$ and $\delta^{15}N_{frustule}$. In some cases these offsets are related to changes in diatom provenance, but they also show that $\delta^{15}N_{frustule}$ records a greater degree of seasonal variation than the $\delta^{15}N_{bulk}$.

2.2 Setting

Sediments of the Guaymas Basin accumulate rapidly and the core top $\delta^{15}N_{bulk}$ is indistinguishable from subeuphotic zone nitrate and sinking particulate N [*Pride et al.*, 1999; *Thunell and Kepple*, 2004]. Subeuphotic zone nitrate in the region today has $\delta^{15}N$ of 10 – 11 ‰ [*Pride et al.*, 1999], elevated well above the global mean of ~5 ‰ by denitrification in the water column of the ETNP [*Cline and Kaplan*, 1975; *Liu and Kaplan*, 1989; *Sigman et al.*, 2003]. The sediments are laminated [*Calvert*, 1964], with alternating opal-rich (~60 % opal) and clay-rich intervals (~30 % opal) and excellent preservation of diatoms, making it a globally significant sink of Si [*Calvert*, 1966].

It is generally thought that opal-rich layers form during fall and winter, when the onset of strong northerlies breaks down stratification, causing a "dump" of the summer diatom growth [*Kemp et al.*, 2000] and, subsequently, upwelling with variably nutrient-rich conditions [*Thunell et al.*, 1993; *Sancetta*, 1995]. The episodic nature of diatom deposition was illustrated by a 6-year sediment trap study that showed an order-of-magnitude increase in opal sinking flux during winter [*Thunell*, 1998]. Nitrogen isotopic measurements of the bulk organic matter collected in the sediment trap study showed a strong anti-correlation to the opal concentration, with $\delta^{15}N$ up to 11.6 ‰ in opal-poor samples and as low as 6.6 ‰ in opal-rich samples. The dark, opal-poor layers are attributed to summer, when diatom sinking-flux is low and aeolian input is accelerated by vigorous convective transport of particles from the Sonora desert [*Baumgartner et al.*, 1991]. As such, one couplet of light and dark sediment (a varve) represents an annual cycle [*Pike and Kemp*, 1997; *Thunell*, 1998]. The visually distinct layers are referred to here simply as D (diatom-rich) and C (Clay-rich). The very low oxygen content of bottom waters at the core depth, within the Pacific Intermediate Water

mass, impeded the activity of macrobenthos within this sediment interval [*van Geen et al.*, 2003], encouraging the preservation of laminae.

Barron et al. [2005] presented a detailed history of diatom species abundances in core JPC-56 (27.5 °N, 112.1 °W, water depth 818 m), very near to our study site. They describe the early Holocene, when the sediments studied here were deposited, as a period of cool and windy conditions with few coccolithophorids or tropical diatoms. They also observed large and highly variable quantities of the shelf-dwelling *Actinoptychus* spp., composing 10 to 70% of the total diatom assemblage, which they interpreted as representing downslope transport by summer storms.

2.3 Methods

Sediment samples were collected from GLC-1 (Guaymas Layer Cake 1), a small block extracted across the sub-bottom depth range 505-512 cm from giant box core MD02-2517SC, which was raised on the western slope of Guaymas Basin (27.4850 °N, 112.0743 °W, 888.5 m water depth) in 2002. This depth range contains sediments of early Holocene age (~ 9 ka, estimated by comparison to MD02-2515, raised from the same site [*Cheshire et al.*, 2005]). The block contains 43 couplets, thought to represent 43 years of sedimentation. The block was dried gently in an oven, and clay-rich layers were separated from diatom-rich layers with a stainless-steel razor blade. Two diatom-rich samples were extracted from single layers (1D1 and 1D2), while the others represent integrations of multiple diatom-rich layers (see Fig 2.1). Cross-sections of the entire block (1X1) as well as smaller sections (1X2 and 1X3) were also included, in order to provide integrated, multi-annual isotopic values.

All samples were freeze-dried and thoroughly stirred with a metal spatula, in order to ensure homogenization. A portion of each stirred sample was ground in an agate mortar and the opal content measured by dissolution with a strong base followed by colorimetric analysis [*Mortlock and Froelich*, 1989]. Total C and N was determined by flash combustion-GC analysis using a Fisons NA-1500 elemental analyser, and $\delta^{15}N_{bulk}$ was measured by combustion EA-IRMS as described by Ganeshram et al. [2000]. An unground portion was floated in Sodium Polytungstate at density 2.15 g cm^{-3} to remove lithogenic material (See Appendix 1 for a more detailed description), and the diatom fraction was cleaned following Robinson et al. [2005] with slight modification. This involved a dithionite-citric acid reductive cleaning

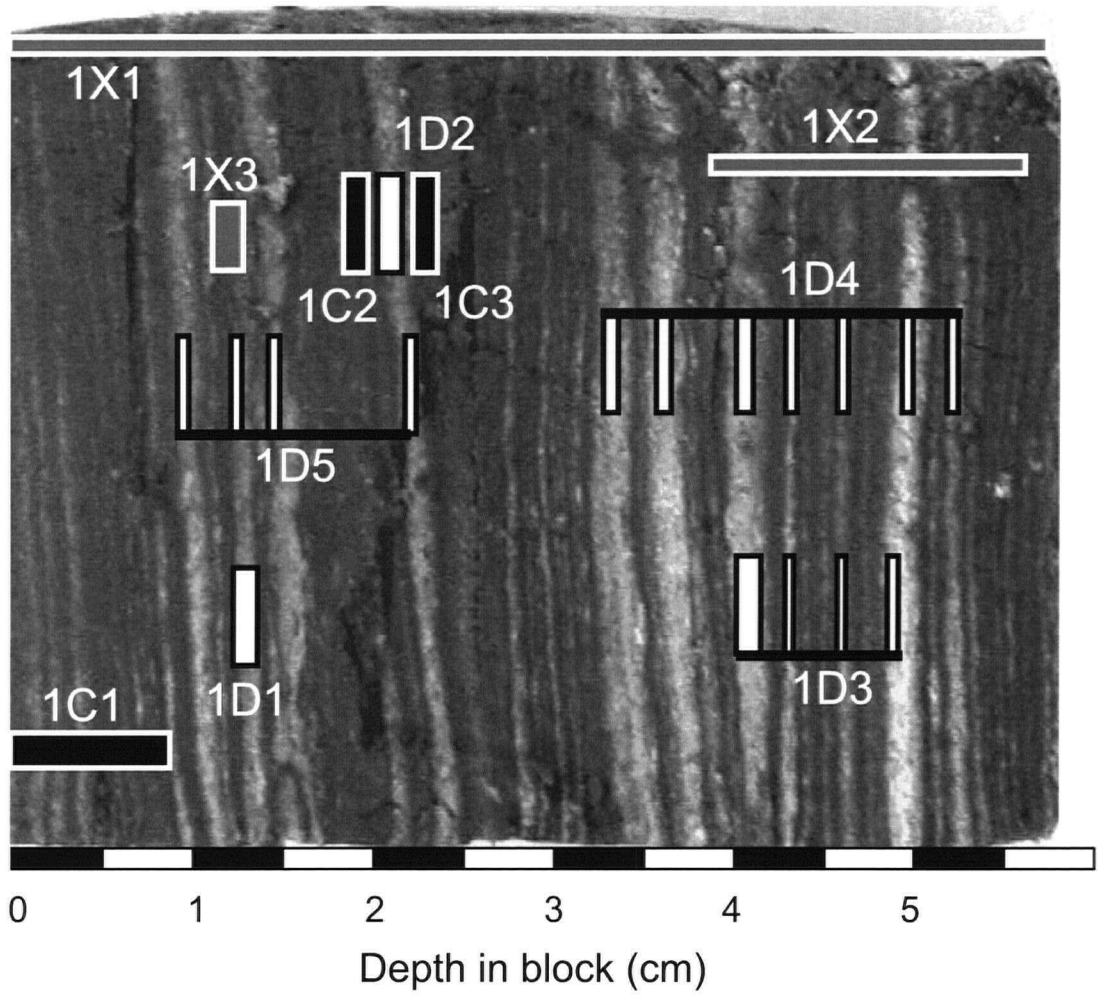

2.1: Photograph of Guyamas Layer Cake (1) showing sample locations. Pale layers are diatom-rich, and samples extracted from those layers are referred to as "D" samples. Samples extracted from dark, clay-rich layers are referred to as "C" samples. Samples that included both C and D layers are labeled "X". Sample depths used in the plots that follow correspond to the intersection of the laminae sampled with the lower side of the block, e.g. sample 1D5 spans 1.1 to 2.5 cm depth in block.

step followed by a single treatment with 30 % H_2O_2 and then a chemical oxidation with 70 % $HClO_4$ at 100 °C. N content and $\delta^{15}N_{frustule}$ were determined by the "persulphate-denitrifier" (here PD) method as described by Robinson et al. [2004]. This involved heating the sample in a solution of potassium persulfate and 1.5 N NaOH, to dissolve the opal and oxidize the liberated organic N to nitrate. Nitrate concentration was then determined by chemiluminescence [*Braman and Hendrix*, 1989] and the N isotopic composition of the nitrate was measured via the "denitrifier" method [*Sigman et al.*, 2001].

Diatom frustules were counted on random traverses across smear slides, using a light microscope. Fragments were counted as fractions of frustules.

2.4 Geochemical observations

The opal concentrations vary as expected, from ~ 60 % in D layers to ~ 36 % in C layers (Figure 2.2). The total N content of the samples follows the inverse pattern, with almost twice as much N in the C layers as in the D layers, by weight. Much of this variability simply reflects the dilution of organic matter by opal. Considering that C layers are also likely to have a higher density than D layers, the C layers contribute a significantly greater fraction to the bulk N than do the D layers.

The $\delta^{15}N_{bulk}$ measurements are shown in Figure 2.3. The $\delta^{15}N_{bulk}$ of the block X-section is 10.7 ‰, identical within measurement error to other X and C samples, and identical to the subsurface $\delta^{15}N_{nitrate}$ of the region today. The D layers all have significantly lower $\delta^{15}N_{bulk}$, particularly those from 1.0 - 2.5 cm, in which the average $\delta^{15}N_{bulk}$ is ~ 9.7 ‰. This anti-correlation of $\delta^{15}N$ and opal is consistent with the multi-year sediment trap data of *Pride et al.* [1999] who showed that sinking particulate nitrogen has an average $\delta^{15}N$ of ~ 10.5 ‰ during modern diatom-poor summers, and ~ 8.5 ‰ during the diatom-rich winters. The consecutive C-D-C samples from 2.2 - 2.6 cm show that the $\delta^{15}N_{bulk}$ varies on a millimetre scale, with near-average values in the C layers, but ~ 1 ‰ lower in the D layer. However, the changes in $\delta^{15}N_{bulk}$ in GLC-1 are smaller than the range observed in sediment traps, and all measurements fall within a total range of 2 ‰.

The $\delta^{15}N_{frustule}$ values, in contrast, span a range of 13 ‰ (Figure 2.4). The $\delta^{15}N_{frustule}$ in D layers is 1 to 6.5 ‰ lower than the corresponding $\delta^{15}N_{bulk}$, while the $\delta^{15}N_{frustule}$ in C layers is 2 to 5 ‰ higher than the corresponding $\delta^{15}N_{bulk}$. The sequential C-D-C samples from

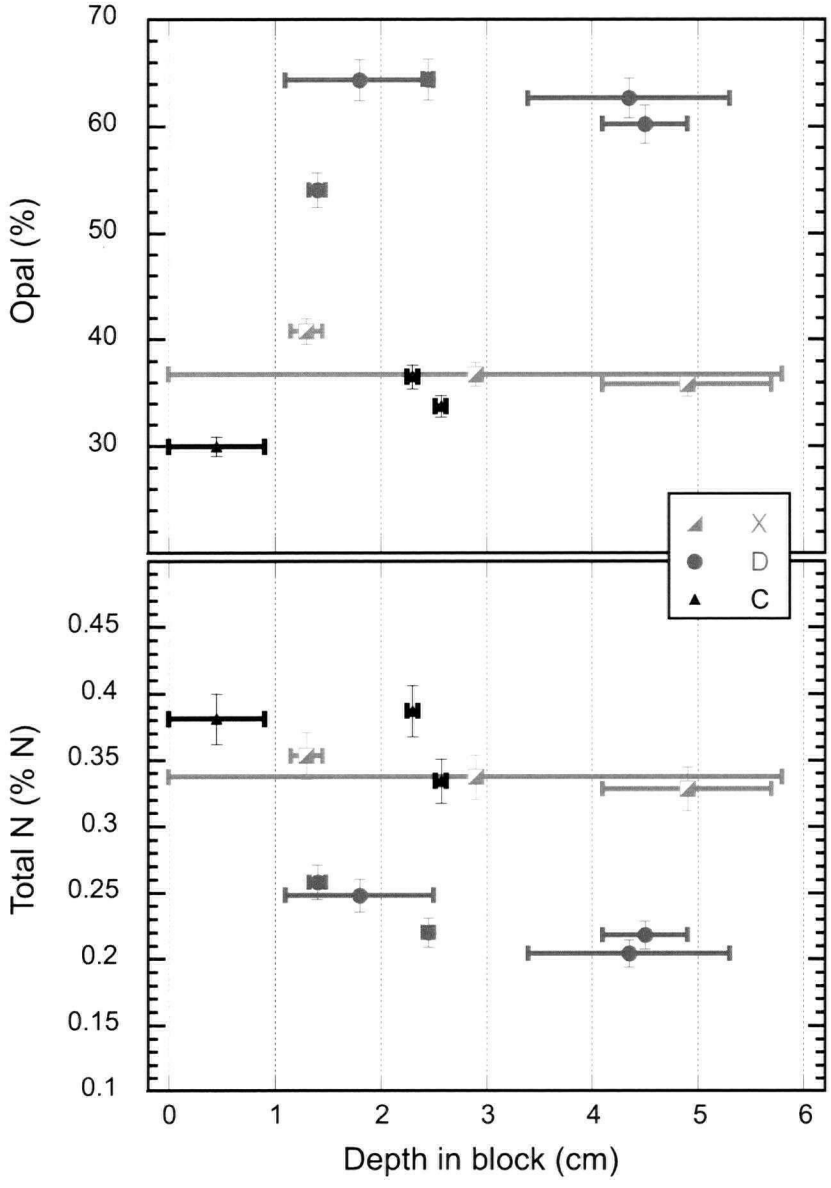

2.2: Bulk geochemistry of GLC-1 samples. The horizontal axis indicates the depth in the GLC block corresponding to the samples; horizontal whiskers indicate the depth range over which each sample was taken (see Figure 2.1). The weight % opal and N concentrations are shown on the vertical axes. Note the average block composition is represented by the 'X' sample that spans the full depth range.

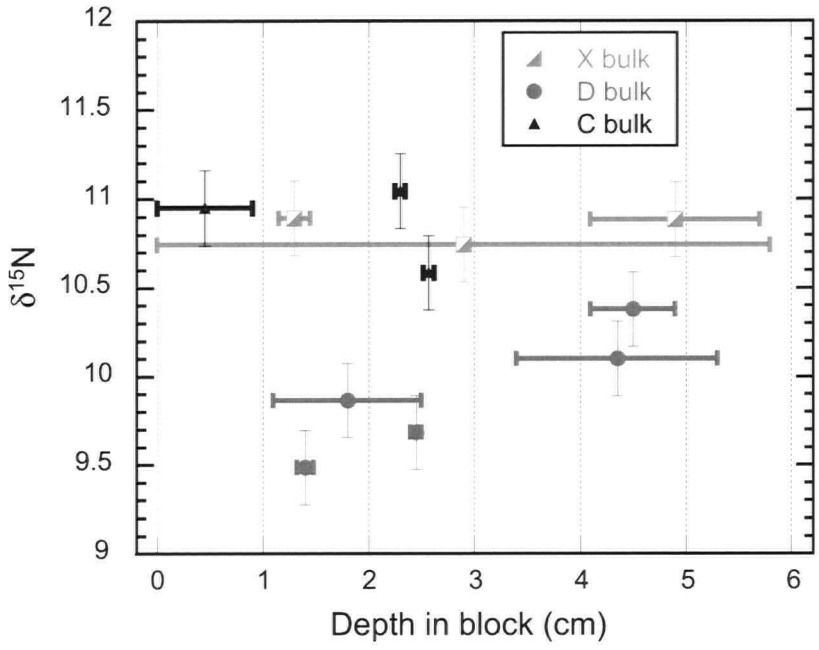

2.3: $\delta^{15}N_{bulk}$ measurements of GLC-1 samples. See Figure 2.2 for explanation of plot.

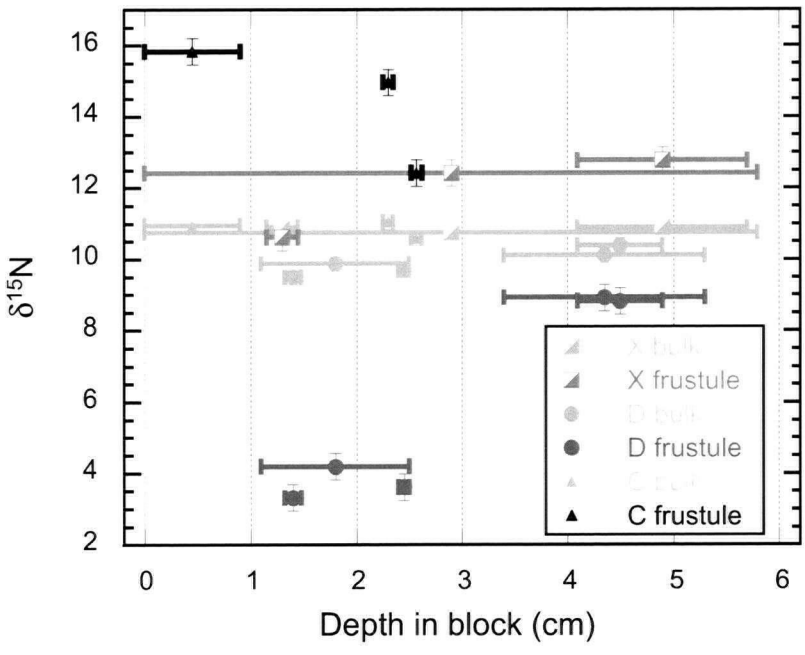

2.4: Comparison of $\delta^{15}N_{bulk}$ and $\delta^{15}N_{frustule}$ for GLC-1 samples. Pale grey symbols show $\delta^{15}N_{bulk}$, colour symbols show $\delta^{15}N_{frustule}$. See Figure 2.2 for explanation of plot.

2.2 - 2.6 cm have $\delta^{15}N_{frustule}$ values of 15 ‰, 3.5 ‰ and 12.5 ‰, respectively, a remarkable variation. Furthermore, the changes measured in the bulk sediment can be accounted for almost entirely by the contribution of extreme changes in the $\delta^{15}N_{frustule}$. Assuming that

$$\delta^{15}N_{bulk} * N_{bulk} = \delta^{15}N_{frustule} * N_{frustule} + \delta^{15}N_{non\text{-}frustule} * (N_{bulk} - N_{frustule}) \quad (2.1)$$

and that

$$N_{frustule} = N_{frustule}(\text{separated sample}) * \text{opal wt\%}, \quad (2.2)$$

the $\delta^{15}N_{non\text{-}frustule}$ can be calculated for all samples, as shown in Figure 2.5. The average $\delta^{15}N_{non\text{-}frustule}$ is 10.55 ‰, with a standard deviation (1σ) of 0.33 ‰ for all samples, which falls within the calculated measurement error of 0.5 ‰ (1σ). This is very close to the block average $\delta^{15}N_{bulk}$ of 10.73‰. Although the $\delta^{15}N_{non\text{-}frustule}$ of D samples is consistently lower than that of C and X samples by ~ 0.6 ‰, this contrast is significantly less than the analagous $\delta^{15}N_{bulk}$ range of ~ 2 ‰. Also, the $\delta^{15}N_{non\text{-}frustule}$ of all D layers is very similar, including the samples from 1.0 – 2.5 cm depth in block, in contrast to the low $\delta^{15}N$ of both $\delta^{15}N_{bulk}$ and $\delta^{15}N_{frustule}$ over this interval. Thus, the isotopic composition of the non-frustule organic N throughout the block, in both C and D layers, is almost identical, despite the very large changes in $\delta^{15}N_{frustule}$.

2.5 Diatom provenance: an unexpected twist

The extremely low $\delta^{15}N_{frustule}$ in the D layers from 1.0 – 2.5 cm depth in block was unexpected. However, a survey of species abundances among the samples revealed tremendous variability, particularly in the abundance of *Actinopytuchus* spp., as previously noted by *Barron et al.* [2005]. The robust frustules of these shelf-dwelling diatoms are apparently swept downslope to the deep Guaymas Basin during intense summer storms. The N contained within their frustules is naturally swept downslope as well.

In order to evaluate the importance of this source of frustular N, a simple 'shelf-diatom index' was calculated as the number of *Actinoptychus* spp. valves divided by the total number of pennate diatom valves present, as shown in Figure 2.6. The values of the index

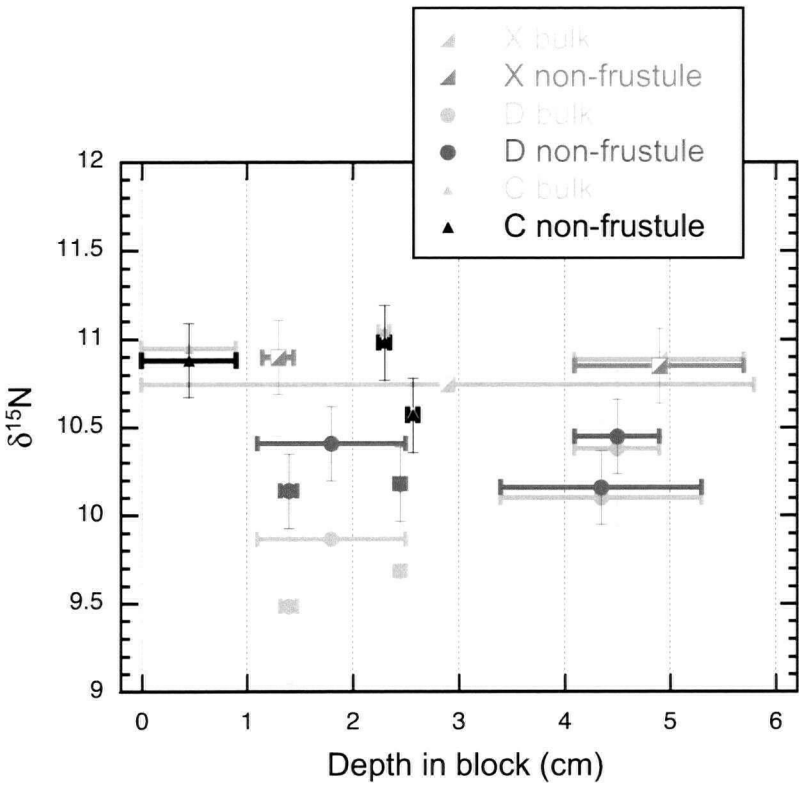

2.5: Comparison of $\delta^{15}N_{bulk}$ with the $\delta^{15}N$ (calculated) of non-frustule bound combustible N. Note that the frustule N content for sample 1X1 was not available. See Figure 2.2 for explanation of plot.

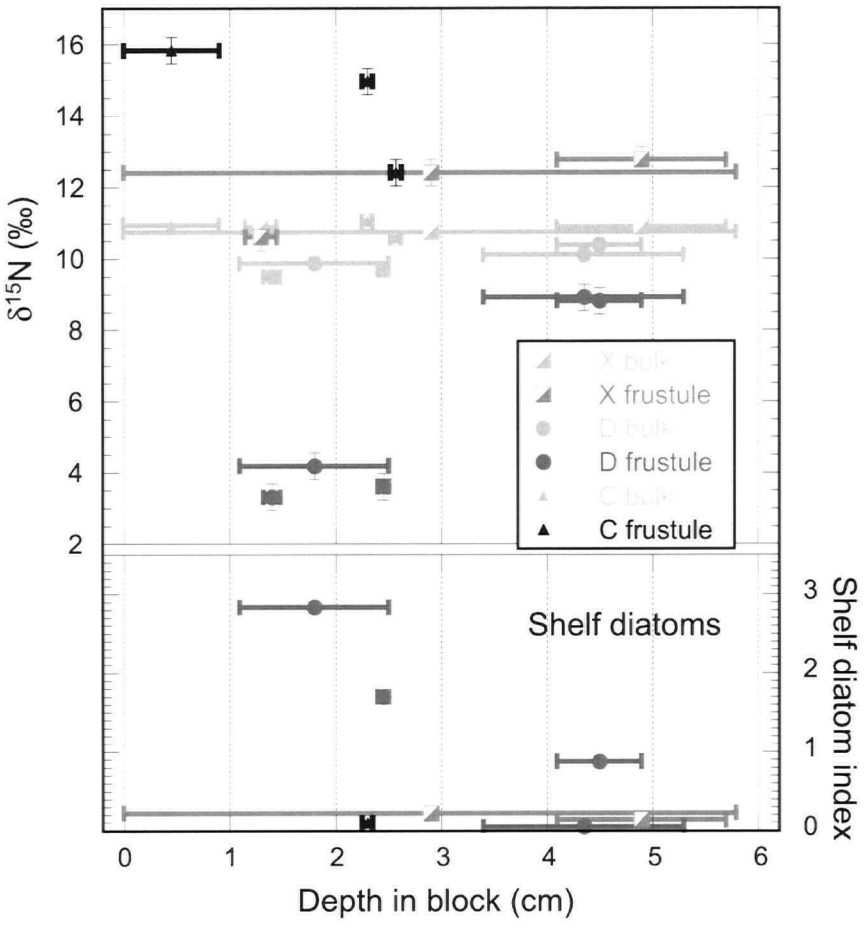

2.6: Comparison of shelf-derived diatom abundance with $\delta^{15}N_{bulk}$ and $\delta^{15}N_{frustule}$. The "shelf diatom index" is a ratio of the number of shelf-dwelling Actinoptychus valves to the number of pelagic pennate diatom valves. Note that diatom counts of four samples are not available.

vary widely, reflecting the abundance range of *Actinoptychus* spp. valves from 2 % to 78 % of all diatom valves. Shelf-derived frustules clearly represent a large portion of the total frustules in the D layers from the upper part of the block.

Nitrogen dynamics are likely to be quite different on the shelf, when compared to the open water column. Denitrification occurs at high rates in sediments on the shelf [*Christensen et al.*, 1987] and releases little or no residual nitrate, precluding significant isotopic enrichment [*Brandes and Devol*, 1997; *Lehmann et al.*, 2004], while any N_2 fixation present would provide new N with a $\delta^{15}N$ of 0 to –1 ‰ [*Wada and Hattori*, 1976; *Liu et al.*, 1996; *Montoya et al.*, 2002]. Therefore, the shelf environment may be awash with newly-fixed N of low $\delta^{15}N$. Also, ammonium excreted by heterotrophs and diffused out of the sediment may provide an important ^{15}N-depleted nitrogen substrate for benthic diatoms. The negative correlation between the shelf index and $\delta^{15}N_{frustule}$ (Figure 2.7) suggests that the extremely low $\delta^{15}N_{frustule}$ measurements are inherited from this shelf N pool. The intensity of this dilution could be expected to exhibit an irregular distribution, depending on local dynamics on the shelf. In contrast, nitrate supplied to the pelagic ecosystem is uniformly dominated by ^{15}N-enriched nitrate from below, diluted to a lesser extent by pelagic N_2 fixation.

The coincidence of variably low $\delta^{15}N_{frustule}$ with high concentrations of shelf-derived frustules in discrete intervals is strong evidence for episodic deposition. The fact that the highest concentrations of shelf diatoms are found among D layers suggests that these particular layers represent neither the "fall dump", nor winter upwelling season, but the sudden deposition of diatoms mobilized by intense summer storms sweeping the shelf [*Barron et al.*, 2005]. This cautions against the interpretation of diatom layers exclusively as the products of seasonally elevated diatom export rates. With this understanding, the upper, generally darker portion of the GLC-1 block can be interpreted as a period of weak pelagic diatom export punctuated by violent storm events. In contrast, the paler, well-banded lower portion of the GLC-1 block contains a higher proportion of diatom mats, more representative of the seasonal cycles of diatom export observed in the present-day Gulf of California (e.g. [*Sancetta*, 1995; *Thunell*, 1998]). The presence of these two end members within a block representing ~ 43 years of deposition could be an expression of the ~ 50 year cyclicity observed by *Pike and Kemp* [1997] in adjacent core JPC-56 during the same time period.

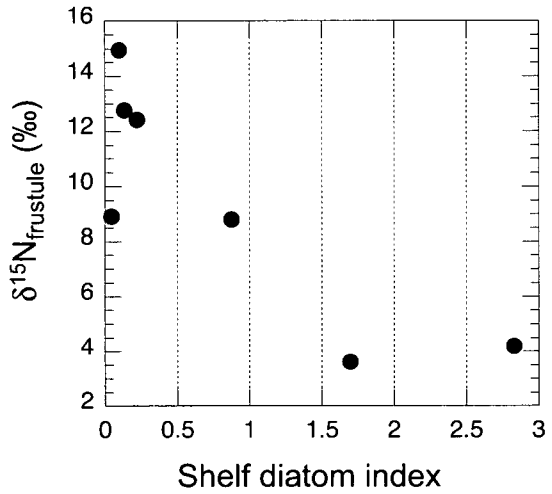

2.7: Shelf diatom index vs. $\delta^{15}N_{frustule}$ for all available samples of GLC-1.

2.6 Linking frustule N to whole diatom and exported N

The episodic abundance of shelf diatoms can account for the very low $\delta^{15}N_{frustule}$ during the upper D layers, but it cannot account for the > 6 ‰ range of $\delta^{15}N_{frustule\text{-}bulk}$ between samples with negligible shelf diatom content. The additional $\delta^{15}N_{frustule}$ variability, and its lack of parallel variation in the $\delta^{15}N_{bulk}$, could result from three factors, singly or in combination: first, that the N isotopic difference between diatom frustules and the diatom biomass, Δ(f-d), is not constant; second, that the relationship between the $\delta^{15}N$ of sedimented diatoms and the total N export, Δ(d-e), is not constant; and/or third, that the bulk organic nitrogen does not preserve the true seasonal changes in $\delta^{15}N_{export}$ due to homogenization of unprotected N during sedimentation and burial, Δ(sed) (see Section 2.7).

Considering the Δ(d-e) relationship, one might expect the great abundance of diatoms in Guaymas Basin to equate to diatom-dominated export and a minimal Δ(d-e). However, given that opal and C_{org} fluxes are strongly decoupled at present in the Guaymas basin [*Thunell*, 1998], much of the sedimented N may be exported from the euphotic zone by other organisms. It has been shown that diatoms have large fractionation factors during nitrate assimilation [*Wada and Hattori*, 1978; *Montoya and McCarthy*, 1995; *Waser et al.*, 1998; *Needoba et al.*, 2003] and can also form symbiotic associations with N_2 fixing cyanobacteria [*Capone et al.*, 2005], both of which would cause $\delta^{15}N_{diatom}$ to be low relative to other phytoplankton. Enrichment of ^{15}N typically occurs at higher trophic levels [*Minagawa and Wada*, 1984; *Montoya and McCarthy*, 1995; *McClelland and Montoya*, 2002] so, in general, the $\delta^{15}N$ of heterotrophic detritus would tend to be higher than $\delta^{15}N_{diatom}$. To maintain mass balance, the phytoplankton community must be depleted in ^{15}N relative to heterotrophs, when integrated over a period of complete mixed-layer nitrate utilization and export. Thus, unless the diatoms preserved in sediment grew under highly atypical conditions, Δ(d-e) should be negative, as shown in Figure 2.8. There is currently no published information with which to assess Δ(f-d), but a degree of constraint is provided by a careful consideration of the data in hand.

The highest $\delta^{15}N_{frustule}$ values are found in C layers. Shelf-derived diatoms are essentially absent from these samples, so these should provide a true measure of the $\delta^{15}N_{frustule}$ of preserved pelagic diatoms. Frustules are heavily fragmented, suggesting that they have been grazed, consistent with oligotrophic conditions and slow export. They may have grown on

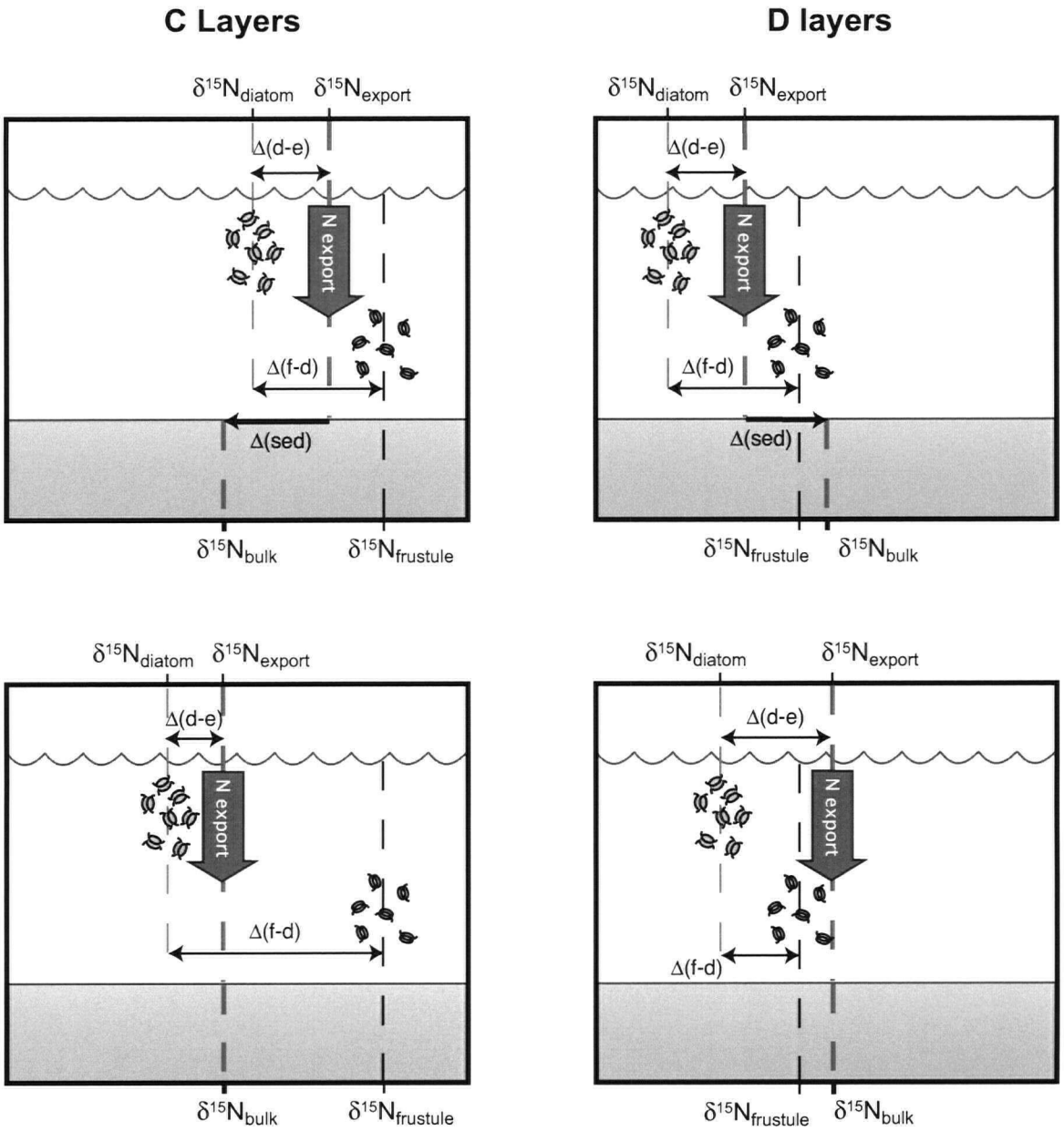

2.8: Schematic diagram illustrating some possible relationships between $\delta^{15}N_{bulk}$, $\delta^{15}N_{export}$, $\delta^{15}N_{diatom}$ and $\delta^{15}N_{frustule}$. Panels on left represent deposition of C layers, while panels on right represent D layer deposition. Upper panels show a scenario to explain the observed relationship between $\delta^{15}N_{bulk}$ and $\delta^{15}N_{frustule}$ with consistent offsets between $\delta^{15}N_{export}$, $\delta^{15}N_{diatom}$ and $\delta^{15}N_{frustule}$, and homogenization during sedimentation. Lower panels show an alternative scenario with no homogenization during sedimentation, but with variable relationships between $\delta^{15}N_{export}$, $\delta^{15}N_{diatom}$ and $\delta^{15}N_{frustule}$. See text for further discussion.

residual nitrate, enriched by Rayleigh fractionation [*Altabet and Francois*, 1994] or during a season when N_2 fixation was less active. However, the highest $\delta^{15}N_{export}$ of any sinking material in *Pride et al.* [1999] was 11.6 ‰, while the $\delta^{15}N_{frustule}$ measurements are as high as 16 ‰. As discussed above, $\delta^{15}N_{diatom}$ should be less than $\delta^{15}N_{export}$. Assuming that the seasonal maximum $\delta^{15}N$ of *Pride et al.* [1999] is representative of the early Holocene within 1 ‰, the maximum $\delta^{15}N_{diatom}$ is 12.6 ‰ and $\delta^{15}N_{frustule}$ must be elevated relative to $\delta^{15}N_{diatom}$ in the C samples, by up to 5 ‰.

In contrast, the $\delta^{15}N_{frustule}$ of D layers dominated by pelagic, pennate mat-formers with negligible shelf diatoms (multi-annual sample 1D4) is 8.9 ‰, slightly lower than $\delta^{15}N_{bulk}$. *Pride et al.* [1999] measured an average $\delta^{15}N$ of 8.5 ‰, with values as low as 6.6 ‰, during the analagous modern diatom export pulse in mid-winter. Again, assuming a similar seasonal contrast during the early Holocene, the $\delta^{15}N_{diatom}$ was probably less than 8.5 ‰ during deposition of these D layers. Thus, these layers are also consistent with a Δ(f-d) greater than zero.

The smaller $\delta^{15}N_{frustule\text{-}bulk}$ of X samples compared to C samples may relate to the substantial proportion of shelf diatoms within them (7 – 12 % *Actinoptychus* spp.). Since the shelf frustules identified have anomalously low $\delta^{15}N$, this would be expected to bias the $\delta^{15}N_{frustule}$ in the X samples toward lower values. Thus, the difference between $\delta^{15}N_{bulk}$ and $\delta^{15}N_{frustule}$ averaged across the entire block of 2 ‰ is a minimum estimate for the ^{15}N-enrichment of pelagic frustules. Assuming, again, that $\delta^{15}N_{diatom}$ is less than $\delta^{15}N_{export}$, and that $\delta^{15}N_{bulk}$ reflects $\delta^{15}N_{export}$ for these multi-annual averages, the average Δ(f-d) must be greater than 2 ‰.

In summary, it is not possible to conclude from these data whether Δ(f-d) is a constant offset of about 2 ‰, or a variable offset with smaller values during rapid diatom export and larger values during slow growth. However, it is certainly nonzero, in agreement with the preliminary culture results shown in Appendix 2. Changes in Δ(f-d) might be expected to occur due to species shifts, or due to variations in growth rates. The measurement of $\delta^{15}N_{frustule}$ in a modern sediment trap study would help to clarify the relationship to $\delta^{15}N_{export}$.

2.7 Low variability of bulk N isotopes

The constancy of $\delta^{15}N_{bulk}$, and even greater constancy of $\delta^{15}N_{non\text{-}frustule}$ across the block, could indicate one of two things. First, that the seasonal contrast of $\delta^{15}N_{frustule}$ is exaggerated in comparison to that of $\delta^{15}N_{export}$, due to variations of Δ(f-d) and/or Δ(d-e), as discussed above and illustrated in Figure 2.8. If the $\delta^{15}N_{non\text{-}frustule}$ is, in fact, an accurate monitor of seasonal variations in $\delta^{15}N_{export}$, the seasonal variability during the period of study must have been less than that shown by the six-year sediment trap study of *Pride et al.* [1999]. The second possibility is that $\delta^{15}N_{export}$ was seasonally variable, but non-frustule N was homogenized during deposition and burial, Δ(sed). This could have occurred through microbioturbation by low-oxygen tolerant microbenthos on a small enough scale to avoid destruction of the laminated fabric [*Pike et al.*, 2001]. Because the relatively large and rigid diatom frustules form a substantial structural matrix, they would be more resistant to microbioturbation. Again, a sediment-trap study including measurements of both bulk and frustule N could help differentiate between these possibilities.

It is also important to note that $\delta^{15}N_{non\text{-}frustule}$ does not mirror the very low $\delta^{15}N_{frustule}$ in the D layers from 1.0 – 2.5 cm depth in block, indicating that the diatom redeposition events are ineffective at transporting unbalasted, bulk organic nitrogen downslope, and therefore have negligible impact on $\delta^{15}N_{bulk}$. Taken together, these observations show that $\delta^{15}N_{bulk}$ is less sensitive to seasonal change than $\delta^{15}N_{frustule}$, relatively insensitive to downslope transport of material from the shelf, and an excellent integrative monitor of the pelagic $\delta^{15}N_{nitrate}$.

2.8 Conclusions

These results show that $\delta^{15}N_{frustule}$ offers additional information, beyond that which can be gleaned from $\delta^{15}N_{bulk}$, and is not simply an equivalent of $\delta^{15}N_{bulk}$ with greater preservation potential. The $\delta^{15}N_{frustule}$ measurements show large seasonal variability, which may be exaggerated beyond the seasonal range of $\delta^{15}N_{export}$. The $\delta^{15}N_{frustule}$ is higher than $\delta^{15}N_{diatom}$, by less than 5 ‰, in all samples for which the difference can be resolved here. We are unable to state, at this point, whether this is a consistent offset or whether the offset varies depending on species and/or growth conditions.

Laminated diatom mats such as those in Guaymas Basin can robustly be interpreted as annual features, and if properly understood, the $\delta^{15}N_{frustule}$ can therefore be used as a high-

resolution monitor of ecosystem dynamics. However, the presence of exogenous frustules from the shelf, with markedly distinct $\delta^{15}N_{frustule}$, alerts us to the transportation potential of diatom frustules. This is likely to be a particularly severe problem at our study site, given its location on a slope with rapidly accumulating sediments, only ~ 16 km from the 100 m isobath, and can be identified by microscopic inspection for *Actinoptychus* spp.; however, it may also be a problem in deep sea, diatom-rich deposits that include potentially redeposited material, such as those found in some regions of the Southern Ocean [*Ingalls et al.*, 2004].

Meanwhile, the $\delta^{15}N_{bulk}$ has little seasonal variability, and what seasonal contrasts exist can be largely accounted for by the highly variable $\delta^{15}N$ of N preserved in diatom frustules. This observation is at odds with the greater seasonal variability in $\delta^{15}N_{export}$ collected by sediment traps. It follows that either the seasonal variability was less during the period of deposition, or the seasonal signal was obliterated by homogenization during burial. In either case it can be concluded that, where diagenesis is either absent or consistently quantifiable, the robust devotion of $\delta^{15}N_{bulk}$ to $\delta^{15}N_{nitrate}$ makes it a very useful quantity.

2.9 References

Altabet, M. A., and R. Francois, Sedimentary Nitrogen Isotopic Ratio As a Recorder For Surface Ocean Nitrate Utilization, *Global Biogeochemical Cycles*, 8, 103-116, 1994.

Altabet, M. A., R. Francois, D. W. Murray, and W. L. Prell, Climate-Related Variations in Denitrification in the Arabian Sea From Sediment $^{15}N/^{14}N$ Ratios, *Nature*, 373, 506-509, 1995.

Altabet, M. A., C. Pilskaln, R. Thunell, C. Pride, D. Sigman, F. Chavez, and R. Francois, The nitrogen isotope biogeochemistry of sinking particles from the margin of the Eastern North Pacific, *Deep-Sea Research Part I-Oceanographic Research Papers*, 46, 655-679, 1999.

Barron, J. A., D. Bukry, and W. E. Dean, Paleoceanographic history of the Guaymas Basin, Gulf of California, during the past 15,000 years based on diatoms, silicoflagellates, and biogenic sediments, *Marine Micropaleontology*, 56, 81-102, 2005.

Baumgartner, T. R., V. Ferreira-Bartrina, and P. Moreno-Hentz, Varve formation in the central Gulf of California: a reconsideration of the origin of the dark laminae from the 20th century varve record. in *The gulf and peninsular province of the Californias: AAPG Memoir 47*, edited by Dauphin, J. P. and B. R. T. Simoneit, pp. 617-635, 1991.

Braman, R. S., and S. A. Hendrix, Nanogram Nitrite and Nitrate Determination in Environmental and Biological-Materials by Vanadium(Iii) Reduction with Chemi-Luminescence Detection, *Analytical Chemistry*, 61, 2715-2718, 1989.

Brandes, J. A., and A. H. Devol, Isotopic fractionation of oxygen and nitrogen in coastal marine sediments, *Geochimica Et Cosmochimica Acta*, 61, 1793-1801, 1997.

Calvert, S. E., Factors affecting distribution of laminated diatomaceous sediments in the Gulf of California. in *Marine geology of the Gulf of California, AAPG Memoir 3*, edited by van Andel, T. H. and G. G. Shor, pp. 311-330, 1964.

Calvert, S. E., Origin of the diatom-rich, varved sediments from the Gulf of California, *Journal of Geology*, 74, 546-565, 1966.

Calvert, S. E., B. Nielsen, and M. R. Fontugne, Evidence From Nitrogen Isotope Ratios For Enhanced Productivity During Formation of Eastern Mediterranean Sapropels, *Nature*, 359, 223-225, 1992.

Capone, D. G., J. A. Burns, J. P. Montoya, A. Subramaniam, C. Mahaffey, T. Gunderson, A. F. Michaels, and E. J. Carpenter, Nitrogen fixation by Trichodesmium spp.: An important source of new nitrogen to the tropical and subtropical North Atlantic Ocean, *Global Biogeochemical Cycles*, 19, 2005.

Cheshire, H., J. Thurow, and A. J. Nederbragt, Late Quaternary climate change record from two long sediment cores from Guaymas Basin, Gulf of California, *Journal of Quaternary Science*, 20, 457-469, 2005.

Christensen, J. J., J. W. Murray, A. H. Devol, and L. A. Codispoti, Denitrification in continental shelf sediments has major impact on the oceanic nitrogen budget, *Global Biogeochemical Cycles*, 1, 97-116, 1987.

Cline, J. D., and I. R. Kaplan, Isotopic fractionation of dissolved nitrate during denitrification in the eastern tropical north Pacific Ocean, *Marine Chemistry*, 3, 271-299, 1975.

Crawford, S. A., M. J. Higgins, P. Mulvaney, and R. Wetherbee, Nanostructure of the diatom frustule as revealed by atomic force and scanning electron microscopy, *Journal of Phycology*, 37, 543-554, 2001.

Crosta, X., and A. Shemesh, Reconciling down core anticorrelation of diatom carbon and nitrogen isotopic ratios from the Southern Ocean, *Paleoceanography*, 17, 2002.

Crosta, X., A. Shemesh, J. Etourneau, R. Yam, I. Billy, and J. J. Pichon, Nutrient cycling in the Indian sector of the Southern Ocean over the last 50,000 years, *Global Biogeochemical Cycles*, 19, 10, 2005.

Falciatore, A., and C. Bowler, Revealing the molecular secrets of marine diatoms, *Annual Reviews of Plant Biology*, 53, 109-130, 2002.

Francois, R., M. A. Altabet, E. F. Yu, D. M. Sigman, M. P. Bacon, M. Frank, G. Bohrmann, G. Bareille, and L. D. Labeyrie, Contribution of Southern Ocean surface-water stratification to low atmospheric CO2 concentrations during the last glacial period, *Nature*, 389, 929-935, 1997.

Ganeshram, R. S., T. F. Pedersen, S. E. Calvert, G. W. McNeill, and M. R. Fontugne, Glacial-interglacial variability in denitrification in the world's oceans: Causes and consequences, *Paleoceanography*, 15, 361-376, 2000.

Ganeshram, R. S., T. F. Pedersen, S. E. Calvert, and J. W. Murray, Large changes in oceanic nutrient inventories from glacial to interglacial periods, *Nature*, 376, 755-758, 1995.

Hazelaar, S., H. J. van der Strate, W. W. C. Gieskes, and E. G. Vrieling, Monitoring rapid valve formation in the pennate diatom Navicula salinarum (Bacillariophyceae), *Journal of Phycology*, 41, 354-358, 2005.

Ingalls, A. E., R. F. Anderson, and A. Pearson, Radiocarbon dating of diatom-bound organic compounds, *Marine Chemistry*, 92, 91-105, 2004.

Ingalls, A. E., C. Lee, S. G. Wakeham, and J. I. Hedges, The role of biominerals in the sinking flux and preservation of amino acids in the Southern Ocean along 170 degrees W, *Deep-Sea Research Part Ii-Topical Studies in Oceanography*, 50, 713-738, 2003.

Kemp, A. E. S., J. Pike, R. B. Pearce, and C. B. Lange, The "Fall dump" - a new perspective on the role of a "shade flora" in the annual cycle of diatom production and export flux, *Deep-Sea Research Part Ii-Topical Studies in Oceanography*, 47, 2129-2154, 2000.

Kienast, M., On the sedimentological origin of down-core variations of bulk sedimentary nitrogen isotope ratios, *Paleoceanography*, 20, 2005.

Kroger, N., R. Deutzmann, C. Bergsdorf, and M. Sumper, Species-specific polyamines from diatoms control silica morphology, *Proceedings National Academy of Science*, 97, 14133-14138, 2000.

Kroger, N., R. Deutzmann, and M. Sumper, Polycationic peptides from diatom biosilica that direct silica nanosphere formation, *Science*, 286, 1129-1132, 1999.

Lehmann, M. F., D. M. Sigman, and W. M. Berelson, Coupling the $^{15}N/^{14}N$ and $^{18}O/^{16}O$ of nitrate as a constraint on benthic nitrogen cycling, *Marine Chemistry*, 88, 1-20, 2004.

Liu, K.-K., and I. R. Kaplan, The eastern tropical Pacific as a source of ^{15}N-enriched nitrate in seawater off southern California, *Limnology and Oceanography*, 34, 820-830, 1989.

Liu, K. K., M. J. Su, C. R. Hsueh, and G. C. Gong, The nitrogen isotopic composition of nitrate in the Kuroshio Water northeast of Taiwan: Evidence for nitrogen fixation as a source of isotopically light nitrate, *Marine Chemistry*, 54, 273-292, 1996.

Macko, S. A., M. L. Fogel, P. E. Hare, and T. C. Hoering, Isotopic fractionation of nitrogen and carbon isotopes in the synthesis of amino acids by microorganisms, *Chemical Geology*, 65, 79-92, 1987.

McClelland, J. W., and J. P. Montoya, Trophic relationships and the nitrogen isotopic composition of amino acids in plankton, *Ecology*, 83, 2173-2180, 2002.

McKay, J. L., T. F. Pedersen, and S. S. Kienast, Organic carbon accumulation over the last 16 kyr off Vancouver Island, Canada: evidence for increased marine productivity during the deglacial, *Quaternary Science Reviews*, 23, 261-281, 2004.

Milligan, A. J., and F. M. M. Morel, A proton buffering role for silica in diatoms, *Science*, 297, 1848-1850, 2002.

Minagawa, M., and E. Wada, Stepwise enrichment of ^{15}N along food chains: Further evidence and the relation between $\delta^{15}N$ and animal age, *Geochimica et Cosmochimica Acta*, 48, 1135-1140, 1984.

Montoya, J. P., E. J. Carpenter, and D. G. Capone, Nitrogen fixation and nitrogen isotope abundances in zooplankton of the oligotrophic North Atlantic, *Limnology and Oceanography*, 47, 1617-1628, 2002.

Montoya, J. P., and J. J. McCarthy, Isotopic fractionation during nitrate uptake by phytoplankton grown in continuous-culture, *Journal of Plankton Research*, 17, 439-464, 1995.

Mortlock, R. A., and P. N. Froelich, A Simple Method for the Rapid-Determination of Biogenic Opal in Pelagic Marine-Sediments, *Deep-Sea Research Part a-Oceanographic Research Papers*, 36, 1415-1426, 1989.

Nakanishi, T., and M. Minagawa, Stable carbon and nitrogen isotopic compositions of sinking particles in the northeast Japan Sea, *Geochemical Journal*, 37, 261-275, 2003.

Needoba, J. A., D. M. Sigman, and P. J. Harrison, The mechanism of isotope fractionation during algal nitrate assimilation as illuminated by the $^{15}N/^{14}N$ of intracellular nitrate, *Journal of Phycology*, 40, 517-522, 2004.

Needoba, J. A., N. A. Waser, P. J. Harrison, and S. E. Calvert, Nitrogen isotope fractionation in 12 species of marine phytoplankton during growth on nitrate, *Marine Ecology-Progress Series*, 255, 81-91, 2003.

Peters, K. E., R. E. Sweeney, and I. R. Kaplan, Correlation of carbon and nitrogen stable isotope ratios in sedimentary organic matter, *Limnology and Oceanography*, 23, 598-604, 1978.

Pike, J., J. M. Bernhard, S. G. Moreton, and I. B. Butler, Microbioirrigation of marine sediments in dysoxic environments: Implications for early sediment fabric formation and diagenetic processes, *Geology*, 29, 923-926, 2001.

Pike, J., and A. E. S. Kemp, Early Holocene decadal-scale ocean variability recorded in Gulf of California laminated sediments, *Paleoceanography*, 12, 227-238, 1997.

Pride, C., R. Thunell, D. Sigman, L. Keigwin, M. Altabet, and E. Tappa, Nitrogen isotopic variations in the Gulf of California since the last deglaciation: Response to global climate change, *Paleoceanography*, 14, 397-409, 1999.

Robinson, R. S., B. G. Brunelle, and D. M. Sigman, Revisiting nutrient utilization in the glacial Antarctic: Evidence from a new method for diatom-bound N isotopic analysis, *Paleoceanography*, 19, 2004.

Robinson, R. S., D. M. Sigman, P. J. DiFiore, M. M. Rohde, T. A. Mashiotta, and D. W. Lea, Diatom-bound N-15/N-14: New support for enhanced nutrient consumption in the ice age subantarctic, *Paleoceanography*, 20, 2005.

Sancetta, C., Diatoms in the Gulf of California: Seasonal flux patterns and the sediment record for the past 15,000 years, *Paleoceanography*, 10, 67-84, 1995.

Schneider-Mor, A., R. Yam, C. Bianchi, M. Kunz-Pirrung, R. Gersonde, and A. Shemesh, Diatom stable isotopes, sea ice presence and sea surface temperature records of the past 640 ka in the Atlantic sector of the Southern Ocean, *Geophysical Research Letters*, 32, 2005.

Schubert, C. J., and S. E. Calvert, Nitrogen and carbon isotopic composition of marine and terrestrial organic matter in Arctic Ocean sediments: implications for nutrient utilization and organic matter composition, *Deep-Sea Research Part I-Oceanographic Research Papers*, 48, 789-810, 2001.

Shemesh, A., S. A. Macko, C. D. Charles, and G. H. Rau, Isotopic Evidence for Reduced Productivity in the Glacial Southern-Ocean, *Science*, 262, 407-410, 1993.

Sigman, D. M., M. A. Altabet, R. Francois, D. C. McCorkle, and J.-F. Gaillard, The isotopic composition of diatom-bound nitrogen in Southern Ocean sediments, *Paleoceanography*, 14, 118-134, 1999.

Sigman, D. M., K. L. Casciotti, M. Andreani, C. Barford, M. Galanter, and J. K. Bohlke, A bacterial method for the nitrogen isotopic analysis of nitrate in seawater and freshwater, *Analytical Chemistry*, 73, 4145-4153, 2001.

Sigman, D. M., R. Robinson, A. N. Knapp, A. van Geen, D. C. McCorkle, J. A. Brandes, and R. C. Thunell, Distinguishing between water column and sedimentary denitrification in the Santa Barbara Basin using the stable isotopes of nitrate, *Geochemistry Geophysics Geosystems*, 4, art. no.-1040, 2003.

Sumper, M., A phase separation model for the nanopatterning of diatom biosilica, *Science*, 295, 2430-2433, 2002.

Thunell, R., C. Pride, E. Tappa, and F. Mullerkarger, Varve Formation in the Gulf-of-California - Insights from Time-Series Sediment Trap Sampling and Remote-Sensing, *Quaternary Science Reviews*, 12, 451-&, 1993.

Thunell, R. C., Seasonal and annual variability in particle fluxes in the Gulf of California: A response to climate forcing, *Deep-Sea Research Part I-Oceanographic Research Papers*, 45, 2059-2083, 1998.

Thunell, R. C., and A. B. Kepple, Glacial-holocene $\delta^{15}N$ record from the Gulf of Tehuantepec, Mexico: Implications for denitrification in the eastern equatorial Pacific and changes in atmospheric N2O, *Global Biogeochemical Cycles*, 18, 2004.

van Geen, A., Y. Zheng, J. M. Bernhard, K. G. Cannariato, J. Carriquiry, W. E. Dean, B. W. Eakins, J. D. Ortiz, and J. Pike, On the preservation of laminated sediments along the western margin of North America, *Paleoceanography*, 18, 2003.

Wada, E., and A. Hattori, Natural abundance of 15N in particulate organic matter in the North Pacific Ocean, *Geochimica Et Cosmochimica Acta*, 40, 249-251, 1976.

Wada, E., and A. Hattori, Nitrogen isotope effects in the assimilation of inorganic nitrogenous compounds by marine diatoms, *Geomicrobiology Journal*, 1, 85-101, 1978.

Waser, N. A. D., P. J. Harrison, B. Nielsen, and S. E. Calvert, Nitrogen isotope fractionation during the uptake and assimilation of nitrate, nitrite, ammonium and urea by a marine diatom, *Limnology and Oceanography*, 43, 215-224, 1998.

CHAPTER III

Nitrogen isotope dynamics of the subarctic Pacific over the past 742,000 years: influences of denitrification, iron fertilization and diagenesis

3.1 Introduction and background

The subarctic Pacific has received scant attention from paleoceanographers, due in part to the paucity of good sedimentary records from the region, and in part to the observation that circulation beneath the subarctic Pacific has not obviously changed a great deal during late Pleistocene glacial cycles [*Keigwin*, 1987]. Yet there is abundant evidence that drastic changes in export production have occurred in the subarctic Pacific, connected with changes in climate, but incompletely understood in terms of timing and mechanisms [*Haug et al.*, 1999; *McDonald et al.*, 1999; *Narita et al.*, 2002; *Kienast et al.*, 2004; *Jaccard et al.*, 2005]. Iron limitation has been definitively demonstrated in the modern subarctic Pacific [*Martin et al.*, 1991; *Tsuda et al.*, 2003; *de Baar et al.*, 2005] yet evidence for variations in iron limitation over past climate cycles remains equivocal [*Kienast et al.*, 2004]. Clear evidence has also been presented for changes in the ventilation of the upper North Pacific water column [*Behl and Kennett*, 1996; *Keigwin*, 1998; *Zheng et al.*, 2000; *Ahagon et al.*, 2003; *Crusius et al.*, 2004; *McKay et al.*, 2005], intimately linked to the subarctic Pacific surface by the circulation of North Pacific Intermediate Water (NPIW), with important implications for past changes in nitrogen cycling. This chapter contributes to the developing understanding of the subarctic Pacific by presenting new data on the nitrogen isotope dynamics of the region, both in the present day and as recorded in sediments, that shed additional light on all of these issues.

Previous work on the nitrogen isotope dynamics of the modern subarctic Pacific includes one profile of the nitrogen isotopic ratio of nitrate thoughout the water column at Ocean Station Papa (OSP) [*Casciotti et al.*, 2002] in the central Gulf of Alaska, four low-resolution profiles spanning the open subarctic [*Minagawa et al.*, 2001], and a series of high-resolution profiles from the Bering Sea and the western subarctic gyre [*Lehmann et al.*, 2005]. Here, isotopic data are presented from a transect spanning the B.C. coast to OSP, a region that forms a critical bridge for water mass mixing between the subtropical and the subarctic gyres. A new water column profile is also presented from the western subarctic Pacific.

Following this sketch of the modern N isotope dynamics, three new sediment records from both the eastern and western subarctic Pacific are explored. Two sites (ODP 882 and MD01-2416) are close together and lie under the Western Subarctic Gyre (WSG), while the third site (ODP 887) is in the eastern subarctic, beneath the northwestern Gulf of Alaska (GA). These are highly complex cores, from an N-isotopic perspective, as they are certain to record impacts of changing relative nitrate utilization, diagenetic alteration, and the nitrogen isotopic composition of the nitrate substrate. However, by using multiple proxies, the three discrete contributions to the bulk N isotope signal are disentangled to provide important new information. It will be shown that the WSG records are dominated by changes in the degree of relative nitrate utilization, likely determined by the balance of macronutrient availability vs. aeolian dust flux, while the GA record is dominated by changes in the nitrogen isotopic composition of nitrate in the subarctic Pacific.

3.1.1 Modern Subarctic Pacific Hydrography

The surface of the subarctic Pacific has lower salinity than any other part of the open ocean, with the exception of the Arctic. This is maintained by a high flux of freshwater to the region, supplied principally by atmospheric moisture advection from the western tropical Pacific [*Emile-Geay et al.*, 2003]. As a result, the maximum density formed at the surface during winter of 26.5 kg m^{-3} [*You*, 2003b] is insufficient to allow exchange below mode water depths [*Reid*, 1965; *Yasuda*, 2004]. Somewhat higher densities are generated in polynyas of the Sea of Okhotsk [*Gladyshev et al.*, 2003], but the ventilation of the NPIW (~26.7 - 27.4 kg m^{-3}) appears to be accomplished principally by the formation of denser waters through

diapycnal diffusion and cabbeling [*Reid*, 1965; *You*, 2003a; *Yun and Talley*, 2003]. This involves lateral subsurface mixing of salty, subtropical gyre waters with cold, fresh Okhotsk Sea Intermediate Water and, to a lesser extent, Gulf of Alaska Intermediate Water [*You*, 2003a; *Yun and Talley*, 2003]. The resultant water mass spreads from the eastern subarctic frontal region towards the south and west, weakly ventilating much of the intermediate North Pacific on a timescale of < 80 years [*Talley*, 1997; *Yasuda et al.*, 2002; *You*, 2003b]. Within the subarctic itself, upper intermediate waters flow eastward into the southern Gulf of Alaska as part of the N Pacific current and are modified as they transit the the Gulf in a cyclonic pattern [*Aydin et al.*, 1998]. They then follow the Aleutians westward into the Western Subarctic Gyre until turning N into the Bering Sea, east of 170 °E [*Ueno and Yasuda*, 2003]. Surface water circulation is more variable, and is heavily influenced by freshwater eddies that form according to a complex interplay between coastal bathymetry and freshwater distribution [*Stabeno et al.*, 2004].

Far below, in the lower deep ocean, lies the Pacific bottom water, a mixture of roughly equal parts Antarctic Bottom Water and North Atlantic Deep Water [*Broecker et al.*, 1998]. Above the northward flowing bottom water, the circulation reverses, such that mass transport is generally southward in upper deep waters [*Ueno and Yasuda*, 2003]. Sluggish horizontal circulation, combined with the great distance from the formation regions, gives this water mass the lowest ^{14}C concentrations anywhere in the world ocean [*Broecker and Peng*, 1982]. Apparent Oxygen Utilization is very high throughout the subsurface of the North Pacific, with a maximum near 1 km depth, and oxygen concentrations below 50 μM can be found within 200 m of the surface of the subarctic Pacific. These low O_2 concentrations can be partly attributed to the poor oxygenation of old, slowly upwelling deep waters, partly due to exchange with the oxygen deficient waters of the Eastern Tropical North Pacific (ETNP) shadow zone, and partly due to the lack of effective exchange between surface and subsurface waters of the subarctic Pacific.

3.1.2 Sediment core sites

The GA site lies ~ 300 km SE of the Alaskan shelf break (Table 3.1), on the gently sloping flank of the Patton-Murray group of seamounts. This site lies squarely underneath the Alaskan Gyre [*Whitney et al.*, 2005] where domal upwelling raises isopycnals into an elon-

Table 3.1

Locations of sediment cores discussed in this chapter

Name	Location	Latitude	Longitude	Depth	References for data shown
ODP 887	Gulf of Alaska	54.37 °N	148.45 °W	3647 m	[*McDonald et al.*, 1999], [*McDonald*, 1997], this study
PAR87A-01	Gulf of Alaska	54.42 °N	149.43 °W	3480 m	[*McDonald et al.*, 1999], this study
ODP 882	Western Subarctic Gyre	50.35 °N	167.58 °E	3244 m	[*Jaccard et al.*, 2005], this study
MD01-2416	Western Subarctic Gyre	51.27 °N	167.73 °E	2317 m	Sarnthein et al in press, Kienast et al., unpublished
W8709-08	Oregon Midway	42.26 °N	127.68 °W	3111 m	[*Kienast et al.*, 2002]
W8709-13	Oregon Nearshore	42.12 °N	125.75 °W	2712 m	[*Kienast et al.*, 2002]
ODP 1017	California margin	34.53 °N	121.10 °W	955 m	[*Hendy et al.*, 2004]
NH15P	Mexican margin	22.68 °N	106.48 °W	420 m	[*Nameroff et al.*, 2004]
NH22P	Mexican margin	23.52 °N	106.52 °W	2025 m	[*Ganeshram et al.*, 1995; *Nameroff et al.*, 2004]

gate bulge and provides a gradual upward flux of cold, salty water (Figure 3.1). As a result, the surface waters above Site 887 are denser and more saline than the rest of the Gulf.

The central Gulf, typified by Ocean Station Papa (OSP), is a classic High Nitrate Low Chlorophyll (HNLC) region in which macronutrients are generally nonzero throughout the year. It is widely suspected that Fe limits the export of nutrients from the surface ocean [*Martin and Fitzwater*, 1988], a concept generally borne out by laboratory and shipboard experiments and recently confirmed by a mesoscale Fe addition experiment ([*Boyd et al.*, 2004] and references therein). Iron limitation seems to be the result of low Fe concentrations in upwelled waters combined with a weak aeolian Fe supply, perhaps exacerbated by the high-Fe requirements of phytoplankton for light-gathering apparatus in these dimly-lit latitudes [*Strzepek and Harrison*, 2004]. The coastal waters that ring the Gulf are Fe-rich, with up to two orders of magnitude higher iron concentrations than central Gulf waters [*Johnson et al.*, 2005], and where coastal waters are transported offshore they allow complete drawdown of macronutrients [*Whitney and Robert*, 2002; *Peterson et al.*, 2005]. Coastal eddies are important vectors of coastal Fe to the central Gulf along the margin of British Columbia [*Johnson et al.*, 2005], and may also be important along the Alaskan slope near Kodiak Island [*Ladd et al.*, 2005; *Whitney et al.*, 2005], particularly during episodic events of widespread eddy formation [*Thomson and Gower*, 1998]. Moreover, the Gyre circulation itself is rapid and can efficiently transport waters from the coastal shelf of Alaska to the vicinity of the GA site within a few months [*Bograd et al.*, 1999; *Whitney et al.*, 2005]. Thus, the supply of trace metals from the Alaskan shelf to the GA site seems likely to exceed significantly that supplied by atmospheric dust in the present day [*Johnson et al.*, 2005; *Lam et al.*, accepted].

Conceivably, biogenic detritus found in the sediment at the GA site could have been produced under a range of conditions, from growth of organisms in Fe-poor upwelled deep waters with little coastal influence, to almost pure coastal water transported offshore. However, for the following reasons, it is most likely to be dominated by detritus representing the fertile coastal-oceanic transition zone. The US NODC World Ocean Atlas 2001 (WOA2001) seasonal climatology shows that, while waters above the GA site have very high nitrate concentrations in winter (~ 20 μM), they neighbour a zone in which nitrate is quickly drawn down during the spring bloom (Apr-Jun), the period of rapid opal export in the subarctic Pacific identified by sediment trap studies [*Wu et al.*, 1999; *Takahashi et al.*, 2000]. The mini-

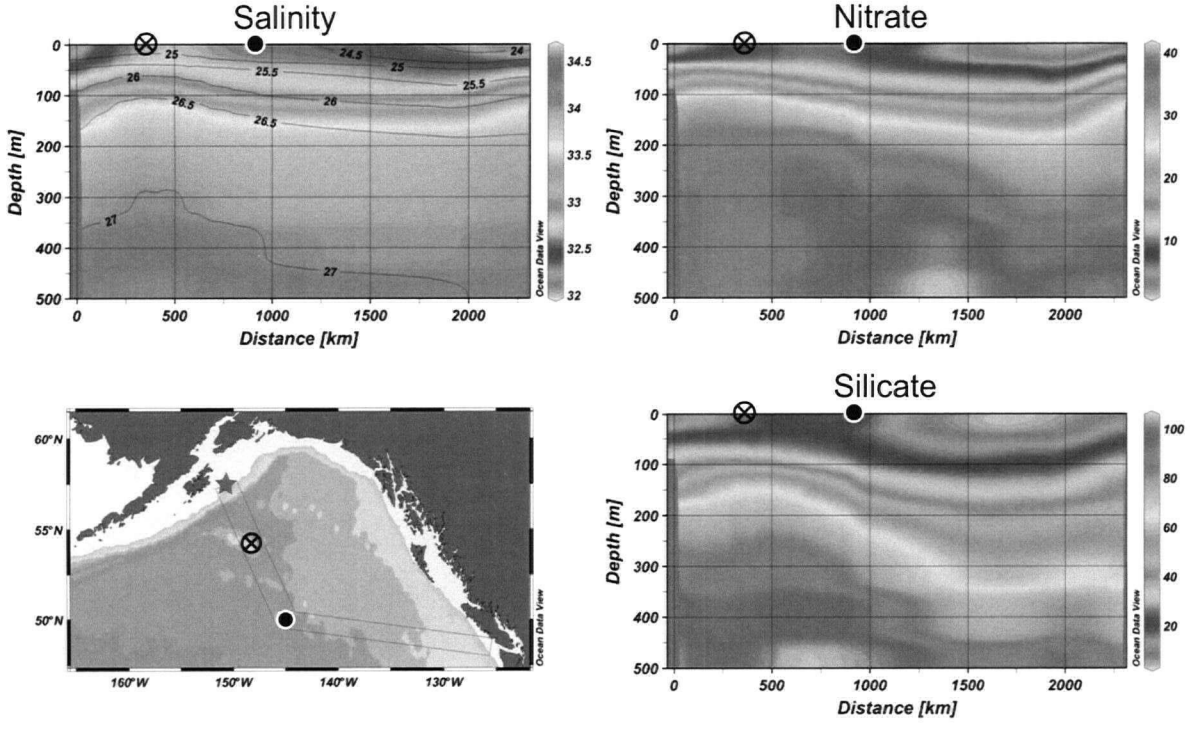

3.1: Average July-September upper water column characteristics across the Gulf of Alaska (WOA01). The distance along the transect, starting from the star shown on the Alaskan shelf, is indicated on the horizontal axis. The location of ODP Site 887 is shown by the circled cross, while OSP is shown by the black dot with white outline. The GA site is beneath domal upwelling, where dense, saline waters are drawn upwards by Ekman divergence. Although winter nutrient concentrations are much higher at the GA site than at OSP (Fig SeasonalSAP), by late summer they are significantly lower, indicating a much larger seasonal nutrient drawdown. This is related to the proximity of the GA site to the shelf break (~320 km) compared to the remote OSP. The offshore shoaling of isopycnals provides a direct lateral route for waters in contact with shelf sediments, rich with micronutrients, to the euphotic zone above the GA site.

mum climatological nitrate concentrations at the GA location itself are ~ 7 μM in the mixed layer during July-September, similar to the concentrations shown between "Line P" stations P20 and P16 (~138 °W on the transect shown in Figure 3.1) where *Whitney et al.* [2005] found complete nitrate utilization in summer; the climatological estimate likely misses the true minimum concentrations, since observations of zero nitrate are obscured by inclusion in the average of occasional measurements of high nitrate. Episodic lateral transport of Fe-rich waters from the shelf is likely to fuel occasional pulses of export with complete nitrate utilization [*Lam et al.*, accepted]. Consistent with this, Banse and English [1999] draw the HNLC region as lying to the south of the GA site; thus, the GA site lies on the margin of the coastal-oceanic transition zone, where nitrate drawdown is complete. Considering the rapid transport of surface waters on the time frame of sinking organic matter (weeks) estimated from surface drifters in the region [*Bograd et al.*, 1999], one would also expect the abundant organic detritus produced in the transition zone to be dispersed over a swath including the GA site. Thus, it seems very likely that the seafloor at the GA site receives abundant organic matter produced across the zone where nitrate drawdown is generally complete. OSP, at which the full seasonal range of nitrate concentrations in the WOA2001 climatology is only from ~13 to ~9 μM, is not a good oceanographic analogue for the more coastally-influenced GA site.

The two WSG cores (Table 3.1) are more than 500 km to SE of the narrow shelf of Kamchatka, on opposite flanks of the Detroit Seamount, squarely within a zone of very high year-round nitrate concentrations. Unlike the GA site, the WSG site is close to the large, arid, dust source region of East Asia [*Duce and Tindale*, 1991; *Mahowald et al.*, 1999]. This gives it the potential to receive a significant aeolian Fe supplement [*Fung et al.*, 2000] although recent measurements show that it currently lies outside the primary corridor of dust deposition and receives much less dust than previously supposed [*Brown et al.*, 2005; *Measures et al.*, 2005]. Mesoscale Fe enrichment experiments have confirmed that the aerosol source is currently insufficient to overcome Fe limitation, as strong responses to Fe additions were observed among the phytoplankton communities in the WSG [*Tsuda et al.*, 2003]. The WSG also differs from the GA in that it is characterized by higher $Si(OH)_4$:NO_3^- ratios, and more of the chlorophyll is accounted for by diatoms [*Harrison et al.*, 2004].

To summarize, both regions have macronutrient-rich surface waters, but the GA site receives significant inputs of micronutrients from the coast, allowing sporadic drawdown of

macronutrients by a cosmopolitan community. In contrast, the WSG site is more isolated from direct coastal influence but has a greater potential for supply of micronutrient via windborne dust. The WSG also hosts surface waters with higher perennial macronutrient concentrations, and a community dominated by diatoms.

3.1.3 General controls on $\delta^{15}N\text{-}NO_3^-$ in the N Pacific

Deep-water $\delta^{15}N\text{-}NO_3^-$ measurements range globally from 4 - 5.5 ‰ [*Sigman*, 1997], and within the N Pacific from 5 - 5.5 ‰. The slight variations depend on the relative inputs of residual nitrate from denitrification, which is enriched in ^{15}N, vs. the nitrification of newly fixed N with $\delta^{15}N$ near 0 ‰ [*Wada and Hattori*, 1976; *Saino and Hattori*, 1987; *Liu et al.*, 1996; *Karl et al.*, 1997; *Minagawa et al.*, 2001]. Because these processes are focused in the thermocline in the modern ocean, the thermocline tends to have much more regionally variable $\delta^{15}N\text{-}NO_3^-$; thermocline variations are essentially modifications of the deep NO_3^- by local processes. Thermocline nitrate wells up and becomes incorporated into organic matter, which then settles and is deposited in the underlying sediments. Therefore we can consider the N source to be a combination of two related, but subtly disconnected pools: a deep water source pool, and a thermocline pool derived from this deep NO_3^- and subsequently modified to some degree. We can take deep Southern Ocean nitrate as the best approximation of a well-mixed, global average, which - today – has an average $\delta^{15}N\text{-}NO_3^-$ of 4.8 ‰ [*Sigman et al.*, 2000]. At 2000 m in the subarctic Pacific, the $\delta^{15}N\text{-}NO_3^-$ is ~ 5.8 ‰ [*Casciotti et al.*, 2002; *Lehmann et al.*, 2005]. This shows a net increase in $\delta^{15}N$ during the transit of deep water across the basin, caused by denitrification in the thermocline of the eastern tropical Pacific, likely diluted to some extent by the addition of ^{15}N-depleted OM from N_2 fixation.

Today, denitrification in the thermocline of the eastern tropical Pacific is quite active, though it may be somewhat less vigorous than it was during the deglacial peak [*Pride et al.*, 1999; *Ganeshram et al.*, 2000; *Deutsch et al.*, 2004] (see also Chapter 4). Nitrate with initial $\delta^{15}N\text{-}NO_3^-$ close to the deep Pacific mean is refined, within the ETNP shadow zone, to produce waters with $\delta^{15}N\text{-}NO_3^-$ as high as 18 ‰ [*Brandes et al.*, 1998; *Voss et al.*, 2001]. The ^{15}N-enriched nitrate seeps out into the adjacent water masses, notably through the California undercurrent [*Liu and Kaplan*, 1989; *Kienast et al.*, 2002] and equatorial countercurrent [*Higginson et al.*, 2003].

3.2 Methods

3.2.1 $\delta^{15}N\text{-}NO_3^-$.

Water samples for $\delta^{15}N\text{-}NO_3^-$ analysis were collected on the February, 2003 Line P hydrographic cruise aboard the CCGS John P. Tully by staff of the Institute of Ocean Sciences (IOS) in Sidney, B.C. Subsamples were collected directly from the rosette into 1 L polypropylene bottles and sterilized by adding 5 mL 25 % HCl (reagent grade), lowering the pH to between 2 and 3. The bottles were then closed and stored at ambient temperature, until analysis at the University of British Columbia following the method of Sigman *et al.* [1997]. Briefly, a 200 mL aliquot of each sample was transferred into a Wheaton glass bottle and 0.500 g of pre-combusted (450 °C), finely powdered MgO was added to raise the pH. Each bottle was incubated at 60 °C for five days, uncapped, to convert NH_4^+ to gaseous NH_3 that escaped. Next, the samples were evaporated to 20 - 45 mL volume at 95 °C, and the volumes adjusted to 50 mL by addition of distilled, de-ionized water. Filter 'sandwiches' were assembled by enclosing a GFD filter, acidified with 25 µL phosphoric acid, between two circular Teflon™ membranes that were then sealed together by pressing firmly with an aluminium ring. One sandwich was placed, floating, in each bottle, and 0.1500 g Devarda's alloy was added before quickly and tightly sealing the lid. The sealed bottles were placed in a 60 °C oven for 10-14 days, and then placed on a circulating table for 14 days, in order to ensure complete conversion of nitrate to ammonia and subsequent trapping of ammonia as ammonium salt on the acidified filter. The sandwiches were then removed, rinsed in 10 % HCl (environmental grade), rinsed again in DDW, and placed in a dessicator alongside a small dish of concentrated phosphoric acid for 24 hours in order to dry the filters. The sandwiches were then disassembled and the GFDs were rolled in tin foil and pelletized before analysis of $\delta^{15}N$ by combustion (see below). Standard deviation for replicate analyses averaged 0.19 ‰ (1 σ, n=14). The single profile from August 1999 was also collected by IOS aboard the CCGS John P. Tully and $\delta^{15}N\text{-}NO_3^-$ measured at Princeton University using the "denitrifier" method [*Sigman et al.*, 2001; *Casciotti et al.*, 2002].

3.2.2 Bulk sediment geochemistry methods.

All bulk samples were freeze-dried and thoroughly ground in an agate mortar to ensure homogenization. Opal concentrations were determined using the method of *Mortlock and Froelich* [1989]. Si and Al were determined by X-ray fluorescence as described by *Calvert and Fontugne* [2001] and the Si/Al was ratio used to estimate opal concentrations where opal measurements were not available, using a polynomial regression of all available data from the GA core (when used, this is indicated as "calculated opal", see Appendix 3 for more information). Carbonate concentrations were determined by coulometry for the GA core [*McDonald*, 1997], and using an X-ray fluorescence core-scanner for WSG core ODP 882 [*Jaccard et al.*, 2005]. The $\delta^{15}N_{bulk}$ was measured by combustion using a Carlo Erba NC 2500 elemental analyzer coupled to a Finnigan Mat Delta Plus mass spectrometer, via a Finnigan Mat ConFlo III. The standard deviation of repeat measurements from the GA site was approximately 0.3 ‰ (1σ).

3.2.3 Diatom frustule-bound $\delta^{15}N$ method.

Diatoms were separated from the bulk sediment at the University of British Columbia as described in Appendix 1, and cleaned and analyzed at Princeton University. Two different cleaning methods were used to remove organic matter not protected within the diatom frustules; despite the problems with more recent and cultured diatoms discussed in Appendices 1 and 2, no significant difference was noted between results obtained using the different methods in these older sediments, and they are presented together here. One cleaning method involved multiple treatments of 30 % H_2O_2 as described by Robinson et al. [2004] while the other employed chemical oxidation with 70 % $HClO_4$ at 100 °C. The N content and $\delta^{15}N_{frustule}$ were determined by the "persulphate-denitrifier" method as described by Robinson et al. [2004]. This involved heating the sample in a solution of potassium persulfate and 1.5N NaOH, to dissolve the opal and oxidize the liberated organic N to nitrate. Nitrate concentration was then determined by chemiluminescence [*Braman and Hendrix*, 1989] and the N isotopic composition of the nitrate was measured via the "denitrifier" method [*Sigman et al.*, 2001].

3.2.4 Chronological control.

The chronology of the GA core is completely independent of those for the WSG sites. The ODP 887 (GA) age model is based on five radiocarbon dates over the upper 25.5 ky and, below, on a correlation of the low-resolution benthic foraminifera $\delta^{18}O$ record of McDonald {, 1997 #973} to the global stacked benthic $\delta^{18}O$ record of *Lisiecki and Raymo* [2005] (see Appendix 4 for more information). The ODP 882 (WSG) age model has two radiocarbon dates (11.7 and 13.8 ka), beyond which it is calibrated by correlation of the high-resolution Ba/Al record to Vostok δD [*Jaccard et al.*, 2005], with additional constraints from benthic foraminiferal $\delta^{18}O$ at Termination II (i.e. the penultimate deglaciation). The MD01-2416 (WSG) age model is based on 19 radiocarbon ages over the past 25 ky [*Sarnthein et al.*, in press], before which it is linked to ODP 882 at 14 points chosen by aligning high-resolution $CaCO_3$ records (not shown) with a linear correlation coefficient of 0.85 (T. Kiefer, pers. comm. 2005).

3.3 Modern water column N isotope dynamics

3.3.1 Line P $\delta^{15}N\text{-}NO_3^-$

Line P is a well-studied transect of twenty-six hydrographic stations from southern British Columbia to OSP, spanning the range from coastal waters on the upper slope to the HNLC waters at the centre of the Alaska Gyre. Our subsurface transect of $\delta^{15}N\text{-}NO_3^-$ from the southern B.C. coast to OSP (P26) shows a relatively homogeneous picture (Figure 3.2), with a total range of only 2.5 ‰, and an even smaller range of < 1.5 ‰ at any given depth. The most obvious departures from homogeneity are: 1) the shallowest samples have higher $\delta^{15}N\text{-}NO_3^-$; and 2) there is a region of high $\delta^{15}N\text{-}NO_3^-$ hugging the coast.

The high $\delta^{15}N\text{-}NO_3^-$ near the surface (at 100 m depth) represents residual nitrate following partial utilization of NO_3^- [*Altabet et al.*, 1991; *Sigman et al.*, 1999; *Lourey et al.*, 2003]. Although NO_3^- uptake occurs at shallower depths than this, deep winter mixing spreads the residual nitrate down the water column to some degree. The slightly depressed $\delta^{15}N\text{-}NO_3^-$ and elevated N* ($N^* = 0.87*(NO_3^- - 16\ PO_4^{3-} + 2.90\ \mu M)$, a gauge of processes that alter nitrate concentrations other than idealized uptake and remineralization [*Gruber and Sarmiento*, 1997]) at mode water depths (200 - 500m) may be due to incorporation of Kuro-

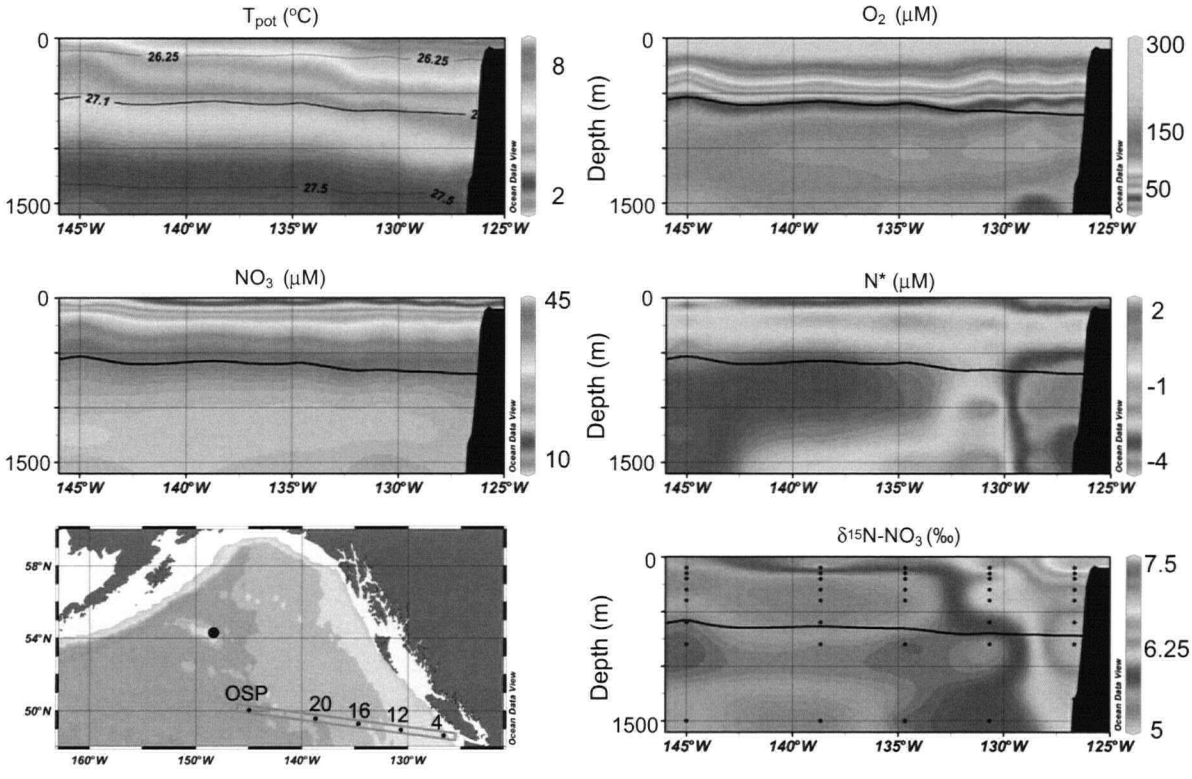

3.2: Water mass characteristics along Line P during February, 2003. Temperature, salinity and nutrient data were provided by the Institute of Ocean Sciences, Sydney, B.C. Stations with $\delta^{15}N\text{-}NO_3^-$ analyses are indicated on the map, where "4" is P4, and OSP is P26. Isopycnals are drawn as black contours, overlain on potential temperature (upper left panel), and the 27.10 kg m^{-3} isopycnal is shown as a black line in all panels. N* is calculated as $0.87*(NO_3^- - 16\ PO_4^{3-} + 2.90\ \mu M)$, following [Gruber and Sarmiento, 1997]. The $\delta^{15}N\text{-}NO_3^-$ is remarkably homogeneous (lower right, measurement locations given as black dots) with most values between 5.0 and 5.7 ‰. Markedly higher $\delta^{15}N\text{-}NO_3^-$ occurs in the shallowest samples, as well as at the two most coastal stations.

shio waters, containing recently fixed, low $\delta^{15}N\text{-}NO_3^-$ [*Liu et al.*, 1996]. Alternatively, this low $\delta^{15}N\text{-}NO_3^-$ layer may reflect the remineralization of low-$\delta^{15}N$, high N:P organic matter exported from the surface under incomplete utilization of surface nitrate. Though the detailed resolution of N isotopic cycling in the near-surface is beyond the scope of this study, the important observation is that there is not a strong gradient in $\delta^{15}N\text{-}NO_3^-$ from Station P to the coast, as might be expected were lateral transport of residual, ^{15}N-enriched nitrate from the HNLC Gyre to the coast significant; instead, the subsurface $\delta^{15}N\text{-}NO_3^-$ is quite homogeneous, with the exception of the two most coastal stations.

The California Undercurrent (CUC) is clearly visible at these coastal stations as a mass of warm, high salinity, low O_2 and low N* water centered over the slope at 400-1000 m depth. The $\delta^{15}N\text{-}NO_3$ shows a maximum of 6.5 ‰ at station P4 where it intersects the N* minimum of the deep CUC, at a density of $\sigma_\theta = 27.10$ kg m^{-3} (Castro et al., 2001). This is unsurprising, as the N* minimum and $\delta^{15}N$ enrichment both represent nitrate loss from the water column during denitrification in the ETNP [*Cline and Kaplan*, 1975; *Liu and Kaplan*, 1989]. Another profile from station P4 collected during August, 1999 (D. Sigman, unpublished), sampled the CUC during its annual peak flow and showed a larger enrichment, with a maximum value of 7.1 ‰, drawn toward the surface by summertime upwelling (Figure 3.3). The relationship between salinity and N*, Si and O_2 is remarkably well conserved when compared with the data compiled by Castro et al. [2001] (Figure 3.4) indicating that sedimentary denitrification, *in situ* oxygen consumption and/or local ventilation, and Si remineralization along the path of the CUC are negligible.

The CUC clearly provides an input of high $\delta^{15}N\text{-}NO_3^-$ into the subarctic Pacific. However, the California Current system does not continue north into the gyre, and the ribbon of low N* extending poleward along the coast does not penetrate significantly north of Line P (Castro, 2001). Instead, the CUC waters must be gradually advected offshore and mixed into the intermediate water circulation of the GA. Therefore, $\delta^{15}N\text{-}NO_3^-$ measured here for the CUC represents the ^{15}N-enriched endmember input to the Alaska Gyre.

3.3.2 $\delta^{15}N\text{-}NO_3^-$ in the vicinity of the GA sediment site

Although on the opposite side of the Gyre, the Line P transect illuminates the factors controlling subeuphotic zone $\delta^{15}N\text{-}NO_3^-$ in the vicinity of GA site. Subeuphotic zone nitrate

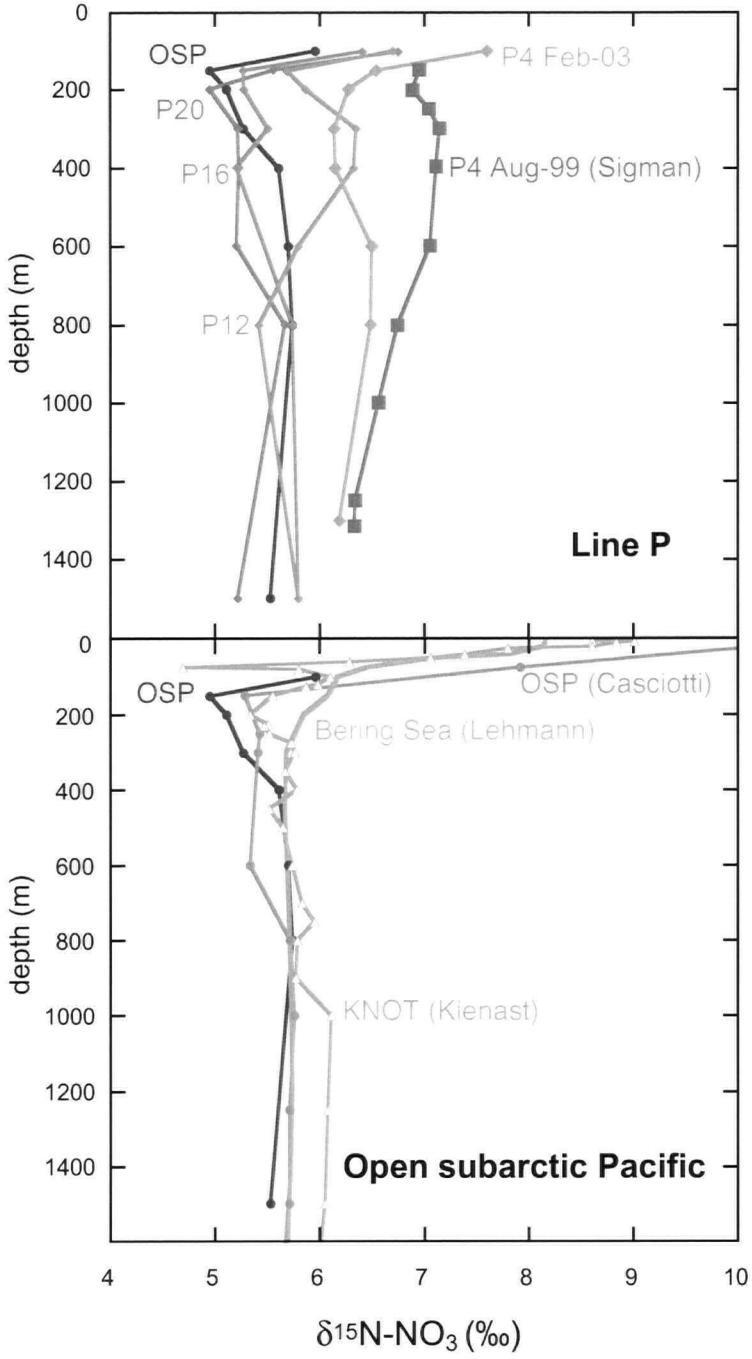

3.3: Profiles of $\delta^{15}N\text{-}NO_3^-$ spanning the subarctic Pacific. The upper panel shows the data from Line P, as in Figure 3.2, but including an additional profile from the most coastal station collected during August 1999 [D. Sigman, unpublished], when the California Undercurrent (CUC) flow was more vigorous. The lower panel shows, again, the February 2003 profile from OSP, in dark blue, along with a July, 1999 profile from OSP in pale blue [Casciotti et al., 2002], a profile from the WSG in orange [M. Kienast, unpublished], and the average Bering Sea profile of *Lehmann et al.* [2005]. Shallow ^{15}N-enrichments result from fractionation during incomplete nitrate consumption. Clearly, there is much more subsurface N isotopic variability between the southern B.C. coast and OSP than within the entire open subarctic Pacific.

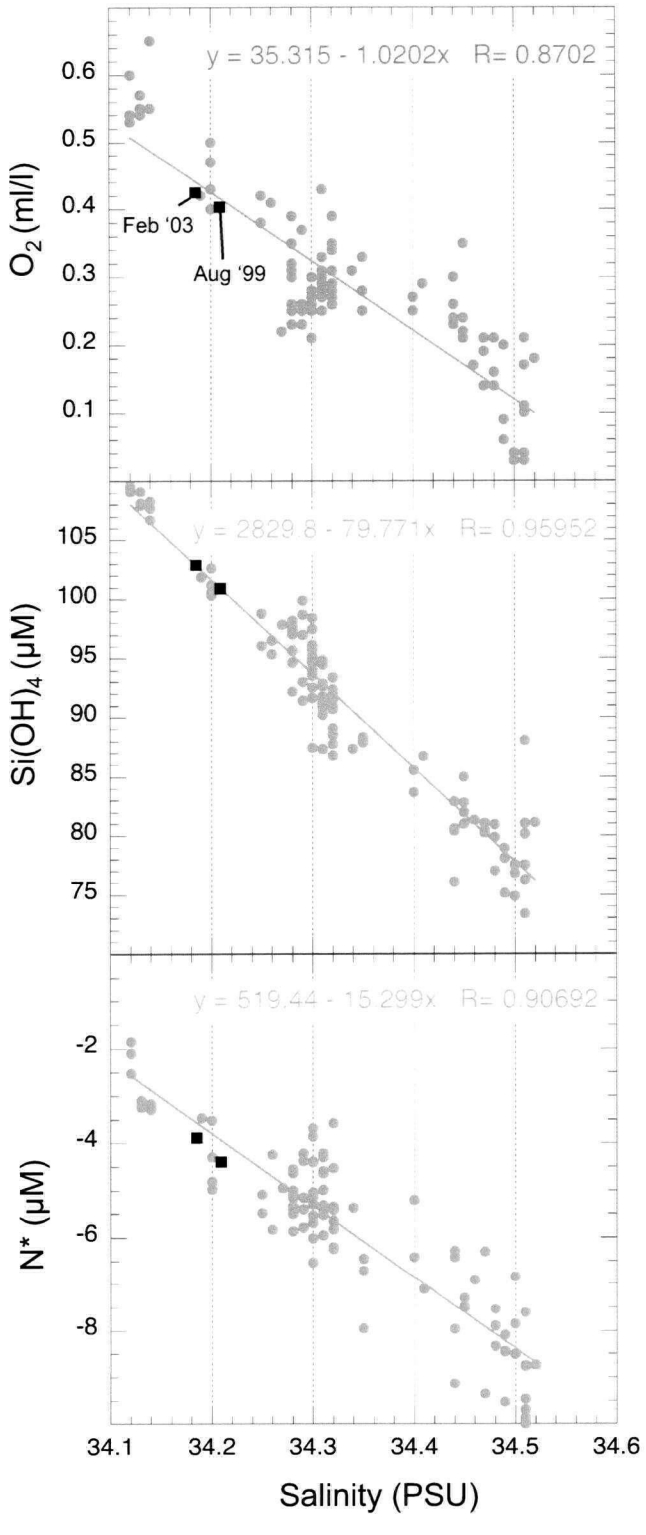

3.4 Water chemistry at 27.10 kg m^{-3} along the western margin of North America. Coloured circles show data from Baja California to Alaska as compiled by *Castro et al.* [2001] with linear regressions (equations as indicated). Black squares show the properties at station P4 using the data presented from the two cruises discussed in the text. The linearity of all relationships vs. salinity implies conservative mixing with negligible water mass alteration by biological processes during transit along the coast.

(200 - 500 m depth) in the central Gulf averages ~5.3 ‰, while near the B.C. coast, nitrate supplied by the upwelling of CUC water averages ~6.8 ‰. Most coastal nitrate is completely consumed on an annual basis (given abundant trace metals and a shallow mixed layer), and annual net Ekman transport is onshore; any offshore transport of coastal nitrate along Line P should be evident as a surface layer of ^{15}N-enriched NO_3^- in the transect shown here. Although there is some enrichment, it is not more than what would be expected for residual nitrate contributed from the HNLC region, particularly at OSP. The coastal-oceanic-transitional production captured at the GA site, located far from the CUC and in a region of intense domal upwelling, should thus be dominantly supported by open ocean nitrate. Considering these factors, we conservatively estimate a value of 5.8 ± 0.5 ‰ as the $\delta^{15}N\text{-}NO_3^-$ of the modern source waters delivered to the mixed layer at the GA site.

3.3.3 Comparing WSG to GA and the Bering Sea

Figure 3.3 shows the $\delta^{15}N\text{-}NO_3^-$ measured in the central Alaskan Gyre at OSP, both the February, 2003 data presented in this study and the July, 1999 data of [*Casciotti et al.*, 2002], as well as a profile collected near Site 882 in the WSG and the average Bering Sea profile of [*Lehmann et al.*, 2005]. Although there are some differences over several depth intervals, on the order of 0.2 ‰, these are near the range of analytical error, and the four profiles are almost indistinguishable over the range of 300 to 900 m. In fact, there is more variability between Line P stations P12 and OSP than between these three sites that represent the entire subarctic Pacific over a multiannual period. Clearly, despite the large contrast in $\delta^{15}N\text{-}NO_3^-$ between the Kuroshio thermocline and that of the California Undercurrent today, the subarctic Pacific subsurface $\delta^{15}N\text{-}NO_3^-$ is remarkably homogeneous. This testifies to the effective circulation of near-surface waters within the subarctic Pacific relative to the rate of external nitrate inputs: the circulation subdues regional isotopic variability.

3.4 Sediment records

3.4.1 Paleoproductivity context

There have been spectacular variations in the proportion of biogenic components in subarctic sediments over the past few million years (e.g. [*Rea et al.*, 1993; *Haug et al.*, 1999]) and continuing through the last few glacial cycles (e.g. [*McDonald et al.*, 1999; *Na-*

rita et al., 2002; *Katsuki et al.*, 2003; *Kienast et al.*, 2004; *Jaccard et al.*, 2005]). As shown in Figure 3.5, during the past 150 ky opal concentrations have spanned a tremendous range, between <10 and >70 %, while calcium carbonate contents have ranged from being undetectable to as high as 40 %. The preservation of these phases in sediments is not linearly related to the export flux of carbonate or opal from the surface; carbonate preservation is very strongly determined by the depth of the lysocline, while opal shows a nonlinear preservation ([*Ragueneau et al.*, 2000] and references therein). Nonetheless, these are second order effects, particularly for opal [*Pondaven et al.*, 2000], and the variations in opal concentration are so large (more than one order of magnitude) that they can be safely assumed to reflect changes in export production. ^{230}Th-normalized accumulation rates have confirmed this, showing changes in mass accumulation-rate of opal of more than 20-fold that closely match the opal concentration changes over the period 50 - 110 ka [*McDonald et al.*, 1999].

The top of the GA core, which is probably no more than a few centuries old [*McDonald*, 1997] has relatively low concentrations of $CaCO_3$ (< 5 %) and moderately low concentrations of opal (< 20 %). Despite the uncertain relationship between export and preservation, the core top values can be taken as indicating that modern environmental conditions are generating a low-to-moderate flux of biogenic materials in the vicinity of the GA core, relative to the past 150 kyr. This is consistent with the micropaleontological reconstruction of *deVernal and Pedersen* [1997], who inferred relatively low productivity from the uppermost sediment of nearby core PAR 87A-10 (raised from within 2 km of the GA site).

The large variations in biogenic components shown in Figure 3.5 do not appear to be synchronous between the WSG and GA, as far as can be distinguished with the available time control. Despite the differences, it is clear that biogenic components are very minor constituents of the sediments at both sites during generally cold periods: early Marine Isotope Stage (MIS) 2, late MIS 3, MIS 4 and MIS 5d. Conversely, biogenic components were delivered to the sediment at high rates during the deglaciation and early Holocene, early MIS 3, late MIS 5 and the penultimate deglaciation through the Eemian. It should be noted that the age control during 60 - 110 ka in the GA record is poor, due to the low-resolution $\delta^{18}O$ stratigraphy and large changes in accumulation rate; the low-opal shown at 90 - 100 ka may in fact be ~10 ka younger, such that it falls during MIS 5b. On the whole, the evidence points towards minimal export production from the subarctic Pacific during globally cold periods,

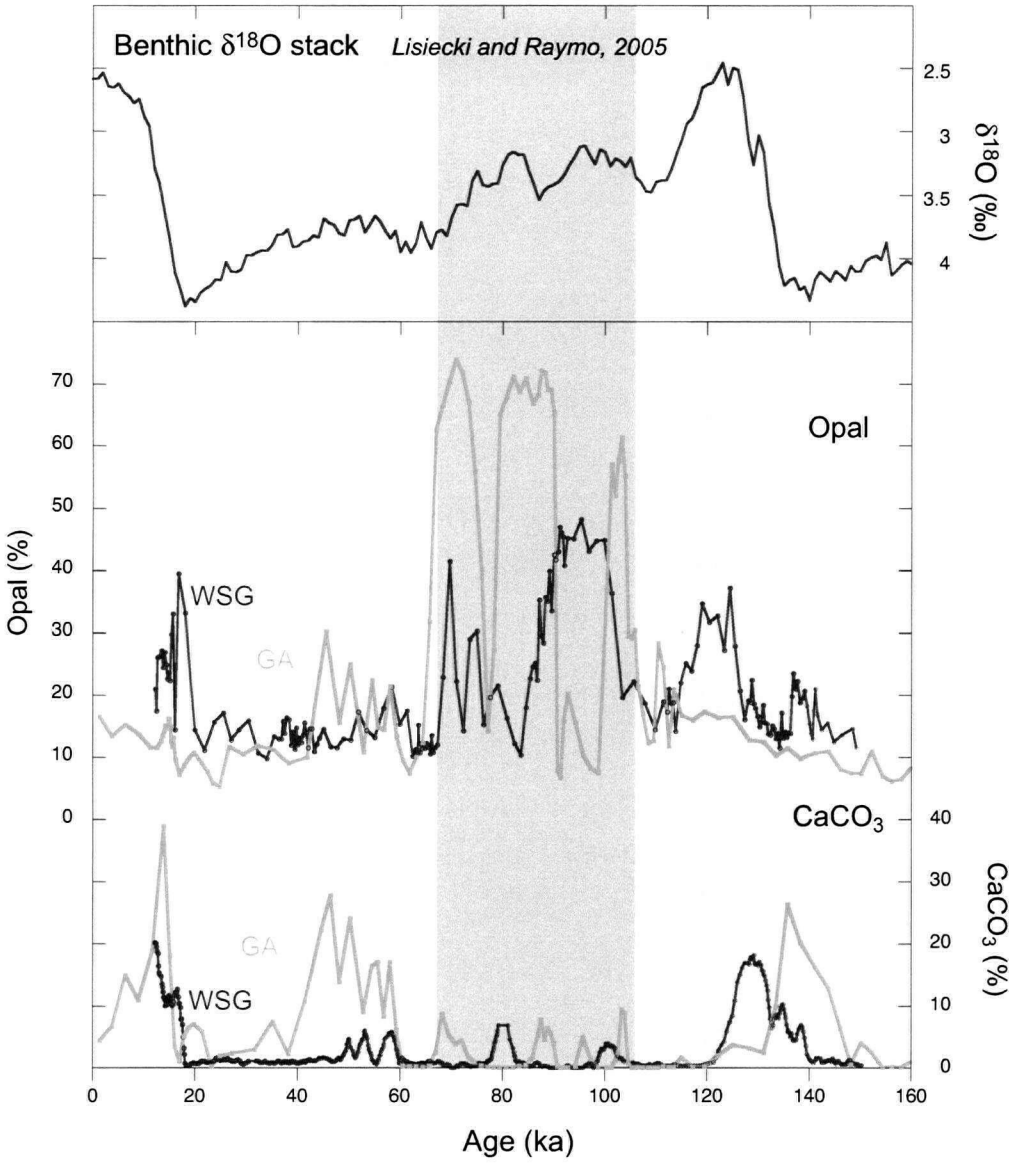

3.5: Variations in the concentrations of biogenic components in the subarctic Pacific sediments over the past 150 ky. The WSG data are as measured in ODP 882. Orange shadings indicate periods of moderately high biogenic concentrations, while the green shading indicates a period of extremely high biogenic concentrations. See text for discussion.

though the highest opal concentrations are found not during the warmest periods, but during glacial advances.

3.4.2 Nitrogen isotopes: Conceptual framework

We define the $\delta^{15}N$ of the nitrogen substrate supplied to the euphotic zone as $\delta^{15}N_{nitrate}$ and the average $\delta^{15}N$ of all N sinking out of the euphotic zone as $\delta^{15}N_{export}$. If we assume a closed system at steady state (applicable to multi-annual timescales), and further assume that N inputs to and outputs from the euphotic zone are entirely accounted for by nitrate and sinking particulate matter, respectively, internal cycling of nitrogen within the euphotic zone has no impact on $\delta^{15}N_{export}$. Given these assumptions, the difference between $\delta^{15}N_{nitrate}$ and $\delta^{15}N_{export}$ is due to fractionation by phytoplankton during incomplete nitrate consumption, referred to here as relative nitrate utilization (RNU) [*Altabet and Francois*, 1994]. The $\delta^{15}N$ of all combustible N in sediment is $\delta^{15}N_{bulk}$. The difference between $\delta^{15}N_{export}$ and the corresponding $\delta^{15}N_{bulk}$ eventually measured is due to 'diagenesis', and includes any N-isotope fractionating processes that affect N during sinking and burial in sediment, such as partial consumption by heterotrophs and the addition of exogenous, isotopically distinct N. Diagenesis is further separated into two phases: that which occurs in contact with the water column (including the sediment-water interface, $DIAG_{WC}$), and that which occurs post-burial ($DIAG_{PB}$). This framework can be expressed as

$$\delta^{15}N_{bulk} = \delta^{15}N_{nitrate} - RNU + DIAG_{WC} + DIAG_{PB} \quad (3.1)$$

and is schematically depicted in Figure 3.6. Note that the low sea surface temperatures and weak insolation of the subarctic Pacific are likely to preclude N_2 fixation, and potential isotopic effects of local N_2 fixation are not considered here.

3.4.3 Nitrogen isotopes: General features of the three records

Figure 3.7 shows the $\delta^{15}N_{bulk}$ records from the three cores for the past 150 ka. The two WSG records are very similar and show the same general features, with minor deviations. The WSG records are also very similar to the Bering Sea diatom frustule-bound ($\delta^{15}N_{frustule}$) record of Brunelle et al. (AGU poster, 2004). The GA record shares some com-

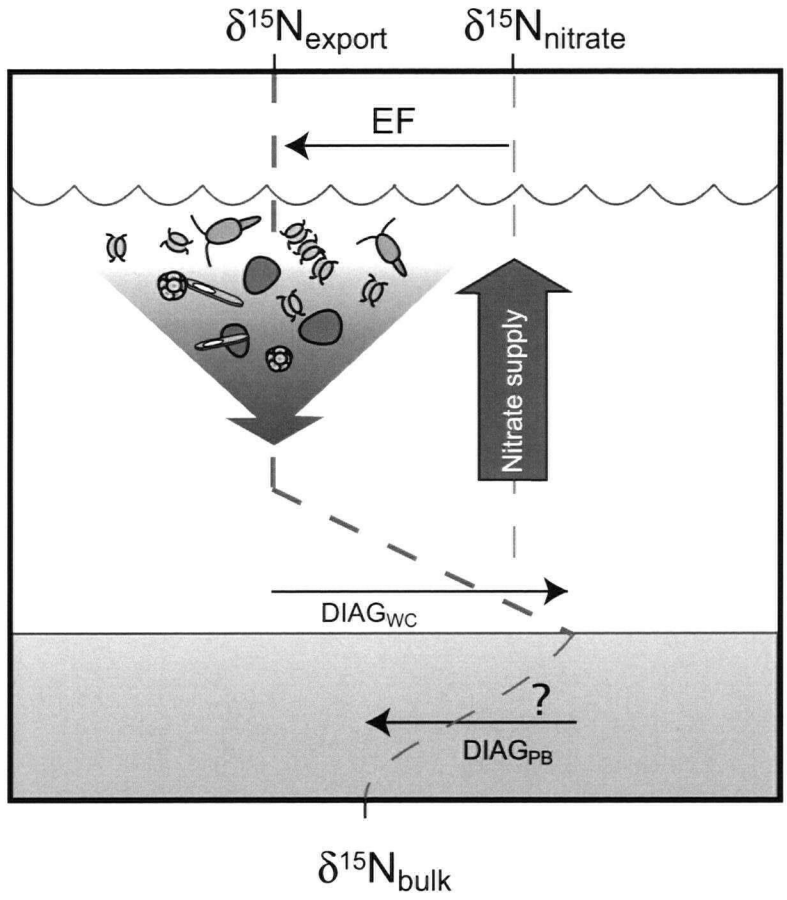

3.6: Conceptual diagram of $\delta^{15}N$ components and transformations. $\delta^{15}N_{nitrate}$ is the isotopic composition of the nitrogen substrate supplied to the mixed layer over a given time interval. $\delta^{15}N_{export}$ is the integrated isotopic composition of all nitrogen exported over the same time interval. The difference between $\delta^{15}N_{nitrate}$ and $\delta^{15}N_{export}$ is due to Export Fractionation, EF, a sum of Rayleigh-type fractionation processes and trophic cycling. $\delta^{15}N_{bulk}$ is the isotopic composition of all combustible N in sediment. The difference between the $\delta^{15}N_{bulk}$ of a given sediment interval and the corresponding $\delta^{15}N_{export}$ is due to diagenesis both in the water column ($DIAG_{WC}$) and post-burial ($DIAG_{PB}$). See text for discussion.

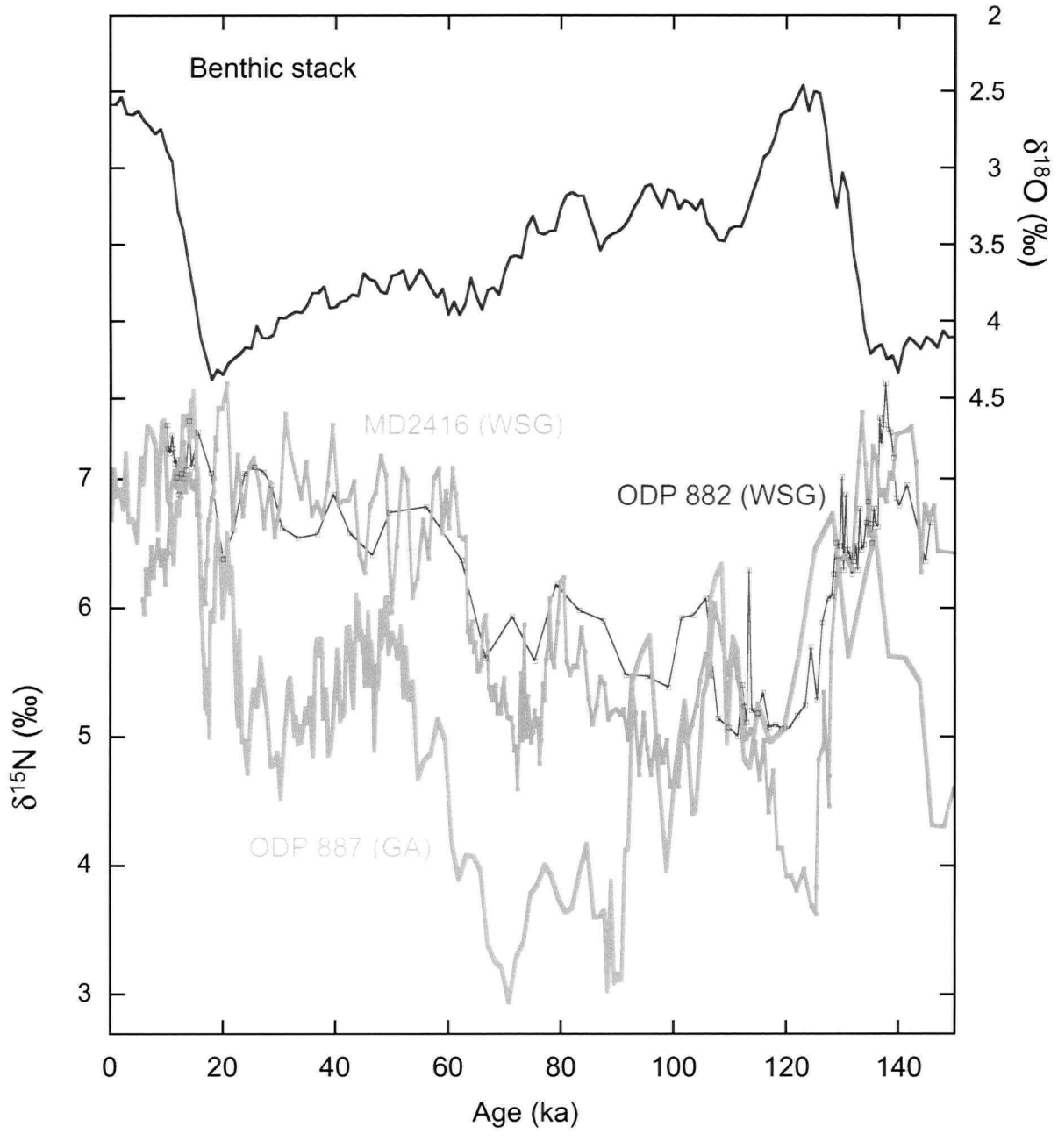

3.7: Three $\delta^{15}N_{bulk}$ records from the subarctic Pacific covering the past 150 ky. The three lower curves show $\delta^{15}N_{bulk}$, with the two WSG sites shown as blue open squares (ODP 882) and purple filled squares (MD01-2416, Kienast et al., unpubl.) and the GA site shown as an orange line with no symbols (ODP 887). The upper, dark grey curve is the benthic $\delta^{18}O$ stack of *Lisiecki and Raymo* [2005] as a proxy for global climate. See text for discussion.

mon features with the WSG, particularly the elevated values during deglaciations, low values between 60 and 100 ka, and a rapid increase near 60-70 ka. However, the GA record also differs substantially. For example, the GA $\delta^{15}N_{bulk}$ is very low between 65 and 90 ka, increasing in one step to intermediate values at ~ 60 ka and increasing again at 22 - 12 ka; meanwhile, the WSG $\delta^{15}N$ increases gradually from a minimum prior to 110 ka to a noisy but grossly consistent plateau, remaining nearly unchanged from the glacial maximum through to the early Holocene.

The GA record, on the other hand, is far more similar to $\delta^{15}N_{bulk}$ records from the North American margin including those from Oregon [*Kienast et al.*, 2002] and California [*Hendy et al.*, 2004] (Figure 3.8). Despite a few notable differences, the overall trends at the GA site are clearly correlated with the changes in $\delta^{15}N_{nitrate}$ along the Western North American margin.

Figure 3.9 shows the full records of the WSG and GA, extending back to 742 ka. A climate link is not immediately clear from the full $\delta^{15}N_{bulk}$ GA record; it has a good deal of variability not clearly related to the previously observed glacial-interglacial pattern of regional changes in $\delta^{15}N_{nitrate}$, shown to reflect increases in thermocline denitrification during more recent periods of ocean warming ([*Ganeshram et al.*, 2000; *Liu et al.*, 2005], Chapter 4). However, the additional variability can be attributed in large part to extreme changes in diatom export that punctuate the history of the site [*McDonald et al.*, 1999]. The opal-rich layers appear to be due to large changes in the surface environment, but there is no consistent relationship between $\delta^{15}N_{bulk}$ and the abundance of opal. It seems likely that these layers are caused by large increases in the supply of nutrients to the surface, so that diatoms become variously limited by the availability of light, macronutrients or micronutrients. As a result, the degree of nitrate utilization within these layers is highly variable. However, if all high opal samples are removed from the record, the remaining $\delta^{15}N_{bulk}$ peaks appear to occur during periods of global warming, within the error of the age model (Figure 3.10). This is consistent with a high fidelity of the GA record as a monitor of regional NE Pacific $\delta^{15}N_{nitrate}$. Meanwhile, the WSG record between 340 and 450 ka has a different pattern than the GA record, just as it does during the past 150 ka.

The contrast between the WSG and GA is intriguing. It is conceivable that the differences between the WSG and GA are due to difference in $\delta^{15}N_{nitrate}$, with the WSG site repre-

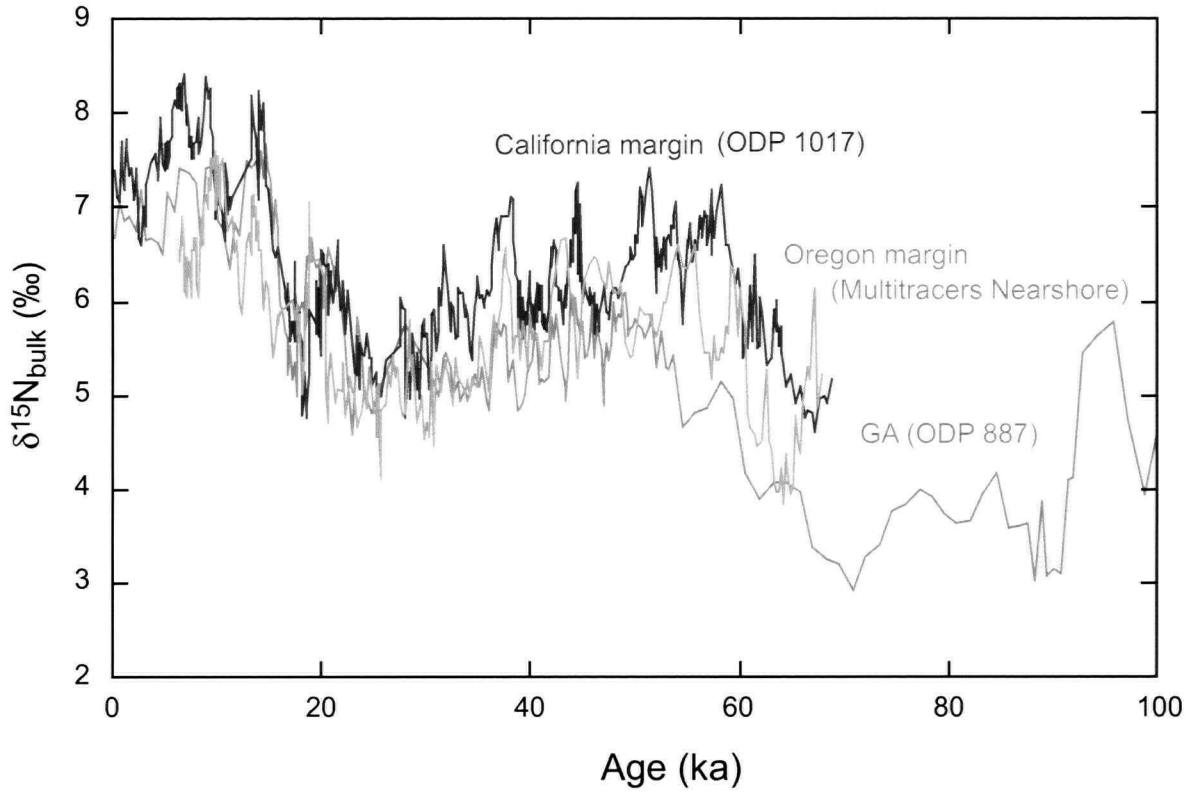

3.8: Parallel changes in $\delta^{15}N_{bulk}$ records throughout the NE Pacific. The GA record is shown in orange, the California margin record of *Hendy et al.* [2004] (ODP Site 1017) is shown in blue, and the *Kienast et al.* [2002] record from the Oregon margin (nearshore, W87-09-13PC) is shown in green. Note that all records are shown on the same vertical axis.

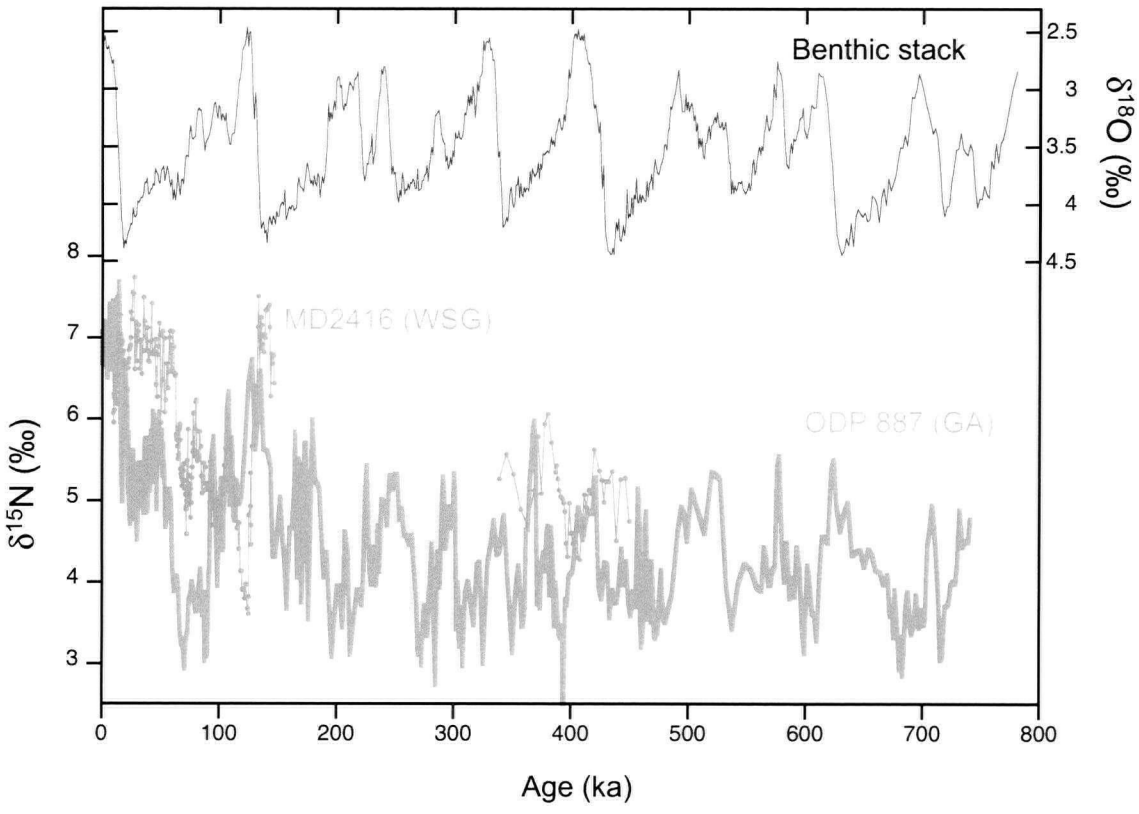

3.9: Two $\delta^{15}N_{bulk}$ records from the subarctic Pacific over the past 742 ky. The two lower curves show $\delta^{15}N_{bulk}$, with the WSG site shown as filled purple circles (MD01-2416, Kienast et al., un-publ.) and the GA site shown as a thick orange line with no symbols (ODP 887). The upper, dark grey curve is the benthic $\delta^{18}O$ stack of *Lisiecki and Raymo* [2005] as a proxy for global climate. See text for discussion.

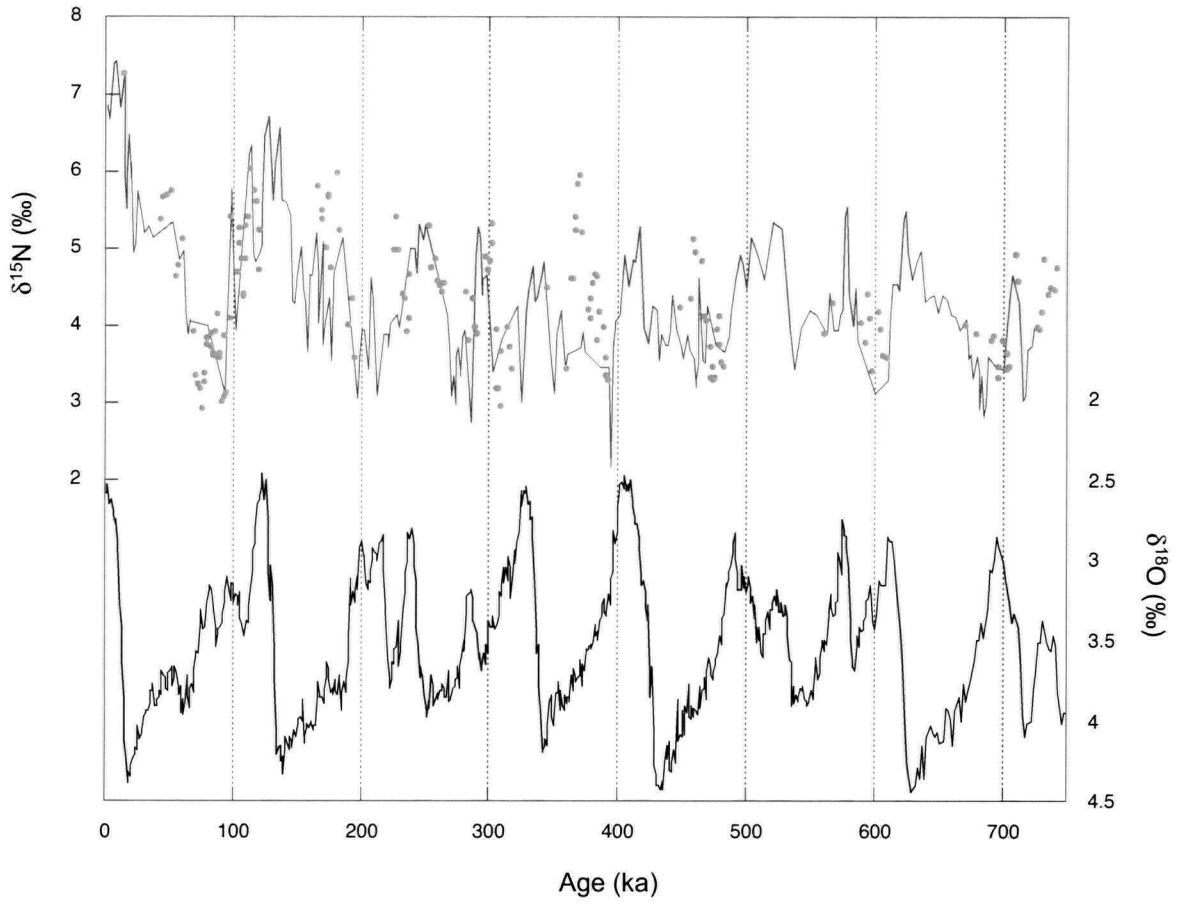

3.10: GA $\delta^{15}N_{bulk}$ record with and without high opal samples. The blue curve shows the $\delta^{15}N_{bulk}$ record from the GA after removing all samples for which opal concentrations are greater than 16%. The $\delta^{15}N_{bulk}$ measurements of >16% opal samples are shown as brown circles. The orange-shaded vertical bars indicate global periods of warming, as identified by the benthic $\delta^{18}O$ stack of *Lisiecki and Raymo* [2005] (bottom), during which the blue curve shows high $\delta^{15}N_{bulk}$. This is consistent with elevated $\delta^{15}N_{nitrate}$ due to enhanced thermocline denitrification during periods of oceanic warming.

senting a western subarctic Pacific – Bering Sea nitrate pool, and the GA representing a North American margin nitrate pool. However, the modern water column data show that the $\delta^{15}N_{nitrate}$ is almost identical at the two sites (Section 3.3.3, Figure 3.4), even though the modern subarctic Pacific receives isotopically distinct end member inputs from the Kuroshio current (low $\delta^{15}N\text{-}NO_3^-$) and California Undercurrent (high $\delta^{15}N\text{-}NO_3^-$). The only way for the $\delta^{15}N_{nitrate}$ at the two sites to have significantly diverged in times past would have been by dramatic alteration of the circulation, such that the mode/intermediate waters of the GA were divorced from those of the WSG. Although this is an interesting possibility, there is no evidence to support it, and thus it will not be considered further here. Instead, it is assumed that the modern pan-subarctic isotopic homogeneity is representative of the past 500 ka, such that both sites were supplied with the same $\delta^{15}N_{nitrate}$ within 0.5 ‰ throughout the past 150 kyr. Accordingly, the differences in $\delta^{15}N_{bulk}$ must be related to relative nitrate utilization and/or diagenesis. We now examine these processes in greater detail.

3.5 Diagenesis

In order to better understand these records, the effects of diagenesis must first be addressed. It has been shown that $DIAG_{WC}$ results in an enrichment of ^{15}N in deep, well-oxygenated, slowly accumulating sediments [*Altabet and Francois*, 1994; *Holmes et al.*, 1999; *Freudenthal et al.*, 2001a], such as those presented here. $DIAG_{PB}$ has little effect in rapidly accumulating sediments [*Prokopenko*, 2005]; however, its effect in slowly accumulating, deep sediments has not been determined.

3.5.1 Evaluating $DIAG_{PB}$

Figure 3.11 shows the full GA and WSG records, vs. depth, alongside three other published deep-sea $\delta^{15}N_{bulk}$ records, all of which are located at substantial distances from the coast. There is a clear trend from ^{15}N-enriched values at the core tops to lower $\delta^{15}N_{bulk}$ at greater depth, of similar magnitudes in all cores (1-2 ‰ over the upper 10 m). This is particularly striking given the fivefold range in accumulation rates: the upper 10 m of the Equatorial Pacific core represents 570 ka while the upper 10 m of the WSG core represents only 110 ka. Thus, this is not a global trend in the isotopic composition of marine nitrogen cycle over time, but is most likely an artifact of burial that varies as a function of burial depth.

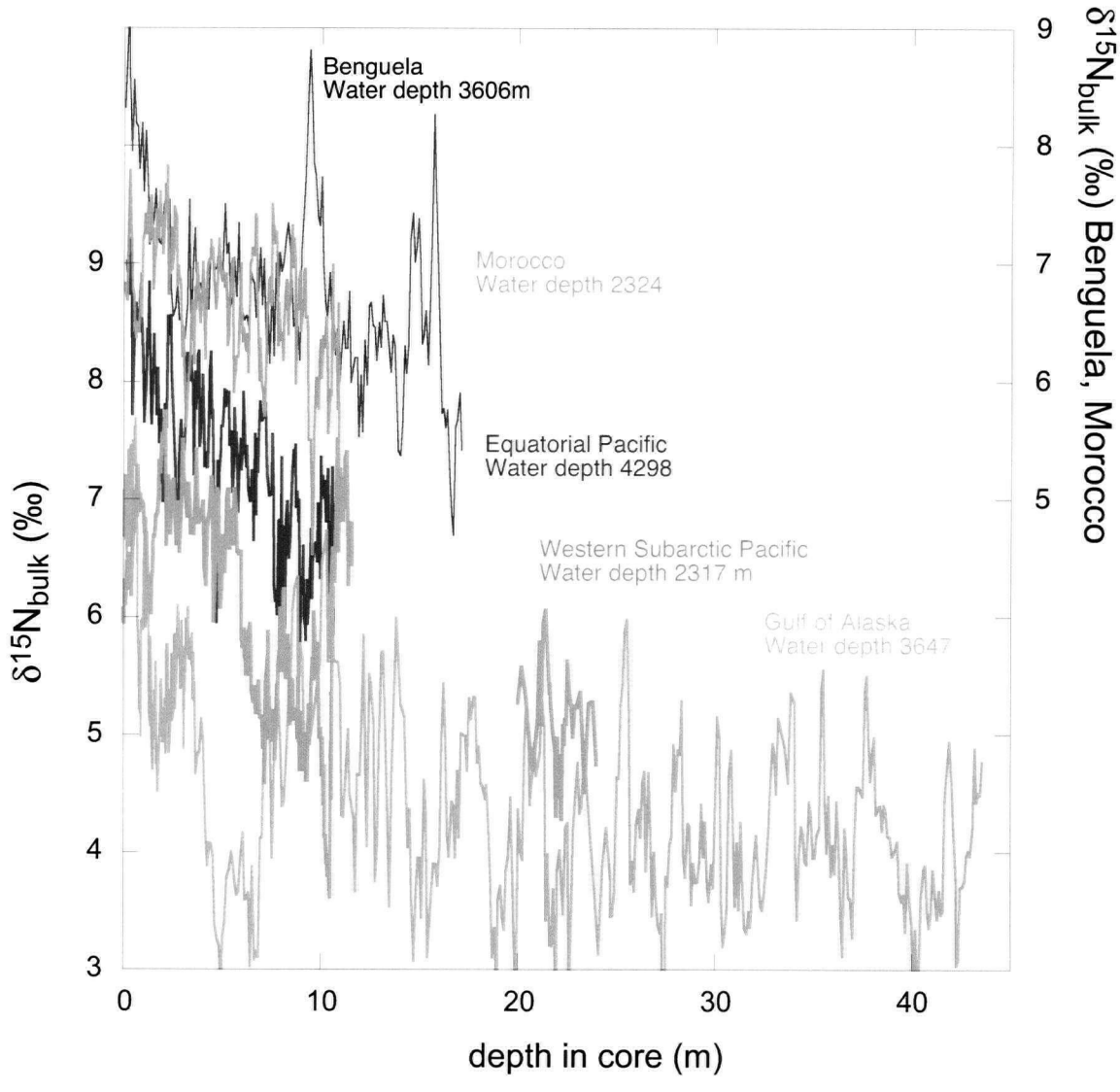

3.11: Five globally-distributed long $\delta^{15}N_{bulk}$ records. Each curve shows a $\delta^{15}N_{bulk}$ record from a deep site at a significant distance from the shelf break, at which sediments accumulate slowly. The grey curve is MD96-2086 near Namibia [Bertrand et al., 2000], khaki is GeoB-4216 from near Morocco [Freudenthal et al., 2002], blue is PC-72 from the equatorial Pacific [Altabet, 2001], purple is MD01-2416 (Kienast et al., unpubl.) from the WSG and orange is 887 from the GA. The records are plotted vs. depth, thus the parallel decreases in $\delta^{15}N_{bulk}$ cannot represent a climatic signal, but more likely represent post-burial diagenesis (see text for discussion).

The GA core is by far the longest of the available records and shows what appears to be a typical decrease in $\delta^{15}N_{bulk}$ over the upper 10 – 20 m, but below this there does not appear to be any trend. In order to quantify the long-term $DIAG_{PB}$ change that lies behind the "noise" of the climate signal, which is apparently dominated by a glacial-interglacial cyclicity, the record (with high-opal intervals removed) was divided into discrete climate cycles, with divisions placed at late interglacial times (Figure 3.12). The average calculated for the uppermost cycle is 1.3 ‰ higher than the average calculated for the lower five cycles (the average $\delta^{15}N_{bulk}$ below 20 m is 4.1 ‰). Considering that $DIAG_{PB}$ is almost certainly due to microbial transformations of N, it seems likely that the process proceeds as approximated by the general formulation of Berner (e.g. [*Rabouille and Gaillard*, 1991]), using the form

$$\partial C/\partial t = - R_{max} * C / (K_m + C) \qquad (3.2)$$

where t is replaced by depth and C is, in this case, $\delta^{15}N_{bulk}$. This equation readily fits the observed averages (Figure 3.13) when the initial C is 2, suggesting that the total magnitude of $DIAG_{PB}$ is on the order of 2 ‰ from the core top to 20 m depth. This matches well with the ~ 2 ‰ decrease in $\delta^{15}N_{bulk}$ observed by [*Prokopenko*, 2005] at ODP Site 1238 (2000 m depth, ~ 200 km offshore). It should be emphasized that this is not a mechanistically-based relationship, but an arbitrary fit using a logical equation, and is merely intended to highlight a diagenetic tendency which is clear in the GA record. As such, it can be subtracted from the original record to produce a detrended $\delta^{15}N$ record (Figure 3.14). This detrended record strongly parallels the $\delta^{15}N_{bulk}$ variations on the North American margin. However, the lack of a mechanistic foundation for the detrending equation precludes its wholesale adoption, and requires further research into the microbial underpinnings that are beyond the scope of this work. Although the detrended record may offer a more accurate representation of the subarctic Pacific response to past climate change, it is not discussed further here, nor is it used in any of the calculations that follow.

3.5.2 Evaluating $DIAG_{WC}$

The magnitude of $DIAG_{WC}$ can be assessed by comparing available sediment trap data to $\delta^{15}N_{nitrate}$ and core-top $\delta^{15}N_{bulk}$. At the WSG site, a sediment trap at 5000 m collected

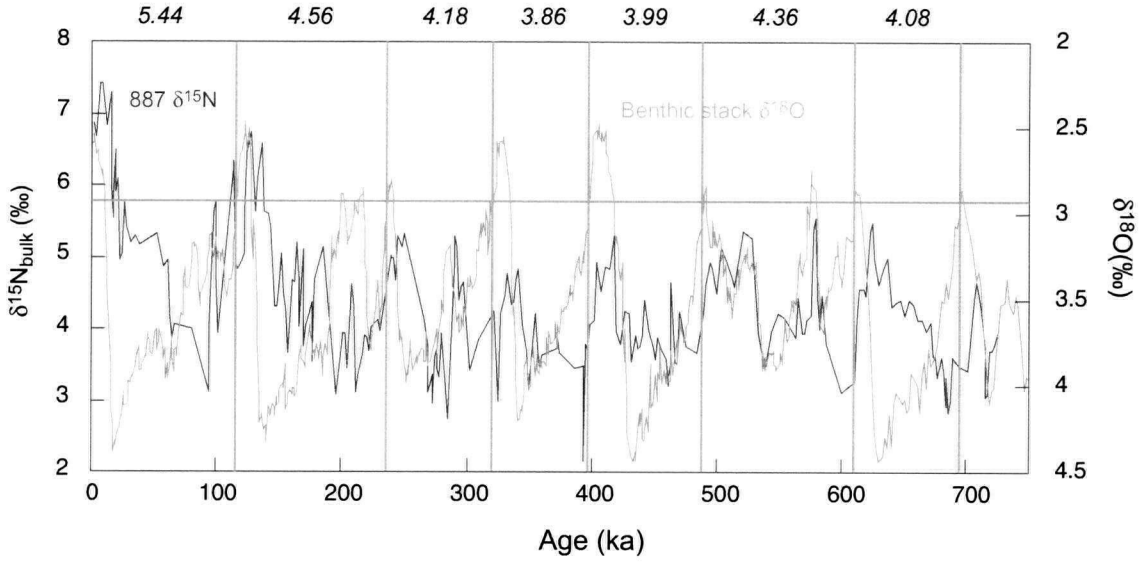

3.12: The Gulf of Alaska $\delta^{15}N_{bulk}$ record over successive climate cycles. The $\delta^{15}N_{bulk}$ record from GA core ODP 887B is shown (with all high (>16 %) opal intervals removed) as a blue curve. The benthic $\delta^{18}O$ stack of *Lisiecki and Raymo* [2005] is shown as a pale grey line. The horizontal grey line indicates the $\delta^{18}O$ used as a signature of late interglacial climate conditions. The $\delta^{15}N_{bulk}$ record is divided where $\delta^{18}O$ intersects this threshold on glacial inception, into the seven bins as shown by the grey vertical lines. The average $\delta^{15}N_{bulk}$ of each bin is listed in italics at the top of the figure.

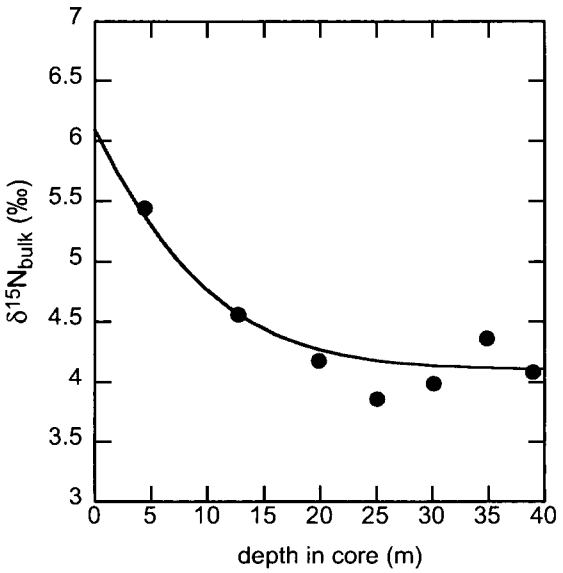

3.13: Diagenetic alteration of $\delta^{15}N_{bulk}$ with increasing depth in the Gulf of Alaska core. The green filled circles are the average $\delta^{15}N_{bulk}$ binned values from Figure 3.12. The green curve represents the postburial diagenetic trend, fit to the average values as described in the text.

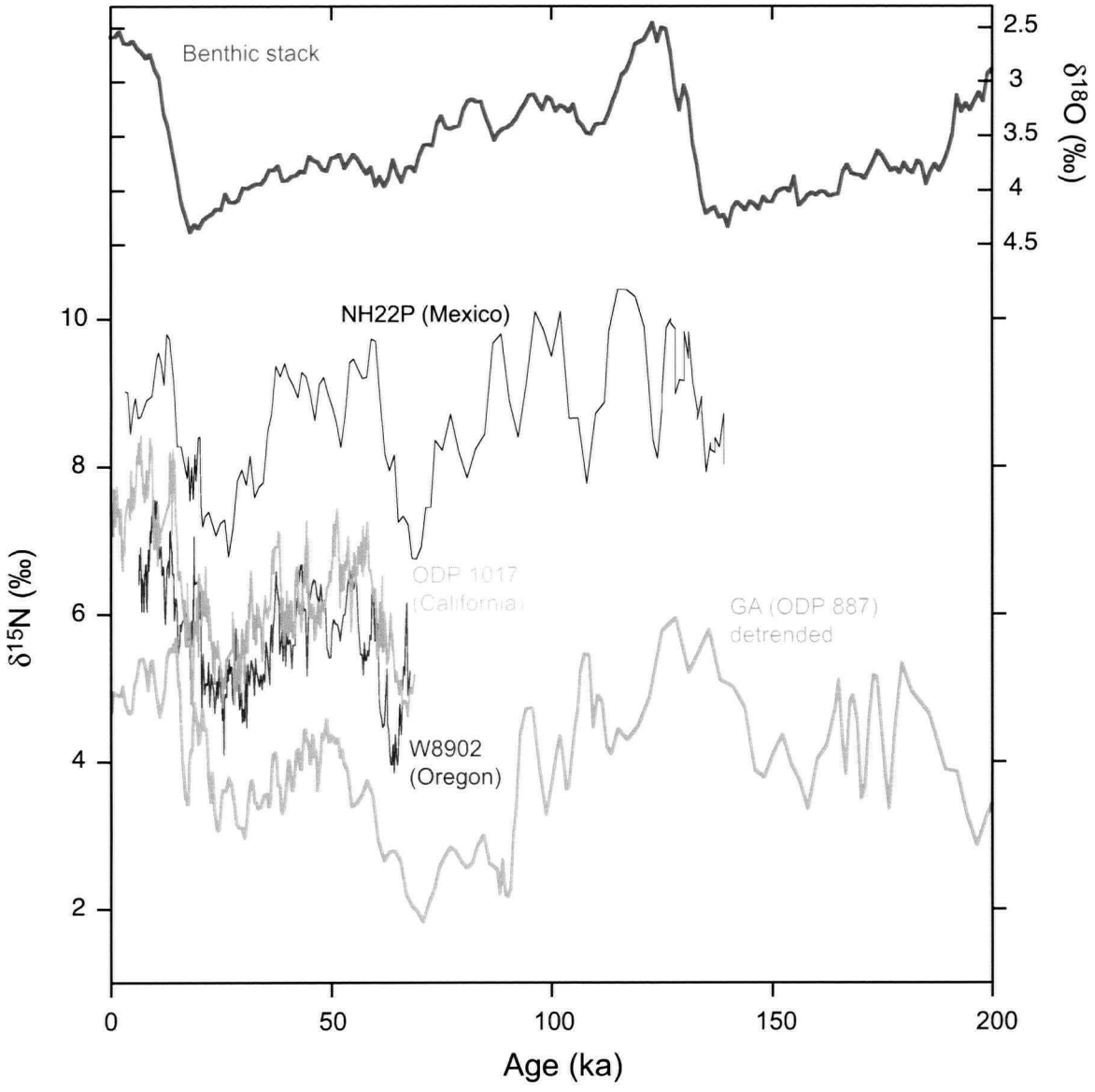

3.14: The detrended GA $\delta^{15}N_{bulk}$ record in a regional context. The orange curve shows the $\delta^{15}N_{bulk}$ record for the GA core, with the postburial diagenetic trend illustrated in figure 3.13 removed. Also shown are records from the California margin [Hendy et al., 2004], Oregon [Kienast et al., 2002], Mexico [Ganeshram et al., 1995], and a benthic $\delta^{18}O$ stack [Lisiecki and Raymo, 2005] as a proxy for global climate.

sinking particulate nitrogen with annually averaged $\delta^{15}N$ of 3.5 ± 0.2 ‰ (Markus Kienast, unpublished data), presumed here to reflect $\delta^{15}N_{export}$ accurately. Although the core top was not recovered in either WSG core, the most recent value of 6.1 ± 0.3 ‰ in MD01-2416 (ca. 6-8 ky before present) suggests that $DIAG_{WC}$ has caused an enrichment of 2.6 ± 0.5 ‰.

It is difficult to estimate the $DIAG_{WC}$ at the GA site, as there are no sediment trap data available from the immediate location. However, given eq. (1) and the fact that $DIAG_{PB}$ is zero at the core top, the difference $\delta^{15}N_{bulk} - \delta^{15}N_{nitrate}$ is equal to $DIAG_{WC}$ – RNU. Since $\delta^{15}N_{nitrate}$ is 5.8 ± 0.5 ‰ (see 3.3.2) and the core top $\delta^{15}N_{bulk}$ is 6.9 ± 0.2 ‰ (average of samples < 1 ky before present), $DIAG_{WC}$ is equal to RNU + 1.1 ± 0.7 ‰. At OSP, where $\delta^{15}N_{nitrate}$ is 5.3 ± 0.1 ‰, an 8-year study of sinking particulate N at 3800 m gave an average $\delta^{15}N$ of 2.8 ± 0.1 ‰ [*Wu et al.*, 1999], suggesting a modern RNU at OSP of 2.5 ± 0.2 ‰. As discussed in section 3.1.2, sediment at the GA site represents at least twice as much seasonal drawdown of nitrate than OSP, and may tend to reflect complete nitrate utilization. A conservative estimate for RNU at the GA site of 0.6 ± 0.6 ‰ therefore suggests $DIAG_{WC}$ is 1.7 ± 1.3 ‰.

3.5.3 Potential for downcore variations in diagenesis

The inference of such significant diagenetic alteration raises the spectre of rapid and time-variable changes in diagenesis. Fortunately, the GA core provides an excellent means by which to evaluate this possibility. The diatom-rich layers that punctuate the background of hemipelagic clay have been shown to accumulate up to an order of magnitude more rapidly [*McDonald et al.*, 1999] and in nearby core PAR87A-01 (at a distance of 64.1 km from Site 887, see Table 1), opal content is strongly correlated with Mo, a trace metal that is enriched in reducing sediments [*Calvert and Pedersen*, 1993]. This suggests that the oxic/anoxic boundary migrated upward toward the sediment-water interface during periods of rapid diatom sedimentation and that associated sulphate reduction produced sufficient HS^- to support sequestration of Mo species [*Helz et al.*, 1996; *Erickson and Helz*, 2000]. Given a host of observations suggesting that diagenesis produces little or no ^{15}N-enrichment in rapidly accumulating, oxygen-poor sediments [*Altabet et al.*, 1999; *Sachs and Repeta*, 1999; *Freudenthal et al.*, 2001b; *Lehmann et al.*, 2002; *Prahl et al.*, 2003; *Thunell et al.*, 2004], one would ex-

pect that, were diagenesis prone to rapid variation at the GA site, it would do so across the interval shown here.

The N isotopic composition of the organic matter bound within diatom frustules ($\delta^{15}N_{frustule}$) represents an N component that is immune to diagenesis (Chapter 2, Appendix 1). The difference between $\delta^{15}N_{frustule}$ and $\delta^{15}N_{bulk}$ ($\Delta^{15}N_{frustule\text{-}bulk}$) therefore reflects the sum of diagenesis and any difference between $\delta^{15}N_{export}$ and $\delta^{15}N_{frustule}$ (Chapter 2). The $\delta^{15}N_{frustule}$ is generally higher than the corresponding $\delta^{15}N_{bulk}$ in the GA core, likely due to an enrichment of $\delta^{15}N_{frustule}$ relative to $\delta^{15}N_{export}$ (consistent with the observations of Chapter 2), counteracted to some degree by the $DIAG_{WC}$ ^{15}N-enrichment of $\delta^{15}N_{bulk}$. Were $DIAG_{WC}$ to have decreased during the deposition of diatom layers while the offset between $\delta^{15}N_{export}$ and $\delta^{15}N_{frustule}$ remained constant, $\Delta^{15}N_{frustule\text{-}bulk}$ would be larger within the reducing diatom layers. In fact, the opposite is the case, as evident by the anticorrelation of Mo and $\Delta^{15}N_{frustule\text{-}bulk}$ shown in Figure 3.15; the $\Delta^{15}N_{frustule\text{-}bulk}$ is lowest during the periods of greatest Mo enrichment. This implies that variable $DIAG_{WC}$ is not the dominant control on the difference between $\delta^{15}N_{bulk}$ and $\delta^{15}N_{frustule}$ on these timescales; rather, it is more likely that $\delta^{15}N_{frustule}$ is varying relative to $\delta^{15}N_{export}$, as a result of ecological changes (Chapter 2). It is possible that significant diagenetic changes co-occur in diametric opposition to ecological changes and that the ecological change is simply larger, masking the changes in diagenesis, but Occam's razor excises this possibility from the current work.

The availability of two sediment cores in the WSG, from different water depths (2317 m and 3244 m), spaced reasonably far apart (102 km), with different accumulation rates (~ 45 % higher at MD01-2416 than at ODP 882) provides a second line of evidence against a large influence of time-variable changes in diagenesis. With the exception of the curious period of very low $\delta^{15}N_{bulk}$ in MD01-2416 near 120 ka, the general features of the two cores are virtually identical within the errors of the age models. This offers additional confirmation that local, time-variable diagenetic changes do not contribute significantly to the $\delta^{15}N_{bulk}$ profiles.

To summarize, cores ODP 887 (GA) and MD01-2416 (WSG) display coretop ^{15}N-enrichments ($DIAG_{WC}$) of ~ 1.7 and 2.6 ‰, respectively. There are gradual, smooth decreases in $\delta^{15}N_{bulk}$ of ~ 2 ‰ over the upper 20 m of both long records ($DIAG_{PB}$). There is no evidence that rapid changes in sedimentation conditions produced time-variable degrees of

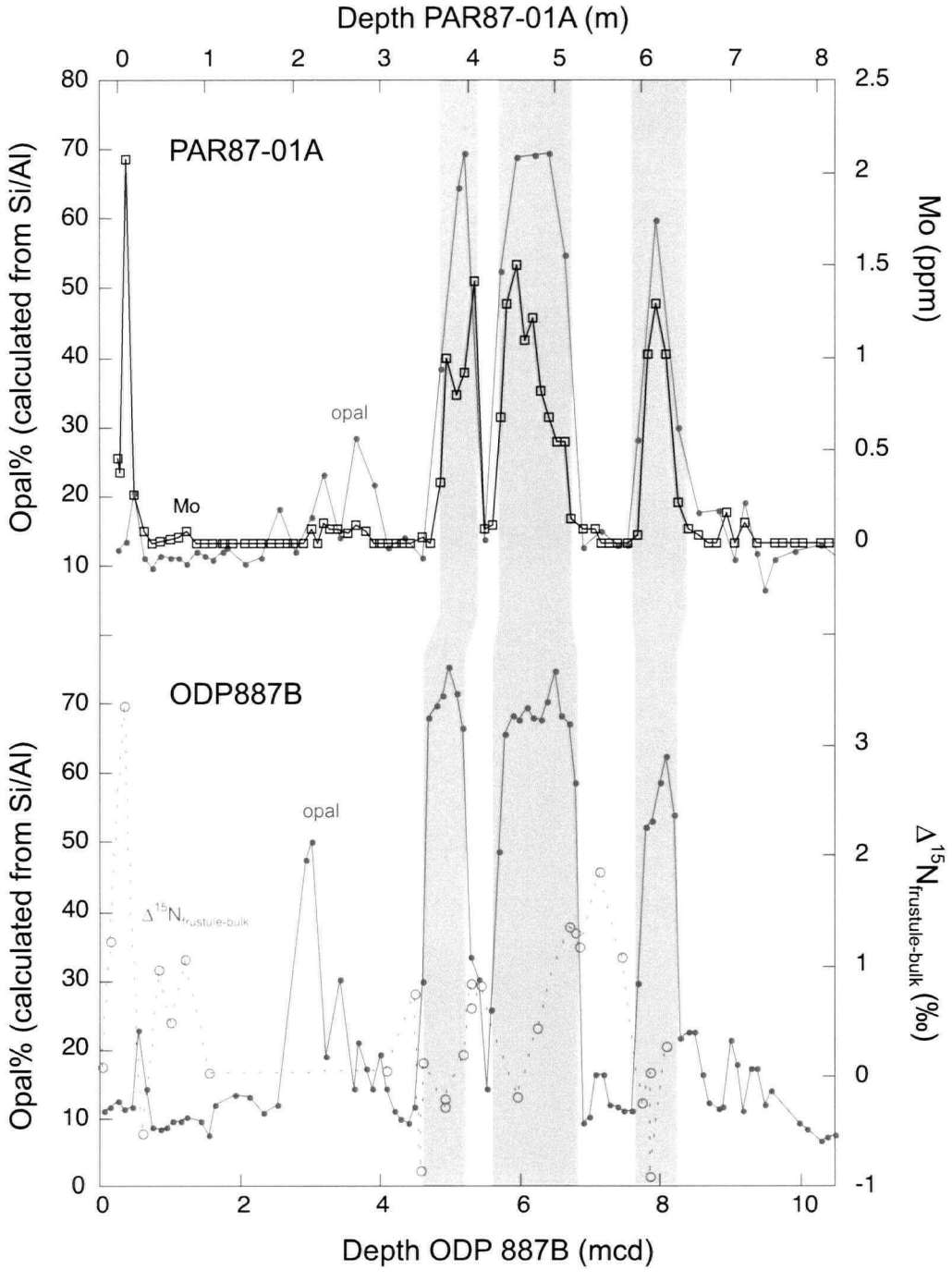

3.15: Bulk and frustule-bound $\delta^{15}N$ under contrasting sedimentary conditions in the Gulf of Alaska. The blue curves with filled circles show opal concentrations (calculated from Si/Al, see Appendix 3) at two adjacent sites in the GA. In the top panel, Mo concentrations are shown by black squares (J. Crusius, unpublished), while open circles show the difference between $\delta^{15}N_{frustule}$ and $\delta^{15}N_{bulk}$ in the lower panel. The rapidly-accumulated opal-rich layers show Mo enrichment, consistent with a shoaling of the sedimentary redoxcline. Yet, $\Delta^{15}N_{frustule-bulk}$ is generally larger in the slowly accumulated, oxic sediments than in the rapidly accumulated, reducing sediments. This is opposite the pattern expected were diagenesis to vary under different sedimentation conditions at a single site.

diagenesis, either in the water column or post-burial. Therefore, the principal differences between the WSG and GA records must be due to differences in RNU.

3.6 Changes in Relative Nitrate Utilization

In the subarctic Pacific on the whole, perennially incomplete nitrate utilization is common. The tendency for phytoplankton to preferentially incorporate ^{14}N causes the $\delta^{15}N_{export}$ to be lower than the $\delta^{15}N\text{-}NO_3^-$ of the subeuphotic source where nitrate is incompletely consumed, generating a significant RNU signal.

The good visual correlation of the GA record to $\delta^{15}N_{bulk}$ records from different oceanographic and productivity regimes along the Western North American margin (Figure 3.8) implies that changes in RNU at this site are, to first order, unimportant. This initially surprising observation can be attributed to two things. First, much of the Fe nutrition at the GA site is supplied from below, including a large component that is transported laterally from the shelf ([*Lam et al.*, accepted], section 3.2). As such, the degree of Fe limitation is relatively insensitive to variations in atmospheric dust input, especially as these inputs are quite subdued when compared to the WSG site; instead, the Fe supply to the surface is generally correlated with the macronutrient supply to the surface. *Altabet* [2001] observed a similar dynamic in the equatorial Pacific, where nitrate supply and export production were both greatly reduced during El Niño but, because limiting micronutrients are supplied by upwelling in a fixed ratio to NO_3^-, RNU remained constant regardless of ENSO state. Second, nitrate utilization in the vicinity of the GA site today is nearly complete, despite a moderately abundant supply of macronutrients and very little atmospheric dust. Since Fe availability is expected to have been greater than today throughout most of the late Pleistocene, the apparently minimal modern RNU of 0.6 ± 0.6 ‰ (estimated above) should represent the high end of the potential range, allowing little leeway for change in the past, with the possible exception of the diatom-rich layers.

The GA profile is therefore primarily a sum of variations in $\delta^{15}N_{nitrate}$ and $DIAG_{PB}$. The WSG profiles are one step more complex, in that they also incorporate significant changes in RNU that, as reasoned above, are the principal sources of discrepancy between

the two sites. The intimate subsurface link (see 3.3.3, [*Ueno and Yasuda*, 2003]) between the two sites makes it very likely that past changes in $\delta^{15}N_{nitrate}$ were nearly identical at the two locations. Furthermore, the decreases in $\delta^{15}N_{bulk}$ of the two long records, MD01-2416 (WSG) and ODP 887 (GA) over the past 450 ka are remarkably similar (Figure 3.9). In fact, the average differences between MD01-2416 and ODP 887 over the upper (9 to 146 ka) and lower (343 to 450 ka) intervals are 0.88 ‰ and 0.94 ‰, respectively, showing that $DIAG_{PB}$ is almost identical at the two sites. Given that downcore variability caused by $\delta^{15}N_{nitrate}$ and $DIAG_{PB}$ is so similar at the GA and WSG sites, and recalling Eq. 3.1, RNU at the WSG can be approximated by subtracting the $\delta^{15}N_{bulk}$ GA record from the WSG records. This was accomplished by linear interpolation of the three records onto a common timescale, with high-opal layers removed from the GA record to minimize the effect of variable RNU in the GA, and subtraction of GA $\delta^{15}N_{bulk}$ from WSG $\delta^{15}N_{bulk}$, using both 1 ky interpolated ages and 9-ky running averages. The interpolated records used for generating the differences are shown in Figure 3.16.

The resulting difference curves show a clear pattern with a consistent relationship to global ice volume (Figure 3.16). The magnitude of change is on the order of 3 ‰, much larger than the estimated potential for RNU variability at the GA site (0.6 ± 0.6 ‰), the primary unknown in this analysis. The generally positive values of the difference curves suggest a larger $DIAG_{WC}$ at the WSG sites, consistent with the range of values estimated in section 3.5.2. Also, the curves for the two WSG sites are almost identical, showing a lack of dependency on local details of the records. As such, the difference curve appears to be a reasonably robust monitor of RNU for the WSG.

3.6.1 Implications for the nutrient status of the WSG over past glacial cycles

According to this reconstruction, RNU in the WSG is most incomplete during interglacial periods and most complete during glacial periods. This is most simply interpreted as reflecting increased nitrate utilization during glacials. During the last glacial cycle, the degree of nitrate utilization increased through MIS 5d-5b, reaching a high degree of utilization by MIS 5a. This was followed by a long 'plateau', then a return to lower degrees of utilization beginning near the LGM. Small decreases in relative nitrate utilization appear to accompany peaks in WSG opal concentration, thought to result from enhanced macronutrient supply.

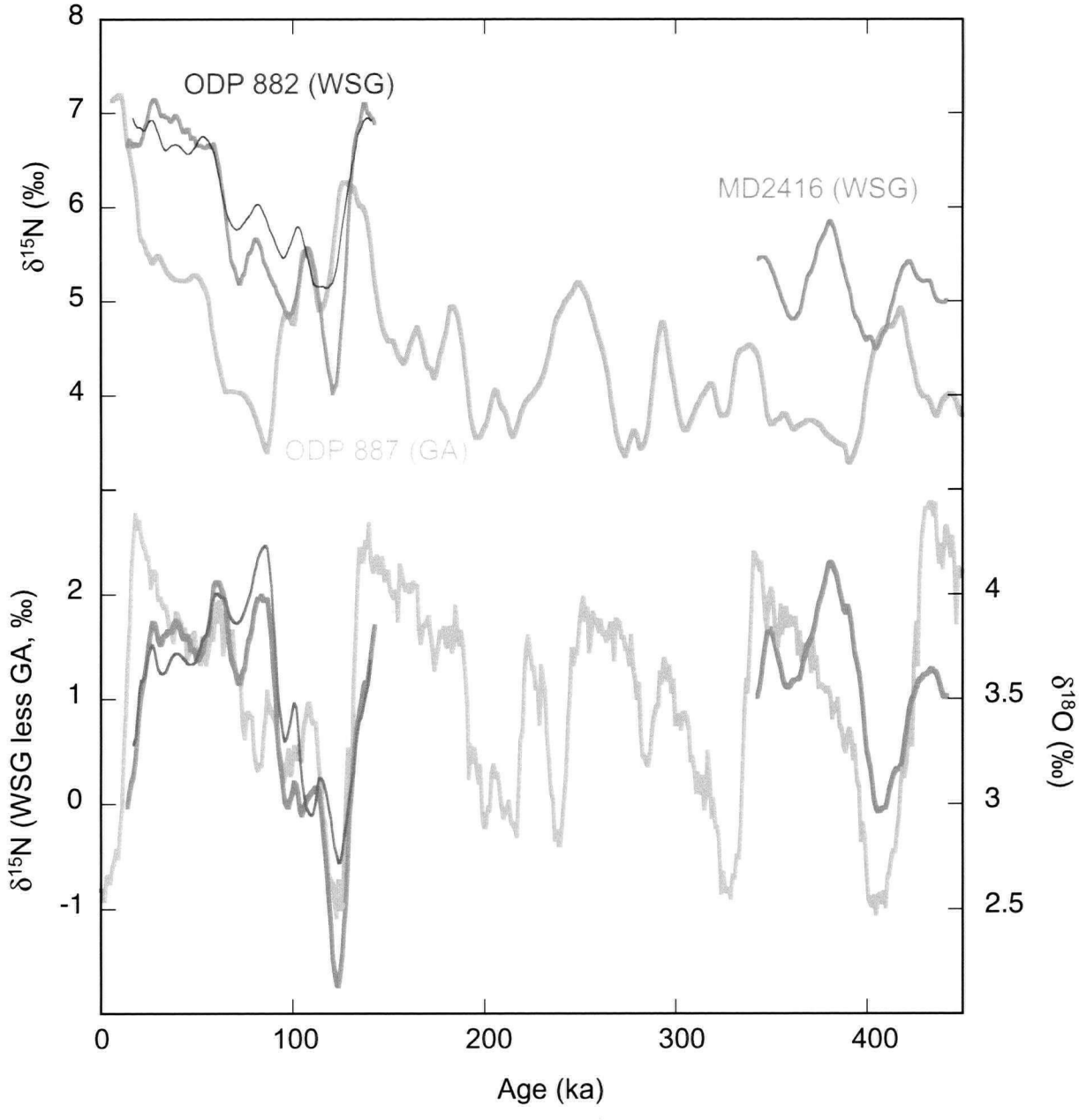

3.16: Difference between $\delta^{15}N_{bulk}$ records of the Gulf of Alaska and the Western Subarctic Gyre. The upper panel shows interpolated, 9 ky running averages for the three subarctic Pacific sediment records. The lower panel shows the difference between the WSG records and the GA record, with the ODP 882 – ODP 887 difference shown by the thin blue line, and the MD01-2416 – ODP 887 difference shown by the thick purple line. The $\delta^{18}O$ stack of *Lisiecki and Raymo* [2005] is shown as a proxy for ice volume in pale grey.

The glacial-interglacial cycle from 343-450 ka follows a similar pattern, with low interglacial values and a rapid, early rise to a long (if bumpy) plateau.

A ready explanation for the observed pattern is that relative nitrate utilization increased due to atmospheric Fe fertilization during periods of increased dust transport, as initially hypothesized by *Martin and Fitzwater* [1988]. Although there are no applicable records of dust transport from the vicinity of the western Pacific itself, ice core records of insoluble particles from both Greenland [*Ruth et al.*, 2003] and central Antarctica [*Petit et al.*, 1999] show similar patterns over the last glacial cycle (Fig 3.17). The fact that the principal source of dust to the NGRIP site in Greenland is the arid portion of East Asia [*Ruth et al.*, 2003], which also supplies dust to the WSG, suggests that it is a reasonable proxy for dust delivery to the WSG. During interglacial periods, dust delivery to the subarctic Pacific was greatly reduced, consistent with Fe-limitation of growth rates and the incomplete nitrate utilization observed in the region today [*Brown et al.*, 2005]. As ice sheets advanced and aridity increased, the dustiness of the atmosphere increased, quickly enhancing Fe delivery to the WSG. The resulting acceleration of algal growth would have allowed more complete utilization of nitrate, reducing the isotopic effect of RNU.

The shape of the WSG RNU curve is notably different from the dust records, however, in that it reached a plateau by ~90 ka, while the dustiness of the atmosphere continued increasing until the Glacial Maximum. This may be, in part, an artifact of the GA subtraction, if RNU at the GA increased gradually throughout the glacial, to the glacial maximum. However, given the small potential for RNU variability at the GA site, this artifact is incapable of producing more than a small difference in the timing and shape of the plateau. The existence of the plateau can be more easily explained as representing a threshold of Fe sufficiency.

Following the rationale of *Brown et al.* [2005], the degree of iron stress that afflicts the diatom community can be illustrated by comparing the ratio of Fe : NO_3^- supplied to the mixed layer with cellular quotas. Coupling the cellular Fe : N quotas of *Sunda and Huntsman* [1995] to the Redfield C : N ratio gives a threshold Fe : NO_3^- ratio of ~ 7×10^{-5}, above which nitrate uptake rates are not limited by Fe. Intermediate waters in the WSG currently have an Fe : NO_3^- ratio of ~ 3×10^{-5} [*Brown et al.*, 2005]. Thus, a supply of Fe from the atmosphere equivalent to ~ 130 % of that delivered from below would be sufficient to alleviate Fe limitation, assuming that deep waters maintained the same Fe : NO_3^-. An annual NO_3^- supply to

the mixed layer of 20 μM would therefore demand an annual aeolian Fe supplement of 80 x 10^{-5} μM, or 0.8 nM. Further additions beyond this relatively minor increase in Fe supply would have no impact on growth rates or relative nitrate utilization. Assuming a 50 m mixed layer, 0.55 mmol Fe g^{-1} dust and 5 % Fe solubility (*Brown et al.* [2005] and references therein), 1 g dust m^{-2} y^{-1} would supply ~ 0.5 nM Fe annually to the entire mixed layer, suggesting that Fe sufficiency would be reached with 1.6 g dust m^{-2} y^{-1}. For comparison, the present-day dust flux was recently estimated as < 0.3 g m^{-2} y^{-1} [*Measures et al.*, 2005], while *Mahowold et al.* [1999] estimate a dust flux to this region during the LGM of > 10 g m^{-2} y^{-1}. Therefore a factor of five increase in the local dust supply above the present-day flux should alleviate the Fe limitation, representing only a fraction of the previously estimated glacial-interglacial range. Any increase in deep water Fe : NO_3^- during the glacial period caused by enhanced Fe deposition throughout the basin would further tend to push the region towards early Fe sufficiency. In addition, any decrease in NO_3^- supply would decrease the amount of Fe required for complete utilization.

The analysis presented here suggests the WSG was Fe-sufficient, ensuring complete drawdown of NO_3^-, for most of the period from ~90 to 18 ka. Indeed, the concentrations of dust in ice cores representing this period are higher than Holocene concentrations, by a factor of at least three at Vostok, and a factor of at least four at Greenland (Figure 3.17). This implies that an increase in average high-latitude atmospheric dust concentrations of only a factor of three to five equates to sufficient dust supply to the WSG site to allow complete utilization of NO_3^-. The similar pattern of variability from 343-450 ka hints that a long period of Fe sufficiency may be a general feature of the WSG during glaciations.

The lack of correspondence between proxy evidence for increased export production and evidence for Fe fertilization may seem surprising; however this points to what may be an important feature of the system. Enhanced nitrate utilization, resulting from Fe fertilization, would indeed be expected to cause an immediate increase in the sinking flux of organic matter. However, a fraction of the nutrient wealth exported from the upper ocean would not be remineralized in the shallow subsurface, but would sink into intermediate water masses and be lost from the local environment. This, in effect, would cause a deepening of the nutricline, so that the availability of Fe would actually impoverish the macronutrient supply to the surface ocean. This reinforces the point that the capacity of the surface ocean to fuel export pro-

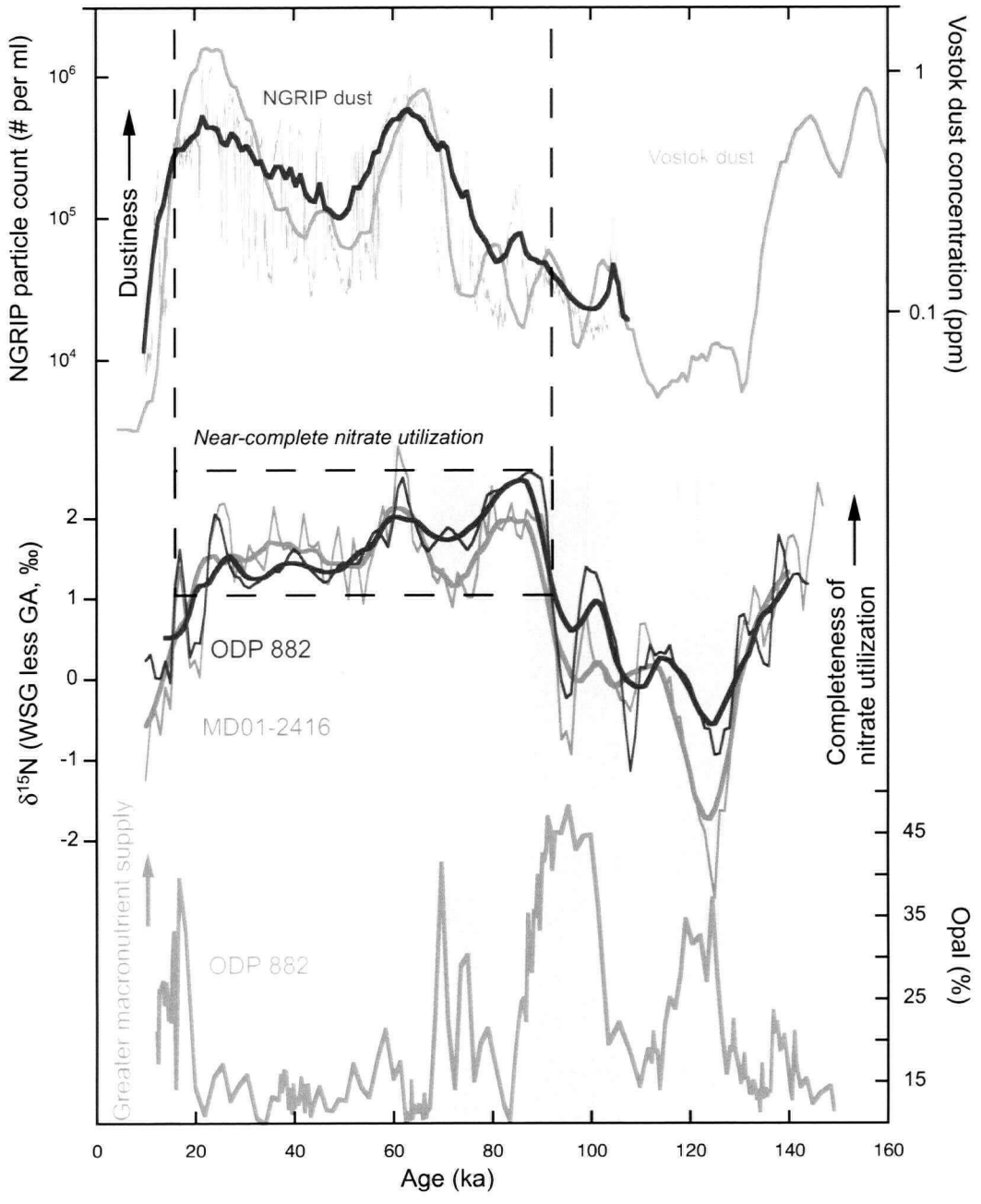

3.17: Changes in nitrate utilization in the Western Subarctic Pacific during the last glacial cycle. The upper panel shows dust records from Greenland [Ruth et al., 2003] in blue, and Antarctica [Petit et al., 1999] in khaki, with smoothed values shown by the heavy lines. The central panel shows the difference curves from 3.16, as heavy lines, as well as the difference between the unsmoothed, interpolated $\delta^{15}N_{bulk}$ records as discussed in the text. The lower panel shows the opal concentration in WSG record of ODP 882. Periods of rapid opal export indicate abundant macronutrient supply to the euphotic zone, and are highlighted by the vertical green shaded rectangles. The lengthy plateau in the difference curve is interpreted as representing near-complete nitrate utilization, and is coincident with a lengthy period of elevated dust levels. The apparent nonlinearity of the relationship between dust and nitrate utilization is discussed in the text.

duction is fundamentally dependent not on a single limiting nutrient, but on the ability of physical mixing and transport to resupply nutrients from below.

Despite the secondary importance of Fe for determining export production fluxes, the enhanced macronutrient uptake has implications for the efficiency of the biological pump and low latitude productivity. Complete utilization of nutrients at high latitudes causes more sequestration of CO_2 in the deep sea [*Sarmiento and Toggweiler*, 1984; *Sigman and Haug*, 2003], while low nutrient concentrations in newly forming mode and intermediate waters reduces the potential fertility of low latitude regions [*Sarmiento et al.*, 2004].

3.7 Temporal change in δ^{15}N-nitrate

The GA $\delta^{15}N_{bulk}$ record is clearly very similar to the $\delta^{15}N_{bulk}$ records of the North American margin, likely due to only small temporal variability of RNU, making it a good monitor of $\delta^{15}N_{nitrate}$. However, the Line P survey of $\delta^{15}N\text{-}NO_3^-$ (section 3.3) shows that despite the relatively high activity of both the ETNP denitrification zone and the CUC today, the enrichment of subeuphotic zone nitrate at the GA site is only ~1 ± 0.5 ‰ above the deep Southern Ocean mean of 4.8 ‰, in contrast to the Californian margin which is enriched by > 3 ‰ (~ 8 ‰ near Site 1017 [*Sigman et al.*, 2003]). This indicates that the ^{15}N-enriched nitrate from the ETNP is mixed into the open North Pacific gyres, via pathways other than the CUC, so that the GA $\delta^{15}N\text{-}NO_3^-$ is not tied particularly closely to the CUC. Thus, although it is very similar to the CUC records, it represents a distinct subarctic Pacific nitrate pool and, as such, an important new perspective on past N cycle changes. Glacial-interglacial changes in the $\delta^{15}N$ of this and other regional nitrate pools over the past 300 ky are discussed in Chapter 4; here, the focus is on the peripheries, the most recent 30 ky and the full 720 ky record.

3.7.1 Implications of the GA record: a 15 ka event

There is a rapid $\delta^{15}N_{bulk}$ rise in the GA record from 5.3 ‰ to 7.8 ‰ over a period of at most 2 ky, centred at approximately 15 ka (Figure 3.18). This occurs over a small depth range in the core (0.20 m) so that the gradual $DIAG_{PB}$ has a negligible impact on the magnitude of the change, which is therefore quite well constrained as 2.5 ± 0.2 ‰. A similar rise is evident in the WSG record of MD01-2416, though the inferred decrease in relative nitrate utilization over this period obscures the magnitude of the rise (see section 3.6). A parallel rise

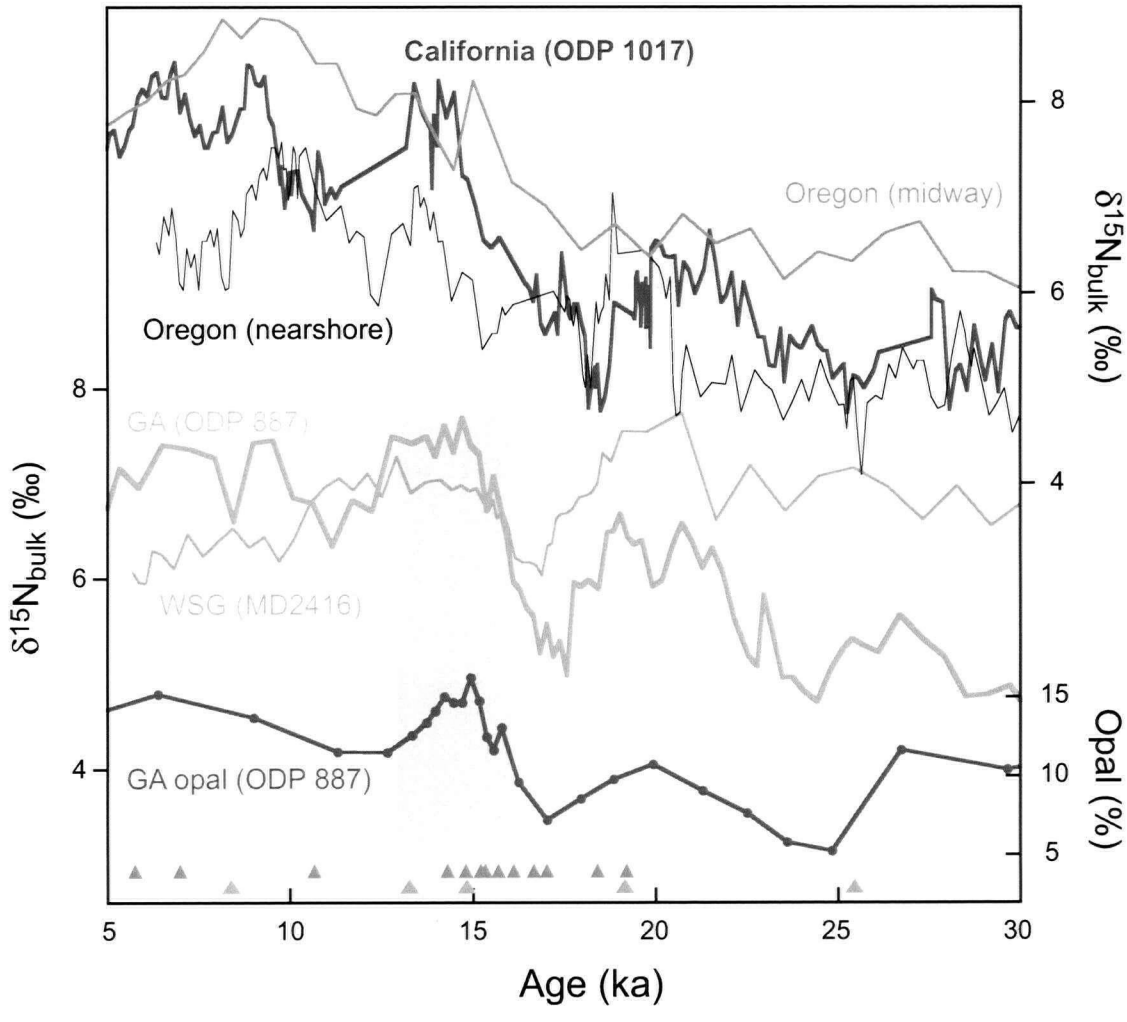

3.18: Nitrogen isotopes and opal concentration in the subarctic and NE Pacific during the past 30 ky. The upper five curves are $\delta^{15}N_{bulk}$ records from the NE Pacific, as shown in previous figures. The lower panel shows the opal concentration in the GA record, which shows a peak typical of a wide-spread increase in export production across the North Pacific *ca* 15 ka, coincident with the rapid rise in $\delta^{15}N_{bulk}$. The time control for the subarctic Pacific records is based on ^{14}C ages at the points indicated by triangles at the bottom of the panel, where narrow purple triangles correspond to MD01-2416 (Kienast et al., unpubl.) and broader orange triangles correspond to ODP 887.

is apparent in the deglacial $\delta^{15}N_{bulk}$ records of Nakatsuka *et al.* [1995] from the deep Bering Sea. The 15 ka rise represents either a rapid increase in the supply of ^{15}N-enriched NO_3^- from outside the subarctic Pacific, or a sudden onset of denitrification in the subarctic Pacific itself. The $\delta^{15}N_{bulk}$ record from the California margin (Figure 3.18) has a similar rise over a similar time period, with a magnitude of 3.2 ‰. At Oregon (Figure 3.18), the magnitude of the rapid change near 15 ka is only about half that at the Californian site (1.6 and 1.8 ‰ for the Nearshore and Midway sites, respectively). The weak signal at Oregon suggests that the large $\delta^{15}N_{nitrate}$ rise evident at the California margin was not effectively communicated further north by the CUC at this time, nor did it reflect a North-Pacific-wide change.

It is clear that suboxia expanded rapidly throughout the North Pacific Ocean at the onset of the "Bolling-Allerod" period [*Zheng et al.*, 2000], and included intensification of the denitrification zone in the ETNP [*Pride et al.*, 1999]. However, the change at the GA site is significantly more pronounced than at the Oregon sites, and appears more rapid than any of the North American margin records, suggesting that there was a proximal source of ^{15}N-enriched NO_3^- to the subarctic Pacific surface at this time. The low O_2 concentrations within the subarctic Pacific subsurface today (as low as 18 μM, WOCE one time sailing) testify to the proximity of this region to the threshold of denitrification. The recent observation of laminated sediments in cores from intermediate and deep sites in the Bering Sea during the Bolling-Allerod [*Cook et al.*, 2005] lends further support to this suggestion. The temporal coincidence of the onset of subarctic Pacific denitrification with an increase in productivity, as shown both by opal concentrations in the GA core as well as in numerous cores from the western subarctic Pacific [*Crusius et al.*, 2004], suggests a mechanistic link. Either the subsurface oxygen deficiency of the subarctic Pacific was exacerbated by the increase in export production, or a change in the physical circulation simultaneously invigorated algal growth while causing the reduction of subsurface oxygen concentrations.

3.7.2 Implications of the GA record: a 20 ka event

An earlier peak in $\delta^{15}N_{bulk}$ appears near 20 ka (Figure 3.19), with a magnitude of 1.4 ‰ in the California and Oregon (Nearshore) records, 1.1 ‰ at Mazatlan, 1.8 ‰ in the GA record and 1.1 ‰ at the WSG record, averaging 1.5 ‰ in the subarctic Pacific. The similarity of the magnitude of this peak across this vast distance suggests that it is not merely a down-

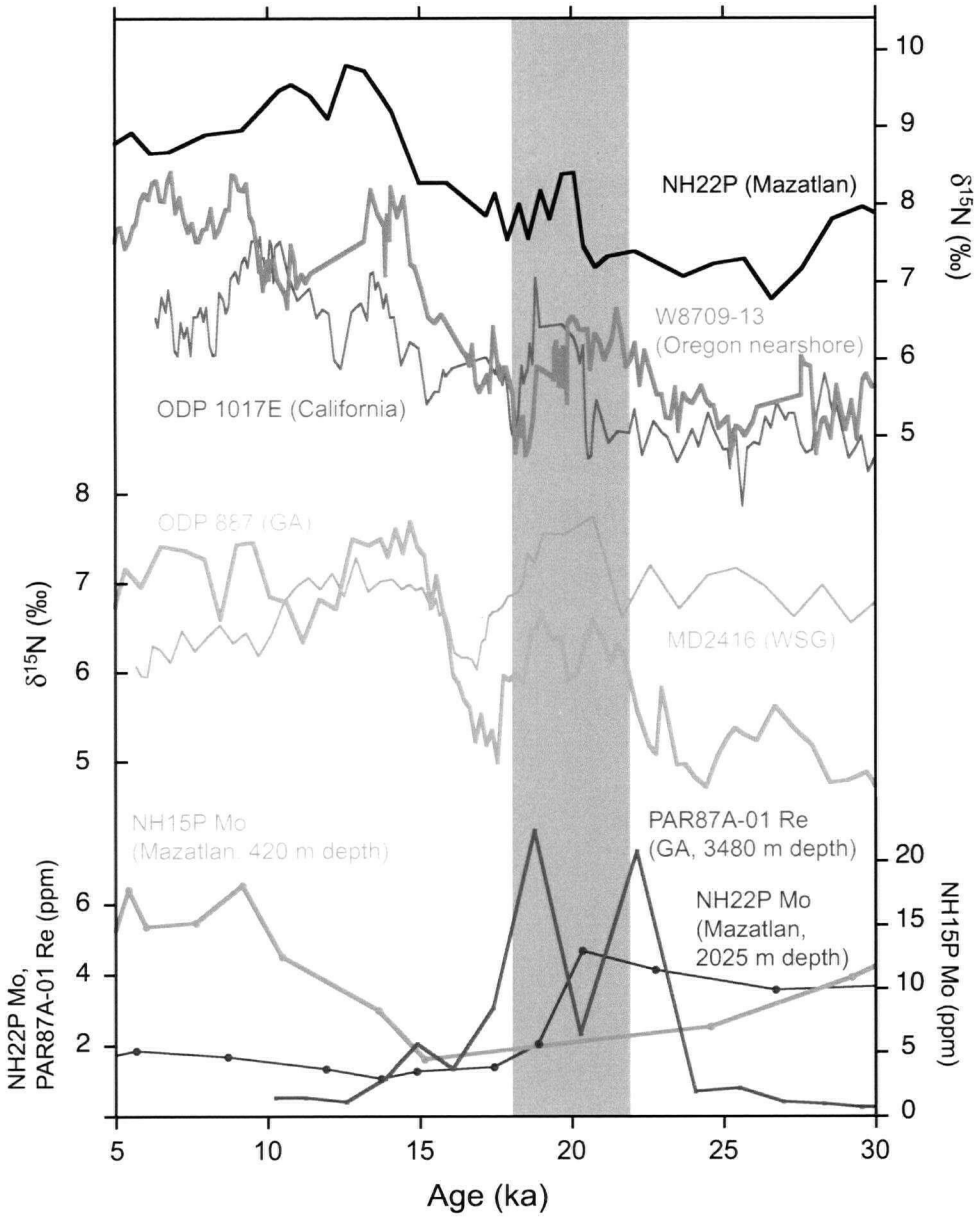

3.19: Nitrogen isotopes and authigenic metals in the NE Pacific during the past 30 ky. The upper five curves are $\delta^{15}N_{bulk}$ records from the NE Pacific, as shown in previous figures. The three curves in the bottom panel show trace metal concentrations from the Mexican margin at Mazatlan [Nameroff et al., 2004] and from the GA (J. Crusius, unpublished). The deep cores show Mo and Re enrichments consistent with poorly oxygenated conditions during the 20 ka $\delta^{15}N_{bulk}$ peak, while the shallow core shows significant Mo enrichment following 15 ka.

stream enrichment from the ETNP, but that it represents an isotopic enrichment throughout the region of ~ 1.5 ‰. There is no evidence for a > 0.5 ‰ increase in $\delta^{15}N_{bulk}$ records of the South China Sea over this interval [*Kienast*, 2000; *Kienast*, 2005], suggesting that the enrichment was not transmitted from the NE Pacific to the Western subtropical Pacific. The signal is most likely muted in the South China Sea due to dilution of the high $\delta^{15}N\text{-}NO_3^-$ waters with low $\delta^{15}N$ organic matter from N_2 fixation in the western tropical Pacific [*Liu et al.*, 1996].

Unlike the ca. 15 ka period, when evidence for intermediate-depth suboxia is widespread throughout the North Pacific, this earlier $\delta^{15}N_{bulk}$ peak occurred during a time of apparently high oxygenation throughout the upper 1 km of the NE Pacific water column. Laminations are not present between 18 and 22 ka in the Santa Barbara Basin [*Behl and Kennett*, 1996], nor were they observed in any of the cores raised along the western north American margin at less than 1000 m water depth that were studied by van Geen *et al.* [2003]. Trace metals in the ETNP show generally oxic conditions from 16 to 22 ka at 803 and 760 m on the California margin [*Zheng et al.*, 2002], at 577 m in the Santa Barbara Basin [*Ivanochko and Pedersen*, 2004] and on the Mexican margin at 420 m water depth [*Nameroff et al.*, 2004]. Thus, it seems unlikely that this period of $\delta^{15}N\text{-}NO_3^-$ enrichment, which is on the order of half the full glacial-interglacial amplitude at the GA site, could have been due to denitrification in the relatively well-oxygenated ETNP thermocline, where it occurs at present.

However, there is evidence that the deep North Pacific was extremely oxygen-poor during this period. Authigenic uranium is enriched in ODP 882 (WSG) during the glacial, with a peak at 18 – 20 ka [*Jaccard*, 2005] and Mo is enriched during the same period at 2025 m on the Mexican margin ([*Nameroff et al.*, 2004], Figure 3.19). It has been noted that the glacial Pacific was typified by relatively low nutrients contents above ~ 2000 m, and relatively high nutrients below [*Herguera et al.*, 1991; *Keigwin*, 1998; *Matsumoto et al.*, 2002]. Thus, it seems plausible that an intense oxygen minimum was present in the middle-deep ocean during the 20 ka peak, and that waters having undergone denitrification at > 1 km depth provided a source of ^{15}N-enriched nitrate at this time. A period of elevated export production throughout the NE Pacific during this period (e.g. [*Hendy et al.*, 2004; *Ortiz et al.*, 2004] may have contributed to intensifying oxidant demand in the deep North Pacific over this period, generating the 20 ka peak. Alternatively, mixing may have been enhanced be-

tween a deep, denitrifying water mass and the overlying intermediate waters, during this period, causing a greater flux of ^{15}N-enriched nitrate from a mass that had been denitrifying steadily for millennia.

The fact that oxygen was not completely absent from the water column at 3085 m in the Panama Basin at this time [*Yang et al.*, 1995] suggests that denitrification did not occur in the deep ETNP. Given that the subarctic Pacific currently has the lowest O_2 contents of anywhere in the deep world ocean, and that deep waters there were not locally ventilated during the LGM [*Keigwin*, 1987; *Keigwin*, 1998; *Matsumoto et al.*, 2002], denitrification in this specific region seems a likely alternative. In this case, denitrification in the poorly ventilated water mass below ~2600 m would have produced ^{15}N-enriched NO_3^- that would have mixed upwards into the Glacial North Pacific Intermediate Water (GNPIW). The resulting elevation of $\delta^{15}N$-NO_3^- in the GNPIW would have been transmitted to upwelling sites along the North American margin, analogous to the transmission of high $\delta^{15}N$-NO_3^- from the ETNP to other parts of the NE Pacific by NPIW today. Because the GNPIW was likely ventilated in the open subarctic Pacific [*Ohkushi et al.*, 2003], the subarctic Pacific would have had the most direct link to the deep $\delta^{15}N$-NO_3^-, consistent with the large magnitude of the 20 ka peak at the GA site.

The end of the $\delta^{15}N_{bulk}$ peak at ~18 ka, coincident with a return to background values of authigenic U in sediments of the deep North Pacific [*Jaccard*, 2005](Figure 3.19) suggests an increase in oxygenation of the deep water mass, and a cessation of denitrification in the deep North Pacific. The fact that this change is contemporaneous with the retreat of sea ice in the Southern Ocean [*Bianchi and Gersonde*, 2004] presents tantalizing support for the hypothesis that sea ice cover significantly impedes gas exchange between the atmosphere and the deep ocean during the glacial period [*Stephens and Keeling*, 2000] and hints that this impedence may extend to oxygen exchange. As the deep sea became better oxygenated, the upper ocean oxygenation diminished, as evinced by trace metal distributions, laminations, and the rapid $\delta^{15}N_{bulk}$ rise at 15 ka. This general view is consistent with the conjecture of van Geen *et al.* [1996], who proposed that ventilation of the deep and shallow water masses of the NE Pacific are antiphased.

3.7.3 Implications: long record

There is a gradual downcore decay in the amplitude of variability in the long $\delta^{15}N_{bulk}$ records from both the WSG and GA (Figure 3.9). This decrease in amplitude is not apparent in the 1.8 My $\delta^{15}N_{bulk}$ record of *Liu et al.* [2005] from the California margin, a region shown to exhibit little diagenetic alteration [*Altabet et al.*, 1999]. Since the primary source of variability at both the GA and Californian sites is denitrification in the ETNP, it seems unlikely that the dwindling amplitude in the GA record reflects a primary signal, but is more likely a dampening effect of deep-sea diagenesis. However, the stability of the average $\delta^{15}N_{bulk}$ below 20 m depth in the GA core (figure 3.12) implies that the average $\delta^{15}N_{nitrate}$ in the subarctic NE Pacific has not changed substantially over the past 740 ky. The amplitude of variability in $\delta^{15}N_{bulk}$ (detrended) is, at most, 3.5 ‰, and the core-top $\delta^{15}N_{bulk}$ (representing a $\delta^{15}N_{nitrate}$ of 5.8 ± 0.5 ‰, as determined in Section 3.3.2) is within the highest 1.2 ‰ of detrended values (Figure 3.14). Therefore, the most ^{15}N-enriched nitrate supplied to the subarctic Pacific surface over the past 742 ka was no more than 7.5 ‰, while the lowest $\delta^{15}N_{nitrate}$ that has occurred in the region was at least 3.0 ‰.

3.8 Conclusions

The subarctic Pacific receives low $\delta^{15}N\text{-}NO_3^-$ from the shallow Kuroshio current (< 4 ‰) [*Liu et al.*, 1996], and high $\delta^{15}N\text{-}NO_3$ from the CUC (> 6.5 ‰), as shown in the Line P transect. However, shallow subsurface waters are very well mixed, with less than 0.5 ‰ variability between the open Gulf of Alaska, the Western Subarctic Gyre, and the Bering Sea. It is likely, therefore, that the $\delta^{15}N$ of nitrate supplied to phytoplankton communities of the three regions was also well coupled in the past.

Diagenesis in the water column imparts a significant enrichment of ^{15}N at the tops of the deep, slowly-accumulating cores studied. Following burial there is a gradual decrease in $\delta^{15}N$ with depth that has essentially terminated by ~ 20 m depth. Postburial diagenesis appears to be identical in the two long records presented. Comparison of $\delta^{15}N_{bulk}$ with $\delta^{15}N_{frustule}$ for the GA core gives no indication of time-variable changes in diagenesis, but suggests that changes in the relationship between $\delta^{15}N_{frustule}$ and $\delta^{15}N_{export}$ are significant.

Despite drawing on a common nitrate pool and undergoing similar diagenesis, the GA and WSG $\delta^{15}N_{bulk}$ records differ markedly. The primary source of this divergence is likely to have been temporal changes in the relative nitrate utilization in the WSG, while the GA record remained a more faithful witness of changes in $\delta^{15}N_{nitrate}$. When variations in nitrate are removed from the WSG record by subtraction of the GA record, a pattern of enhanced NO_3^- utilization during glacials is clear. The pattern of variability suggests relatively small increases in dust flux are sufficient to allow complete nitrate utilization, so that iron limitation is significant only during interglacial periods. The large changes in relative nitrate utilization are largely unrelated to export production, which must be determined instead by macronutrient supply and/or the physical surface conditions, in agreement with the conclusions of Kienast *et al.* [2004]. However, it is possible that glacial increases in nutrient drawdown impacted the nutrient richness of mode and intermediate waters formed in the subarctic Pacific, thereby decreasing low latitude fertility while increasing the effectiveness of the biological pump.

Changes in the $\delta^{15}N_{nitrate}$ of the subarctic Pacific illuminated by the GA core suggest the rapid onset of denitrification in the subarctic Pacific at 15 ka, in parallel to the $\delta^{15}N$ increase in the thermocline of the ETNP. An earlier regional $\delta^{15}N$ peak, near 20 ka, has previously escaped comment in the literature, and is tentatively ascribed to denitrification in a deep, oxygen-poor water mass of the North Pacific. This opens the possibility that denitrification occurred sporadically, or in patches, within the poorly ventilated deep glacial Pacific. Deep denitrification may have represented a source of ^{15}N -enriched NO_3^- to the glacial ocean, counterbalancing the reduction of thermocline denitrification and maintaining a relatively stable isotopic budget as suggested by the observations of Kienast [2000]. This conjecture requires further testing.

References

Ahagon, N., K. Ohkushi, M. Uchida, and T. Mishima, Mid-depth circulation in the northwest Pacific during the last deglaciation: Evidence from foraminiferal radiocarbon ages, *Geophysical Research Letters*, 30, 2003.

Altabet, M. A., Nitrogen isotopic evidence for micronutrient control of fractional NO_3^- utilization in the equatorial Pacific, *Limnology and Oceanography*, 46, 368-380, 2001.

Altabet, M. A., W. G. Deuser, S. Honjo, and C. Stienen, Seasonal and Depth-Related Changes in the Source of Sinking Particles in the North-Atlantic, *Nature*, 354, 136-139, 1991.

Altabet, M. A., and R. Francois, Sedimentary Nitrogen Isotopic Ratio As a Recorder For Surface Ocean Nitrate Utilization, *Global Biogeochemical Cycles*, 8, 103-116, 1994.

Altabet, M. A., C. Pilskaln, R. Thunell, C. Pride, D. Sigman, F. Chavez, and R. Francois, The nitrogen isotope biogeochemistry of sinking particles from the margin of the Eastern North Pacific, *Deep-Sea Research Part I-Oceanographic Research Papers*, 46, 655-679, 1999.

Aydin, M., Z. Top, R. A. Fine, and D. B. Olson, Modification of the intermediate waters in the northeastern subpolar Pacific, *Journal of Geophysical Research-Oceans*, 103, 30923-30940, 1998.

Banse, K., and D. C. English, Comparing phytoplankton seasonality in the eastern and western subarctic Pacific and the western Bering Sea, *Progress in Oceanography*, 43, 235-288, 1999.

Behl, R. J., and J. P. Kennett, Brief interstadial events in the Santa Barbara basin, NE Pacific, during the past 60 kyr, *Nature*, 379, 243-246, 1996.

Bianchi, C., and R. Gersonde, Climate evolution at the last deglaciation: the role of the Southern Ocean, *Earth and Planetary Science Letters*, 228, 407-424, 2004.

Bograd, S. J., R. E. Thomson, A. B. Rabinovich, and P. H. LeBlond, Near-surface circulation of the northeast Pacific Ocean derived from WOCE-SVP satellite-tracked drifters, *Deep-Sea Research Part II-Topical Studies in Oceanography*, 46, 2371-2403, 1999.

Boyd, P. W., C. S. Law, C. S. Wong, Y. Nojiri, A. Tsuda, M. Levasseur, S. Takeda, R. Rivkin, P. J. Harrison, R. Strzepek, J. Gower, R. M. McKay, E. Abraham, M. Arychuk, J. Barwell-Clarke, W. Crawford, D. Crawford, M. Hale, K. Harada, K. Johnson, H. Kiyosawa, I. Kudo, A. Marchetti, W. Miller, J. Needoba, J. Nishioka, H. Ogawa, J. Page, M. Robert, H. Saito, A. Sastri, N. Sherry, T. Soutar, N. Sutherland, Y. Taira, F. Whitney, S. K. E. Wong, and T. Yoshimura, The decline and fate of an iron-induced subarctic phytoplankton bloom, *Nature*, 428, 549-553, 2004.

Braman, R. S., and S. A. Hendrix, Nanogram Nitrite and Nitrate Determination in Environmental and Biological-Materials by Vanadium(III) Reduction with Chemi-Luminescence Detection, *Analytical Chemistry*, 61, 2715-2718, 1989.

Brandes, J. A., A. H. Devol, T. Yoshinari, D. A. Jayakumar, and S. W. A. Naqvi, Isotopic composition of nitrate in the central Arabian Sea and eastern tropical North Pacific: A tracer for mixing and nitrogen cycles, *Limnology and Oceanography*, 43, 1680-1689, 1998.

Broecker, W., and T. H. Peng, *Tracers in the sea*, ELDIGIO Press, New York, 1982.

Broecker, W. S., S. L. Peacock, S. Walker, R. Weiss, E. Fahrbach, M. Schroeder, U. Mikolajewicz, C. Heinze, R. Key, T. H. Peng, and S. Rubin, How much deep water is formed in the Southern Ocean?, *Journal of Geophysical Research-Oceans*, 103, 15833-15843, 1998.

Brown, M. T., W. M. Landing, and C. I. Measures, Dissolved and particulate Fe in the western and central North Pacific: Results from the 2002 IOC cruise, *Geochemistry Geophysics Geosystems*, 6, 2005.

Calvert, S. E., and M. R. Fontugne, On the late Pleistocene-Holocene sapropel record of climatic and oceanographic variability in the eastern Mediterranean, *Paleoceanography*, 16, 78-94, 2001.

Calvert, S. E., and T. F. Pedersen, Geochemistry of Recent Oxic and Anoxic Marine-Sediments - Implications for the Geological Record, *Marine Geology*, 113, 67-88, 1993.

Casciotti, K. L., D. M. Sigman, M. G. Hastings, J. K. Bohlke, and A. Hilkert, Measurement of the oxygen isotopic composition of nitrate in seawater and freshwater using the denitrifier method, *Analytical Chemistry*, 74, 4905-4912, 2002.

Castro, C. G., F. P. Chavez, and C. A. Collins, Role of the California Undercurrent in the export of denitrified waters from the eastern tropical North Pacific, *Global Biogeochemical Cycles*, 15, 819-830, 2001.

Cline, J. D., and I. R. Kaplan, Isotopic fractionation of dissolved nitrate during denitrification in the eastern tropical north Pacific Ocean, *Marine Chemistry*, 3, 271-299, 1975.

Cook, M., L. Keigwin, and C. Sancetta, The deglacial history of surface and intermediate water of the Bering Sea, *Deep-Sea Research II*, 52, 2163-2173, 2005.

Crusius, J., T. F. Pedersen, S. Kienast, L. Keigwin, and L. Labeyrie, Influence of northwest Pacific productivity on North Pacific Intermediate Water oxygen concentrations during the Boiling-Allerod interval (14.7-12.9 ka), *Geology*, 32, 633-636, 2004.

de Baar, H. J. W., P. W. Boyd, K. H. Coale, M. R. Landry, A. Tsuda, P. Assmy, D. C. E. Bakker, Y. Bozec, R. T. Barber, M. A. Brzezinski, K. O. Buesseler, M. Boye, P. L. Croot, F. Gervais, M. Y. Gorbunov, P. J. Harrison, W. T. Hiscock, P. Laan, C. Lancelot, C. S. Law, M. Levasseur, A. Marchetti, F. J. Millero, J. Nishioka, Y. Nojiri, T. van Oijen, U. Riebesell, M. J. A. Rijkenberg, H. Saito, S. Takeda, K. R. Timmermans, M. J. W. Veldhuis, A. M. Waite, and C. S. Wong, Synthesis of iron fertilization experiments: From the iron age in the age of enlightenment, *Journal of Geophysical Research-Oceans*, 110, 2005.

Deutsch, C., D. M. Sigman, R. C. Thunell, A. N. Meckler, and G. H. Haug, Isotopic constraints on glacial/interglacial changes in the oceanic nitrogen budget, *Global Biogeochemical Cycles*, 18, 2004.

deVernal, A., and T. F. Pedersen, Micropaleontology and palynology of core PAR87A-10: A 23,000 year record of paleoenvironmental changes in the Gulf of Alaska, northeast North Pacific, *Paleoceanography*, 12, 821-830, 1997.

Duce, R. A., and N. W. Tindale, Atmospheric Transport of Iron and Its Deposition in the Ocean, *Limnology and Oceanography*, 36, 1715-1726, 1991.

Emile-Geay, J., M. A. Cane, N. Naik, R. Seager, A. C. Clement, and A. van Geen, Warren revisited: Atmospheric freshwater fluxes and "Why is no deep water formed in the North Pacific", *Journal of Geophysical Research-Oceans*, 108, 2003.

Erickson, B. E., and G. R. Helz, Molybdenum(VI) speciation in sulfidic waters: Stability and lability of thiomolybdates, *Geochimica Et Cosmochimica Acta*, 64, 1149-1158, 2000.

Freudenthal, T., S. Neuer, H. Meggers, R. Davenport, and G. Wefer, Influence of lateral particle advection and organic matter degradation on sediment accumulation and stable nitrogen isotope ratios along a productivity gradient in the Canary Islands region, *Marine Geology*, 177, 93-109, 2001a.

Freudenthal, T., T. Wagner, F. Wenzhofer, M. Zabel, and G. Wefer, Early diagenesis of organic matter from sediments of the eastern subtropical Atlantic: Evidence from stable nitrogen and carbon isotopes, *Geochimica Et Cosmochimica Acta*, 65, 1795-1808, 2001b.

Fung, I. Y., S. K. Meyn, I. Tegen, S. C. Doney, J. G. John, and J. K. B. Bishop, Iron supply and demand in the upper ocean, *Global Biogeochemical Cycles*, 14, 281-295, 2000.

Ganeshram, R. S., T. F. Pedersen, S. E. Calvert, G. W. McNeill, and M. R. Fontugne, Glacial-interglacial variability in denitrification in the world's oceans: Causes and consequences, *Paleoceanography*, 15, 361-376, 2000.

Ganeshram, R. S., T. F. Pedersen, S. E. Calvert, and J. W. Murray, Large changes in oceanic nutrient inventories from glacial to interglacial periods, *Nature*, 376, 755-758, 1995.

Gladyshev, S., L. Talley, G. Kantakov, G. Khen, and M. Wakatsuchi, Distribution, formation, and seasonal variability of Okhotsk Sea Mode Water, *Journal of Geophysical Research-Oceans*, 108, 2003.

Gruber, N., and J. L. Sarmiento, Global patterns of marine nitrogen fixation and denitrification, *Global Biogeochemical Cycles*, 11, 235-266, 1997.

Harrison, P. J., F. A. Whitney, A. Tsuda, H. Saito, and K. Tadokoro, Nutrient and plankton dynamics in the NE and NW gyres of the subarctic Pacific Ocean, *Journal of Oceanography*, 60, 93-117, 2004.

Haug, G. H., D. M. Sigman, R. Tiedemann, T. F. Pedersen, and M. Sarnthein, Onset of permanent stratification in the subarctic Pacific Ocean, *Nature*, 401, 779-782, 1999.

Helz, G. R., C. V. Miller, J. M. Charnock, J. F. W. Mosselmans, R. A. D. Pattrick, C. D. Garner, and D. J. Vaughan, Mechanism of molybdenum removal from the sea and its concentration in black shales: EXAFS evidence, *Geochimica Et Cosmochimica Acta*, 60, 3631-3642, 1996.

Hendy, I. L., T. F. Pedersen, J. P. Kennett, and R. Tada, Intermittent existence of a southern Californian upwelling cell during submillennial climate change of the last 60 kyr, *Paleoceanography*, 19, 2004.

Herguera, J. C., L. D. Stott, and W. H. Berger, Glacial Deep-Water Properties in the West-Equatorial Pacific - Bathyal Thermocline Near a Depth of 2000 M, *Marine Geology*, 100, 201-206, 1991.

Higginson, M. J., J. R. Maxwell, and M. A. Altabet, Nitrogen isotope and chlorin paleoproductivity records from the Northern South China Sea: remote vs. local forcing of millennial- and orbital-scale variability, *Marine Geology*, 201, 223-250, 2003.

Holmes, M. E., C. Eichner, U. Struck, and G. Wefer, Reconstruction of Surface Ocean Nitrate Utilization Using Stable Nitrogen Isotopes in Sinking Particles and Sediments. in *The Use of Proxies in Paleoceanography: Examples from the South Atlantic*, edited by Fischer, G. and G. Wefer, pp. 447-468, Springer, 1999.

Ivanochko, T. S., and T. F. Pedersen, Determining the influences of Late Quaternary ventilation and productivity variations on Santa Barbara Basin sedimentary oxygenation: a multi-proxy approach, *Quaternary Science Reviews*, 23, 467-480, 2004.

Jaccard, S. L., The history of the biological pump in the subarctic Pacific: Implications for past atmospheric CO_2 variability and abrupt climate change, Ph.D., ETHZ, Zurich, 2005.

Jaccard, S. L., G. H. Haug, D. M. Sigman, T. F. Pedersen, H. R. Thierstein, and U. Rohl, Glacial/interglacial changes in subarctic North Pacific stratification, *Science*, 308, 1003-1006, 2005.

Johnson, W. K., L. A. Miller, N. E. Sutherland, and C. S. Wong, Iron transport by mesoscale Haida eddies in the Gulf of Alaska, *Deep-Sea Research Part II-Topical Studies in Oceanography*, 52, 933-953, 2005.

Karl, D., R. Letelier, L. Tupas, J. Dore, J. Christian, and D. Hebel, The role of nitrogen fixation in biogeochemical cycling in the subtropical North Pacific Ocean, *Nature*, 388, 533-538, 1997.

Katsuki, K., K. Takahashi, and M. Okada, Diatom assemblage and productivity changes during the last 340,000 years in the subarctic Pacific, *Journal of Oceanography*, 59, 695-707, 2003.

Keigwin, L. D., North Pacific Deep-Water Formation During the Latest Glaciation, *Nature*, 330, 362-364, 1987.

Keigwin, L. D., Glacial-age hydrography of the far northwest Pacific Ocean, *Paleoceanography*, 13, 323-339, 1998.

Kienast, M., Unchanged nitrogen isotopic composition of organic matter in the South China Sea during the last climatic cycle: Global implications, *Paleoceanography*, 15, 244-253, 2000.

Kienast, M., On the sedimentological origin of down-core variations of bulk sedimentary nitrogen isotope ratios, *Paleoceanography*, 20, 2005.

Kienast, S. S., S. E. Calvert, and T. F. Pedersen, Nitrogen isotope and productivity variations along the northeast Pacific margin over the last 120 kyr: Surface and subsurface paleoceanography, *Paleoceanography*, 17, art. no.-1055, 2002.

Kienast, S. S., I. L. Hendy, J. Crusius, T. F. Pedersen, and S. E. Calvert, Export production in the subarctic North Pacific over the last 800 kyrs: No evidence for iron fertilization?, *Journal of Oceanography*, 60, 189-203, 2004.

Ladd, C., P. Stabeno, and E. D. Cokelet, A note on cross-shelf exchange in the northern Gulf of Alaska, *Deep-Sea Research Part II-Topical Studies in Oceanography*, 52, 667-679, 2005.

Lam, P. J., J. K. B. Bishop, C. C. Henning, M. A. Marcus, G. A. Waychunas, and I. Fung, Wintertime phytoplankton bloom in the Subarctic Pacific supported by continental margin iron, *Global Biogeochemical Cycles*, accepted.

Lehmann, M. F., S. M. Bernasconi, A. Barbieri, and J. A. McKenzie, Preservation of organic matter and alteration of its carbon and nitrogen isotope composition during simulated and in situ early sedimentary diagenesis, *Geochimica Et Cosmochimica Acta*, 66, 3573-3584, 2002.

Lehmann, M. F., D. M. Sigman, D. C. McCorkle, B. G. Brunelle, S. Hoffmann, M. Kienast, G. Cane, and J. Clement, Origin of the deep Bering Sea nitrate deficit: Constraints from the nitrogen and oxygen isotopic composition of water column nitrate and benthic nitrate fluxes, *Global Biogeochemical Cycles*, 19, 2005.

Lisiecki, L. E., and M. E. Raymo, A Pliocene-Pleistocene stack of 57 globally distributed benthic delta ^{18}O records, *Paleoceanography*, 20, 2005.

Liu, K.-K., and I. R. Kaplan, The eastern tropical Pacific as a source of ^{15}N-enriched nitrate in seawater off southern California, *Limnology and Oceanography*, 34, 820-830, 1989.

Liu, K. K., M. J. Su, C. R. Hsueh, and G. C. Gong, The nitrogen isotopic composition of nitrate in the Kuroshio Water northeast of Taiwan: Evidence for nitrogen fixation as a source of isotopically light nitrate, *Marine Chemistry*, 54, 273-292, 1996.

Liu, Z., M. Altabet, and T. Herbert, Glacial-interglacial modulation of eastern tropical North Pacific denitrification over the last 1.8-Myr, *Geophysical Research Letters*, 32, 10.1029/2005GL024439, 2005.

Lourey, M. J., T. W. Trull, and D. M. Sigman, Sensitivity of $\delta^{15}N$ of nitrate, surface suspended and deep sinking particulate nitrogen to seasonal nitrate depletion in the Southern Ocean, *Global Biogeochemical Cycles*, 17, 2003.

Mahowald, N., K. Kohfeld, M. Hansson, Y. Balkanski, S. P. Harrison, I. C. Prentice, M. Schulz, and H. Rodhe, Dust sources and deposition during the last glacial maximum and current climate: A comparison of model results with paleodata from ice cores and marine sediments, *Journal of Geophysical Research-Atmospheres*, 104, 15895-15916, 1999.

Martin, J. H., and S. E. Fitzwater, Iron-Deficiency Limits Phytoplankton Growth in the Northeast Pacific Subarctic, *Nature*, 331, 341-343, 1988.

Martin, J. H., R. M. Gordon, and S. E. Fitzwater, The Case for Iron, *Limnology and Oceanography*, 36, 1793-1802, 1991.

Matsumoto, K., T. Oba, J. Lynch-Stieglitz, and H. Yamamoto, Interior hydrography and circulation of the glacial Pacific Ocean, *Quaternary Science Reviews*, 21, 1693-1704, 2002.

McDonald, D., The Late Quaternary History of Primary Productivity in the Subarctic East Pacific, M.Sc., University of British Columbia, Vancouver, 1997.

McDonald, D., T. F. Pedersen, and J. Crusius, Multiple late Quaternary episodes of exceptional diatom production in the Gulf of Alaska, *Deep-Sea Research II*, 46, 2993-3017, 1999.

McKay, J. L., T. Pedersen, and J. R. Southon, Intensification of the oxygen minimum zone in the northeast Pacific off Vancouver Island during the last deglaciation: Ventilation and/or export production?, *Paleoceanography*, 20, doi: 10.1029/2003PA000979, 2005.

Measures, C. I., M. T. Brown, and S. Vink, Dust deposition to the surface waters of the western and central North Pacific inferred from surface water dissolved aluminum concentrations, *Geochemistry Geophysics Geosystems*, 6, 2005.

Minagawa, M., M. Ohashi, T. Kuramoto, and N. Noda, $\delta^{15}N$ of PON and nitrate as a clue to the origin and transformation of nitrogen in the subarctic North Pacific and its marginal sea, *Journal of Oceanography*, 57, 285-300, 2001.

Mortlock, R. A., and P. N. Froelich, A Simple Method for the Rapid-Determination of Biogenic Opal in Pelagic Marine-Sediments, *Deep-Sea Research Part A-Oceanographic Research Papers*, 36, 1415-1426, 1989.

Nakatsuka, T., K. Watanabe, N. Handa, E. Matsumoto, and E. Wada, Glacial to Interglacial Surface Nutrient Variations of Bering Deep Basins Recorded By $\delta^{13}C$ and $\delta^{15}N$ of Sedimentary Organic-Matter, *Paleoceanography*, 10, 1047-1061, 1995.

Nameroff, T. J., S. E. Calvert, and J. W. Murray, Glacial-interglacial variability in the eastern tropical North Pacific oxygen minimum zone recorded by redox-sensitive trace metals, *Paleoceanography*, 19, 2004.

Narita, H., M. Sato, S. Tsunogai, M. Murayama, M. Ikehara, T. Nakatsuka, M. Wakatsuchi, N. Harada, and Y. Ujiie, Biogenic opal indicating less productive northwestern North Pacific during the glacial ages, *Geophysical Research Letters*, 29, 2002.

Ohkushi, K., T. Itaki, and N. Nemoto, Last Glacial-Holocene change in intermediate-water ventilation in the Northwestern Pacific, *Quaternary Science Reviews*, 22, 1477-1484, 2003.

Ortiz, J. D., S. B. O'Connell, J. DelViscio, W. Dean, J. D. Carriquiry, T. Marchitto, Y. Zheng, and A. van Geen, Enhanced marine productivity off western North America during warm climate intervals of the past 52 ky, *Geology*, 32, 521-524, 2004.

Peterson, T. D., F. A. Whitney, and P. J. Harrison, Macronutrient dynamics in an anticyclonic mesoscale eddy in the Gulf of Alaska, *Deep-Sea Research Part II-Topical Studies in Oceanography*, 52, 909-932, 2005.

Petit, J. R., J. Jouzel, D. Raynaud, N. I. Barkov, J. M. Barnola, I. Basile, M. Bender, J. Chappellaz, M. Davis, G. Delaygue, M. Delmotte, V. M. Kotlyakov, M. Legrand, V. Y. Lipenkov, C. Lorius, L. Pepin, C. Ritz, E. Saltzman, and M. Stievenard, Climate and atmospheric history of the past 420,000 years from the Vostok ice core, Antarctica, *Nature*, 399, 429-436, 1999.

Pondaven, P., O. Ragueneau, P. Treguer, A. Hauvespre, L. Dezileau, and J. L. Reyss, Resolving the 'opal paradox' in the Southern Ocean, *Nature*, 405, 168-172, 2000.

Prahl, F. G., G. L. Cowie, G. J. De Lange, and M. A. Sparrow, Selective organic matter preservation in "burndown" turbidites on the Madeira Abyssal Plain, *Paleoceanography*, 18, 2003.

Pride, C., R. Thunell, D. Sigman, L. Keigwin, M. Altabet, and E. Tappa, Nitrogen isotopic variations in the Gulf of California since the last deglaciation: Response to global climate change, *Paleoceanography*, 14, 397-409, 1999.

Prokopenko, M., Fractionation of nitrogen isotopes during early diagenesis, PhD, University of Southern California, Los Angeles, 2005.

Rabouille, C., and J. F. Gaillard, Towards the Edge - Early Diagenetic Global Explanation - a Model Depicting the Early Diagenesis of Organic-Matter, O_2, NO_3, Mn, and PO_4, *Geochimica Et Cosmochimica Acta*, 55, 2511-2525, 1991.

Ragueneau, O., P. Treguer, A. Leynaert, R. F. Anderson, M. A. Brzezinski, D. J. DeMaster, R. C. Dugdale, J. Dymond, G. Fischer, R. Francois, C. Heinze, E. Maier-Reimer, V. Martin-Jezequel, D. M. Nelson, and B. Queguiner, A review of the Si cycle in the modern ocean: recent progress and missing gaps in the application of biogenic opal as a paleoproductivity proxy, *Global and Planetary Change*, 26, 317-365, 2000.

Rea, D. K., I. A. Basov, T. R. Janacek, and A. Palmer-Julson, Introduction to Leg 145: North Pacific Transect. in *Proceedings of ODP Initial Reports*, pp. 85-120, College Station, Texas, 1993.

Reid, J. L., Intermediate waters of the Pacific Ocean, *Johns Hopkins Oceanographic Studies*, 5, 1-96, 1965.

Robinson, R. S., B. G. Brunelle, and D. M. Sigman, Revisiting nutrient utilization in the glacial Antarctic: Evidence from a new method for diatom-bound N isotopic analysis, *Paleoceanography*, 19, 2004.

Ruth, U., D. Wagenbach, J. P. Steffensen, and M. Bigler, Continuous record of microparticle concentration and size distribution in the central Greenland NGRIP ice core during the last glacial period, *Journal of Geophysical Research-Atmospheres*, 108, 2003.

Sachs, J. P., and D. J. Repeta, Oligotrophy and nitrogen fixation during eastern Mediterranean sapropel events, *Science*, 286, 2485-2488, 1999.

Saino, T., and A. Hattori, Geographical variation of the water column distribution of suspended particulate organic nitrogen and its ^{15}N natural abundance in the Pacific and its marginal seas, *Deep-Sea Research*, 34, 807-827, 1987.

Sarmiento, J. L., N. Gruber, M. A. Brzezinski, and J. P. Dunne, High-latitude controls of thermocline nutrients and low latitude biological productivity, *Nature*, 427, 56-60, 2004.

Sarmiento, J. L., and J. R. Toggweiler, A New Model for the Role of the Oceans in Determining Atmospheric Pco2, *Nature*, 308, 621-624, 1984.

Sigman, D. M., The Role of Biological Production in Pleistocene Atmospheric Carbon Dioxide Variations and the Nitrogen Isotope Dynamics of the Southern Ocean, Doctoral, MIT/WHOI, Cambridge, Massachusetts, 1997.

Sigman, D. M., M. A. Altabet, D. C. McCorkle, R. Francois, and G. Fischer, The $\delta^{15}N$ of nitrate in the Southern Ocean: Consumption of nitrate in surface waters, *Global Biogeochemical Cycles*, 13, 1149-1166, 1999.

Sigman, D. M., M. A. Altabet, D. C. McCorkle, R. Francois, and G. Fischer, The $\delta^{15}N$ of nitrate in the Southern Ocean: Nitrogen cycling and circulation in the ocean interior, *Journal of Geophysical Research-Oceans*, 105, 19599-19614, 2000.

Sigman, D. M., K. L. Casciotti, M. Andreani, C. Barford, M. Galanter, and J. K. Bohlke, A bacterial method for the nitrogen isotopic analysis of nitrate in seawater and freshwater, *Analytical Chemistry*, 73, 4145-4153, 2001.

Sigman, D. M., and G. H. Haug, The Biological Pump in the Past. in *Treatise on Geochemistry*, edited by Holland, D. and K. K. Turekian, pp. 491-528, Elsevier, Amsterdam, 2003.

Sigman, D. M., R. Robinson, A. N. Knapp, A. van Geen, D. C. McCorkle, J. A. Brandes, and R. C. Thunell, Distinguishing between water column and sedimentary denitrification in the Santa Barbara Basin using the stable isotopes of nitrate, *Geochemistry Geophysics Geosystems*, 4, art. no.-1040, 2003.

Stabeno, P. J., N. A. Bond, A. J. Hermann, N. B. Kachel, C. W. Mordy, and J. E. Overland, Meteorology and oceanography of the Northern Gulf of Alaska, *Continental Shelf Research*, 24, 859-897, 2004.

Stephens, B. B., and R. F. Keeling, The influence of Antarctic sea ice on glacial-interglacial CO_2 variations, *Nature*, 404, 171-174, 2000.

Strzepek, R. F., and P. J. Harrison, Photosynthetic architecture differs in coastal and oceanic diatoms, *Nature*, 431, 689-692, 2004.

Sunda, W., and S. Huntsman, Iron uptake and growth limitation in oceanic and coastal phytoplankton, *Marine Chemistry*, 50, 189-206, 1995.

Takahashi, K., N. Fujitani, M. Yanada, and Y. Maita, Long-term biogenic particle fluxes in the Bering Sea and the central subarctic Pacific Ocean, 1990-1995, *Deep-Sea Research Part I-Oceanographic Research Papers*, 47, 1723-1759, 2000.

Talley, L. D., North Pacific intermediate water transports in the mixed water region, *Journal of Physical Oceanography*, 27, 1795-1803, 1997.

Thomson, R. E., and J. F. R. Gower, A basin-scale oceanic instability event in the Gulf of Alaska, *Journal of Geophysical Research-Oceans*, 103, 3033-3040, 1998.

Thunell, R. C., D. M. Sigman, F. Muller-Karger, Y. Astor, and R. Varela, Nitrogen isotope dynamics of the Cariaco Basin, Venezuela, *Global Biogeochemical Cycles*, 18, 2004.

Tsuda, A., S. Takeda, H. Saito, J. Nishioka, Y. Nojiri, I. Kudo, H. Kiyosawa, A. Shiomoto, K. Imai, T. Ono, A. Shimamoto, D. Tsumune, T. Yoshimura, T. Aono, A. Hinuma, M. Kinugasa, K. Suzuki, Y. Sohrin, Y. Noiri, H. Tani, Y. Deguchi, N. Tsurushima, H. Ogawa, K. Fukami, K. Kuma, and T. Saino, A mesoscale iron enrichment in the western Subarctic Pacific induces a large centric diatom bloom, *Science*, 300, 958-961, 2003.

Ueno, H., and I. Yasuda, Intermediate water circulation in the North Pacific subarctic and northern subtropical regions, *Journal of Geophysical Research-Oceans*, 108, 2003.

van Geen, A., Y. Zheng, J. M. Bernhard, K. G. Cannariato, J. Carriquiry, W. E. Dean, B. W. Eakins, J. D. Ortiz, and J. Pike, On the preservation of laminated sediments along the western margin of North America, *Paleoceanography*, 18, 2003.

vanGeen, A., R. G. Fairbanks, P. Dartnell, M. McGann, J. V. Gardner, and M. Kashgarian, Ventilation changes in the northeast Pacific during the last deglaciation, *Paleoceanography*, 11, 519-528, 1996.

Voss, M., J. W. Dippner, and J. P. Montoya, Nitrogen isotope patterns in the oxygen-deficient waters of the Eastern Tropical North Pacific Ocean, *Deep-Sea Research Part I-Oceanographic Research Papers*, 48, 1905-1921, 2001.

Wada, E., and A. Hattori, Natural abundance of ^{15}N in particulate organic matter in the North Pacific Ocean, *Geochimica Et Cosmochimica Acta*, 40, 249-251, 1976.

Whitney, F., and M. Robert, Structure of Haida eddies and their transport of nutrient from coastal margins into the NE Pacific Ocean, *Journal of Oceanography*, 58, 715-723, 2002.

Whitney, F. A., W. R. Crawford, and P. Harrison, Physical processes that enhance nutrient transport and primary productivity in the coastal and open ocean of the subarctic NE Pacific, *Deep-Sea Research Part II-Topical Studies in Oceanography*, 52, 681-706, 2005.

Wu, J. P., S. E. Calvert, C. S. Wong, and F. A. Whitney, Carbon and nitrogen isotopic composition of sedimenting particulate material at Station Papa in the subarctic northeast Pacific, *Deep-Sea Research Part II-Topical Studies in Oceanography*, 46, 2793-2832, 1999.

Yang, Y. L., H. Elderfield, T. F. Pedersen, and M. Ivanovich, Geochemical Record of the Panama Basin During the Last Glacial Maximum Carbon Event Shows That the Glacial Ocean Was Not Suboxic, *Geology*, 23, 1115-1118, 1995.

Yasuda, I., North Pacific intermediate water: Progress in SAGE (SubArctic Gyre Experiment) and related projects, *Journal of Oceanography*, 60, 385-395, 2004.

Yasuda, I., S. Kouketsu, K. Katsumata, M. Ohiwa, Y. Kawasaki, and A. Kusaka, Influence of Okhotsk Sea Intermediate Water on the Oyashio and North Pacific Intermediate Water, *Journal of Geophysical Research-Oceans*, 107, 2002.

You, Y. Z., Implications of cabbeling on the formation and transformation mechanism of North Pacific Intermediate Water, *Journal of Geophysical Research-Oceans*, 108, 2003a.

You, Y. Z., The pathway and circulation of North Pacific Intermediate Water, *Geophysical Research Letters*, 30, 2003b.

Yun, J. Y., and L. D. Talley, Cabbeling and the density of the North Pacific Intermediate Water quantified by an inverse method, *Journal of Geophysical Research-Oceans*, 108, 2003.

Zheng, Y., R. F. Anderson, A. Van Geen, and M. Q. Fleisher, Preservation of particulate non-lithogenic uranium in marine sediments, *Geochimica Et Cosmochimica Acta*, 66, 3085-3092, 2002.

Zheng, Y., A. van Geen, R. F. Anderson, J. V. Gardner, and W. E. Dean, Intensification of the northeast Pacific oxygen minimum zone during the Bolling-Allerod warm period, *Paleoceanography*, 15, 528-536, 2000.

Chapter IV [1]

Glacial-interglacial modulation of the marine nitrogen cycle by high latitude O_2 supply to the global thermocline

4.1 Introduction

Analyses of marine sediment core samples recovered from a growing number of sites have made it clear that, to first order, sedimentary $\delta^{15}N$ records do not uniformly covary over glacial-interglacial timescales, as do, for example, downcore benthic foraminiferal $\delta^{18}O$ records. Instead, downcore $\delta^{15}N$ profiles from different parts of the globe vary greatly in both the magnitude and even the sign of change over climatic cycles. In light of the numerous isotopic fractionation effects observed in the modern ocean (see *Sigman and Casciotti* [2001] for a review), many sedimentary $\delta^{15}N$ records have been interpreted as representing increasingly complex combinations of local processes.

Yet, despite the apparent contrasts between different oceanic regimes, a degree of correspondence has been observed among sedimentary $\delta^{15}N$ records located close to regions of modern Thermocline Denitrification (TD) [*Ganeshram et al.*, 2000; *Kienast et al.*, 2002]. This chapter shows that these correspondences extend to areas with strong oxygen minima but without present-day TD activity. Furthermore, when we examine a region dominated by local inputs of bioavailable N by N_2-fixation as well as those regions which lie between zones of fixation and denitrification, there is evidence for an effective global coupling of the rates of fixation and denitrification, as speculated by other authors [*Tyrrell*, 1999; *Ganeshram et al.*, 2002] but previously uncorroborated by the sedimentary record.

---

[1] A version of this chapter has been published as Galbraith, E.D., Kienast, M., Pedersen, T.F. and Calvert, S.E., "Glacial-interglacial modulation of the marine nitrogen cycle by O_2 supply to the global thermocline", *Paleoceanography*, 19, 2004.

It is proposed here that the link amongst disparate TD zones can be parsimoniously explained by global changes in the marine nitrogen cycle that are fundamentally driven by the flux of dissolved oxygen to the major denitrification zones via lateral advection of waters within the permanent thermocline. The term 'thermocline' is used here to denote the water masses variously referred to as 'central', 'mode', or 'intermediate', which span the potential density range of ~25 to 27.3 kg m^{-3}, in the sense of *Luyten et al.* [1983], *Slowey and Curry* [1995] and *Karstensen and Quadfasel* [2002]. The base of the thermocline varies between a few hundred metres at high latitudes to over 1000 m depth in the central subtropical gyres. The oxygen flux is physically dependent on the combined effects of the temperature dependence of oxygen solubility and the vigour of thermocline ventilation, crucially influenced by wind and sea-ice processes. All of these factors are linked to the sea-surface conditions in the high-latitude source areas where the thermocline is ventilated [*Luyten et al.*, 1983] in the North Pacific, North Atlantic and, most importantly, the Southern Ocean [*Sarmiento et al.*, 2004]. We provide a conceptual model to show how the response of the nitrogen system to changes in the dissolved oxygen supply can produce $\delta^{15}N$ records that vary according to a common rhythm, but which differ in regionally distinct ways.

4.2 Materials and Methods

Downcore $\delta^{15}N$ records have been compiled mainly from the literature, the sources of which are shown in Table 4.1. The records are presented on their original timescales, as per the cited publications, with no modifications. It is important to note that many of these age models rely exclusively on low resolution $\delta^{18}O$ records; errors of > 10 ky are possible, though these errors are significantly reduced near marine isotope stage boundaries. A $\delta^{15}N$ record from ODP Site 887 in the Gulf of Alaska is also included, as discussed in Chapter 3.

4.3 Past changes in sedimentary $\delta^{15}N$

The N isotopic ratio of organic matter accumulated on the seafloor provides a tool with which to characterize past states of the marine N budget, as discussed in Chapter 1. Many local processes introduce fractionation of N isotopes from the initial N pool and have been cited as potential contributors to the $\delta^{15}N$ signal recorded in bottom sediments at a given site. Among these are relative nutrient utilization [*Altabet and Francois*, 1994], phytoplankton

Table 4.1
Sedimentary $\delta^{15}N$ records shown in this chapter

Core	Location	Depth (m)	Reference
ODP 722	Arabian Sea (16°37'N, 59°48'E)	2028	*Altabet et al.*[1999]
ODP 887	Gulf of Alaska (54°21.92'N, 148°26.78'W)	3647	This study
NH22P	Mexico (23°31.1'N, 106°31.1W)	2025	*Ganeshram et al.* [2000]
CD 38-02	Peru (14°56'S, 77°04'W)	2525	*Ganeshram et al.* [2000]
SEDORQUA 20bK	Mauritania (25°02'N, 16°39'W)	1445	*Bertrand et al.* [2000]
GeoB 1016-3	Angola (11°46'S, 11°41'E)	3411	*Holmes et al.* [1999]
MD 96-2086	Namibia (25.81°S, 12.13°E)	3606	*Bertrand et al.* [2002]
SO95 17961	South China Sea (8°30.4N, 112°19.9E)	1795	*Kienast* [2000]
MD 84641	Eastern Mediterranean (33°02'N, 32°38'E)	1375	*Calvert et al.* [1992]

species effects shown in culture [*Montoya and McCarthy*, 1995], trophic exchanges shown in food web studies [*Minagawa and Wada*, 1984], sea-level effects [*Giraud et al.*, 2003] and diagenesis [*Freudenthal et al.*, 2001]. However, it has not been proven that, at a given site, changes in any of these local parameters have large impacts on downcore $\delta^{15}N$ profiles over long time periods; the fact that some records show very little change in $\delta^{15}N$ over hundreds of thousands of years despite significant potential for local influences (e.g. [*Kienast*, 2000]) demonstrates that these processes do not necessarily generate significant variability over time. Consequently, it can be reasonably assumed that local factors – although important in determining the absolute magnitude of the $\delta^{15}N$ signal recorded – are probably relatively invariant on millennial time scales for many fixed locations on the seafloor. Sedimentation is a potent averaging mechanism, involving both areal averaging, through the large-scale lateral advection of sinking and sedimented particles (particularly fine-grained organic matter) [*Mollenhauer et al.*, 2003] and temporal averaging through bioturbation and sampling. As a result, only at sites subject to unusually large, sustained changes in relative nutrient drawdown, plankton community structure, or sedimentary environment do these local processes generate impacts on $\delta^{15}N$ that dominate downcore profiles [*Kienast*, 2005].

Many sedimentary $\delta^{15}N$ records are, instead, overwhelmed by temporal variations in the isotopic signature of the regional nitrogen pools that support plankton growth, determined by the relative importance of N fixation and denitrification within the region [*Altabet et al.*, 1995; *Ganeshram et al.*, 2000; *Struck et al.*, 2001]. Because water column denitrification and N_2 fixation are localized in discrete volumes of the ocean, their isotopic impacts are not evenly distributed. Instead, the ocean will be divisible into those regions in which TD dominates the isotopic signal, those in which N_2 fixation dominates, and those which receive significant influences from both. We look first to regions with 'denitrification-type' records.

4.4 Global changes in denitrification over the past 200 ky

Denitrification in the thermocline currently accounts for 25-60 % of the loss of fixed N from the marine system [*Gruber and Sarmiento*, 1997; *Codispoti et al.*, 2001]; the remainder is lost predominantly by sedimentary denitrification. Strong isotopic fractionation during the incomplete bacterial reduction of NO_3^- to N_2 in the water column leaves a residual NO_3^- pool enriched in ^{15}N. As a result, the $\delta^{15}N$ of nitrate ($\delta^{15}N_{nitrate}$) in the immediate vicinity

of TD zones is higher than the global average $\delta^{15}N_{nitrate}$ of ~ 5 ‰ [*Sigman et al.*, 1999], typically 9 to 18 ‰ [*Brandes et al.*, 1998; *Voss et al.*, 2001]. This isotopically heavy NO_3^- is mixed upwards or wells up, incorporated into phytoplankton and transferred to the sediment, which thereby records a high $\delta^{15}N$ signal. TD is confined to regions where dissolved oxygen concentrations are below 5 μmol/kg [*Codispoti et al.*, 2001] (Figure 4.1), which currently includes the Eastern Tropical North Pacific (ETNP), Eastern Tropical South Pacific (ETSP) and the Arabian Sea (AS). Two other regions, the Subarctic Pacific and the Angola-Benguela system, are only marginally more oxygenated, with $[O_2]$ as low as 18 μmol/kg reported in both regions during the World Ocean Circulation Experiment (WOCE online dataset). Denitrification can occur throughout the upper 1 km of the water column, although the most intense denitrification intervals are found between 150 and 500 m [*Codispoti et al.*, 2001], the upper-central portion of the permanent thermocline, as defined above. Because the locations of these poorly-ventilated cul-de-sacs are defined by large scale gyre circulation, it is unlikely that their gross distribution has changed over the Quaternary.

Previous compilations of sedimentary $\delta^{15}N$ records from regions of modern TD in the Eastern Pacific and the Arabian Sea [*Ganeshram et al.*, 2000] have shown patterns of enhanced denitrification during interglacials and reduced denitrification during glacials. We extend this correspondence to $\delta^{15}N$ records near the remaining low oxygen zones: those of the Subarctic Pacific and western Africa (Figure 4.2). When this is done, a number of strongly coherent characteristics over the past 200 ky emerge. In particular, all have high $\delta^{15}N$ during interglacial periods, both during the 20 ky since the Last Glacial Maximum (LGM) and during the previous interglacial, 135 to 115 ky ago. Particularly consistent is an early Holocene peak, common to all records in which the core top was recovered. Also, pronounced minima occur during cold periods, particularly between ~75 and ~60 ky ago. It is important to note that the chronologies of these records are all based on their original foraminiferal $\delta^{18}O$ timescales; in order to present an unbiased comparison, no attempt has been made to improve temporal agreement by 'tuning' the $\delta^{15}N$ records (although doing so could undoubtedly improve the visual agreement). In spite of our reluctance to fine tune the published records, and as noted previously, it is likely that at least the isotope stage boundaries can be reasonably well correlated, providing some confidence in the identification of the stages themselves and the coherence of the isotopic records displayed.

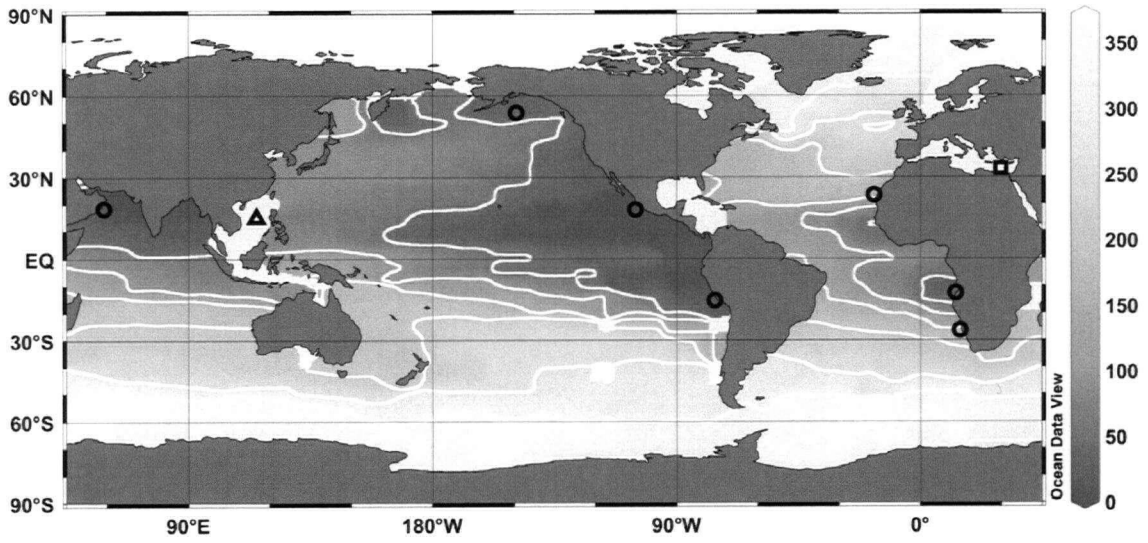

4.1: Dissolved O_2 (μmol/kg) on the 27.0 σ_θ isopycnals; white contour lines are at 50 μmol/kg intervals. This potential density surface lies near the core of the AAIW and intersects the mid-depths of the world's TD zones: the Eastern Tropical North Pacific, Eastern Tropical South Pacific, and Arabian Sea. Also visible are the low O_2 zones of Angola-Benguela, NW Africa and the Subarctic Pacific. The locations of cores discussed in this paper are shown according to their dominant isotopic influence, as discussed in the text, indicated by a circle (denitrification), square (fixation) and triangle (mixed). Oxygen minima zones form where high oxidant demand, generated by the respiration of sinking organic matter from highly productive surface waters, coincides with low rates of oxygen renewal as determined by water mass circulation. Figure generated with Ocean Data View (Schlitzer, R., Ocean Data View, http://www.awi-bremerhaven.de/GEO/ODV, 2003) with the WOCE one-time data set.

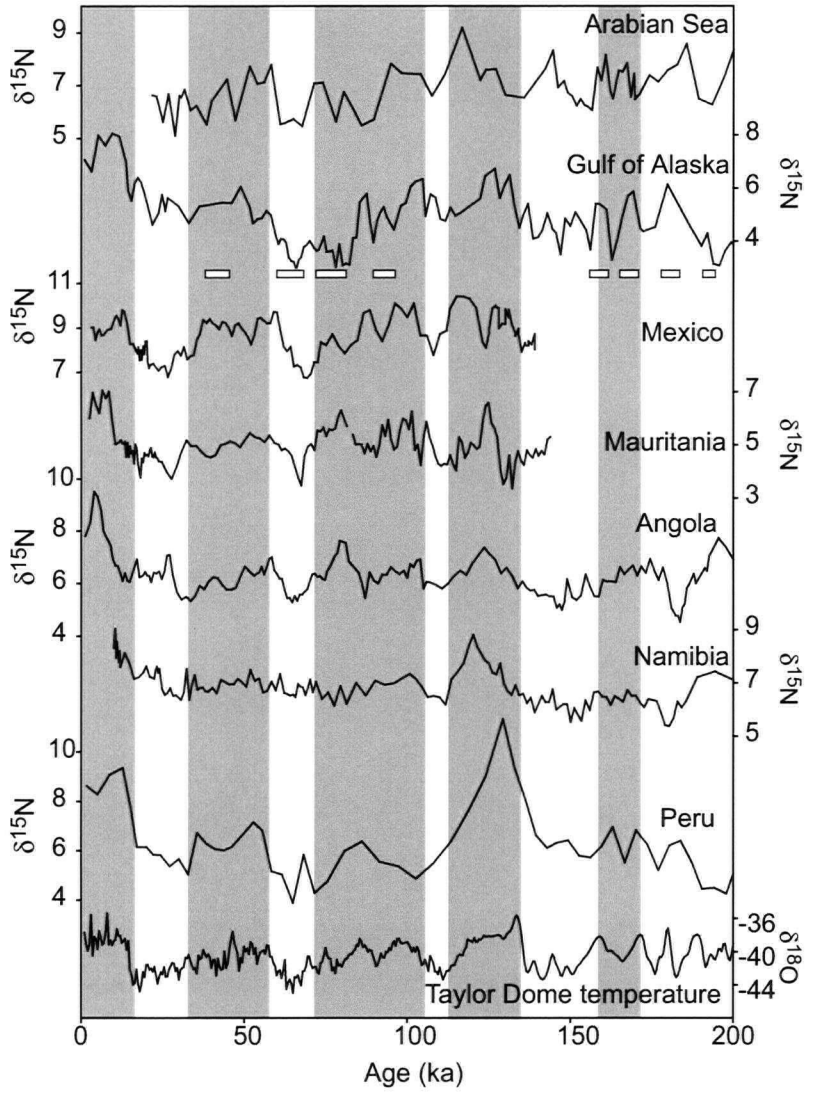

4.2: Sedimentary $\delta^{15}N$ records from areas of present and/or potential TD for the last 200 ky. Shaded bars highlight generally warmer periods. Although the records are by no means identical, they reveal a number of striking similarities. Particularly evident are two maxima (within the last 18 ky and between 135 and 115 ky ago) and two minima (during 74-59 ky ago and 115-108 ky ago), although there are numerous other similar features. It is important to note that all data are plotted vs. the original age models as provided by the authors, with no alteration: Gulf of Alaska [McDonald et al., 1999], Arabian Sea [Altabet et al., 1999], Mazatlan [Ganeshram et al., 2000], Mauritania [Bertrand et al., 2000], Angola [Holmes et al., 1999], Namibia [Bertrand et al., 2002], Peru [Ganeshram et al., 2000]. All timescales are based on $\delta^{18}O$-foraminifera and therefore the age models may have large errors, on the order of 10^4 y. The features discussed are generally synchronous within this error. White rectangles indicate the locations of rapidly deposited diatom-rich layers in the Gulf of Alaska core that interrupt the background of hemipelagic clay without any consistent impact on $\delta^{15}N$. Also shown is a record of $\delta^{18}O_{ice}$, a proxy for atmospheric temperature, from the Taylor Dome ice core, Antarctica [Masson et al., 2000]; [Grootes et al., 2001].

Intervals of high $\delta^{15}N$ in sediments that underlie regions of modern TD clearly indicate periods of enhanced interglacial denitrification, as previously established [*Altabet et al.*, 1995; *Ganeshram et al.*, 1995; *Ganeshram et al.*, 2000]. These have been linked to both climatic changes and to fluctuations in atmospheric concentrations of the radiatively active gases N_2O and CO_2 [*Suthhof et al.*, 2001; *Altabet et al.*, 2002]. However, the explanation for the correspondence observed in the other records is less obvious.

The Gulf of Alaska record (Figure 4.2) shows the presence of grossly simultaneous $\delta^{15}N$ variations, of similar magnitude, far from the nearest recognized location of modern TD (the ETNP). This is the first deep-sea location (3647m water depth) we are aware of that yields a $\delta^{15}N$ record that parallels recognized climate-related changes in denitrification. Drastic changes in productivity, evident as rapidly deposited diatom oozes that punctuate a background of hemipelagic mud over this interval [*McDonald et al.*, 1999] (indicated on Figure 4.2) are associated with only minor fluctuations in $\delta^{15}N$, making a local ecosystem or diagenesis-related explanation for the glacial-interglacial scale downcore variability unlikely (see Chapter 3 for a more in-depth discussion), while the location precludes an influence of sea-level/shelf interactions [*Bertrand et al.*, 2000]. Contemporaneous variations in $\delta^{15}N$ on the western margin of North America recorded as far north as the Oregon margin, where TD does not occur today, have been shown to result from the advection of isotopically heavy nitrate from the ETNP TD zone [*Liu and Kaplan*, 1989; *Pride et al.*, 1999; *Kienast et al.*, 2002], proving that substantial regional signals can emanate beyond a relatively small TD zone; thus, the Gulf of Alaska $\delta^{15}N$ signal may be due solely to advected high $\delta^{15}N_{nitrate}$ from the ETNP. However, given that the amplitude of the Gulf of Alaska signal (2-3 ‰) is comparable to those observed on the Oregon margin [*Kienast et al.*, 2002], despite the much greater distance from the ETNP, it seems unlikely that this can be the sole explanation. An additional contribution has potentially come from local denitrification in the oxygen minimum zone of the subarctic Pacific that has fluctuated in its local intensity. The fact that denitrification has not previously been described in the region may indicate that it has been overlooked, or more likely, that it waned following the early Holocene, due to factors discussed below, and is no longer operational. This is consistent with core-top values >1 ‰ lower than those of the early Holocene maximum, and with a well-documented deglacial

period of widespread oxygen deficiency throughout the North Pacific [*Zheng et al.*, 2000; *Ohkushi et al.*, 2003].

The west African records present a similar situation. Although it has previously been suggested that small amounts of TD occur in the Angola-Benguela system off southwestern Africa [*Dittmar and Birkicht*, 2001; *Tyrrell and Lucas*, 2002], most sedimentary $\delta^{15}N$ records from western Africa have been interpreted as dominantly reflecting changes in local relative nitrate utilization related to wind-driven upwelling dynamics [*Holmes et al.*, 1999; *Martinez et al.*, 2000; *Freudenthal et al.*, 2002]. Nonetheless, it has recently been suggested that enhanced periods of denitrification in the past may have played a role in generating variability in sediment $\delta^{15}N$ records from coastal Namibia [*Lavik*, 2002]. Given the near zero oxygen concentrations in modern thermocline waters of the Angola basin, it seems reasonable that TD may have occurred there in the past, and perhaps also in the low oxygen zone off NW Africa. If so, the lack of significant TD and the relatively low $\delta^{15}N$ of late Holocene sediments in the region could be explained by a decline of local denitrification following the early Holocene, as suggested above for the Gulf of Alaska and as discussed further below. The observed anticorrelation between $\delta^{15}N$ and C_{org} on the SW African margin [*Holmes et al.*, 1999] is consistent with this interpretation, as high rates of TD could reduce the available NO_3^- concentration, limiting C export during production of high $\delta^{15}N_{nitrate}$, and vice versa. Hence, we propose that the majority of large $\delta^{15}N$ variations on glacial-interglacial timescales reflect changes in TD activity on the African margin. Again, the $\delta^{15}N$ increases could be attributed to an intensification of remote denitrification zones and an ensuing reduction in nitrate concentrations on the African coast, leading to higher relative nitrate utilization. In either case, these records testify that changes in denitrification have been broadly global and co-ordinated.

In summary, despite the potential for obfuscation by local processes, sedimentary $\delta^{15}N$ fluctuations chronicle broadly synchronous glacial-interglacial increases and decreases in TD in all oceanic regions with oxygen deficient intermediate waters. In general, it appears that TD is less active during cold periods, more active during warm periods, and most active when the ocean is warming after a cold period. Were the global aggregate TD rate to have changed in the absence of corresponding changes in N_2 fixation, the isotopic signature of the global average $\delta^{15}N$ pool would be expected to have followed the magnitude of TD [*Brandes*

and Devol, 2002] and all $\delta^{15}N$ records would parallel those from TD zones. The fact that they do not provides important information on the operation of the marine N system, as discussed next.

4.5 Coupling of N_2 fixation to denitrification

High denitrification rates in geographically confined regions of the subsurface generate waters depleted in N, i.e. with a relatively low N:P, clearly observed as regions of negative N* in the modern ocean [*Gruber and Sarmiento*, 1997]. Nitrogen fixation counters the loss of N by generating biomass with high N:P [*Karl et al.*, 1997] in shallow, warm, stratified surface waters with sufficient micronutrient input [*Carpenter et al.*, 1997; *Falkowski*, 1997], restoring the water mass N:P to near (or locally above) the 16:1 'Redfield' ratio. The long residence time of marine P (20-30 ky) [*Delaney*, 1998] is generally thought to limit the potential for glacial-interglacial changes in P inventory, and certainly rules out rapid change; thus, it has long been considered the ultimate limiting nutrient on multi-millennial time scales [*Tyrrell*, 1999; *Ganeshram et al.*, 2002]. Nitrogen fixation has thus been regarded as a process that maintains a biologically suitable N:P in the face of N losses from denitrification. Indeed, given a preindustrial rate of total global denitrification of ~0.25 Pg N yr^{-1}, a terrestrial source to the oceans of ~ 0.05 Pg N yr^{-1} and a global inventory of ~1000 Pg N [*Gruber and Sarmiento*, 1997], the oceans would be devoid of N in 5 ky in the absence of N_2 fixation.

However, the spatial separation of these two processes limits the ability of fixation to keep up with denitrification [*Codispoti et al.*, 2001]; the response is not immediate, and the coupling is therefore imperfect. The highest N:P will be found in areas that receive a significant N input from fixation, while elsewhere partially denitrified waters are bound to be N deficient. Thus, during times of high denitrification rates, N limitation will develop throughout large regions of the surface ocean where N_2 fixation is prohibited by other factors [*Codispoti*, 1989; *Falkowski*, 1997]; meanwhile, during times of less extensive denitrification, N limitation will be relieved and global N:P will approach a higher value, as discussed by [*Ganeshram et al.*, 2002].

We propose that the response of regions capable of supporting N_2 fixation to enhanced denitrification occurs via the supply of excess P to such regions. When thermocline

waters that have undergone denitrification (low N:P) well up, NO_3^- is depleted first, leaving excess P. This can be seen in the modern ocean, in that surface waters of the ETNP, ETSP and Arabian Sea become exhausted in nitrate during high production periods while 0.2 - 0.7 μM phosphate remains [*Codispoti*, 1989; *Fanning*, 1992]. The nitrate-depleted surface waters of the ETSP present a particularly good example, maintaining high concentrations of unused phosphate (>0.5 μM) over thousands of km. These high-P waters remain relatively barren until advected, potentially across long distances, to regions with warm (>20 °C), stratified surface waters, with sufficient micronutrient input (including Fe), where they can fuel the growth of N_2 fixers [*Carpenter et al.*, 1997], known often to be limited by P in the modern world [*Sanudo-Wilhelmy et al.*, 2001; *Mills et al.*, 2004]. As a result, N may become more limiting in nitrate-supported upwelling zones while fixation-supported communities, potentially far from denitrification zones, will enjoy relatively high production.

In contrast, when denitrification rates are low, upwelling waters will develop higher N:P ratios. As a result, associated biota will be able to completely utilize P with the upwelled NO_3^- supply, such that very little P is available for nitrogen fixers. This would lead to high productivity in and around upwelling zones and very low productivity in N_2 fixation basins. Because N limitation would be alleviated in most of the ocean, overall productivity would likely be higher during these cold periods. This scenario suggests an interesting relationship with Fe-limitation of N_2 fixers: if dustborne Fe supply is reduced during warm periods [*Falkowski*, 1997] when TD is most active, Fe could limit N_2 fixation in many regions during the periods when it is most needed. On the other hand, abundant Fe supply during cold periods may have little effect on the N inventory, as low P-availability would limit N fixation under cold, windy conditions due to diminished TD.

4.6 Isotopic record of the fixation response

Because of the spatial partitioning of TD and N_2 fixation between localized thermocline waters and warm stratified basins, respectively, we can look to sedimentary $\delta^{15}N$ records in potential N_2 fixation basins for fixation responses corresponding to changes in denitrification, as postulated by [*Ganeshram et al.*, 2002]. Because newly fixed N is isotopically similar to atmospheric N (~-1 ‰) [*Wada and Hattori*, 1976; *Brandes and Devol*, 2002], fixation should leave an imprint of low $\delta^{15}N$ in sediments. However, because N_2

fixation is dispersed across large expanses of tropical and subtropical seas, the isotopic signal will be more dilute than the strongly localized signals of TD zones. An exception to this circumstance would be found in regions with permanently low concentrations of nitrate, where local diazotrophy would constitute the primary N supply. Unfortunately, there are no published $\delta^{15}N$ records from oligotrophic gyres with which to test this hypothesis, because the sediments in such regimes accumulate slowly (generating low resolution records) and often lack foramaniferal age models (because of their great water depth).

However, the eastern Mediterranean is a potentially sensitive region in which to look for changes in N_2 fixation in response to a variable P supply. The deep waters are isolated due to the 500 m deep Straits of Sicily, such that only shallow waters are able to exchange with the western Mediterranean and, ultimately, the North Atlantic. In the modern anti-estuarine situation, shallow (<100 m) nutrient-depleted waters flow into the eastern Mediterranean, maintaining its oligotrophic status and strong P limitation [*Krom et al.*, 1991]. Although the N:P in much of the Mediterranean is already quite high, the surface conditions are apparently so conducive to N_2 fixation that up to 30 % of modern new production is supported by diazotrophic N [*Gruber and Sarmiento*, 1997; *Struck et al.*, 2001; *Pantoja et al.*, 2002]. This, combined with the minimal supply of high $\delta^{15}N$-nitrate from outside the basin, leads to the relatively low $\delta^{15}N$ of surface sediments in the eastern Mediterranean (4 - 4.5 ‰). According to the reasoning presented above, the periods of enhanced denitrification in the eastern Atlantic should have generated low N:P waters which would have spread throughout the region, largely through subsurface circulation. These N-poor waters would have been mixed into the Mediterranean, either at surface or at depth (depending on the circulation regime at the time), encouraging N limitation and, thus, stimulating N_2 fixation resulting in low $\delta^{15}N$.

As shown in Figure 4.3, the $\delta^{15}N$ record from the eastern Mediterranean is entirely consistent with this scenario. All of the $\delta^{15}N$ *maxima* on the west African margin correspond to $\delta^{15}N$ *minima* in the eastern Mediterranean. This diametric opposition can be explained as an overall decrease in the availability of fixed N_2 relative to P and a corresponding increase in N_2 fixation in the ideally suited environment of the Mediterranean. The close relationship between the isotopically-light $\delta^{15}N$ sapropels and hydrographic changes in the basin [*Calvert and Fontugne*, 2001; *Struck et al.*, 2001] may reflect the need for an abundant relative P

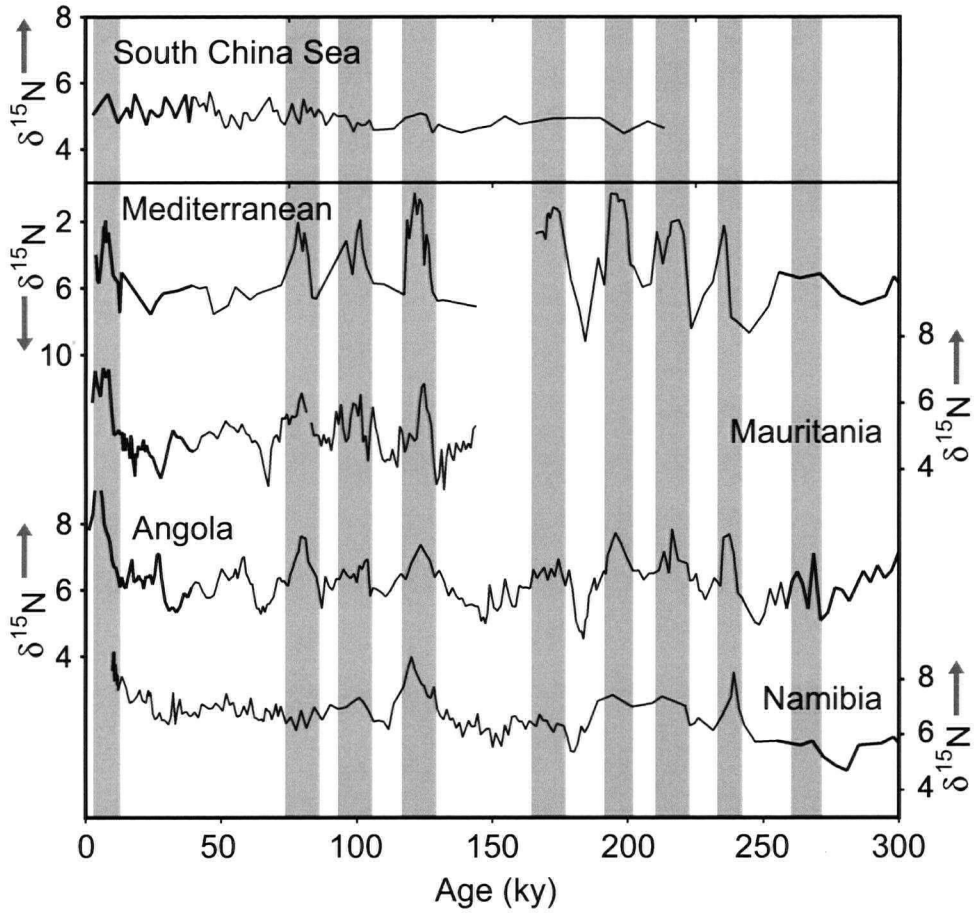

4.3: Sedimentary $\delta^{15}N$ records from fixation, denitrification and well-mixed areas. Denitrification off W Africa is indicated by the $\delta^{15}N$ records of Mauritania, Angola and Namibia, as discussed in the text. The Eastern Mediterranean [Calvert et al., 1992] records low $\delta^{15}N$ (note reversed axes), indicating nitrogen fixation, during the same periods as high denitrification is recorded on the African margin. Sedimentary $\delta^{15}N$ records from the South China Sea [Kienast, 2000] are relatively invariant over the same time period, suggesting that this is a region of globally well-mixed N, which does not register changes in fixation or denitrification.

supply (due to remote denitrification) to promote extensive N fixation, as well as a suitable local physical environment. Precessionally-driven, monsoon-related changes in precipitation have been shown to impact the evaporative balance of the Mediterranean, reducing the anti-estuarine character of the basin during moist periods; we suggest that the difference between the poorly developed 'ghost' sapropels [*Calvert and Fontugne*, 2001] and the well-developed sapropels (characterized by low $\delta^{15}N$) is the externally-controlled relative availability of P in waters supplied to the basin. As such, the sapropels present a particularly clear example of the direct response of nitrogen fixers to global denitrification rates, communicated by the advection into the basin of relatively P-rich waters.

This interpretation is similar to that of [*Struck et al.*, 2001], who also invoked enhanced nutrient supply with N-limitation leading to N_2 fixation during sapropel formation; however they suggested that the denitrification took place within the Mediterranean itself, requiring water-column suboxia, and incompatible with the emerging view of sapropel anoxia as being restricted to a blanket at the sediment-water interface [*Casford et al.*, 2003]. The enhanced runoff during sapropel formation could also promote P supply, but would simultaneously provide additional N and seems therefore less likely to promote the massive amounts of N_2 fixation required to explain the $\delta^{15}N$ record. Of course, correlation is not proof of causation, and the inference that high rates of denitrification in the eastern Atlantic could contribute to sapropel formation needs to be tested further.

4.7 Mixed TD/Fixation d^{15}N records

The arguments presented here support the inference of [*Ganeshram et al.*, 2002] that the global aggregate rates of both TD and N_2 fixation covary over glacial-interglacial time periods. These changes produce symmetrically opposing isotopic signals in TD dominated (high $\delta^{15}N$) and N_2 fixation (low $\delta^{15}N$) regions. Because of the antagonistic relationship between these influences, globally synchronous variations of both should define geographically intermediate regions with less temporal variability in $\delta^{15}N$, in the absence of unusually strong local effects.

In keeping with this prediction, $\delta^{15}N$ records from many regions away from oxygen minimum zones show little or no glacial-interglacial variability. In particular, most records from the South China Sea [*Kienast*, 2000]; [*Tamburini et al.*, 2003] (Figure 4.3) and the

North Atlantic [*Huon et al.*, 2002] show nearly invariant $\delta^{15}N$ records over the last 200 ky. Also, $\delta^{15}N$ records from the Southern Ocean show either little glacial-interglacial change [*Robinson et al.*, 2004] or a pattern clearly unlike that of the TD records [*Francois et al.*, 1997; *Sigman et al.*, 1997]. We note that the recently published $\delta^{15}N$ record of ODP Site 1144, from a drift deposit near the connection of the South China Sea with the open Pacific [*Higginson et al.*, 2003] shows some degree of variability (<2.5 ‰) which has been construed as reflecting glacial-interglacial changes; however, based on sedimentological data, we suspect that the complex sediment mixing dynamics incorporated in the creation of this drift deposit are responsible for many elements of this $\delta^{15}N$ record and its difference from the nearby piston core SO95 17940 [*Kienast et al.*, 2003]. The seven other published $\delta^{15}N$ records of [*Kienast*, 2000] and [*Tamburini et al.*, 2003], representing diverse sedimentary environments throughout the South China Sea, do not display significant glacial-interglacial variability, and show that, on the whole, the isotopic signature of nitrogen in the basin has remained constant within ± 1 ‰ over the past two glacial cycles. This represents a strong constraint on the variation of global average $\delta^{15}N$ over time: the lack of glacial-interglacial $\delta^{15}N$ changes in such regions is difficult to reconcile with whole ocean changes in aggregate TD rates unless these changes are directly matched by changes in N_2 fixation rates. In other words, because fixation supplies isotopically light N to replace the isotopically light N removed through TD [*Brandes and Devol*, 2002], the ratio of fixation:TD must have remained roughly constant during the late Quaternary in order for a global isotopic balance to have been maintained over periods significantly longer than 10^3 years. Additional sedimentary $\delta^{15}N$ records, spatially remote from both potential TD and N_2 fixation basins, are required to test the robustness of this global isotopic balance.

We turn now to the underlying cause driving these changes in the nitrogen cycle. Since it is improbable that simultaneous variations in TD in the Pacific, Atlantic and Indian Oceans (Figure 4.2) could have occurred fortuitously through local processes, we propose a simple global mechanism.

4.8 Surface ocean link to global denitrification

TD occurs in the small fraction of the ocean (~0.1% by volume) in which oxygen has been almost completely consumed by the respiration of organic matter. Only in regions of the

permanent thermocline (150-800 m) with relatively low rates of oxygen supply, which have been exposed to high oxidant demand (OxD) due to the heterotrophic respiration of abundant sinking organic matter, does this happen in the modern ocean (Figure 4.1). Elsewhere, dissolved oxygen is always present in concentrations greater than 5 μmol/kg, which inhibits TD.

Virtually all modern TD takes place in waters in the density range 26.3 – 27.2 kg m^{-3} that are laterally ventilated to some degree by mode and intermediate waters of similar density formed at high latitudes [*Luyten et al.*, 1983; *Sarma*, 2002; *Russell and Dickson*, 2003]. The most important of these are cold, relatively low-salinity waters from the Southern Ocean: the intimately linked Subantarctic Mode Water and Antarctic Intermediate Water, which together span the range σ = 26.0 – 27.4 kg m^{-3}, are ventilated at the rate of ~80 * 10^6 m^3 s^{-1} [*Sloyan and Rintoul*, 2001] and are hereafter collectively referred to as SAMW-AAIW. Because the SAMW-AAIW is of the greatest global importance, providing a dominant input of waters to the thermoclines of the Arabian Sea [*Olson et al.*, 1993], the ETSP [*Toggweiler et al.*, 1991], and the SE Atlantic [*You*, 2002], as well as making a contribution to the ETNP [*Talley*, 1999], we focus our attention on it in this discussion, though other mid-high latitude intermediate water sources (particularly the North Pacific and North Atlantic Intermediate Waters) would be expected to follow most of the same general trends.

SAMW-AAIW leaving the high latitude southern Pacific today, for example, contains roughly 250 μmol/kg O_2 [*Russell and Dickson*, 2003]. As it circuits the subtropical gyre beneath the surface layer, respiration of sinking organic matter provides an OxD that gradually consumes dissolved O_2. While most of this water will well up or mix with more oxygen-rich water masses before the O_2 is fully depleted, a small fraction of this water will follow a path of high OxD. In any region where the total OxD exceeds ~245 μM O_2 equivalent, the suboxic threshold will be passed and denitrification will ensue. Nitrate is slightly more efficient as an electron acceptor on a mol:mol basis than O_2 (5:4), but nonetheless the concentration is much lower – at most about 45 μmol/kg in intermediate depths. Yet, despite the low concentration, denitrification never goes to completion in the modern open ocean water column (though it does in some restricted basins and in all organic-rich sediments). At most, TD currently consumes 12-16 μmol/kg NO_3^- [*Brandes et al.*, 1998; *Voss et al.*, 2001], roughly a third of the nitrate available. This means that even those

thermocline waters that have undergone the highest integrated OxD in the open ocean have >90 % of their oxidant needs met by oxygen. It follows that the presence (or absence) of TD activity is extremely sensitive to both the dissolved oxygen supply and OxD in all thermocline waters that have dissolved oxygen concentrations near zero.

Greater OxD through increased local export productivity, driven by enhanced upwelling, has often been invoked as an explanation for past variations in TD [*Altabet et al.*, 1995; *Ganeshram et al.*, 2000]. Although high rates of export productivity are unquestionably important in generating TD zones, the relevant issue for this discussion is whether or not glacial-interglacial changes in productivity are sufficiently large (and sufficiently uncorrelated with the thermocline O_2 supply) to dominate the TD changes on multi-millennial timescales. The following lines of reasoning lead us to suspect that the oxygen supply term commonly dominates the TD balance on these (and perhaps shorter) timescales.

It has recently been pointed out that productivity increases lag the sedimentary $\delta^{15}N$ enrichments on the western Mexican margin [*Kienast et al.*, 2002], while $\delta^{15}N$ and productivity proxies in the Angola Basin are actually anti-correlated [*Holmes et al.*, 1999]. Meanwhile, productivity changes in the ETNP over the last 140 ky, reconstructed from biogenic Ba data, are insufficient to drive the changes in bottom water oxygenation recorded by redox-sensitive trace metals [*Nameroff et al.*, 2004]. In the Arabian Sea, paleoceanographic studies have often argued for productivity-dominated control of thermocline oxygen concentrations [*Altabet et al.*, 1999; *Schulte et al.*, 1999; *Suthhof et al.*, 2001; *Reichart et al.*, 2002] in spite of the fact that *Olson et al.* [1993] showed that the presence of low-oxygen waters derived from SAMW-AAIW maintained the modern TD. Furthermore, new work by *Sarma* [2002] shows that increased monsoon-driven upwelling in the modern Arabian Sea enhances productivity (and thus OxD) but simultaneously draws in more shallow thermocline water from roughly those depths that host the maximal rates of TD (150-400 m). This replenishes the thermocline O_2 at a rate proportional to the rate of nutrient supply to the surface [*Sarma*, 2002]; therefore, changes in the nutrient:O_2 ratio of subsurface waters advected from the south would be expected to have a greater impact on water-column oxygenation than would changes in upwelling rates. Because all the potential TD-hosting

upwelling zones in question draw waters up from the depths of the most intense oxygen minimum zone, this mechanism should hold true for all of them.

These reasons, coupled with the globally coherent character of $\delta^{15}N$ shifts on glacial-interglacial time scales, lead us to believe that local productivity variations, although undoubtedly important, are not the primary control on the temporal variability of water column suboxia over glacial-interglacial cycles. Instead, local productivity variations modulate the fundamental signal of physically controlled changes in the dissolved O_2 supply. Excluding oxygen consumption during transit of subsurface waters, the supply of O_2 to thermocline waters is essentially a function of two variables: the $[O_2]$ when the water mass leaves the surface, and the rate at which thermocline waters are flushed. As we discuss next, both of these factors are likely to have favoured higher O_2 supply during glacial periods.

4.9 Climatically driven changes in O_2 supply

The solubility of O_2 in seawater is strongly dependent on temperature, with solubility increasing rapidly as the temperature nears the freezing point. At the same time, the degree of O_2 saturation is dependent on the efficiency of wind mixing in the formation region; poor mixing limits the modern SAMW-AAIW initial $[O_2]$ to roughly 50 μmol/kg below saturation [*Russell and Dickson*, 2003]. Palaeoceanographic evidence shows that the surface of the Southern Ocean cooled by 4-5 °C during the LGM [*Mashiotta et al.*, 1999], while proxies of thermocline water temperature are consistent with a glacial SAMW-AAIW that was 4-5 °C colder [*Herguera et al.*, 1991; *Lynchstieglitz and Fairbanks*, 1994; *Matsumoto et al.*, 2002] and a glacial NAIW that was 4 °C colder [*Slowey and Curry*, 1995]. A 4 °C temperature decrease corresponds to an increase in oxygen saturation of ~32 μmol/kg. Meanwhile, dust records have been interpreted as reflecting increased windiness during glacial periods [*Petit et al.*, 1999], which would have driven the initial $[O_2]$ of SAMW-AAIW toward saturation. Combining the temperature effect with some degree of enhanced saturation suggests an increase in initial $[O_2]$ during glacial periods of 30 to 80 μmol/kg above the modern value, an increase of 12 to 32 %. Given that the most intense modern TD zones require an increase in $[O_2]$ of only 20 μmol/kg in order to shut down denitrification altogether, this change in surface ocean conditions is capable of providing a first order control on global intermediate water $[O_2]$ and, consequently, the extent of global TD over glacial-interglacial time scales.

The rate of SAMW-AAIW formation is also likely to have been generally higher during glacial periods. Stronger Southern Hemisphere high-latitude winds would have enhanced Ekman convergence, driving more cold, low salinity surface water northwards into the permanent thermocline [*Karstensen and Quadfasel*, 2002]. An abundant supply of cool, low salinity surface water appropriate for subduction would have been ensured by the glacially enhanced distillation effect of seasonal sea-ice formation, which increases salinity through brine rejection during freezing near Antarctica, while decreasing salinity in the more northerly latitudes where the ice is blown by wind and subsequently melts [*Saenko and Weaver*, 2001]. Accelerated formation of SAMW-AAIW, consistent with heavy benthic foraminiferal $\delta^{13}C$ in intermediate depths [*McCorkle et al.*, 1998; *Matsumoto et al.*, 2002] would have enhanced the O_2 supply to the global thermocline by increasing flow rates. The effects of high latitude surface processes on the nitrogen cycle are shown schematically in Figure 4.4.

Although SAMW-AAIW is the single most important global source of O_2 to the thermocline [*Russell and Dickson*, 2003], the Northern Hemisphere mid-high latitude thermocline ventilation should also be enhanced under cold, windy conditions. However, it must also be recognized that the O_2 budgets of potential TD zones in different locations will also depend on low-latitude O_2 sources, such as local intermediate water formation and diapycnal mixing of O_2-rich waters from above, as well as currently unresolvable possibilities of altered circulation pathways. These impacts would introduce additional spatio-temporal complexity, superimposed upon the long-term global trends. Furthermore, even if changes in O_2 supply were globally uniform, the response of geographically separated TD zones to gradual changes in thermocline O_2 supply would be neither linear nor synchronous.

This important corollary follows from the spatial complexity and temporal variability of marine export production (and hence OxD), which engenders a range of TD thresholds as illustrated schematically in Figure 4.5. Some regions of the world ocean would be expected to experience consistently high OxD and be sites of significant TD during all but the coldest and windiest periods (eg. western Mexican margin, Figure 4.2 and schematically illustrated by line a in Figure 4.5), while others only experience enough OxD to instigate TD during the warmest and calmest conditions (eg. Peru, Figure 4.2, line b of Figure 4.5). It follows that

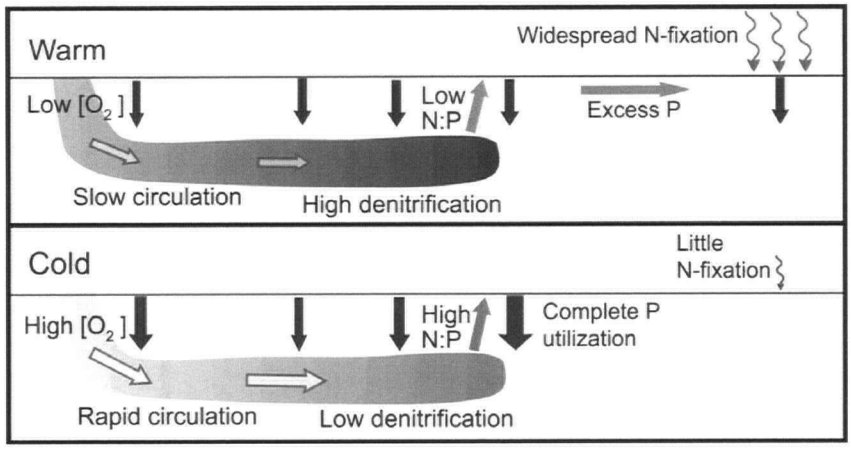

4.4: Schematic illustration of high latitude surface control on denitrification and the fixation response. Downward pointing arrows represent export production. Intermediate waters that form under warm conditions (top) carry relatively less O_2 and circulate more slowly, thus encouraging suboxia and denitrification. Under cold conditions (bottom), high dissolved [O_2] and rapid circulation reduce the extent of suboxia, impeding denitrification. Denitrification zones remove fixed-N from intermediate waters, exporting low N:P waters which, when upwelled, produce N-limited communities; excess-P is then advected to regions with warm, stratified surface waters where it fuels nitrogen fixation. When high O_2 inhibits denitrification, high N:P ratios in upwelling zones allow complete utilization of P to the detriment of N_2-fixation communities elsewhere.

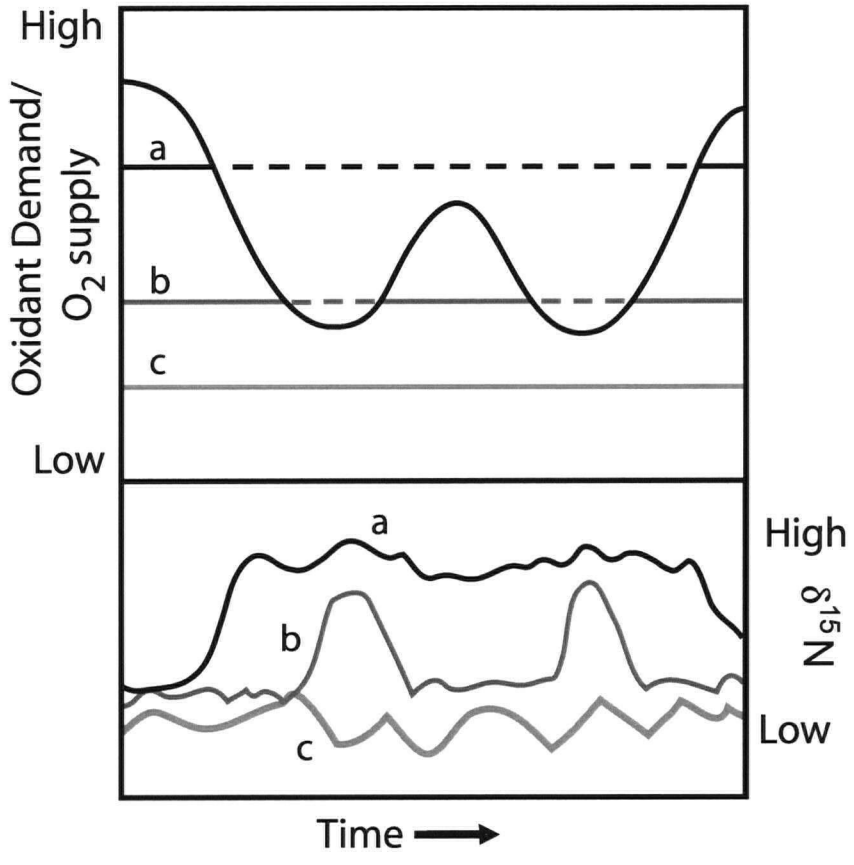

4.5: A schematic illustration showing expected temporal contrasts in the activity of TD in three different water masses subjected to identical changes in O_2 supply over time (top) and the local $\delta^{15}N$ records that would result (bottom). Each horizontal line in the top panel represents a hypothetical water mass that is subject to a constant oxidant demand (OxD) over time. Water mass 'a' receives the greatest oxidant demand, while water mass 'c' receives the least. The curved line represents the changing O_2 supply over time, driven by physical processes. The solid horizontal segments indicate time periods when oxygenation is sufficient to inhibit denitrification, while dashed horizontal segments indicate periods when oxygen is insufficient and denitrification is active. As shown, the onsets and cessations of denitrification are not exactly synchronous among the water masses, even in this highly idealized case in which local temporal variation of OxD is ignored, simply due to different threshold sensitivities to O_2 supply. Nonetheless, the $\delta^{15}N$ records follow the same general trends over long time scales.

contrasts in sensitivity to both O_2 supply and fluctuations in the local distributions of OxD should produce regional phase offsets in the onsets and cessations of denitrification amongst the different OMZs on millennial time scales. This critical feature of the proposed model is illustrated by the $\delta^{15}N$ curves sketched in the bottom panel of Figure 4.5. As a result, tuning of distant $\delta^{15}N$ records to each other on millennial timescales is unjustified without independent time control, and time series analyses of multiple records must be interpreted cautiously.

4.10 Early Holocene $\delta^{15}N$ maxima

As mentioned earlier, all $\delta^{15}N$ records from within or near potential TD zones show maxima during the early Holocene (Figure 4.2). We suggest two complementary mechanisms to explain a maximum in TD after the LGM, followed by a decline to modern values.

First, circum-Antarctic atmospheric and sea surface temperatures peaked [*Ikehara et al.*, 1997; *Mashiotta et al.*, 1999; *Masson et al.*, 2000] while sea ice extent reached a minimum near 11 to 10 ky ago [*Hodell et al.*, 2001]. Thus, O_2 supply to intermediate waters would have reached a minimum at this time. This minimum remained roughly unchanged until 5-6 ky ago, when Southern Ocean temperatures began to decrease and sea ice extent expanded, thus increasing the O_2 supply and reducing the oxygen deficiency in distant denitrification zones. However, the Holocene climatic deterioration was relatively minor and it seems unlikely that a linear dependence on O_2 supply can be the sole explanation for the $\delta^{15}N$ decline.

More importantly, it is likely that the deglacial increase in denitrification would have reduced global N:P because of the imperfect coupling of denitrification and fixation, as discussed above. The expansion of oceanic regimes limited by NO_3^- (i.e. those in which fixation is incapable of compensating N loss due to micronutrient limitation or inappropriate physical conditions) is likely to have reduced export productivity over the deglaciation, decreasing the OxD (the 'slow' feedback of *Codispoti* [1989]). Because TD zones occur near large upwelling-driven ecosystems that are prone to nitrate limitation, this feedback would be effective in reducing OxD in the most sensitive regions (see Chapter 5).

As an example, consider the ETNP. Today, in the heart of the denitrification zone, nitrate concentrations average roughly 30 μmol/kg, while phosphate concentrations are ~ 2.5

μmol/kg (a nitrate deficit of 10 μmol/kg). If oxygen supply were sufficient during the LGM to have completely inhibited thermocline denitrification, immediately-upwelled water might be expected to have an N/P near 16; thus, we would have concentrations of 40 μmol/kg NO_3^- and 2.5 μmol/kg PO_4^{3-}. If the oxygen minimum were then to become suboxic early in the deglaciation, and the denitrification zone were to intensify to roughly double that of today, denitrified waters would contain only 20 μmol/kg NO_3^-. When welled up, these waters would only be able to support half the export production of their glacial equivalents in the absence of immediate N_2 fixation.

Such a negative feedback between denitrification and OxD would serve to stabilize the system once the O_2 supply had ceased its downward trend. In effect, global OxD would readjust to changes in O_2 supply over $10^2 - 10^3$ years in order to bring the N system into balance. We speculate that this homeostatic mechanism may be responsible for maintaining the global OxD in near-balance with O_2 supply over long timescales, preventing widespread water column anoxia despite variable environmental conditions.

Denitrification in bottom sediments could also have a complicated effect on the N balance of the ocean via the change in the locus of organic matter oxidation due to sea level fluctuations. As discussed by *Christensen et al.* [1987] (see also Chapter 1), the exposure of ~75 % of the world's continental shelves during glacial lowstand would have reduced the amount of remineralization in shelf sediments, and shifted more of the remineralization burden (hence OxD) to the water column. As long as O_2 supply to the thermocline remained vigorous, this OxD would have been largely satisfied by dissolved O_2. However, during the deglaciation, the decrease in O_2 supply would have preceded the resumption of sediment denitrification, as shelves were not yet flooded, causing an intervening period of high water column OxD and declining O_2. The subsequent decline in Holocene $\delta^{15}N$ could then reflect the short-circuiting of water column remineralization by the 'trap' of submerged continental shelves.

The early Holocene $\delta^{15}N$ maximum highlights an important feature of the marine nitrogen system: productivity feedbacks on TD are likely to complicate the temporal-spatial pattern, such that the global aggregate rates of TD are not strictly correlated with temperature and winds. The accumulated evidence shows that, instead, TD is maximal during the

transitions from cold to warm periods as the marine nitrogen cycle adjusts to the diminishing oxygen supply.

4.11 Summary and Conclusions

This paper has presented a parsimonious reconciliation of diverse nitrogen isotope records on long timescales (>10 ky), which calls on a strong temporal coupling of denitrification to N_2 fixation as has been suggested previously [*Ganeshram et al.*, 2002]. As the fundamental driver, a direct link is proposed between oceanic surface conditions and the oxygenation of the global permanent thermocline, which modulates the nutrient dynamics of the marine biosphere. This relatively simple, physical mechanism has the potential to explain much of the variability in sedimentary $\delta^{15}N$ records as well as some contribution to the known atmospheric pCO_2 and pN_2O fluctuations [*Fluckiger et al.*, 2004] over the past 200 ky. Furthermore, it can be readily tested by developing records of thermocline water temperature and ventilation-related parameters in the 200 – 1000 m depth range, and through modeling studies, as presented in the following chapter.

4.12 References

Altabet, M. A., and R. Francois, Sedimentary Nitrogen Isotopic Ratio As a Recorder For Surface Ocean Nitrate Utilization, *Global Biogeochemical Cycles*, 8, 103-116, 1994.

Altabet, M. A., R. Francois, D. W. Murray, and W. L. Prell, Climate-Related Variations in Denitrification in the Arabian Sea From Sediment $^{15}N/^{14}N$ Ratios, *Nature*, 373, 506-509, 1995.

Altabet, M. A., M. J. Higginson, and D. W. Murray, The effect of millennial-scale changes in Arabian Sea denitrification on atmospheric CO2, *Nature*, 415, 159-162, 2002.

Altabet, M. A., D. W. Murray, and W. L. Prell, Climatically linked oscillations in Arabian Sea denitrification over the past 1 m.y.: Implications for the marine N cycle, *Paleoceanography*, 14, 732-743, 1999.

Bertrand, P., J. Giraudeau, B. Malaize, P. Martinez, M. Gallinari, T. F. Pedersen, C. Pierre, and M. T. Venec-Peyre, Occurrence of an exceptional carbonate dissolution episode during early glacial isotope stage 6 in the Southeastern Atlantic, *Marine Geology*, 180, 235-248, 2002.

Bertrand, P., T. F. Pedersen, P. Martinez, S. Calvert, and G. Shimmield, Sea level impact on nutrient cycling in coastal upwelling areas during deglaciation: Evidence from nitrogen isotopes, *Global Biogeochemical Cycles*, 14, 341-355, 2000.

Brandes, J. A., and A. H. Devol, A global marine-fixed nitrogen isotopic budget: Implications for Holocene nitrogen cycling, *Global Biogeochemical Cycles*, 16, art. no.-1120, 2002.

Brandes, J. A., A. H. Devol, T. Yoshinari, D. A. Jayakumar, and S. W. A. Naqvi, Isotopic composition of nitrate in the central Arabian Sea and eastern tropical North Pacific: A tracer for mixing and nitrogen cycles, *Limnology and Oceanography*, 43, 1680-1689, 1998.

Calvert, S. E., and M. R. Fontugne, On the late Pleistocene-Holocene sapropel record of climatic and oceanographic variability in the eastern Mediterranean, *Paleoceanography*, 16, 78-94, 2001.

Calvert, S. E., B. Nielsen, and M. R. Fontugne, Evidence From Nitrogen Isotope Ratios For Enhanced Productivity During Formation of Eastern Mediterranean Sapropels, *Nature*, 359, 223-225, 1992.

Carpenter, E. J., H. R. Harvey, B. Fry, and D. G. Capone, Biogeochemical tracers of the marine cyanobacterium Trichodesmium, *Deep-Sea Research Part I*, 44, 27-38, 1997.

Casford, J. S. L., E. J. Rohling, R. H. Abu-Zied, C. Fontanier, F. J. Jorissen, M. J. Leng, G. Schmiedl, and J. Thomson, A dynamic concept for eastern Mediterranean circulation and oxygenation during sapropel formation, *Palaeogeography Palaeoclimatology Palaeoecology*, 190, 103-119, 2003.

Christensen, J. J., J. W. Murray, A. H. Devol, and L. A. Codispoti, Denitrification in continental shelf sediments has major impact on the oceanic nitrogen budget, *Global Biogeochemical Cycles*, 1, 97-116, 1987.

Codispoti, L. A., Phosphorus vs nitrogen limitation of new and export production. in *Productivity of the ocean: Present and past*, edited by Berger, W., V. Smetacek and G. Wefer, pp. 377-394, John Wiley and Sons, Chichester, 1989.

Codispoti, L. A., J. A. Brandes, J. P. Christensen, A. H. Devol, S. W. A. Naqvi, H. W. Paerl, and T. Yoshinari, The oceanic fixed nitrogen and nitrous oxide budgets: Moving targets as we enter the anthropocene?, *Scientia Marina*, 65, 85-105, 2001.

Delaney, M. L., Phosphorus accumulation in marine sediments and the oceanic phosphorus cycle, *Global Biogeochemical Cycles*, 12, 563-572, 1998.

Dittmar, T., and M. Birkicht, Regeneration of nutrients in the northern Benguela upwelling and the Angola-Benguela Front areas, *South African Journal of Science*, 97, 239-246, 2001.

Falkowski, P. G., Evolution of the nitrogen cycle and its influence on the biological sequestration of CO_2 in the ocean, *Nature*, 387, 272-275, 1997.

Fanning, K. A., Nutrient Provinces in the Sea - Concentration Ratios, Reaction-Rate Ratios, and Ideal Covariation, *Journal of Geophysical Research-Oceans*, 97, 5693-5712, 1992.

Fluckiger, J., T. Blunier, B. Stauffer, M. Chappellaz, R. Spahni, K. Kawamura, J. Schwander, T. F. Stocker, and D. Dahl-Jensen, N_2O and CH_4 variations during the last glacial epoch: Insight into global processes, *Global Biogeochemical Cycles*, 18, 2004.

Francois, R., M. A. Altabet, E. F. Yu, D. M. Sigman, M. P. Bacon, M. Frank, G. Bohrmann, G. Bareille, and L. D. Labeyrie, Contribution of Southern Ocean surface-water stratification to low atmospheric CO_2 concentrations during the last glacial period, *Nature*, 389, 929-935, 1997.

Freudenthal, T., H. Meggers, J. Henderiks, H. Kuhlmann, A. Moreno, and G. Wefer, Upwelling intensity and filament activity off Morocco during the last 250,000 years, *Deep-Sea Research Part II-Topical Studies in Oceanography*, 49, 3655-3674, 2002.

Freudenthal, T., T. Wagner, F. Wenzhofer, M. Zabel, and G. Wefer, Early diagenesis of organic matter from sediments of the eastern subtropical Atlantic: Evidence from stable nitrogen and carbon isotopes, *Geochimica Et Cosmochimica Acta*, 65, 1795-1808, 2001.

Ganeshram, R. S., T. F. Pedersen, S. E. Calvert, and R. Francois, Reduced nitrogen fixation in the glacial ocean inferred from changes in marine nitrogen and phosphorus inventories, *Nature*, 415, 156-159, 2002.

Ganeshram, R. S., T. F. Pedersen, S. E. Calvert, G. W. McNeill, and M. R. Fontugne, Glacial-interglacial variability in denitrification in the world's oceans: Causes and consequences, *Paleoceanography*, 15, 361-376, 2000.

Ganeshram, R. S., T. F. Pedersen, S. E. Calvert, and J. W. Murray, Large changes in oceanic nutrient inventories from glacial to interglacial periods, *Nature*, 376, 755-758, 1995.

Giraud, X., P. Bertrand, V. Garcon, and I. Dadou, Interpretation of the nitrogen isotopic signal variations in the Mauritanian upwelling with a 2D physical-biogeochemical model, *Global Biogeochemical Cycles*, 17, 2003.

Gruber, N., and J. L. Sarmiento, Global patterns of marine nitrogen fixation and denitrification, *Global Biogeochemical Cycles*, 11, 235-266, 1997.

Herguera, J. C., L. D. Stott, and W. H. Berger, Glacial Deep-Water Properties in the West-Equatorial Pacific - Bathyal Thermocline Near a Depth of 2000 m, *Marine Geology*, 100, 201-206, 1991.

Higginson, M. J., J. R. Maxwell, and M. A. Altabet, Nitrogen isotope and chlorin paleoproductivity records from the Northern South China Sea: remote vs. local forcing of millennial- and orbital-scale variability, *Marine Geology*, 201, 223-250, 2003.

Hodell, D. A., S. L. Kanfoush, A. Shemesh, X. Crosta, C. D. Charles, and T. P. Guilderson, Abrupt cooling of Antarctic surface waters and sea ice expansion in the South Atlantic sector of the Southern Ocean at 5000 cal yr B.P, *Quaternary Research*, 56, 191-198, 2001.

Holmes, M. E., C. Eichner, U. Struck, and G. Wefer, Reconstruction of Surface Ocean Nitrate Utilization Using Stable Nitrogen Isotopes in Sinking Particles and Sediments. in *The Use of Proxies in Paleoceanography: Examples from the South Atlantic*, edited by Fischer, G. and G. Wefer, pp. 447-468, Springer, 1999.

Huon, S., F. E. Grousset, D. Burdloff, G. Bardoux, and A. Mariotti, Sources of fine-sized organic matter in North Atlantic Heinrich layers: $\delta^{13}C$ and $\delta^{15}N$ tracers, *Geochimica Et Cosmochimica Acta*, 66, 223-239, 2002.

Ikehara, M., K. Kawamura, N. Ohkouchi, K. Kimoto, M. Murayama, T. Nakamura, T. Oba, and A. Taira, Alkenone sea surface temperature in the Southern Ocean for the last two deglaciations, *Geophysical Research Letters*, 24, 679-682, 1997.

Karl, D., R. Letelier, L. Tupas, J. Dore, J. Christian, and D. Hebel, The role of nitrogen fixation in biogeochemical cycling in the subtropical North Pacific Ocean, *Nature*, 388, 533-538, 1997.

Karstensen, J., and D. Quadfasel, Formation of southern hemisphere thermocline waters: Water mass conversion and subduction, *Journal of Physical Oceanography*, 32, 3020-3038, 2002.

Kienast, M., Unchanged nitrogen isotopic composition of organic matter in the South China Sea during the last climatic cycle: Global implications, *Paleoceanography*, 15, 244-253, 2000.

Kienast, M., On the sedimentological origin of down-core variations of bulk sedimentary nitrogen isotope ratios, *Paleoceanography*, 20, 2005.

Kienast, M., M. J. Higginson, G. Mollenhauer, T. I. Eglinton, and S. E. Calvert, On the potential sedimentological origin of downcore variations of bulk sedimentary $\delta^{15}N$, paper presented at EOS Trans. AGU, 2003.

Kienast, S. S., S. E. Calvert, and T. F. Pedersen, Nitrogen isotope and productivity variations along the northeast Pacific margin over the last 120 kyr: Surface and subsurface paleoceanography, *Paleoceanography*, 17, art. no.-1055, 2002.

Krom, M. D., N. Kress, S. Brenner, and L. I. Gordon, Phosphorus limitation of primary productivity in the eastern Mediterranean Sea, *Limnology and Oceanography*, 36, 424-432, 1991.

Lavik, G., Nitrogen isotopes of sinking matter and sediments in the South Atlantic, Doctoral, University of Bremen, Bremen, 2002.

Liu, K.-K., and I. R. Kaplan, The eastern tropical Pacific as a source of ^{15}N-enriched nitrate in seawater off southern California, *Limnology and Oceanography*, 34, 820-830, 1989.

Luyten, J. R., J. Pedlosky, and H. Stommel, The Ventilated Thermocline, *Journal of Physical Oceanography*, 13, 292-309, 1983.

Lynchstieglitz, J., and R. G. Fairbanks, Glacial-Interglacial History of Antarctic Intermediate Water - Relative Strengths of Antarctic Versus Indian-Ocean Sources, *Paleoceanography*, 9, 7-29, 1994.

Martinez, P., P. Bertrand, S. E. Calvert, T. F. Pedersen, G. B. Shimmield, E. Lallier-Verges, and M. R. Fontugne, Spatial variations in nutrient utilization, production and diagenesis in the sediments of a coastal upwelling regime (NW Africa): Implications for the paleoceanographic record, *Journal of Marine Research*, 58, 809-835, 2000.

Mashiotta, T. A., D. W. Lea, and H. J. Spero, Glacial-interglacial changes in Subantarctic sea surface temperature and $\delta^{18}O$-water using foraminiferal Mg, *Earth and Planetary Science Letters*, 170, 417-432, 1999.

Masson, V., F. Vimeux, J. Jouzel, V. Morgan, M. Delmotte, P. Ciais, C. Hammer, S. Johnsen, V. Y. Lipenkov, E. Mosley-Thompson, J. R. Petit, E. J. Steig, M. Stievenard, and R. Vaikmae, Holocene climate variability in Antarctica based on 11 ice-core isotopic records, *Quaternary Research*, 54, 348-358, 2000.

Matsumoto, K., T. Oba, J. Lynch-Stieglitz, and H. Yamamoto, Interior hydrography and circulation of the glacial Pacific Ocean, *Quaternary Science Reviews*, 21, 1693-1704, 2002.

McCorkle, D. C., D. T. Heggie, and H. H. Veeh, Glacial and Holocene stable isotope distributions in the southeastern Indian Ocean, *Paleoceanography*, 13, 20-34, 1998.

McDonald, D., T. F. Pedersen, and J. Crusius, Multiple late Quaternary episodes of exceptional diatom production in the Gulf of Alaska, *Deep-Sea Research II*, 46, 2993-3017, 1999.

Mills, M. M., C. Ridame, M. Davey, J. La Roche, and R. J. Geider, Iron and phosphorus co-limit nitrogen fixation in the eastern tropical North Atlantic, *Nature*, 429, 292-294, 2004.

Minagawa, M., and E. Wada, Stepwise enrichment of ^{15}N along food chains: Further evidence and the relation between $\delta^{15}N$ and animal age, *Geochimica et Cosmochimica Acta*, 48, 1135-1140, 1984.

Mollenhauer, G., T. I. Eglinton, N. Ohkuchi, R. R. Schneider, P. J. Muller, P. M. Grootes, and J. Rullkotter, Asynchronous alkenone and foraminfera records from the Benguela Upwelling System, *Geochimica Et Cosmochimica Acta*, 67, 2157-2171, 2003.

Montoya, J. P., and J. J. McCarthy, Isotopic fractionation during nitrate uptake by phytoplankton grown in continuous-culture, *Journal of Plankton Research*, 17, 439-464, 1995.

Nameroff, T. J., S. E. Calvert, and J. W. Murray, Glacial-interglacial variability in the eastern tropical North Pacific oxygen minimum zone recorded by redox-sensitive trace metals, *Paleoceanography*, 19, 2004.

Ohkushi, K., T. Itaki, and N. Nemoto, Last Glacial-Holocene change in intermediate-water ventilation in the Northwestern Pacific, *Quaternary Science Reviews*, 22, 1477-1484, 2003.

Olson, D. B., G. L. Hitchcock, R. A. Fine, and B. A. Warren, Maintenance of the Low-Oxygen Layer in the Central Arabian Sea, *Deep-Sea Research Part II-Topical Studies in Oceanography*, 40, 673-685, 1993.

Pantoja, S., D. J. Repeta, J. P. Sachs, and D. M. Sigman, Stable isotope constraints on the nitrogen cycle of the Mediterranean Sea water column, *Deep-Sea Research Part I-Oceanographic Research Papers*, 49, 1609-1621, 2002.

Petit, J. R., J. Jouzel, D. Raynaud, N. I. Barkov, J. M. Barnola, I. Basile, M. Bender, J. Chappellaz, M. Davis, G. Delaygue, M. Delmotte, V. M. Kotlyakov, M. Legrand, V. Y. Lipenkov, C. Lorius, L. Pepin, C. Ritz, E. Saltzman, and M. Stievenard, Climate and atmospheric history of the past 420,000 years from the Vostok ice core, Antarctica, *Nature*, 399, 429-436, 1999.

Pride, C., R. Thunell, D. Sigman, L. Keigwin, M. Altabet, and E. Tappa, Nitrogen isotopic variations in the Gulf of California since the last deglaciation: Response to global climate change, *Paleoceanography*, 14, 397-409, 1999.

Reichart, G. J., S. Schenau, G. J. de Lange, and W. J. Zachariasse, Synchroneity of oxygen minimum zone intensity on the Oman and Pakistan Margins at sub-Milankovitch time scales, *Marine Geology*, 185, 403-415, 2002.

Robinson, R., B. G. Brunelle, and D. M. Sigman, Revisiting nutrient utilization in the glacial Antarctic: Evidence from a new method for diatom-bound N isotopic analysis, *Paleoceanography*, 19, doi:10.1029/2003PA000996, 2004.

Russell, J. L., and A. G. Dickson, Variability in oxygen and nutrients in South Pacific Antarctic Intermediate Water, *Global Biogeochemical Cycles*, 17, art. no.-1033, 2003.

Saenko, O. A., and A. J. Weaver, Importance of wind-driven sea ice motion for the formation of Antarctic Intermediate Water in a global climate model, *Geophysical Research Letters*, 28, 4147-4150, 2001.

Sanudo-Wilhelmy, S. A., A. B. Kustka, C. J. Gobler, D. A. Hutchins, M. Yang, K. Lwiza, J. Burns, D. G. Capone, J. A. Raven, and E. J. Carpenter, Phosphorus limitation of nitrogen fixation by Trichodesmium in the central Atlantic Ocean, *Nature*, 411, 66-69, 2001.

Sarma, V., An evaluation of physical and biogeochemical processes regulating perennial suboxic conditions in the water column of the Arabian Sea, *Global Biogeochemical Cycles*, 16, art. no.-1082, 2002.

Sarmiento, J. L., N. Gruber, M. A. Brzezinski, and J. P. Dunne, High-latitude controls of thermocline nutrients and low latitude biological productivity, *Nature*, 427, 56-60, 2004.

Schulte, S., F. Rostek, E. Bard, J. Rullkotter, and O. Marchal, Variations of oxygen-minimum and primary productivity recorded in sediments of the Arabian Sea, *Earth and Planetary Science Letters*, 173, 205-221, 1999.

Sigman, D. M., M. A. Altabet, D. C. McCorkle, R. Francois, and G. Fischer, The $\delta^{15}N$ of nitrate in the Southern Ocean: Consumption of nitrate in surface waters, *Global Biogeochemical Cycles*, 13, 1149-1166, 1999.

Sigman, D. M., M. A. Altabet, R. Michener, D. C. McCorkle, B. Fry, and R. M. Holmes, Natural abundance-level measurement of the nitrogen isotopic composition of oceanic nitrate: an adaptation of the ammonia diffusion method, *Marine Chemistry*, 57, 227-242, 1997.

Sigman, D. M., and K. L. Casciotti, Nitrogen isotopes in the ocean. in *Encyclopedia of Ocean Sciences*, edited by Steele, J. H., K. K. Turekian and S. A. Thorpe, pp. 2249, Academic Press, London, 2001.

Slowey, N. C., and W. B. Curry, Glacial-Interglacial Differences in Circulation and Carbon Cycling Within the Upper Western North-Atlantic, *Paleoceanography*, 10, 715-732, 1995.

Sloyan, B. M., and S. R. Rintoul, Circulation, renewal, and modification of Antarctic mode and intermediate water, *Journal of Physical Oceanography*, 31, 1005-1030, 2001.

Struck, U., K. C. Emeis, M. Voss, M. D. Krom, and G. H. Rau, Biological productivity during sapropel S5 formation in the Eastern Mediterranean Sea: Evidence from stable isotopes of nitrogen and carbon, *Geochimica Et Cosmochimica Acta*, 65, 3249-3266, 2001.

Suthhof, A., V. Ittekkot, and B. Gaye-Haake, Millennial-scale oscillation of denitrification intensity in the Arabian Sea during the late Quaternary and its potential influence on atmospheric N_2O and global climate, *Global Biogeochemical Cycles*, 15, 637-649, 2001.

Talley, L. D., Some aspects of ocean heat transport by the shallow, intermediate and deep overturning circulations. in *Mechanisms of Global Climate Change at Millennial Time Scales*, edited by Clark, P. U., R. S. Webb and L. D. Keigwin, pp. 394, American Geophysical Union, 1999.

Tamburini, F., T. Adatte, K. Follmi, S. M. Bernasconi, and P. Steinmann, Investigating the history of East Asian monsoon and climate during the last glacial-interglacial period (0-140 000 years): mineralogy and geochemistry of ODP Sites 1143 and 1144, South China Sea, *Marine Geology*, 201, 147-168, 2003.

Toggweiler, J. R., K. Dixon, and W. S. Broecker, The Peru Upwelling and the Ventilation of the South-Pacific Thermocline, *Journal of Geophysical Research-Oceans*, 96, 20467-20497, 1991.

Tyrrell, T., The relative influences of nitrogen and phosphorus on oceanic primary production, *Nature*, 400, 525-531, 1999.

Tyrrell, T., and M. I. Lucas, Geochemical evidence of denitrification in the Benguela upwelling system, *Continental Shelf Research*, 22, 2497-2511, 2002.

Voss, M., J. W. Dippner, and J. P. Montoya, Nitrogen isotope patterns in the oxygen-deficient waters of the Eastern Tropical North Pacific Ocean, *Deep-Sea Research Part I-Oceanographic Research Papers*, 48, 1905-1921, 2001.

Wada, E., and A. Hattori, Natural abundance of ^{15}N in particulate organic matter in the North Pacific Ocean, *Geochimica Et Cosmochimica Acta*, 40, 249-251, 1976.

You, Y. Z., Quantitative estimate of Antarctic Intermediate Water contributions from the Drake Passage and the southwest Indian Ocean to the South Atlantic, *Journal of Geophysical Research-Oceans*, 107, -, 2002.

Zheng, Y., A. van Geen, R. F. Anderson, J. V. Gardner, and W. E. Dean, Intensification of the northeast Pacific oxygen minimum zone during the Bolling-Allerod warm period, *Paleoceanography*, 15, 528-536, 2000.

Chapter V

Physical sensitivities and stabilizing feedbacks: Numerical simulations of the marine nitrogen cycle under present-day and glacial climates

5.1 Introduction

The marine nitrogen cycle is intimately linked to the distribution of dissolved oxygen. Oxygen supports the vast majority of organic matter respiration in the ocean interior, but where it is almost depleted microbes turn to nitrate as a terminal electron acceptor. In these environments, fixed nitrogen is rapidly converted to N_2 via denitrification. Denitrification represents the dominant loss term of fixed marine nitrogen [*Codispoti et al.*, 2001], about half of which takes place in sediments and half in the water column, at rates that result in a residence time for fixed N of ~ 3 ky. The rapid loss of N is compensated for by nitrogen fixation, but this compensation is not immediate, leading to an ocean in which nitrate abundance limits growth [*Tyrrell*, 1999]. The oceans therefore appear poised on the brink of widespread nitrogen limitation, yet denitrification is presently confined to only three pockets of the modern thermocline (the eastern tropical North and South Pacific, as well as the Arabian Sea). This apparently precarious balance begs explanation: why is denitrification just barely present, and neither widespread with attendant sulphate reduction, nor completely absent? Is it simply coincidence that the oceans contain almost exactly the appropriate amount of O_2 to respire the organic matter produced from the average nitrate content of seawater? Does this tightly coupled system change over time?

Geological evidence shows that the intensity of thermocline denitrification has fluctuated significantly in the past (Chapter 4, [*Altabet et al.*, 1995; *Ganeshram et al.*, 1995]). These fluctuations can be related to a climatic dependency of the oxygen flux to the global

thermocline, via the solubility and saturation of oxygen in subduction regions, and by the efficiency of circulation in exchanging waters quickly between the formation regions and the most oxygen-deficient subsurface regions (Chapter 4). Also, climate has the capacity to determine the fertility of the surface ocean through its control on the global distribution of nutrients [*Sigman and Boyle*, 2000; *Schmittner*, 2005], which modulates the demand for oxidant in the ocean interior. Meanwhile, nitrogen fixation appears to be hindered at present by low Fe concentrations [*Falkowski*, 1997], and it has been suggested that greater Fe supply to the oceans from dust supply during windy, arid glacials, allowed the marine N inventory to swell. In order to investigate this web of interactions that lies at the heart of the marine biosphere, we develop here a novel, fully prognostic global model of the marine nitrogen cycle in a GCM, based on simple, widely accepted concepts. The model reveals a strong stabilization of the marine N cycle through feedbacks with dissolved oxygen, but with a pronounced climatic sensitivity, consistent with observations.

5.2 Model description

The physical model is based on the University of Victoria Earth System Model [*Weaver et al.*, 2001], modified as described by *Schmittner et al.* [2005]. Briefly, it includes a global, three dimensional ocean of 1.8° x 3.6° grid cells and 19 depth levels, with state of the art dynamic-thermodynamic sea ice and a tidal mixing scheme. The atmosphere is a simple, two-dimensional energy balance scheme with moisture advection and prescribed winds.

The nitrogen cycle biogeochemical model (Figure 5.1) is based on seven prognostic variables and is embedded within the ocean circulation model. The inorganic variables include oxygen (O_2) and two nutrients, nitrate (NO_3) and phosphate (PO_4). The biological variables include two classes of phytoplankton, nitrogen-fixing diazotrophs (P_D), and other phytoplankton (P_O), as well as zooplankton (Z) and particulate detritus (D); all biological variables are expressed in units of mmol nitrogen per m^3 (roughly equivalent to μM). Although very simple, this ecological structure captures the essential dynamic of competition for phosphorus highlighted by Tyrell (1999), in which phytoplankton capable of rapid growth using available nitrate (P_O) are pitted against slow growers capable of fixing their own supply of nitrogen (P_D).

Each variable changes its concentration C according to the equation

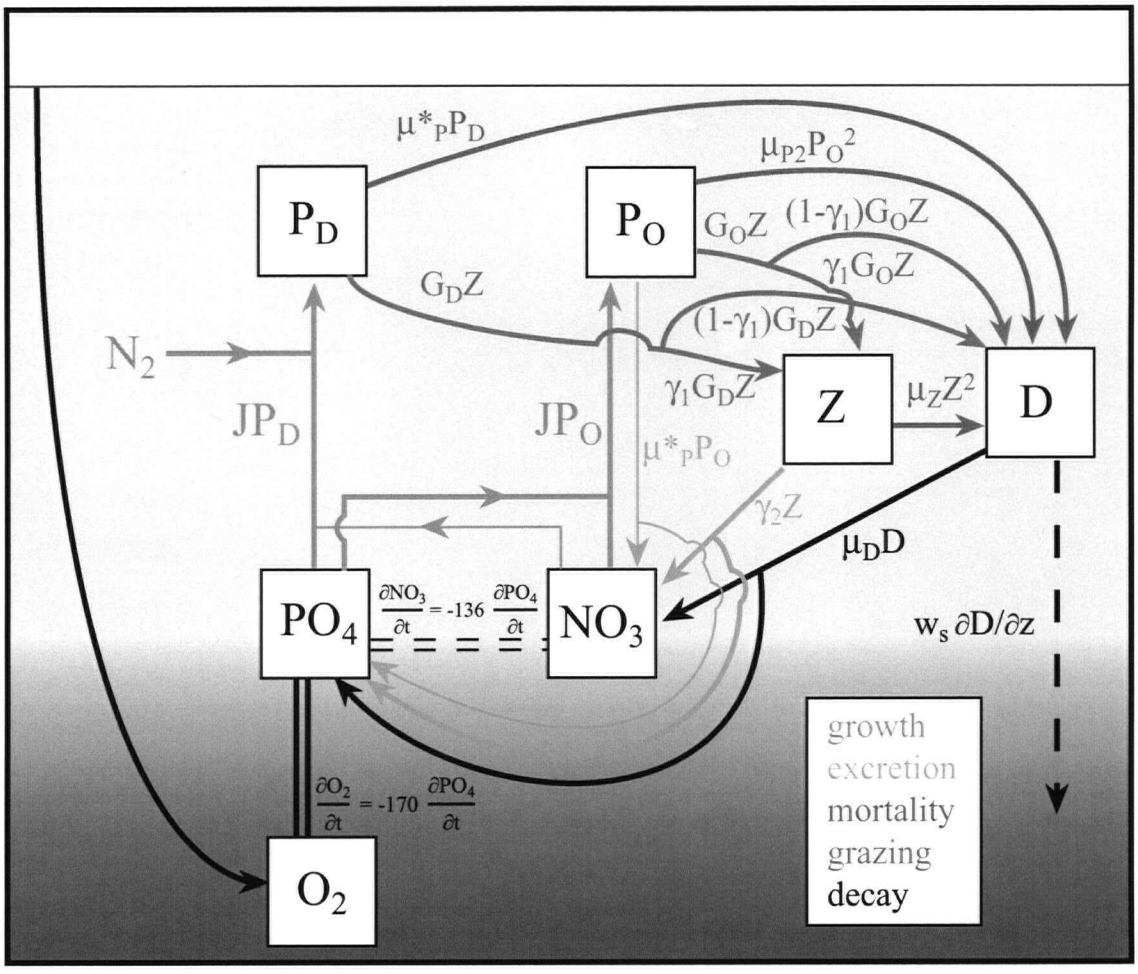

5.1. Schematic illustration of the ecosystem model. Tracers are shown by white boxes, fluxes by coloured arrows. See text for discussion and Table 1 for parameters.

$$\frac{\partial C}{\partial t} = T + S, \tag{5.1}$$

where T represents all transport terms including advection, isopycnal and diapycnal diffusion, and convection. S denotes the source minus sink terms, which describe the biogeochemical interactions as follows:

$$S(\mathrm{PO_4}) = (\mu_D \mathrm{D} + \mu^*_P \mathrm{P}_O + \gamma_2 \mathrm{Z} - J_O \mathrm{P}_O - J_D \mathrm{P}_D) R_{P:N} \tag{5.2}$$

$$S(\mathrm{NO_3}) = (\mu_D \mathrm{D} + \mu^*_P \mathrm{P}_O + \gamma_2 \mathrm{Z} - J_O \mathrm{P}_O - u_\mathrm{N} J_D \mathrm{P}_D)(1 - 0.8 R_{O:N} r_{sox}^{NO3}) \tag{5.3}$$

$$S(\mathrm{P}_O) = J_O \mathrm{P}_O - \mu^*_P \mathrm{P}_O - G(\mathrm{P}_O)\mathrm{Z} - \mu_{P2} \mathrm{P}^2_O \tag{5.4}$$

$$S(\mathrm{P}_D) = J_D \mathrm{P}_D - G(\mathrm{P}_D)\mathrm{Z} - \mu_P \mathrm{P}_D \tag{5.5}$$

$$S(\mathrm{Z}) = \gamma_1 [G(\mathrm{P}_O) + G(\mathrm{P}_D)]\mathrm{Z} - \gamma_2 \mathrm{Z} - \mu_Z \mathrm{Z}^2 \tag{5.6}$$

$$S(\mathrm{D}) = (1-\gamma_1)[G(\mathrm{P}_O)+G(\mathrm{P}_D)]\mathrm{Z} + \mu_P \mathrm{P}_D + \mu_{P2} \mathrm{P}^2_O + \mu_Z \mathrm{Z}^2 - \mu_D \mathrm{D} - w_\mathrm{D} \partial \mathrm{D}/\partial z \tag{5.7}$$

$$S(\mathrm{O_2}) = F_{sfc} - S(\mathrm{PO_4}) R_{O:P} r_{sox}^{O2} \tag{5.8}$$

Parameters and their values are given in Table 5.1. The function $J_O = J(I, \mathrm{NO_3}, \mathrm{PO_4})$ provides the growth rate of non-diazotrophic phytoplankton, determined from irradiance (I), $\mathrm{NO_3}$ and $\mathrm{PO_4}$:

$$J(I, \mathrm{NO_3}, \mathrm{PO_4}) = min(J_{OI}, J_{Omax} u_N, J_{Omax} u_P), \tag{5.9}$$

The maximum, non-limited growth rate is dependent on temperature (T):

$$\mathrm{J}_{Omax} = ab^{cT} \tag{5.10}$$

such that growth rates increase by a factor of ten over the temperature range of -2 to 34 °C. Under nutrient-replete conditions, the light-limited growth rate J_{OI} is calculated according to:

$$J_{OI} = \frac{J_{Omax} \alpha I}{[J^2_{Omax} + (\alpha I)^2]^{1/2}} \tag{5.11}$$

Table 5.1: Ecosystem model parameters.

Parameter	Symbol	Value	Units
	Phytoplankton (P) Coefficients		
Initial slope of P-I curve	α	0.256	$(Wm^{-2})^{-1}d^{-1}$
Maximum growth rate parameter	a	0.15	d^{-1}
Half-saturation constant for NO3 uptake	k_N	0.7	mmol N m^{-3}
Half-saturation constant for PO4 uptake	k_P	0.7 $R_{P:N}$	mmol P m^{-3}
Linear mortality rate	μ_P	0.02	d^{-1}
Quadratic mortality rate	μ_{P2}	0.025	$(mmol\ m^{-3})^{-1}d^{-1}$
	Zooplankton (Z) Coefficients		
Assimilation efficiency	γ_1	0.925	
Maximum grazing rate	g	1.575	d^{-1}
Prey capture rate	ε	1.6	$(mmol\ m^{-3})^{-1}d^{-1}$
Mortality	μ_Z	0.34	$(mmol\ m^{-3})^{-1}d^{-1}$
Excretion	γ_2	0.01 b^{cT}	d^{-1}
	Detritus (D) Coefficients		
Remineralization rate	μ_{D0}	0.048	d^{-1}
	Common Parameters		
Temperature function	b	1.066	
	c	1	$(°C)^{-1}$
Organic matter P:N	$R_{P:N}$	1/16	
Photosynthesis/respiration O:P	$R_{O:P}$	170/16	

where α is the initial slope of the photosynthesis vs. irradiance (*P-I*) curve. The calculation of the photosynthetically active shortwave radiation I and the method of averaging Eq. 5.11 over one day is given in *Schmittner et al.* [2005]. Nutrient limitation is represented by the product of J_{Omax} and the nutrient uptake rates, where $u_N = NO_3/k_N+NO_3$ and $u_P = PO_4/k_P + PO_4$ provide the respective nutrient uptake rates.

Diazotrophs grow according to the same principles as the other phytoplankton, but are disadvantaged by a lower maximum growth rate, J_{Dmax} (see Fig. 2), which is zero below 15°C [*Breitbarth*, 2004]:

$$J_{Dmax} = c_D \, max[0, a(b^{cT} - b^{c15°C})] \tag{5.12}$$

The coefficient c_D handicaps diazotrophs by dampening the increase of their maximal growth rate versus that of other phytoplankton as temperature rises. If, for example, $c_D = 0.5$, the increase per °C warming of diazotrophs is 50 % that of other phytoplankton (Figure 5.2). The precise mechanisms that put diazotrophs at an ecological disadvantage remain unclear, and may be related to a stronger temperature dependence (as we have implemented) or a stronger dependence on light and stratified water conditions (e.g. [*Hood et al.*, 2004]); however, the salient features are simply that diazotrophs are concentrated in tropical surface waters [*Capone et al.*, 2005] and that they grow more slowly than other phytoplankton when nitrate is available [*Tyrrell*, 1999], both of which are captured by our formulation. Diazotrophs have an ecological advantage in that their growth rate is not limited by low NO_3 concentrations:

$$J_D(I, PO_4) = min(J_{DI}, J_{Dmax}u_P). \tag{5.13}$$

Diazotrophs do take up NO_3 if it is available, but some newly fixed nitrogen is always incorporated as a consequence of their growth (see fifth term in the right hand side of Eq. 5.3) as shown in cultures of *Trischodesmium* spp. [*Holl*, 2004]. The N:P of model diazotrophs is equal to other phytoplankton (16:1). Although there is evidence that the best-studied diazotrophs of the genus *Trichodesmium* can have much higher N:P (e.g. [*Sanudo-Wilhelmy et al.*, 2004]), the abundant unicellular diazotrophs are uncharacterized and their N:P is un-

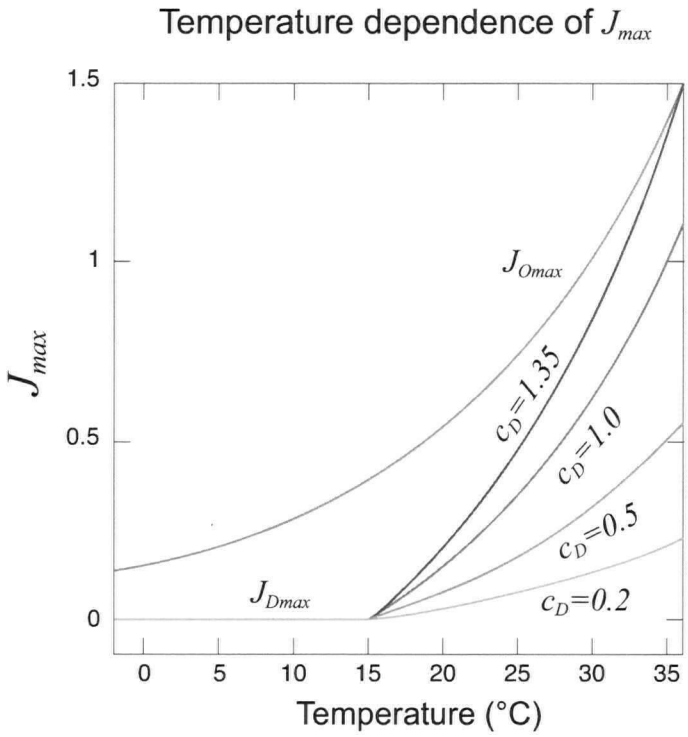

5.2. Increase of maximum growth rate vs. temperature for diazotrophs (J_{Dmax}) and other phytoplankton (J_{Omax}). Other phytoplankton have higher maximum (i.e. nutrient- and light- replete) growth rates than diazotrophs at all temperatures, handicaping the diazotrophs. The impact of the severity of the diazotroph handicap is investigated by varying c_D from 1.35 (very weak handicap) to 0.2 (very strong handicap).

known [*Montoya et al.*, 2004]. For simplicity of interpretation the N:P of both phytoplankton groups were made identical.

The mortality rate of non-diazotrophic phytoplankton is a quadratic function of phytoplankton biomass, representative of viral infections under bloom conditions. DOM and the microbial loop are folded into a single fast-remineralization process, which is the product of P_O and the temperature dependent term $\mu^*_P = \mu_P \cdot b^{cT}$. Diazotrophs do not undergo this fast remineralization, but die at a linear rate that is higher than the non-diazotrophic mortality rate at low biomass.

Detritus is generated from sloppy zooplankton feeding and mortality among the three classes of plankton, and is the only component of the ecosystem model to sink. It does so at a speed of

$$w_D = 2\text{md}^{-1} + 6.8 \times 10^{-2}\text{d}^{-1}z, \qquad (5.14)$$

increasing linearly with depth z from 2 md^{-1} at the surface to 340 md^{-1} at 5km depth, consistent with observations [*Berelson*, 2002]. The remineralization rate of detritus is temperature dependent and, following the observations of Devol and Hartnett [2001], decreases in oxygen-poor waters:

$$\mu_D = \mu_{D0}\, b^{cT}[0.65 + 0.35\tanh(O_2 - 6)] \qquad (5.15)$$

The inclusion of this reduction in remineralization rate under suboxic conditions causes only a minor decrease on the global rate of denitrification (~10%) but expands the suboxic zone slightly. Remineralization returns the N and P of detritus to NO_3 and PO_4. Photosynthesis produces oxygen, while respiration consumes oxygen, at rates equal to the consumption and remineralization rates of PO_4, respectively, multiplied by the constant ratio $R_{O:P}$. Dissolved oxygen exchanges with the atmosphere in the surface layer (F_{sfc}) according to the OCMIP protocol [*Najjar and Orr*, 1998].

Oxygen consumption in suboxic waters (<5 μM) is inhibited, according to

$$r_{sox}^{O2} = 0.5[\tanh(O_2 - 5) + 1] \qquad (5.16)$$

but is replaced by the oxygen-equivalent oxidation of nitrate,

$$r_{sox}^{NO3} = 0.5[1 - \tanh(O_2 - 5)]. \quad (5.17)$$

Denitrification consumes nitrate at a rate of 80% of the oxygen equivalent rate, as NO_3 is a more efficient oxidant on a mol per mol basis (i.e. one mol of NO_3^- can accept 5 mol e^- while 1 mol of O_2 can accept only 4 mol e^-). Although the model does not explicitly include sulfate reduction under anoxic conditions, remineralization is not impeded by a lack of nitrate and, regardless, nitrate is never depleted in the runs presented here. Note that the model does not include sedimentary denitrification, which would provide a large and less time-variant sink for fixed nitrogen. Because sedimentary denitrification would not change the qualitative dynamics of the model's behavior, it is not included in the version presented here.

5.2.1 A note on Anammox

Recent research has suggested that anaerobic ammonium oxidation, "anammox", may be a major sink for nitrate in OMZs [*Kuypers et al.*, 2005]. If true this would mean that, rather than the traditional understanding by which NO_3^- is converted to N_2 in order to oxidize C_{org} to CO_2, NO_3^- and NH_4^+ would instead be combined to produce N_2 directly. Both of these processes result in a net loss of fixed N from the marine environment, and both occur only under oxygen-depleted conditions in the presence of NO_3^-. Most importantly, both require organic matter - the difference is essentially whether N_{org} or C_{org} forms the primary reduced substrate. This has an impact on the stoichiometry of N loss, because N_{org} is lost along with NO_3^- during anammox. However, it does not affect the fact that fixed N loss occurs under suboxic conditions, and requires the presence of both NO_3^- and organic matter. As such, it is essentially a component of what is referred to here as "denitrification". Therefore it is unlikely that anammox, whatever its importance for microbial ecology and reaction stoichiometry, will significantly influence the dynamics discussed here.

5.3 Model runs

For a given ocean P inventory, the intensity of denitrification in the model is primarily determined by the growth rate of diazotrophs and the physical climate state (See Table 5.2). We present six model runs that illustrate these sensitivities. Runs 1-5 represent the "present day" climate, while run 6 represents last glacial maximum (LGM) conditions. Run 1 is identical to runs 2-5, but there is no denitrification or N_2 fixation. Runs 2 to 5 are identical to each other except for differences in the growth rate handicaps of diazotrophs, c_D. Run 4, with a strong growth rate handicap, is used as the present day reference (PD).

5.3.1 Oxygen minimum zones

When initialized with an average PO_4 concentration of 1.82 μM and NO_3 concentration of 29.12 μM (the "Redfield" concentration of $16*PO_4$) and allowed to run for a few centuries, the model develops stable Oxygen Minimum Zones (OMZs) in which denitrification occurs, generating low N:P ratios. Waters transported out of the denitrification zones carry an N deficit (a negative $N^* = NO_3 - 16*PO_4$, simplified after Gruber and Sarmiento [1997]) until they encounter N_2 fixation in tropical surface regions. The distribution of N* in the shallow ocean of the standard PD run is broadly similar to observations (Figure 5.3), indicating that the rates of N cycling are of the right order of magnitude relative to the circulation. The resulting global distribution of NO_3 and PO_4 is similar to that observed in the real ocean (Figure 5.4), with N limitation of surface waters indicated by the positive intercept on the PO_4 axis. This is similar to the model result of Tyrell [1999], despite the very different model architecture and the fact that our diazotrophs are handicapped by a low, temperature-dependent maximum growth rate instead of a fixed lower PO_4 uptake rate. The model has a tendency to produce thermocline OMZs in the eastern tropical shadow zones of the three ocean basins, with the strongest OMZ in the Pacific, intermediate in the Atlantic, and weakest in the Indian Ocean (Figure 5.5). The general distribution is similar to observations, although the Indian Ocean OMZ is much too weak and occurs on the eastern side of the basin rather than in the north, likely due to an underestimate of productivity and lack of a Red Sea Intermediate Water. For these, and perhaps additional reasons, denitrification does not occur in the Indian Ocean. The oxygen minimum of the northern North Pacific is also strongly underestimated, probably as a result of the unrealistically low productivity of the region, a

Table 5.2: Model runs.

Run	c_D	OMZ volume	WCD	NO_3-average	Surplus[1]	NPP
		x 1000 km^3	Tg N y^{-1}	μM	Tg N y^{-1}	Gt C y^{-1}
1. No N cycle (NoN)	-	1010	-	29.1	-	90
2. Very small handicap	1.35	1326	154	32.0	34	92
3. Minor handicap	1.0	887	96	31.2	19	99
4. Strong handicap (PD)	0.5	363	42	27.8	-5	94
5. Very strong handicap	0.2	138	21	25.5	-21	78
6. Last Glacial (LGM)	0.5	304	7	28.1	-1	67

1: Surplus calculated over years 1400-1500 of integration (not equilibrium)

Characteristics of model runs, as described in text, where c_D is the growth rate multiplier for diazotrophs, 'OMZ' is the global volume of grid cells with < 5 μM O_2 and NPP is global net primary production.

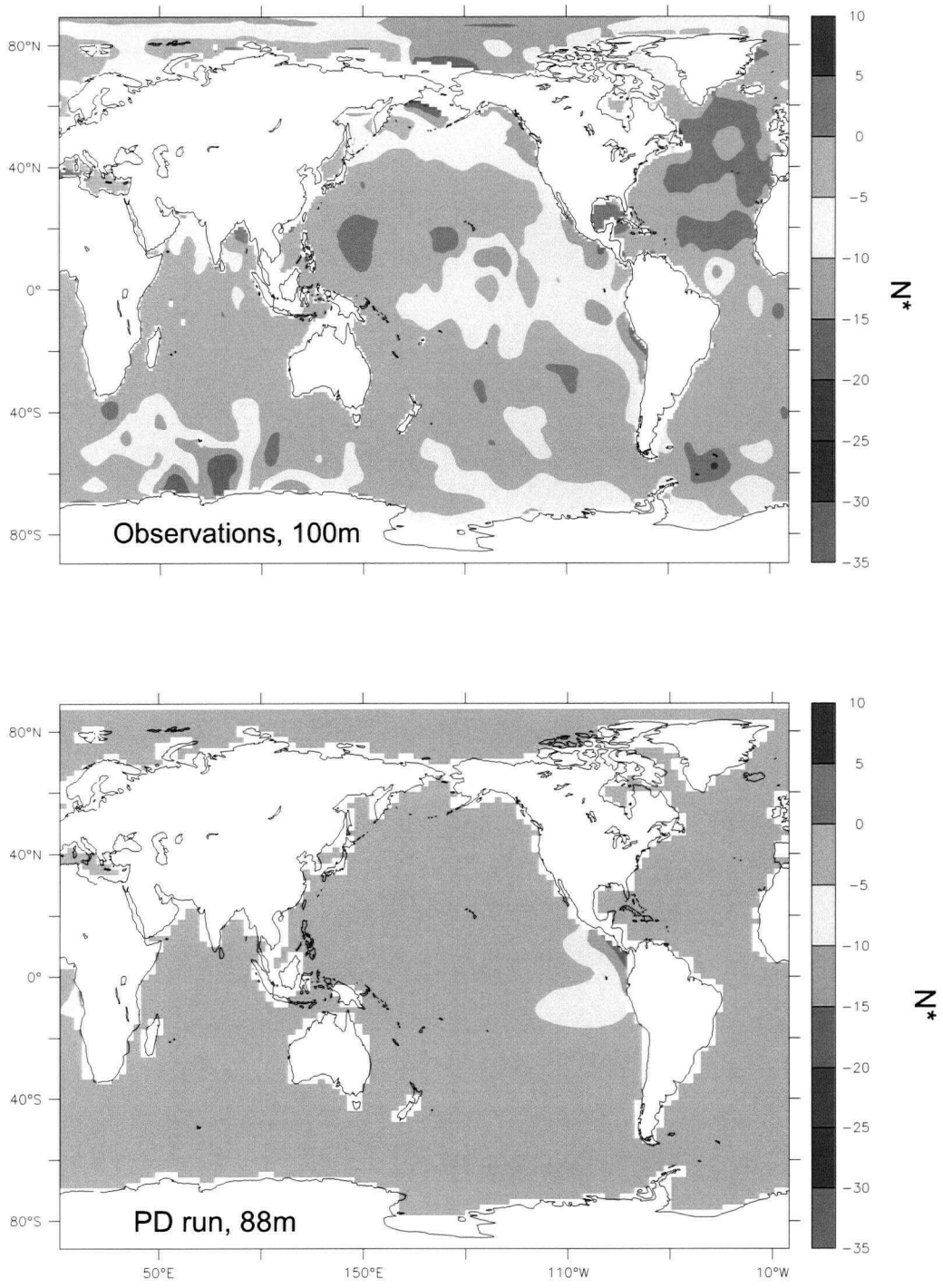

5.3. Shallow N* distributions in the World Ocean Atlas annual climatology [Conkright et al., 1998] and model run PD. The model shows the same general distributions and magnitudes of N* as the observations, with N:P near Redfield throughout the shallow ocean except where denitrified waters abound. The lack of negative N* in the modeled high latitude oceans is likely due to the lack of sedimentary denitrification, while the underestimate of N* in the gyres may result from the use of a strict N:P of 16 for all phytoplankton.

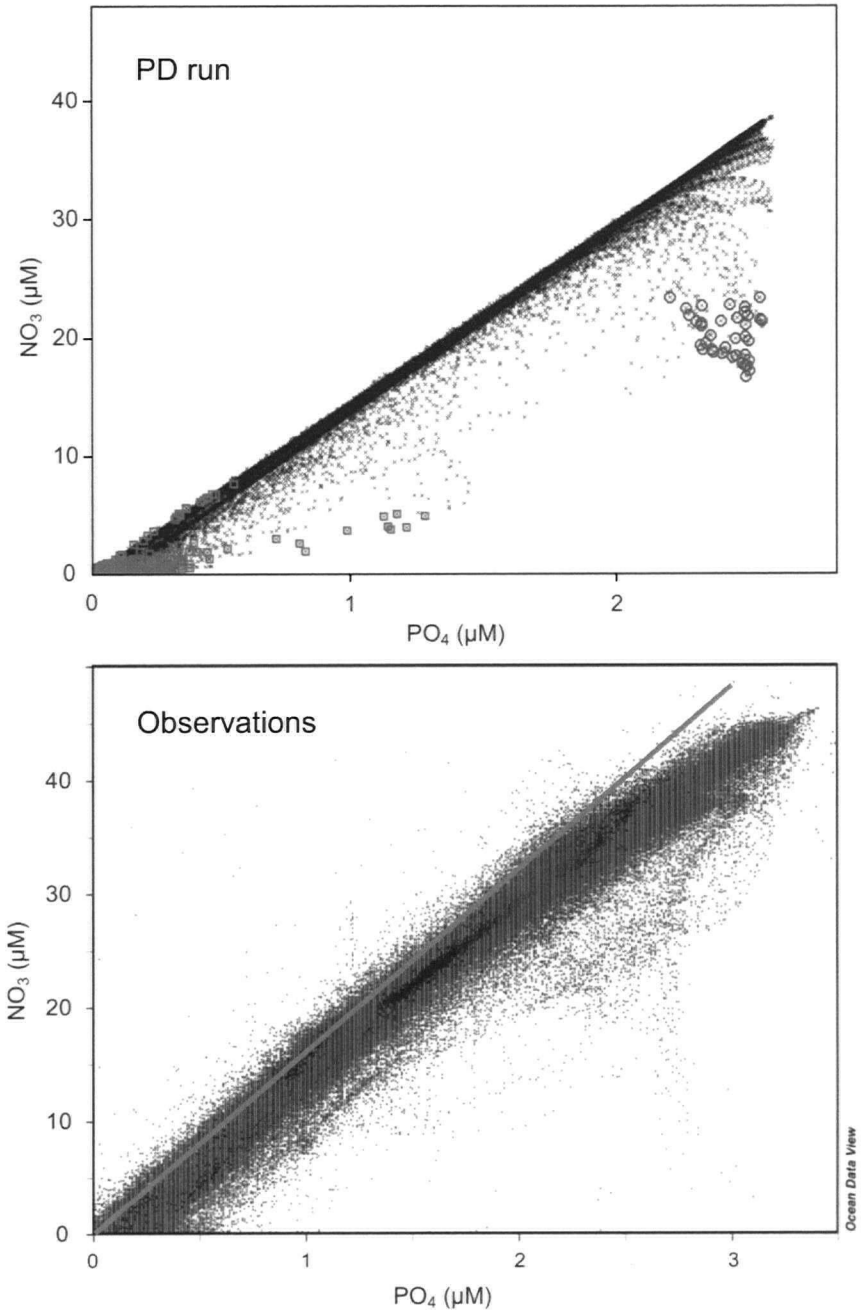

5.4. Global plot of PO_4 vs. NO_3 concentrations in model run PD (#2) and observations. In the top panel, black 'x' symbols show all grid cells, red squares show grid cells in which N_2 fixation is active, and blue circles show grid cells in which denitrification is active. The vast majority of grid cells fall along the 'Redfield' 16:1 line, due to the strict Redfield stoichiometry of all phytoplankton and remineralization. The bottom panel shows all data from the WOCE one-time sailing hydrographic program, with the Redfield ratio shown by the green line. In both model and observations, water column denitrification produces downward 'tufts', pulled away from the nearly linear trend of uptake and remineralization.

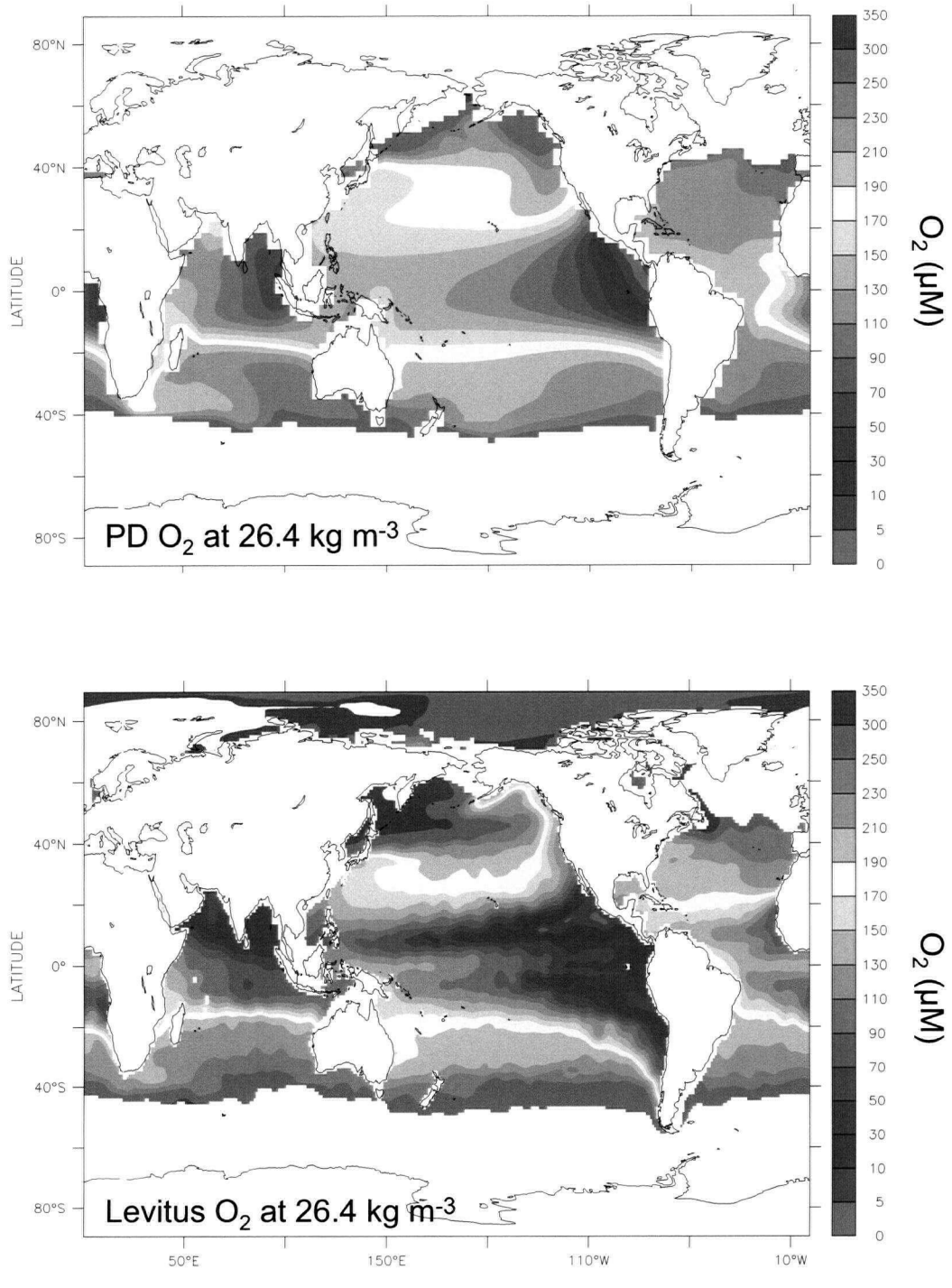

5.5. PDO2. Shallow subsurface O_2 in the PD run and observations. Concentrations are shown on the 26.4 kg m^{-3} isopycnal surface; the white, high latitude regions indicate the area of outcropping. Oxygen minima are well developed in the eastern tropical shadow zones of the three ocean basins of the model. Observations are from the World Ocean Atlas [Conkright et al., 1998]. See text for discussion.

common feature of models (eg. [*Gnanadesikan et al.*, 2004; *Sarmiento et al.*, 2004]. The equatorial currents are also poorly simulated due to the coarse resolution of the model, leading to unrealistically low O_2 concentrations in the equatorial Pacific and a lack of differentiation of the northern and southern OMZs into separate lobes.

5.3.2 N_2 fixation

Nitrogen fixation occurs exclusively in the tropics, because of the strong requirement of model diazotrophs for high temperatures (Figure 5.6). The concentration of diazotroph biomass is always less than that of other phytoplankton. Because diazotrophs are outcompeted by other phytoplankton for phosphate when nitrate is available, they are pushed away from upwelling areas to a degree strongly dependent on their growth rate handicap (see below). N_2 fixation is most abundant in the tropical Pacific, with lesser amounts in the tropical Indian and Atlantic. The distribution of N_2 fixation in the central Atlantic is remarkably similar to that modeled by *Hood et al.* [2004], with a high concentration in the eastern equatorial Atlantic and smaller concentrations in the western tropical Atlantic. This is striking, considering that our diazotrophs are limited by light, temperature and PO_4, while those of *Hood et al.* are determined by mixed layer depth, light and the absence of nitrate, with nitrate inputs determined from climatological values along the boundaries of their much higher-resolution model. Local rates of N_2 fixation are on the same order as those estimated from field observations by *Capone et al.* [2005]. It should be noted that total N_2 fixation is significantly underestimated in our model due to the absence of sedimentary denitrification, which would enhance N deficits globally.

The global N inventory was larger for runs with smaller diazotroph handicaps. Although the runs with smallest handicaps (#2 and #3) had not reached equilibrium after 1500 years, the N inventory trends (not shown) suggest a quadratic relationship over time with peaks in the N inventory of < 20 % above the Redfield value, i.e. an N : P ~ 19, reached ~ 4000 years after run initialization. It is interesting that the gradual increases in these runs arise despite the fact that all phytoplankton have N:P of 16, simply because diazotrophs always amend their N nutrition with a small amount of N_2 fixation, even if their principal N substrate is NO_3, leaving some NO_3 unutilized. As a result, NO_3 concentrations in tropical surface waters exceed 10 μM after a few thousand years, and surface N* values in the South-

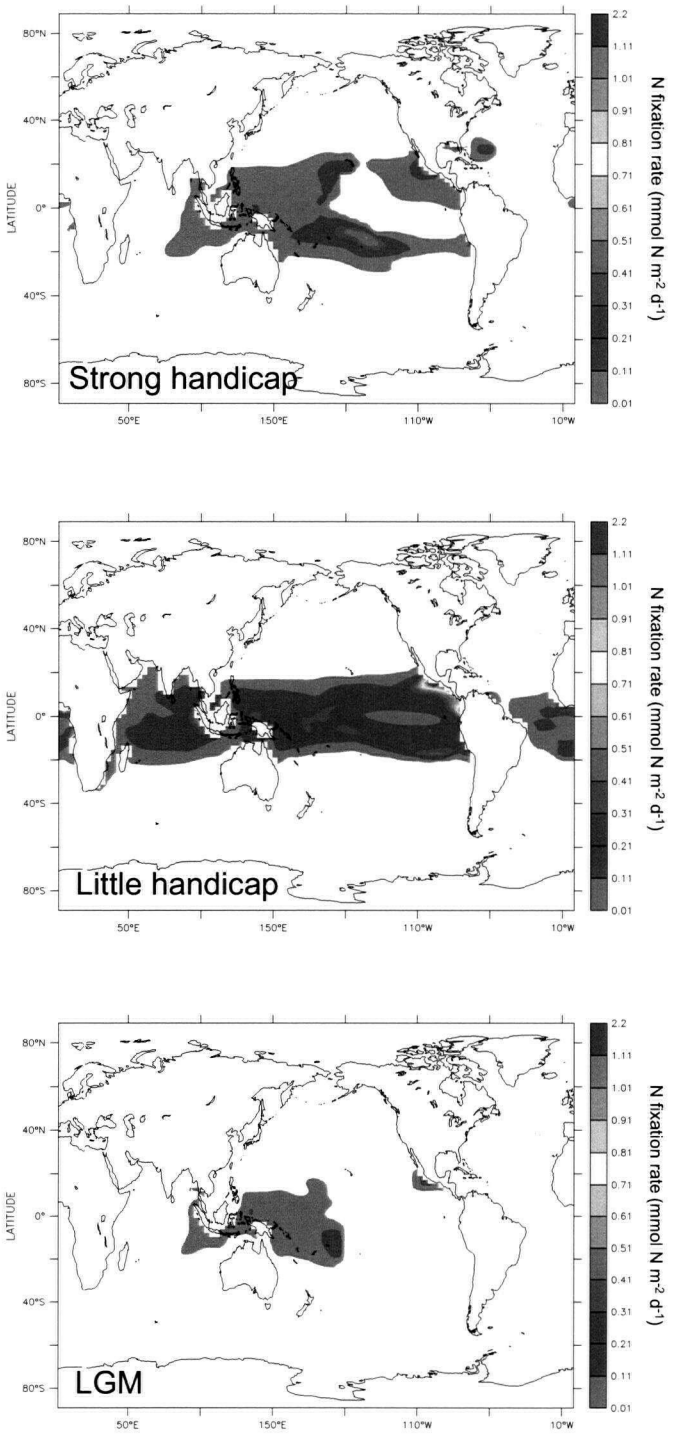

5.6. N_2 fixation rates in three model runs. Nitrogen fixation occurs only in the tropical surface. There is a large increase in N_2 fixation rates when the diazotroph handicap is diminished, particularly in nutrient-rich upwelling areas. Under LGM conditions, fixation is strongly reduced due to lackluster denitrification and abundant nitrate.

ern Ocean are as high as 30. This is clearly not representative of the modern ocean, where NO_3^- is zero throughout the tropical surface ocean and N* does not rise significantly above 5 (Figure 5.3). This indicates that the weak diazotroph handicap is unreasonable. At the other end of the spectrum, the diazotrophs in Run 5 are so disadvantaged as to be on the verge of extinction, and the N inventory was in free fall after 1500 years. With an intermediate diazotroph handicap, the N cycle quickly approaches a balanced budget with the given P inventory and present day climate, suggesting that these intermediate handicaps best approximate the true growth rate disadvantage.

The absence of Fe-limitation of diazotrophs in the model certainly reduces its accuracy, but is not likely to have a strong bearing on the results presented here. Culture studies of *Trichodesmium* spp. have shown high requirements for Fe [*Berman-Frank et al.*, 2001; *Kustka et al.*, 2003] and field studies have confirmed the acceleration of N_2 fixation under Fe addition [*Mills et al.*, 2004]. However, there is little evidence that Fe is a limiting factor for unicellular diazotrophs. Moreover, the effect of exacerbating global micronutrient limitation of diazotrophs is crudely simulated by reducing our handicap parameter, c_D. Hence, a world in which diazotrophs grow more quickly due to alleviation of Fe limitation (e.g. [*Falkowski*, 1997; *Broecker and Henderson*, 1998]) is approximated by the runs with small handicaps (runs 2 and 3). We use the Strong handicap case for the standard PD run, such that the maximum growth rate of diazotrophs is markedly less than other phytoplankton as would be expected in an Fe-limited ocean. Of course, this does not take into account the variable pattern of Fe limitation, and may overestimate N_2 fixation in the Fe-poor eastern tropical Pacific while underestimating it in the tropical Atlantic.

5.4 Model stability

The global OMZ volume varies by a factor of more than four between model runs, while the global water column denitrification rate varies by a factor of more than 20 (Table 5.2). This testifies to the sensitivity of the rates of nitrogen cycling to both the diazotroph handicap and to the physical environment. However, denitrification never proceeds to completion, in accord with the real ocean, and for intermediate diazotroph handicaps the N budget approaches a balanced budget on the order of centuries to millennia. This inventory stability can be attributed to two feedback mechanisms.

First, the extent of a denitrification zone is restrained by nitrate limitation of local phytoplankton export in the immediate vicinity. This is illustrated by the fact that the OMZ is large in the NoN run, but of minimal size in the strong handicap run. If denitrification rates increase, the resulting expansion of nitrate limitation reduces the local export of organic matter, alleviating the subsurface oxygen deficit. The slow growth of diazotrophs prevents immediate compensation of the upwelled nitrate deficit, ensuring that productivity shifts away from the denitrifying region as seen in Figure 5.7. The strength of this stability mechanism is dependent on the degree by which diazotrophs are handicapped relative to other phytoplankton. The faster diazotrophs grow, and hence the more competitive they are for PO_4 uptake relative to other phytoplankton, the more they encroach on the PO_4-rich territory near OMZs (Figure 5.7). Thus, the run with very small handicap has the largest OMZs and most rapid denitrification. This mechanism prevents denitrification from expanding beyond the ability of diazotrophs to restore nitrate concentrations, and maintains most of the surface ocean near Redfield. It also tends to prevent the complete consumption of nitrate, explaining the lack of sulphate reduction in the water column.

Second, the handicap of diazotrophs prevents the N inventory from growing significantly above 16 times the P inventory (Redfield). Where NO_3 is restored to near Redfield values, the growth rates of diazotrophs are so slow compared to other phytoplankton that they are unable to compete for P, maintaining proximate N-limitation as shown by Tyrell [1999]. The exception to this is within warm tropical gyres, where the growth rate handicap of diazotrophs is smallest. Here, though still much less abundant than other phytoplankton, slowly-growing diazotrophs provide a gradual trickle of new N to the surface ocean, allowing the N inventory to rise slightly above Redfield N:P in the Minor handicap run. This would not be likely to occur if the model included sedimentary denitrification, which removes N rapidly from the margins of the upper ocean.

5.5 Glacial run

In order to test the sensitivity of the model N cycle to the physical climate state, we ran the model under climate forcing approximating that of the Last Glacial Maximum (LGM). The only prescribed differences in the LGM run are decreased incoming solar radiation, decreased thermal opacity of the atmosphere (mimicking lower CO_2) and presence of

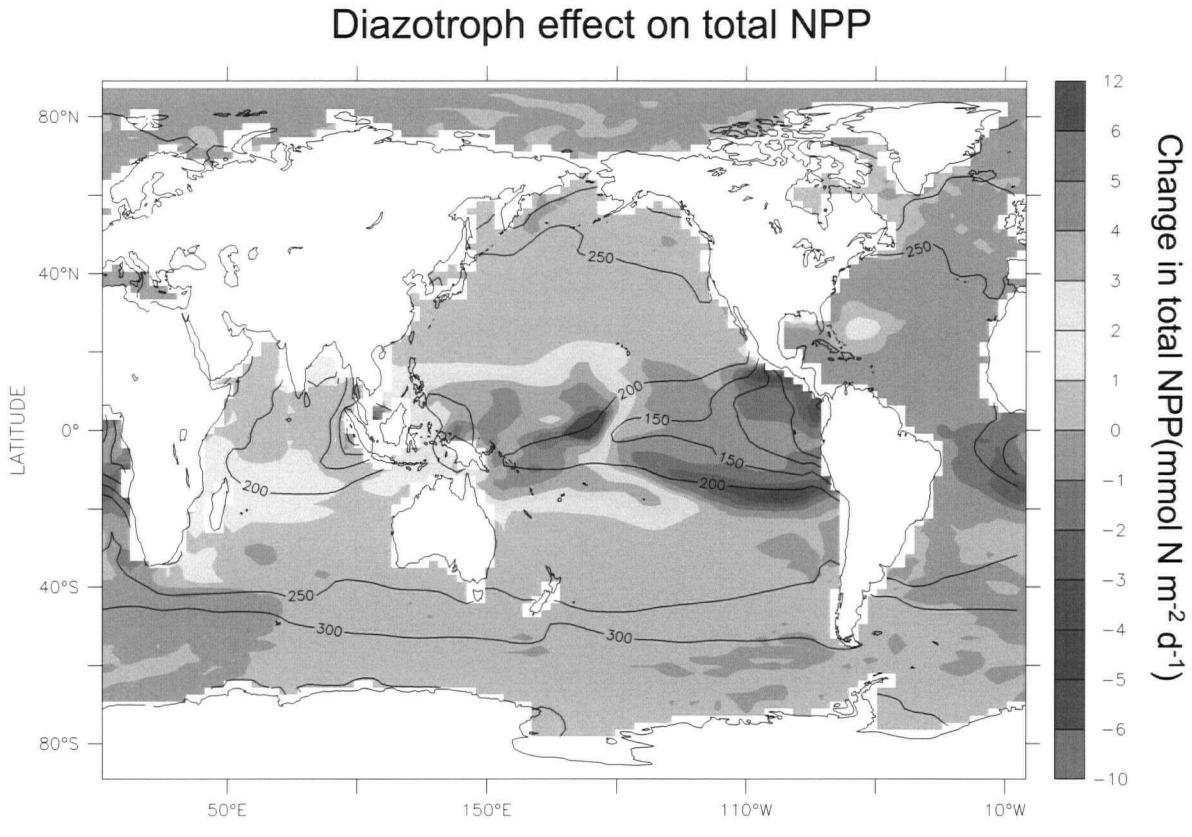

5.7. Differences in net primary production due to diazotrophy. This shows the difference in total water-column-integrated NPP between the standard PD run and the run with no N cycle (run 1, NoN). Contours show O_2 concentrations in NoN at 292m depth. NO_3^- limitation near the denitrification zone in the ETP causes a shift in NPP to more oligotrophic regions where diazotrophs eliminate the N deficit. This geographical shift in NPP limits the size of the denitrification zone.

terrestrial ice sheets. All other parameters, including the wind field, were unchanged from the reference PD run.

There is a large increase in oxygen concentration within the thermocline in the LGM run, when compared to the present day (PD) run (Figures 5.7, 5.8). As a result, the rate of denitrification is sharply decreased (Table 5.2), and the rate of N_2 fixation falls, bringing the budget into balance (Figure 5.6). The decrease in denitrification can be attributed to a combination of both increased oxygen supply and decreased oxygen demand. The physical oxygen supply itself is primarily a function of water temperature and circulation in the upper ocean (Chapter 4). The glacial temperature decrease is responsible for roughly half the increase in O_2 shown in the sensitive low latitudes of the LGM case. The other half is due partly to an increase in ventilation rates, as shown by *Meissner et al.* [2005] using a similar variant of the UVic physical model, and partly by a glacial decrease in ocean fertility.

Decreased oceanic fertility occurs under LGM conditions, as nutrients accumulate in a relatively poorly ventilated deep Atlantic at the expense of the shallow ocean (Figure 5.9 [*Schmittner*, 2005]). Quantitatively, this change is poorly constrained, as effects such as iron fertilization [*Martin and Fitzwater*, 1988], ecosystem composition [*Matsumoto et al.*, 2002] and upper ocean stability [*Sigman et al.*, 2004] may have pronounced impacts on preformed nutrients in high latitude waters [*Sarmiento and Toggweiler*, 1984; *Boyle*, 1988; *Sigman and Boyle*, 2000; *Sarmiento et al.*, 2004] that are not accounted for here. However, the bulk of sedimentary evidence from the high latitude regions ventilating the shallow ocean suggest greater nutrient utilization during the glacial [*Francois et al.*, 1997; *Robinson et al.*, 2004; *Crosta et al.*, 2005] (see also Chapter 3) which would amplify the transfer of nutrients to the deep sea. Thus, the sense of change is consistent with the available evidence.

Interestingly, despite the global trend of lower fertility during the glacial, phytoplankton growth rates in the eastern tropical Pacific actually increase. This can be attributed to the weakening of nitrate limitation in the eastern Tropical Pacific in the LGM run, caused by the decrease in denitrification, allowing phytoplankton growth there to increase. The corresponding redistribution of subsurface oxygen demand, increasing in the most oxygen-starved region, serves to maintain a small amount of denitrification. If not for this feedback, denitrification would have been completely eliminated by the physically-driven increase in subsurface oxygenation during the LGM run.

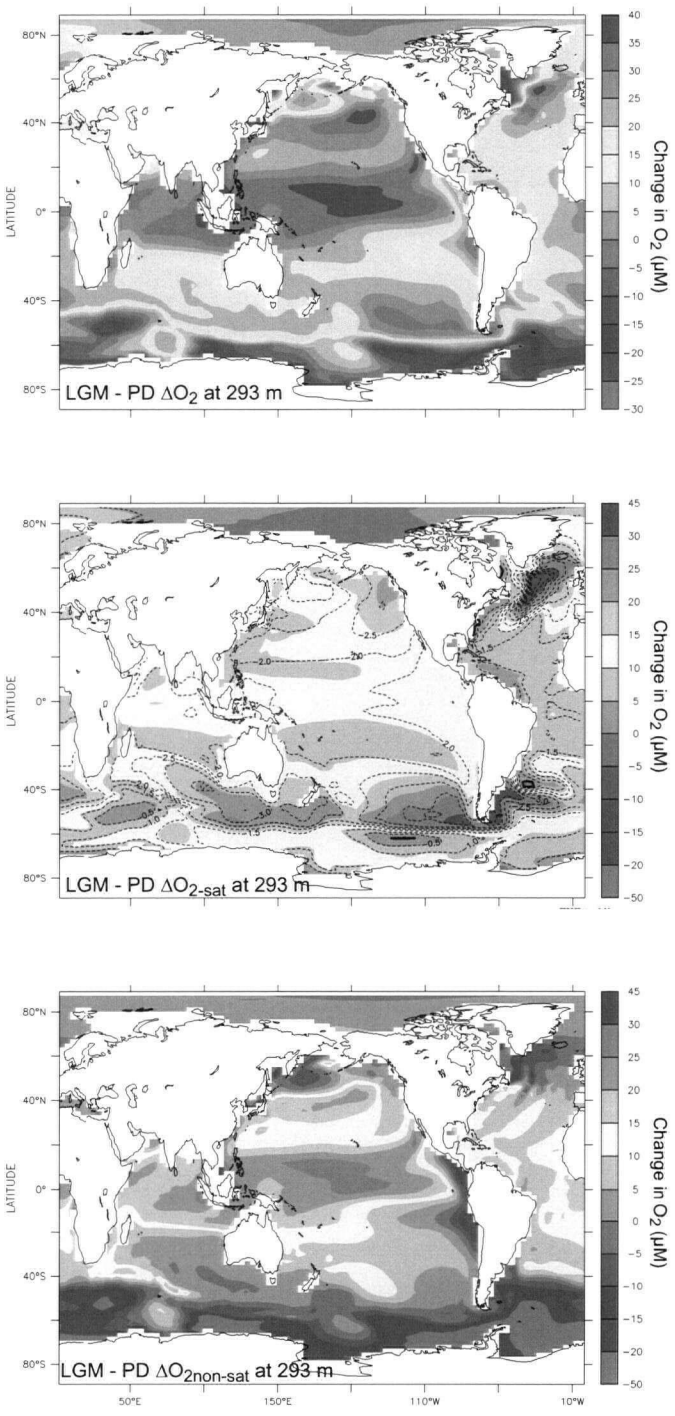

5.8. LGM-PDO2. Increase of subsurface O_2 concentrations in the LGM run vs. the PD run. The top panel shows the increase in O_2 during the LGM run, at the depth of maximum denitrification (293 m). The middle panel shows the change in O_2 saturation concentration on the same level, which is dominantly a function of temperature (shown as contours in °C, with temperature decreases shown by dashed lines). The bottom panel shows the residual of the upper two panels, i.e. the change in O_2 not accounted for by the temperature-driven increase in O_2 solubility: a combination of changes in subsurface remineralization rates and exchange rate with surface waters.

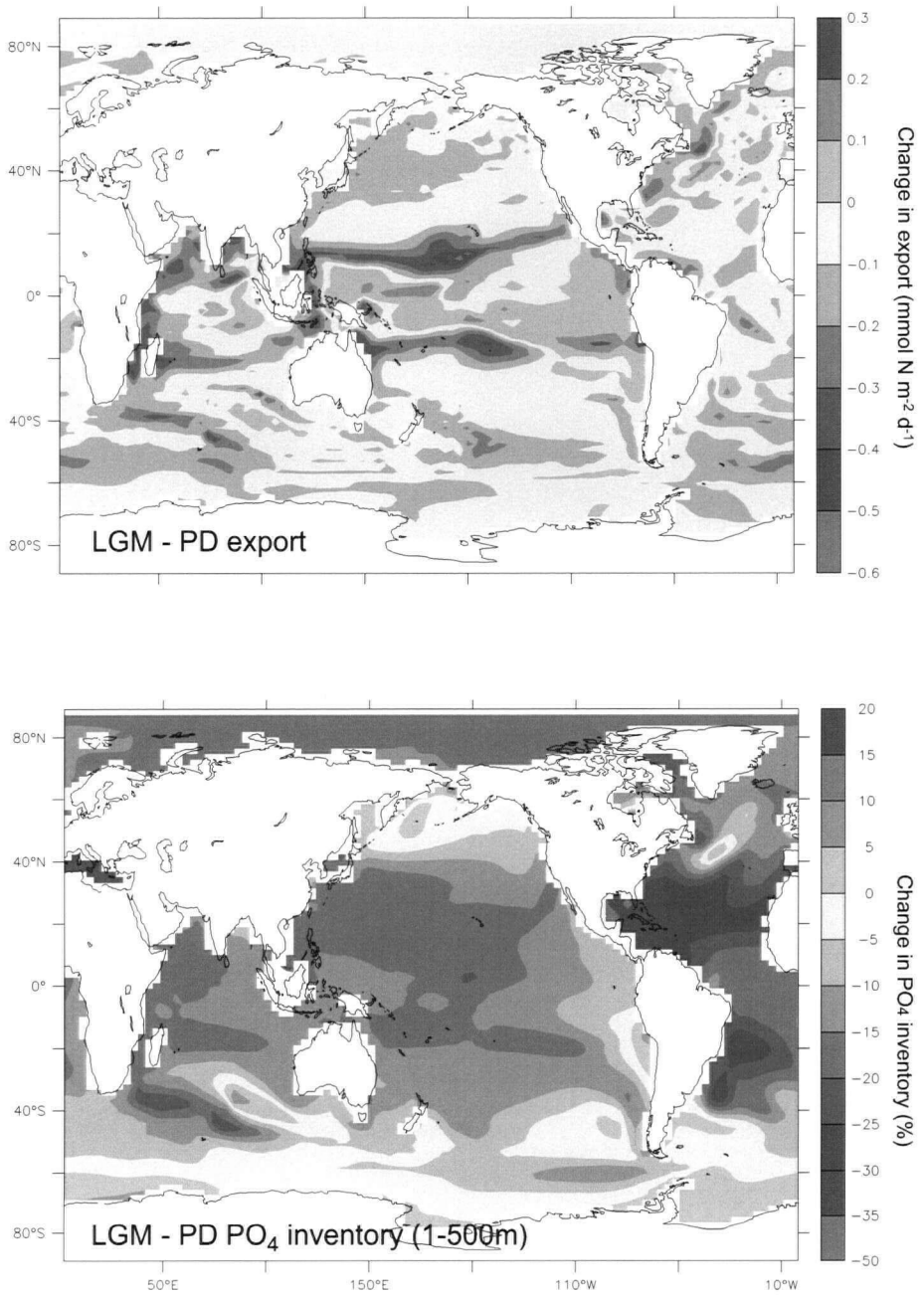

5.9. Decrease of ocean fertility in the LGM vs. the PD run. The top panel shows the change in export of organic matter across 126 m. Throughout most of the ocean there is a slight to moderate decrease in export, except in the equatorial and eastern tropical Pacific where there is a minor increase in export. The bottom panel shows the change in the PO_4 inventory of the upper ocean (1-500m). There is a general decrease in the upper ocean PO_4 inventory globally, as nutrients are shifted to the deep Atlantic, a direct result of the shoaling and weakening of NADW formation in the model.

5.6 Conclusions

A conceptually simple model of the marine N cycle, founded on basic ecological principles, displays many characteristics that are consistent with observations, including reasonable rates of denitrification and patterns of N_2 fixation. Therefore, the model architecture used here appears to be appropriate for studying the relationships between different components of the nitrogen cycle and its relationship to the rest of the climate system.

For a given P inventory, the modeled extent of subsurface oxygen depletion is variable, and denitrification rates vary widely, depending on the degree to which diazotroph growth rates are handicapped relative to other phytoplankton, and the climate state. However, the model displays very strong stabilizing feedbacks that encourage minor denitrification while preventing water column anoxia under all conditions tested here. In particular, the geographical separation of N_2 fixers from denitrifying regions, driven by diazotroph ecophysiology, is highlighted as a primary feature of the nitrogen cycle worthy of further investigation.

Under glacial climate conditions, the model exhibits greatly reduced rates of denitrification and N_2 fixation, both of which decrease by a factor of six. This is attributed primarily to an increase in subsurface oxygen supply and, secondarily, to a general decrease in ocean fertility. This result arises in the complete absence of any wind-driven changes in upwelling, often cited as the primary modulator of denitrification in the ETNP and AS (e.g. [*Altabet et al.*, 1999]).

The results provide further support for the sensitivity of denitrification rates to changes in physical climate, as previously postulated based on sedimentary nitrogen isotope archives (Chapter 4). Despite the large changes in rates, the N inventory itself is relatively stable under the conditions tested here, with intermediate diazotroph handicaps. However, the relationship between N and the P inventory, and potential changes thereof, remains unresolved and demands further enquiry. Future research is also required to test the strengths and limits of the mechanisms that serve to stabilize the N inventory.

5.7 References

Altabet, M. A., R. Francois, D. W. Murray, and W. L. Prell, Climate-Related Variations in Denitrification in the Arabian Sea From Sediment $^{15}N/^{14}N$ Ratios, *Nature*, 373, 506-509, 1995.

Altabet, M. A., D. W. Murray, and W. L. Prell, Climatically linked oscillations in Arabian Sea denitrification over the past 1 m.y.: Implications for the marine N cycle, *Paleoceanography*, 14, 732-743, 1999.

Berelson, W. M., Particle settling rates increase with depth in the ocean, *Deep-Sea Research Part II-Topical Studies in Oceanography*, 49, 237-251, 2002.

Berman-Frank, I., J. T. Cullen, Y. Shaked, R. M. Sherrell, and P. G. Falkowski, Iron availability, cellular iron quotas, and nitrogen fixation in Trichodesmium, *Limnology and Oceanography*, 46, 1249-1260, 2001.

Boyle, E. A., Vertical Oceanic Nutrient Fractionation and Glacial Interglacial CO_2 Cycles, *Nature*, 331, 55-56, 1988.

Breitbarth, E., Ecophysiology of the marine cyanobacterium Trichodesmium, Ph.D., Christian-Albrechts University, Kiel, 2004.

Broecker, W. S., and G. M. Henderson, The sequence of events surrounding Termination II and their implications for the cause of glacial-interglacial CO_2 changes, *Paleoceanography*, 13, 352-364, 1998.

Capone, D. G., J. A. Burns, J. P. Montoya, A. Subramaniam, C. Mahaffey, T. Gunderson, A. F. Michaels, and E. J. Carpenter, Nitrogen fixation by Trichodesmium spp.: An important source of new nitrogen to the tropical and subtropical North Atlantic Ocean, *Global Biogeochemical Cycles*, 19, 2005.

Codispoti, L. A., J. A. Brandes, J. P. Christensen, A. H. Devol, S. W. A. Naqvi, H. W. Paerl, and T. Yoshinari, The oceanic fixed nitrogen and nitrous oxide budgets: Moving targets as we enter the anthropocene?, *Scientia Marina*, 65, 85-105, 2001.

Crosta, X., A. Shemesh, J. Etourneau, R. Yam, I. Billy, and J. J. Pichon, Nutrient cycling in the Indian sector of the Southern Ocean over the last 50,000 years, *Global Biogeochemical Cycles*, 19, 10, 2005.

Devol, A. H., and H. E. Hartnett, Role of the oxygen-deficient zone in transfer of organic carbon to the deep ocean, *Limnology and Oceanography*, 46, 1684-1690, 2001.

Falkowski, P. G., Evolution of the nitrogen cycle and its influence on the biological sequestration of CO_2 in the ocean, *Nature*, 387, 272-275, 1997.

Francois, R., M. A. Altabet, E. F. Yu, D. M. Sigman, M. P. Bacon, M. Frank, G. Bohrmann, G. Bareille, and L. D. Labeyrie, Contribution of Southern Ocean surface-water stratification to low atmospheric CO_2 concentrations during the last glacial period, *Nature*, 389, 929-935, 1997.

Ganeshram, R. S., T. F. Pedersen, S. E. Calvert, and J. W. Murray, Large changes in oceanic nutrient inventories from glacial to interglacial periods, *Nature*, 376, 755-758, 1995.

Gnanadesikan, A., J. P. Dunne, R. M. Key, K. Matsumoto, J. L. Sarmiento, R. D. Slater, and P. S. Swathi, Oceanic ventilation and biogeochemical cycling: Understanding the physical mechanisms that produce realistic distributions of tracers and productivity, *Global Biogeochemical Cycles*, 18, 2004.

Gruber, N., and J. L. Sarmiento, Global patterns of marine nitrogen fixation and denitrification, *Global Biogeochemical Cycles*, 11, 235-266, 1997.

Holl, C. M., Regulation of Trichodesmium Nitrogen Fixation by Combined Nitrogen and Growth Rate: A Field and Culture Study, Ph.D., Georgia Institute of Technology, 2004.

Hood, R. R., V. J. Coles, and D. G. Capone, Modeling the distribution of Trichodesmium and nitrogen fixation in the Atlantic Ocean, *Journal of Geophysical Research-Oceans*, 109, 2004.

Kustka, A. B., S. A. Sanudo-Wilhelmy, E. J. Carpenter, D. Capone, J. Burns, and W. G. Sunda, Iron requirements for dinitrogen- and ammonium-supported growth in cultures of Trichodesmium (IMS 101): Comparison with nitrogen fixation rates and iron: carbon ratios of field populations, *Limnology and Oceanography*, 48, 1869-1884, 2003.

Kuypers, M. M. M., G. Lavik, D. Woebken, M. Schmid, B. M. Fuchs, R. Amann, B. B. Jorgensen, and M. S. M. Jetten, Massive nitrogen loss from the Benguela upwelling system through anaerobic ammonium oxidation, *Proceedings of the National Academy of Sciences of the United States of America*, 102, 6478-6483, 2005.

Martin, J. H., and S. E. Fitzwater, Iron-Deficiency Limits Phytoplankton Growth in the Northeast Pacific Subarctic, *Nature*, 331, 341-343, 1988.

Matsumoto, K., J. L. Sarmiento, and M. A. Brzezinski, Silicic acid leakage from the Southern Ocean: A possible explanation for glacial atmospheric pCO_2, *Global Biogeochemical Cycles*, 16, 2002.

Meissner, K. J., E. D. Galbraith, and C. Volker, Denitrification under glacial and interglacial conditions: A physical approach, *Paleoceanography*, 20, 2005.

Mills, M. M., C. Ridame, M. Davey, J. La Roche, and R. J. Geider, Iron and phosphorus co-limit nitrogen fixation in the eastern tropical North Atlantic, *Nature*, 429, 292-294, 2004.

Montoya, J. P., C. M. Holl, J. P. Zehr, A. Hansen, T. A. Villareal, and D. G. Capone, High rates of N_2 fixation by unicellular diazotrophs in the oligotrophic Pacific Ocean, *Nature*, 430, 1027-1031, 2004.

Najjar, R., and J. C. Orr, Design of OCMIP-2 simulations of chlorofluorocarbons, the solubility pump and common biogeochemistry, available at http://www.ipsl.jussieu.fr/OCMIP, 1998.

Robinson, R. S., B. G. Brunelle, and D. M. Sigman, Revisiting nutrient utilization in the glacial Antarctic: Evidence from a new method for diatom-bound N isotopic analysis, *Paleoceanography*, 19, 2004.

Sanudo-Wilhelmy, S. A., A. Tovar-Sanchez, F. X. Fu, D. G. Capone, E. J. Carpenter, and D. A. Hutchins, The impact of surface-adsorbed phosphorus on phytoplankton Redfield stoichiometry, *Nature*, 432, 897-901, 2004.

Sarmiento, J. L., N. Gruber, M. A. Brzezinski, and J. P. Dunne, High-latitude controls of thermocline nutrients and low latitude biological productivity, *Nature*, 427, 56-60, 2004.

Sarmiento, J. L., and J. R. Toggweiler, A New Model for the Role of the Oceans in Determining Atmospheric Pco2, *Nature*, 308, 621-624, 1984.

Schmittner, A., Decline of the marine ecosystem caused by a reduction in the Atlantic overturning circulation, *Nature*, 434, 628-633, 2005.

Schmittner, A., A. Oschlies, X. Giraud, M. Eby, and H. L. Simmons, A global model of the marine ecosystem for long-term simulations: Sensitivity to ocean mixing, buoyancy forcing, particle sinking, and dissolved organic matter cycling, *Global Biogeochemical Cycles*, 19, 2005.

Sigman, D. M., and E. A. Boyle, Glacial/interglacial variations in atmospheric carbon dioxide, *Nature*, 407, 859-869, 2000.

Sigman, D. M., S. L. Jaccard, and G. H. Haug, Polar ocean stratification in a cold climate, *Nature*, 428, 59-63, 2004.

Tyrrell, T., The relative influences of nitrogen and phosphorus on oceanic primary production, *Nature*, 400, 525-531, 1999.

Weaver, A. J., M. Eby, E. C. Wiebe, C. M. Bitz, P. B. Duffy, T. L. Ewen, A. F. Fanning, M. M. Holland, A. MacFadyen, H. D. Matthews, K. J. Meissner, O. Saenko, A. Schmittner, H. X. Wang, and M. Yoshimori, The UVic Earth System Climate Model: Model description, climatology, and applications to past, present and future climates, *Atmosphere-Ocean*, 39, 361-428, 2001.

Chapter VI

Concluding remarks

6.1 Perspective on progress

The synthesis of past changes in the marine N cycle, as presented in the preceding pages, retains many uncertainties, but this should be viewed in the context of the past two decades. The first proposition that climate change can influence the marine N cycle was made by *McElroy* [1983], who pointed out that the short residence time of fixed marine N (then believed to be ~ 10^4 y) made it a good candidate for change on glacial-interglacial cycles. The marine nitrogen budget estimates of the day appeared to show a large deficit, so McElroy suggested that the present-day situation was part of a grand ~100 ka cycle: during ice age inception, advancing glaciers would have bulldozed terrestrial N into the ocean, while the erosion of continental shelves exposed by sea level drop would have flushed N-rich sediments into the deep-sea, to create a glacial ocean rich with nitrogen in which greater productivity was limited by the availability of phosphate. When shelf sediments were worn down and the ice sheets reached their maximum extents, the supply of terrestrial N would have returned to something like its low, modern rate. Denitrification would have eaten away at the accumulated surplus of N, bringing us eventually to the modern-day position of a nitrogen-limited ocean with a large inferred N deficit. This hypothesis, which was novel and fully defensible at the time, was predicated on the view of the marine N cycle as unresponsive, in that the marine fluxes of fixation and denitrification were assumed to be ineffective at compensating for changes in the external supply of N.

Over the past twenty years, however, modern process studies have shown that the input and output fluxes of the marine N cycle are dominated by marine microbes, not by terrestrial inputs or sediment burial. These point towards a marine nitrogen cycle that is

reactive on a millennial timescale, internally stabilized by homeostatic feedbacks, and largely independent of the terrestrial nitrogen cycle. As a result, the changes in the marine nitrogen cycle discussed here are couched in oceanic processes.

6.2 Contributions of this thesis

This thesis has approached past changes in the global marine nitrogen cycle on multiple fronts. These help overcome some of the uncertainties that have plagued the field, and present a more coherent picture on both regional and global scales.

The emerging understanding of bulk sedimentary $\delta^{15}N$ is, in many environments, as a remarkably reliable monitor of changes in the $\delta^{15}N$ of the nitrogen substrate. This can be attributed to homogenization during sedimentation, as seen in the Guaymas Basin study (Chapter 2), as well as the integrative effect of averaging over seasons or decades, as occurs in slowly accumulating cores. This diminishes the importance of local nutrient cycling in many contexts, but emphasizes the importance of regional changes in $\delta^{15}N_{nitrate}$ for generating downcore variability in $\delta^{15}N$. Diagenesis alters the $\delta^{15}N$ of bulk sediment in cores from the deep sea, but the subarctic Pacific study (Chapter 3) suggests that this may be a relatively straightforward and resolvable matter. The study of targeted sedimentary N components, such as that of diatom frustules, offers an additional avenue of information. As shown in Chapter 2, frustule N is not equivalent to bulk N and appears more sensitive to environmental changes, but offers complementary information.

Regional studies, using multiple $\delta^{15}N$ records, can circumvent many of the uncertainties confronted when considering a record in isolation. The subarctic Pacific study (Chapter 3) shows the importance of recognizing controls on the modern regional variability of $\delta^{15}N_{nitrate}$, which is of fundamental importance for the variability in $\delta^{15}N$ over time. The homogeneity of $\delta^{15}N_{nitrate}$ across the modern subarctic Pacific suggests that the principal discrepancies between local records of change were caused by variable nitrate utilization in the western subarctic Gyre. This is consistent with an alleviation of iron limitation throughout most of the last glacial period, caused by increased dust deposition. The record of $\delta^{15}N_{nitrate}$ suggests that denitrification occurred in the subarctic Pacific during the deglaciation, and hints that denitrification may have occurred in the deep North Pacific during the glacial maximum.

The accumulated sedimentary $\delta^{15}N$ evidence shows that the nitrogen cycle responds dramatically to climate changes, as discussed in Chapter 4. Under globally cool conditions, oxygen supply to the global thermocline is increased due to enhanced solubility and change in circulation. An additional effect is likely to arise from a decrease in the surface ocean fertility, caused by a sequestration of nutrients in the deep sea, as shown by the model described in Chapter 5. Together, these fundamentally physical changes reduce the oxygen deficiency in the global thermocline during cold periods, leading to a decrease in denitrification there. The ensuing reduction in nitrate deficits allows non-diazotrophic phytoplankton to consume all available phosphate and N_2 fixation is correspondingly decreased, as previously suggested by *Ganeshram et al.* [2002]. In contrast, during warmer periods N cycling is more vigorous, nitrogen limitation is exacerbated, and the residence time of fixed N is shorter. These central findings are summarized in Figure 6.1. The numerical model of Chapter 5 suggests that glacial-interglacial changes in water column denitrification rates of an order of magnitude are possible.

It is hoped that this thesis will provide a useful overview of past changes in the marine nitrogen cycle, interpreted within a new conceptual framework with a mechanistic, global view.

6.3 Future work

There is much more variability evident within the $\delta^{15}N$ records than can be described by the broad, glacial-interglacial strokes painted here. Furthermore, many assumptions were made in order to arrive at the conclusions, and some of these assumptions are likely to prove false.

In particular, successful diatom cultures and sediment trap time series are required to confirm the relationship between $\delta^{15}N_{frustule}$ and $\delta^{15}N_{export}$ inferred in Chapter 2. The development of compound-specific techniques, such as for chlorophyll and amino acids, coupled with the use of microfossil-bound organic matter, holds great promise for future investigations [*Ingalls et al.*, 2003; *McCarthy et al.*, 2003].

Detailed measurements of modern $\delta^{15}N\text{-}NO_3^-$ and $\delta^{18}O\text{-}NO_3^-$ throughout the North Pacific would provide valuable information on N cycling rates, physical connections between sources of low and high $\delta^{15}N_{nitrate}$, and the potential for variations in isotopic heterogeneity.

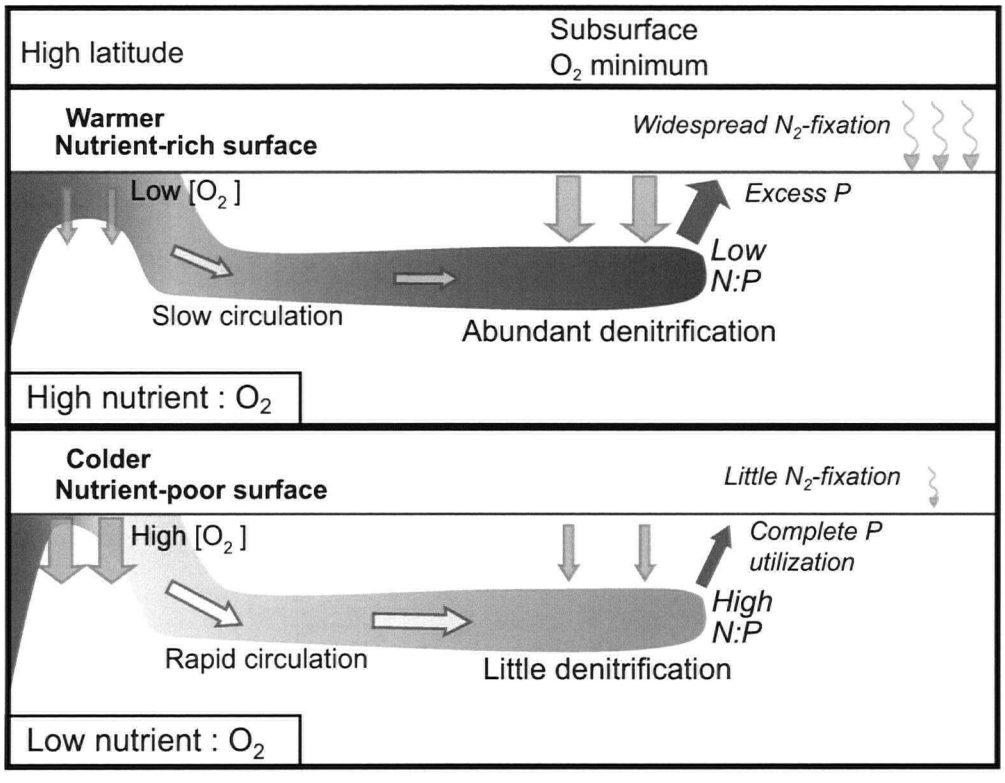

6.1. Modulation of marine N cycle by high latitude influences on global thermocline. The coloured layer indicates the ventilated thermocline, in which darker blue represents greater phosphate concentrations. Downward-pointing green arrows represent export production, which consumes subsurface oxygen, while the upward pointing blue arrows represent the upwelling of nutrients. In the upper panel, effective vertical exchange and low relative nutrient utilization in the high latitudes produce a nutrient-rich thermocline, fuelling abundant low-latitude export production. Meanwhile, warm conditions produce low initial O_2 concentrations and thermocline waters generally circulate more slowly. The low O_2 : nutrient ratio maintains abundant suboxia, with widespread denitrification and, consequently, low N : P in thermocline water (i.e. waters with excess phosphate) which is subsequently upwelled to the surface. Algal growth in this upwelled water eventually yields nitrate-free, phosphate-bearing water, which drives N_2-fixation. In contrast, the lower panel shows poor vertical exchange and high nutrient utilization in the high latitudes, producing a nutrient-poor thermocline that limits export production at low-latitudes. In addition, cool conditions produce high initial O_2 and rapid thermocline circulation. As a result, thermocline suboxia and denitrification are reduced. With high O_2: nutrient conditions inhibiting denitrification, the N:P ratio in upwelling water will be approach the 'Redfield' ratio of 16:1, allowing complete P utilization by non-N_2 fixing algae, shutting down N_2 fixation.

An apparently systematic postburial $\delta^{15}N_{bulk}$ decrease was identified in Chapter 3, which can be readily tested by comprehensive downcore study of sedimentary N components in slowly accumulating, deep-sea cores. Many more sediment records from the subarctic Pacific, from a range of depths and with better temporal control, are also warranted.

Chapter 4 suggests a close reappraisal of Mediterranean sapropels, in order to test the sensitivity of the Mediterranean to the N:P of subsurface eastern Atlantic waters. The precise role of changes in intermediate water mass temperature and circulation can be elucidated with new records of intermediate water temperature, nutrient content, $\delta^{13}C$, and salinity.

Chapter 5 points to the importance of poorly characterized aspects of the marine N cycle, including the N:P ratio and the mechanistic nature of competition between diazotrophs and other phytoplankton. Although it received scant mention in this thesis, the potential remains for significant changes in the P inventory on glacial-interglacial timescales that cry out for better constraints.

6.4 References

Ganeshram, R. S., T. F. Pedersen, S. E. Calvert, and R. Francois, Reduced nitrogen fixation in the glacial ocean inferred from changes in marine nitrogen and phosphorus inventories, *Nature*, 415, 156-159, 2002.

Ingalls, A. E., C. Lee, S. G. Wakeham, and J. I. Hedges, The role of biominerals in the sinking flux and preservation of amino acids in the Southern Ocean along 170 degrees W, *Deep-Sea Research Part II-Topical Studies in Oceanography*, 50, 713-738, 2003.

McCarthy, M., J. I. Hedges, R. Benner, and M. Fogel, Compound-specific delta N-15 measurements of amino acids in dissolved organic matter from the central Pacific Ocean, *Geochimica Et Cosmochimica Acta*, 67, A284-A284, 2003.

McElroy, M. B., Marine biological controls on atmospheric CO2 and climate, *Nature*, 302, 328-329, 1983.

Appendix 1

Isolating frustule-bound nitrogen from sediments: progress and pitfalls

This appendix details the method used for separating and analyzing the nitrogen isotopic composition of frustule-bound nitrogen ($\delta^{15}N_{frustule}$), developed following Sigman [1997] and incorporating the "Liquid Fire" oxidation protocol. Following the method description are discussions of a series of tests used in method development that revealed potential pitfalls, including problems when cleaning with seemingly innocuous H_2O_2. Also included is a discussion of the problems encountered regarding adsorption of N_2 to diatom frustules during analysis by combustion, and a comparison to measurements made using the "denitrifier" method [*Sigman et al.*, 2001; *Robinson et al.*, 2004].

A1.1 General protocol

Sediment samples were collected directly from the refrigerated cores using a syringe and/or a metal spatula. The required sample size was estimated from the Si/Al content (ranging from approximately 2 mL for Si/Al = 25 to 25 mL for Si/Al = 3.5). Samples were placed immediately in acid-cleaned 50 mL polypropylene centrifuge tubes and closed tightly to maintain hydration. They were placed in a refrigerator until preparation.

Large, opal-poor samples were homogenized in Distilled, Deionized Water (DDW) by vigorous shaking and stirring, and subdivided into multiple samples each <8 mL sediment volume to improve the physical separation, after which they were recombined prior to cleaning. All samples were decarbonated using 25 % HCl (Environmental Grade) in DDW. Approximately 35 mL of acid was added to each vial, shaken vigorously, allowed to sit with top loosened for 30 minutes, shaken again, and allowed to sit for another hour. The vials were then centrifuged at 2500 RPM for 3 minutes and the supernatant acid decanted. Next

the samples were rinsed with 35 mL DDW (by shaking, centrifuging and decanting the supernatant) three times. During all separations made following July, 2002, the samples were also partially oxidized in 10% H_2O_2 for 30 minutes prior to rinsing, as this greatly improved the floatation.

A1.1.1 Physical separation

Sodium Polytungstate (SPT, available as powder from Sigma) forms a clear solution when dissolved in DDW, with a density adjustable from 1.0 to over 3.2 g mL^{-1}. An SPT solution of desired density was prepared by adding DDW and powdered SPT to a graduated cylinder on a robust balance until the desired density was achieved. During adjustment it is important to account for the significant expansion of the solution which occurs as SPT is added; it is best to start with approximately half the volume of DDW desired, add SPT until the weight is w-(v-x) where w is the desired weight, v is the desired volume and x is the actual volume, then top up to the desired volume with DDW. Accuracy was generally +/- 0.01 g ml^{-1}.

The prepared SPT solution was added to the vial until the total volume was 40 mL. Because the sediment samples were not dried (in order to prevent potentially irreversible agglomeration of clays, organics and frustules), they contained a substantial amount of water. Therefore, to obtain an SPT solution density of 2.15 (approximately equal to that of opal) in the vial, it was necessary to use an SPT solution of density given by the approximate empirical formula (2.35 + (x-5)) g mL^{-1} where x is the volume of sediment. The result was generally 2.18 +/- 0.05 g mL^{-1}. It was decided to err on the denser side, as this would result in a greater yield of diatoms. Any clays recovered accidentally due to the greater density were subsequently removed by the addition of a repeat step using an SPT solution of exactly 2.15 g mL^{-1}.

The sediment-SPT mixtures were subjected to ultrasonication using a probe at medium power for 6-8 minutes, in order to completely disaggregate the sediment. Next, separation was achieved by centrifuging the samples for 25 minutes at 2500 RPM. This usually produced a well-differentiated floating fraction composed of diatoms and organic material and a sediment dominated by aluminosilicates. The intervening liquid was usually clear, but occasionally contained significant suspended material (presumably neutrally-

buoyant aggregates formed during centrifugation). If the separation was very poor, resulting in a dark, murky mixture, the tube was vortexed well and centrifuged a second time; this usually resulted in a good separation.

The floating fraction was removed, by a combination of scooping with a metal spatula and gentle pouring, into a clean centrifuge tube. The tube was then filled to 40 mL with SPT solution of exactly 2.15 g mL^{-1}. Ultrasonication was repeated, followed by a second round of separation by centrifuge. The floating fraction was gently transferred onto a 45 mm diameter 5.0 micron polycarbonate membrane (Whatman Nuclepore), and filtered to dryness at approximately 10" Hg negative pressure. All SPT was recovered for reuse by further vacuum filtration through a 0.4 micron polycarbonate membrane (PM, Poretics) with a GFF prefilter (to speed filtration), and the density readjusted by evaporation or addition of new SPT powder. Recovery of SPT was 85-90%. The sample was then rinsed with 50 mL DDW from a squirt bottle, at least three times, to remove all traces of SPT. The membrane (with sample) was then placed in a petri dish, dried in a 50 °C oven and stored in a dessicator until oxidation.

The efficacy of the method was tested by measuring Ti in the separated sample by graphite-furnace atomic adsorption spectroscopy. The fractions separated from the most clay-rich samples had less than 4 % of the original Ti content remaining. Considering that there is likely some small amount of Ti in diagenetic aluminosilicate grown on the frustules, this remaining 4 % Ti is equivalent to an upper limit on the amount of clay remaining, showing at least 96 % clay removal.

A1.1.2 Oxidation by liquid fire

The 'periodic acid liquid fire reaction' [*Smith and Diehl*, 1960] takes advantage of what appears to be a synergy between periodic and perchloric acids, increasing oxidative capacity while stabilizing the solution against potentially explosive decomposition. Oxidations were carried out in a round reaction flask, with two openings. The dry diatom sample was introduced to the flask, along with 1.5 g of crystalline periodic acid, and 15 mL of concentrated perchloric acid were added by pipette. The two openings were sealed by inserting a thermometer into one and a reflux column into the other, and pressed tightly together in order to prevent vapour leakage. The flask was placed in a heating mantle, the

temperature of which was controlled by varying the current supplied. A steady flow of water was pumped through the reflux column while the temperature of the reaction liquid was raised quickly to 145 °C, after which it was maintained above 130 °C for 75 - 100 minutes. The mixture was then allowed to cool, and was filtered onto a 5 μm polycarbonate membrane and rinsed with at least 1 L of DDW. Unusual colours were sometimes observed during the oxidation, including greenish fumes and a fuschia condensate of unknown origin, probably an iodide compound. The oxidized diatoms frequently had a pale beige-red-pink hue, which may have indicated the presence of metal oxides on the opal surface.

A1.1.3 C and N measurements

Total carbon and total nitrogen were measured by high temperature combustion using a Carlo Erba 1500 CNS analyzer (referred to here as "CNS"). Repeat measurements of sediment standards typically yield relative standard deviations (RSD, 1σ) for C and N of 3 % and 5 %, respectively. However, because of the very small N and C content of oxidized diatom frustules, the error was much larger; five repeat measurements for each of two samples (OG 9 and 10) yielded an RSD (1σ) of 14 % for C and 19 % for N. These are the reported errors.

A1.1.4 Isotopic analysis

The $\delta^{15}N_{bulk}$ was measured by combustion EA-IRMS as described by Ganeshram et al. [2000]. The $\delta^{15}N_{frustule}$ was determined by two methods. First, by Combustion (here "Cmb") at the University of British Columbia, by packing large tin cups full of cleaned diatoms (50 – 100 mg of sample), pelletizing them, and measuring them by EA-IRMS identical to the $\delta^{15}N_{bulk}$ method. Samples were also measured by the "persulphate-denitrifier" method (here "PD") at Princeton University, as described by Robinson et al. [2004]. This involved heating the sample in a solution of potassium persulfate and 1.5N NaOH, to dissolve the opal and oxidize the liberated organic N to nitrate. Nitrate concentration was then determined by chemiluminescence [*Braman and Hendrix*, 1989] and the N isotopic composition of the nitrate was measured via the "denitrifier" method [*Sigman et al.*, 2001].

A1.2 Oxidation tests: Liquid fire

The "liquid fire" oxidation method was tested using two sediment samples from ODP 887B, one diatom-rich (OT-D, 16.90 – 16.95 mcd, ~ 235 ka) and one clay-rich (OT-C, 8.56 – 8.70 mcd, ~ 107 ka). Following separation of the diatoms, they were exposed to the liquid fire solution for varying lengths of time. OT-D oxidations ranged from no heat applied to heated to temperatures > 130 °C for 210 minutes; two OT-C oxidations were carried out for 90 and 200 minutes.

The results, shown in Figure A1.1, indicate a reduction in the residual N fraction during the first 50 minutes of oxidation, following which the residual N fraction remained constant within error, consistent with the results of [*Sigman*, 1997]. The loss of total dry mass was fairly consistent at ~ 10 %, which could be due to loss of water from the silica, or entirely to mechanical fragmentation by stirring and loss of material through the membrane during filtration. Larger mass losses, as observed by *Sigman* [1997] (up to 25 %) did not occur. Diatom frustules cleaned by the liquid fire method were clearly intact, as revealed by SEM imagery (Figures A1.2, A1.3).

The $\delta^{15}N_{frustule}$ (Cmb) of separated diatoms was lower than that of the bulk sample. Following cleaning, the $\delta^{15}N_{frustule}$ (Cmb) of residual matter decreased very slightly for the OG-D samples (~ 0.5 ‰), during the first 90 minutes, and by somewhat more for the OG-C samples (~ 1 ‰). This is consistent with the sense of change observed by *Sigman* [1997], although the magnitude is less. The absolute $\delta^{15}N_{frustule}$ values as determined by Cmb must be viewed with caution, however, in light of the N_2 adsorption problem discussed below (Section A1.4).

A1.3 Oxidation tests: Peroxide

Oxidation tests were conducted on Guaymas Basin sample GB-1, a large, thoroughly homogenized bag of mud, collected from the box core MD02-2517SC (27.4850 °N, 112.0743 °W, 887 m water depth, 5.6 m length) over a diatom-rich interval at ~1.8 - 2.0 m below sea floor (deposited < 5 ka). The sample was split into 12 aliquots, decarbonated with 25% HCl, and diatoms were separated from each by floatation. The separated diatoms were combined to make a homogenized sample, 'Separate'. This was then subdivided into ten samples of 400 ± 5 mg that were oxidized by different means. The cleanings included the hot $HClO_4$+ HI

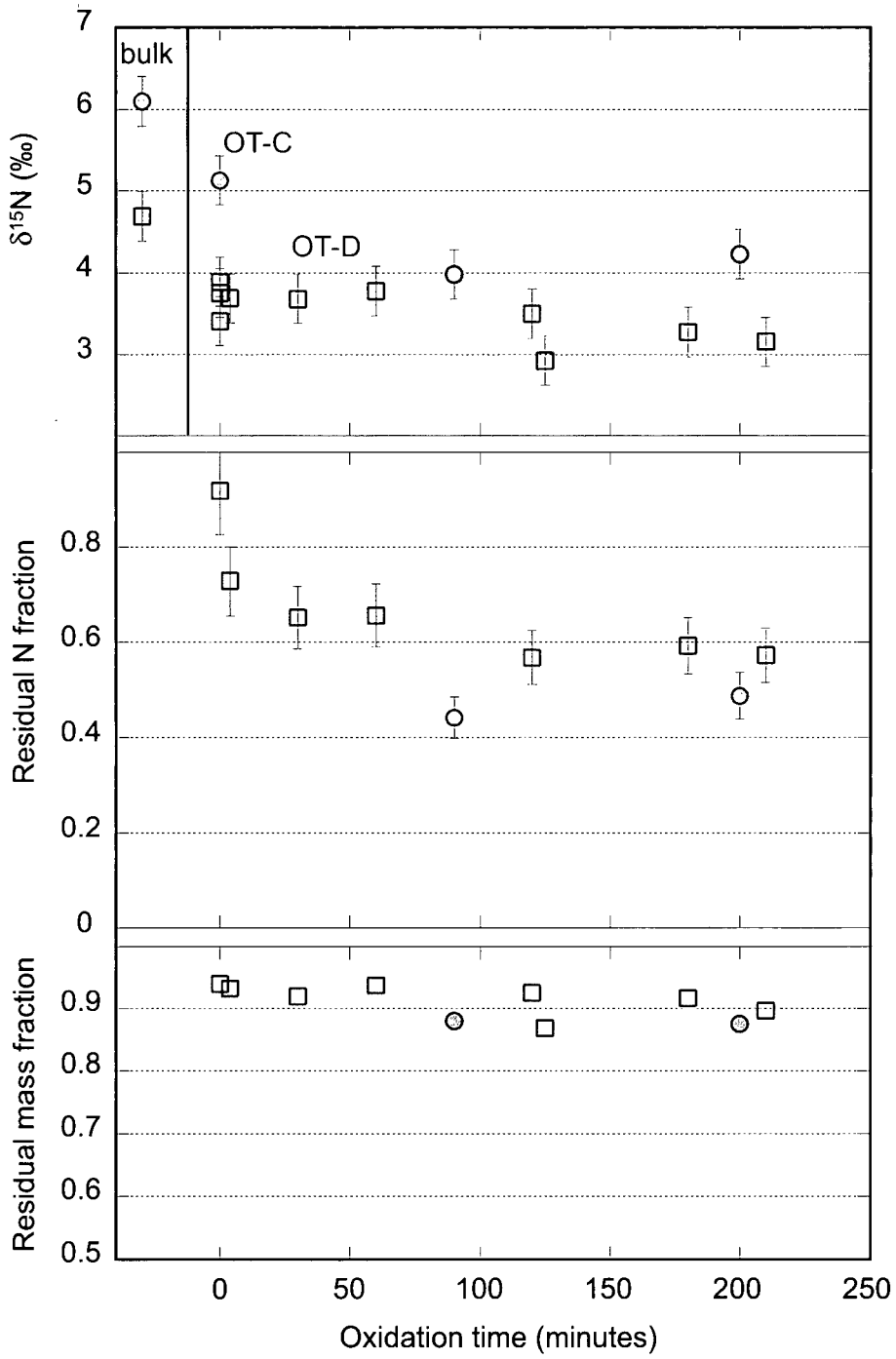

A1.1: Results of the liquid fire oxidation tests. Brown circles correspond to the clay-rich sample, while green squares correspond to the diatom-rich sample. The top panel shows a decrease in $\delta^{15}N_{frustule}$ with increasing oxidation time, with all values identical within error following 90 minutes. The centre panel shows the residual mass of N following oxidation, relative to the initial mass, while the bottom panel shows the residual total dry mass following oxidation, relative to the initial dry mass.

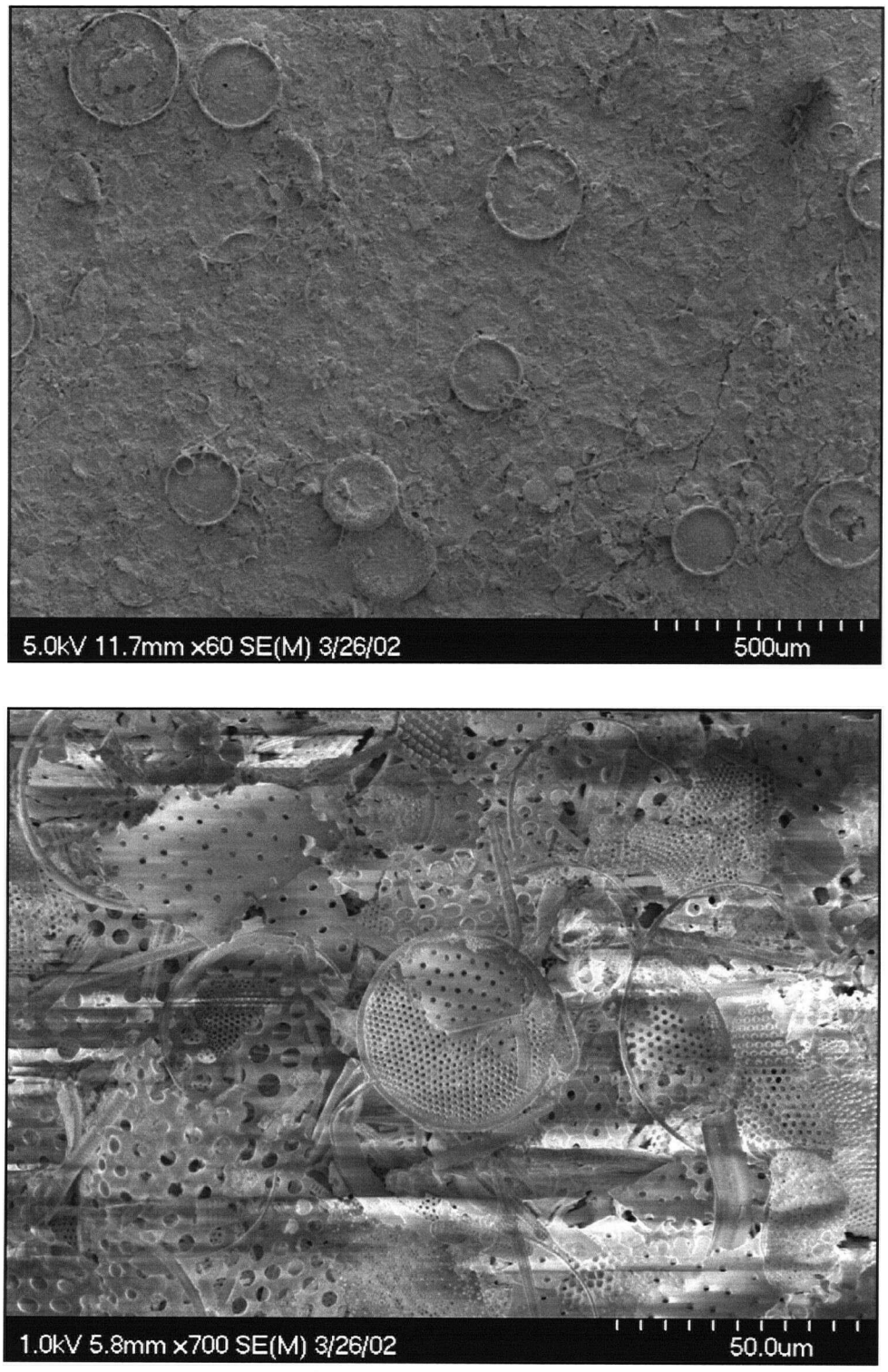

A1.2: Gulf of Alaska sediment samples before and after diatom separation and cleaning. The upper panel shows an SEM image of unprocessed sediment (ODP 887B, 5.54 m composite depth). The lower panel shows an SEM image of separated diatoms (ODP 887B, 4.45m composite depth), cleaned with the liquid fire protocol. The bright, horizontal streaks are due to the semi-conducting nature of the silica, the effect of which is enhanced by the removal of organics.

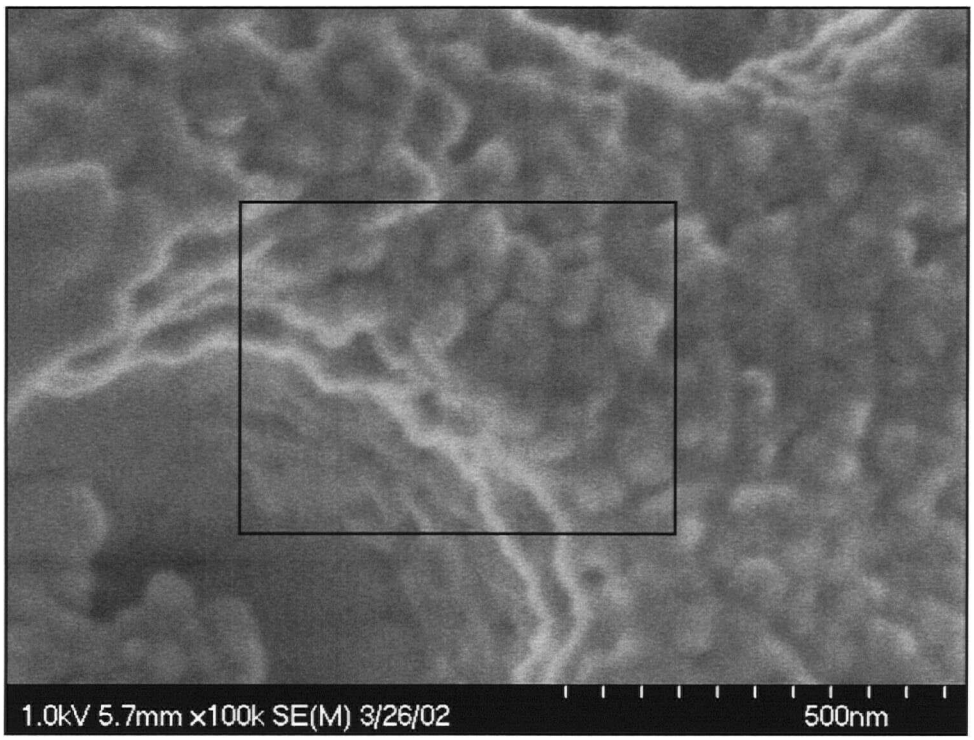

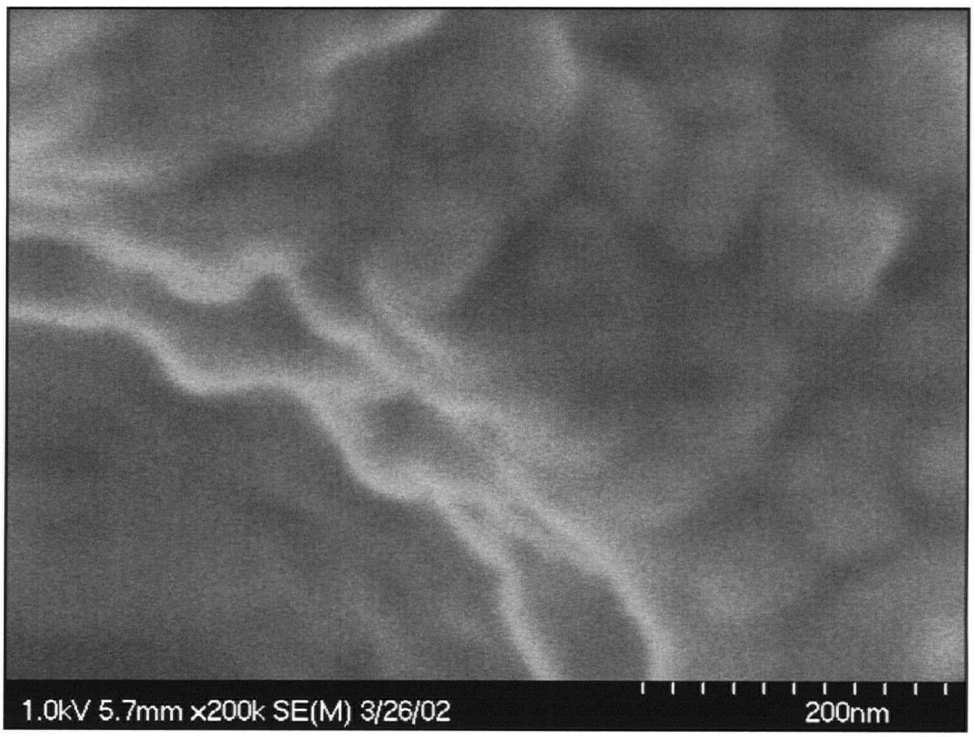

A1.3: Silica nanospheres of an oxidized frustule. These SEM images show the surface of a *Coscino-discus* spp. frustule, cleaned with the liquid fire protocol, (ODP 887B, 4.45m composite depth). The lower image shows a higher magnification of the region outlined by the black rectangle in the upper image.

cleaning described above (here liquid fire, or "LF"), as well as combinations of H_2O_2, sodium pyrophosphate (here 'PyP,' which enhances the effectiveness of H_2O_2, posssibly by chelating metals [*Sequi and Aringhieri*, 1977]), and HCl (to maintain a low pH), as indicated in Table A.1.1. All cleanings with H_2O_2were carried out in polypropylene centrifuge tubes and placed in a water bath to maintain temperatures of 90 - 100 C (time hot, Table A1.1). After cleaning in the oxidizing solutions, each sample was poured onto a 5 μm polycarbonate membrane and filtered to dryness under a gentle vacuum. Residual N and C contents are corrected for total mass loss, as (Residual-concentration) / (Initial-concentration) * (Residual mass fraction), so that they represent the fraction of the total initial N and C contents.

As shown in Figure A1.4, the Perox cleaning was ineffective at removing organic matter, and left a large amount of apparently recalcitrant organic matter (C/N of 13.6 +/- 0.1). The PyP showed a significant improvement in the removal of C, although it was belatedly discovered that the PyP solution had a pH of 10 and may have caused enhanced loss of opal, particularly when left in the solution for multiple days. The PyP-a method resulted in still lower carbon concentrations, although this may have been due to the much longer oxidation time (Table A1.1), with similar % Corg to the LF method. The CNS analyzer measurements seem to show that the N content of all PyP and LF methods are similar, but this is probably compromised by the N_2 adsorption problem (see section A1.4). N contents determined by the PD method show that the PyP-a method produces similar results to the LF method, and compared to the CNS-analyzer C % content gives a C/N of 5.7 +/- .3.

The mass loss of ~10% during the LF cleaning may be entirely due to oxidation of organic matter, with perhaps a small fraction due the mechanical fragmentation of diatoms, and loss of < 5 μm sized particles through the membrane during filtration. However, the more significant mass loss using H_2O_2 during long oxidations (up to 39 %) must be due to a loss of silica, since the initial samples contained only silica and ~ 10% organic matter (bulk C_{org} = 3.9 %, assumed to represent 40 % of organic matter by weight). Dehydration may cause an additional mass loss, but since water typically constitutes only 10-20 % opal by weight [*Mortlock and Froelich*, 1989] this is unlikely to be the only contributing factor. Although H_2O_2 is mildly acidic, and thus would be expected to reduce silica solubility, it has been shown to weaken bonds in glass by inducing a weakly positive charge on exposed Si atoms [*Guyer and Dauskardt*, 2004]. As such, it may tend to weaken the silica structure and

Table A1.1: Oxidation test cleaning methods (OG)

Name	H_2O_2	HCl	$Na_4P_2O_7$	DDW	$HClO_4$	H_5IO_6	Time Hot	Time after[1]
Perox	45 mL	5 mL					20 h	5 d
PyP (1)	10 mL		2.260 g	40 mL			20 h	5 d
PyP (2)	10 mL		2.260 g	40 mL			20 h	-
PyP-a	10 mL	3 mL	2.260 g	40 mL			68 h	-
LF					15 mL	1.5 g	1.5 h	-

1: This represents time the samples remained in the oxidizing solution after removal from the water bath.

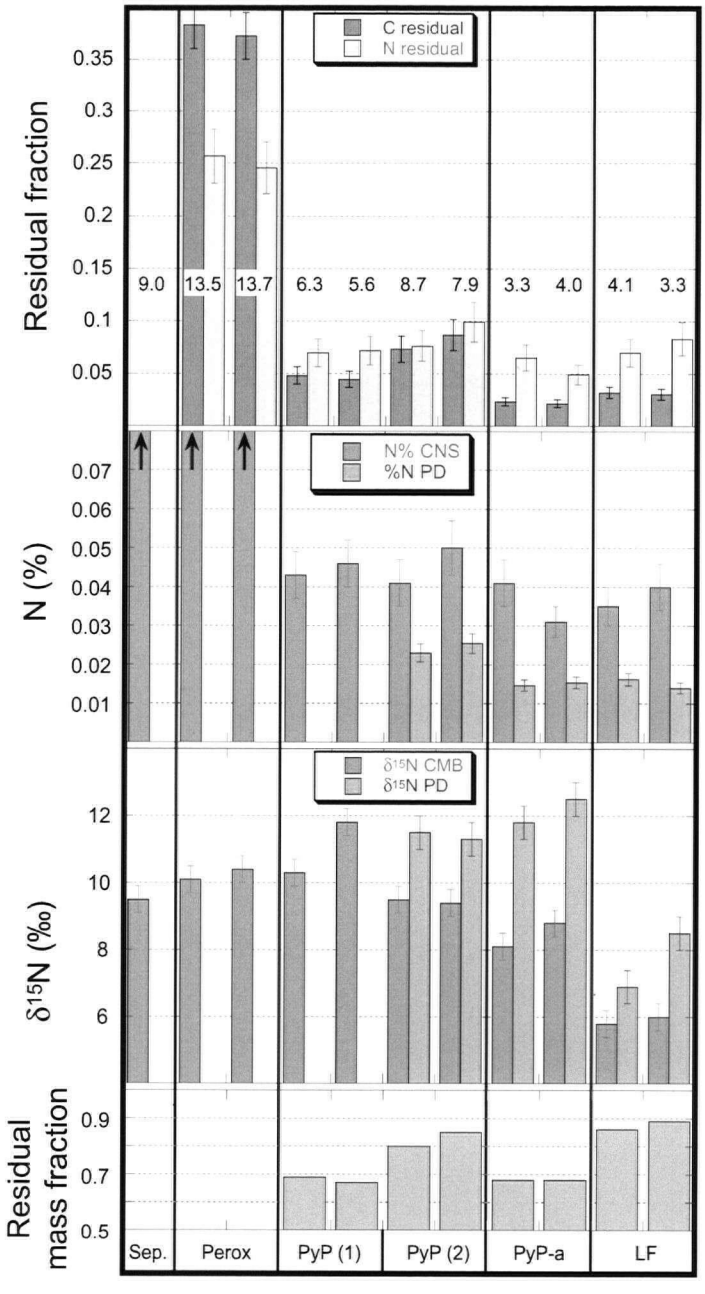

A1.4: Results of the peroxide oxidation tests. "Sep" is the initial, unoxidized, separated diatom sample. Cleaning methods are given in Table A1.1. The top panel shows the residual fraction of the original C and N (i.e. corrected for total mass loss), as determined by CNS, with the C/N ratio from CNS for each sample listed across the panel; note the CNS C/N ratio is erroneously low due to N_2 adsorption, as discussed in the text. The second panel shows the nitrogen concentration as a weight percentage of the oxidized sample, determined by CNS in red and by PD in blue; the N concentrations of Sep and the two Perox samples were much higher (0.429, 0.173 and 0.175 %, respectively). The third panel shows the $\delta^{15}N_{frustule}$ as determined by Cmb in red, and by PD in blue. The bottom panel shows the residual total dry mass following oxidation. Note that the Perox samples overflowed the centrifuge tubes due to their vigorous ebullience, causing additional mass loss, and are not shown in the bottom panel.

break up silica nanospheres, leading to the large loss of mass in both the basic PyP and the acidified PyP-a cleanings. This might expose a significant amount of organic matter initially within the frustule to oxidation, contributing to the very low C_{org} concentrations in PyP-a.

The LF cleaning, on the other hand, causes very little damage to the opal, as evidenced by SEM images (Figure A1.1) and the minor mass loss. The C:N of the LF samples calculated using the PD N% and the CNS C% is 5.5 +/- 0.4. This is slightly higher than expected for mixture of exclusively polyamines and polypeptides [*Sumper*, 2002], which should have a C:N of 2.5 - 4. Assuming the PD conversion of organic N to NO_3 was complete, this suggests that either organic molecules other than polyamines and polypeptides are significant components of the frustules, or some non-frustule carbon has survived the oxidations.

The $\delta^{15}N$ of LF-cleaned frustules, measured by both PD and Cmb methods, is lower than by any other methods, but the PD method exhibited very poor reproducibility. This is difficult to explain, and may simply reflect analytical error, although this is well outside the normal range of error [*Robinson et al.*, 2004]. An alternate explanation is that the oxidizing solution is so powerful that nitrate is formed from organic N, which is then adsorbed by the frustules. The total organic N present in each sample prior to oxidation was 230 μmol N (750 mg aliquot, 0.429 % N), equivalent to a N concentration of ~15 mM in the 15 mL solution. Given the affinity of clean frustules for NO_3^- (discussed further below), any nitrate formed in this vigorous reaction environment could have been adsorbed to the surface of the frustules, some quantity of which is likely to have remained tightly adsorbed despite rinsing with DDW. A persistently adsorbed fraction of only 3 μmol N / g sample, or 1.95 μmol on each ~ 650 mg oxidized sample (i.e. < 1 % of the total initial N) could be significant. The formation of NO_3^- could involve strong fractionation, causing a wide range in measured $\delta^{15}N$ dependent on minor changes in the amount of NO_3^- adsorbed. This could be a particular problem for these samples, which did not receive a pre-treatment by H_2O_2 and thus were unusually organic-rich when introduced to the $HClO_4$ solution.

In summary, the cleaning tests showed that different oxidants produce a wide range of variability in the degree of mass loss, destruction of organic matter, and the $\delta^{15}N$ of the 'frustule' N. They also present a strong warning that the frustules can be altered or destroyed by cleaning methods that may not be expected to be "harsh" [*Robinson et al.*, 2004] such as

H_2O_2. Of the oxidation methods tested here, the LF method was the most effective, with the least apparent impact on frustule integrity, and is therefore the oxidant of choice.

A1.4 A sticky problem: adsorption on diatom frustules

"Diatomaceous earth", the common name for fossilized diatom frustules, has long been known as an excellent adsorbent and has many industrial applications, including as a filtrant for beer and sewage, as well as the adsorbent to which nitroglycerine is bound in dynamite. The strong adsorption of nitroglycerine to diatoms occurs via electrostatic interaction between its three NO_3 esters and the frustule surface. A similar adsorption of ^{15}N-enriched nitric acid during the cleaning method of *Shemesh et al.* [1993], *Crosta and Shemesh* [2002] and *Crosta et al.* [2005] may explain the high $\delta^{15}N$ and %N values these studies found relative to those using other oxidants. Diatom frustules are also excellent adsorbents of gases, including N_2, particularly if treated to partly dissolve the outermost layer of silica [*Fowler et al.*, 2004].

The Brunauer-Emmett-Teller (BET) method [*Brunauer et al.*, 1938] is used to measure the surface area of particles. This measurement involves placing a sample in a sealed chamber, evacuating all gases, lowering the temperature to 77 K, and then reintroducing dinitrogen gas. Two cleaned diatom samples (from the peroxide tests described above, those cleaned by PyP-a and LF) were measured by this method. Both adsorbed large amounts of N_2 gas. For example, at a chamber pressure of only 0.2 bar, the PyP-a sample adsorbed 491 μmol N g^{-1} (0.6875 wt%), while the LF sample adsorbed 750 μmol N g^{-1} (1.05 wt%). Although this is far more N_2 than would be adsorbed at standard temperature and pressure, these measurements testify to the tremendous adsorptive capacity of cleaned diatom frustules. These diatoms have similar surface areas to that of diatomaceous earth cleaned by nitric acid: 39.35 and 59.25 m^2 g^{-1} for the PyP-a and LF samples, respectively, compared to 22 m^2 g^{-1} for diatomaceous earth, and fall within the range of 9.3 - 123 m^2 g^{-1} measured for acid-cleaned, cultured diatoms representing a broad variety of species [*Vrieling et al.*, 1999].

It has been observed that Cu sites on zeolite surfaces greatly enhance their capacity to adsorb N_2 at room temperature [*Kuroda et al.*, 2003]. The presence of metal oxides on the surface of diatoms, suggested by the pale beige-pink hue of samples cleaned by LF, may therefore increase their affinity for N_2. Although most adsorbed N_2 would be quickly

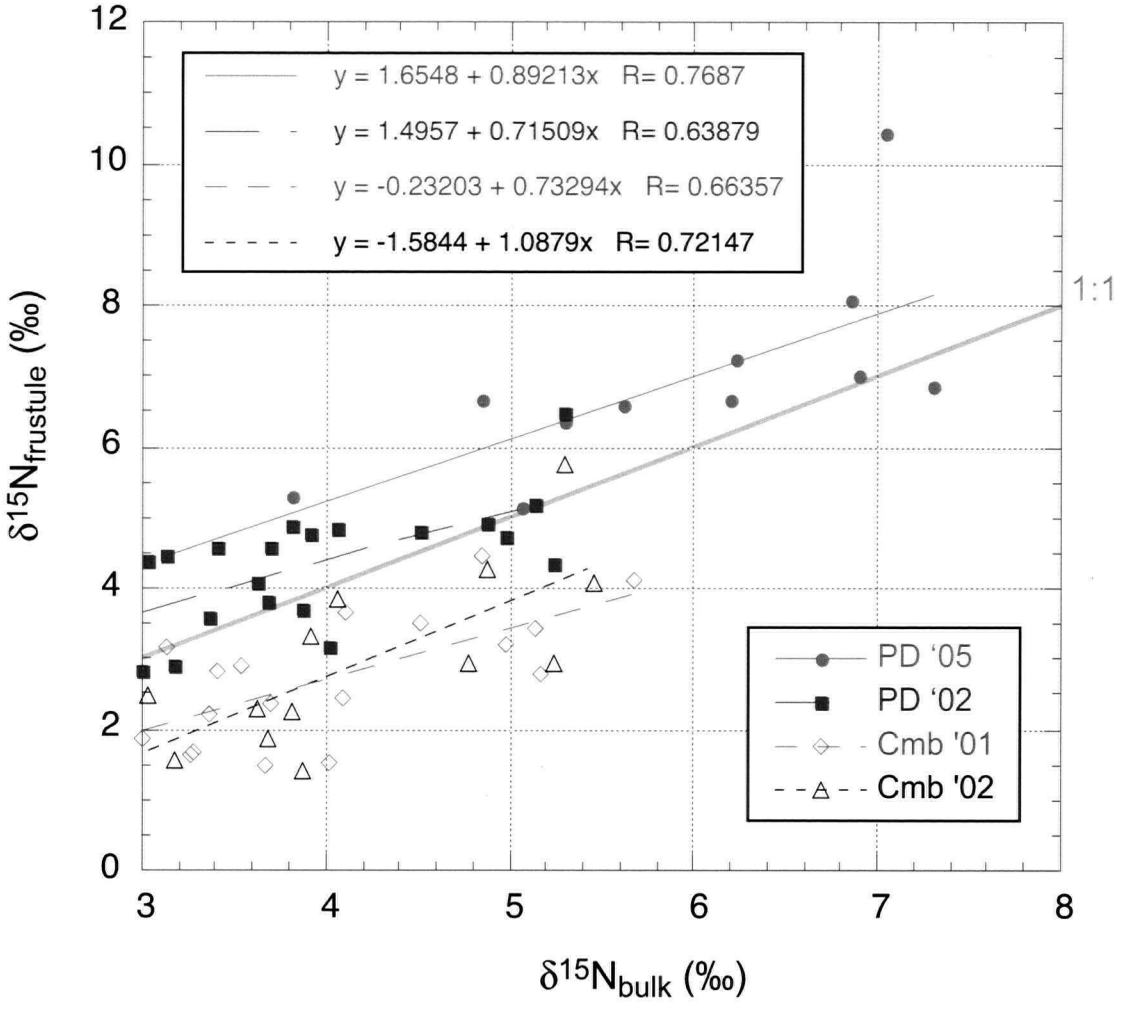

A1.5: The N isotopic composition of diatom frustules vs bulk sediment from the Gulf of Alaska. $\delta^{15}N_{frustule}$ was measured by the two methods, PD and Cmb (described in the text), during the years indicated. The correlations with $\delta^{15}N_{bulk}$ are significant and close to 1:1 as shown, with separate regressions for each group of analyses also shown. The $\delta^{15}N_{frustule}$ measurements made by Cmb are lower, consistent with a low-$\delta^{15}N$ contaminant, though the relationship is not straightforward, as discussed in the text.

evacuated from the frustule surface upon introduction to the vacuum of the EA, some small quantity would remain tightly adsorbed, and it seems likely that this is the source of the contaminant in Cmb samples. Isotopic fractionation may occur during the release of N_2 from the frustule surface, resulting in a contaminant pool that would vary in size and isotopic composition according to the adsorptive environment of the frustule surface.

A1.5 Comparison of Combustion and PD measurements

Natural abundance water-column $\delta^{15}N\text{-}NO_3$ measurements made on the same samples by ammonium-diffusion/combustion at UBC and by the denitrifier method at Princeton, show no consistent offset. The discrepancy in frustule measurements can therefore be attributed to one of two things. It is possible that the PD method fails to completely oxidize organic N in the frustules to NO_3^-. In this case, any fractionation would likely cause the converted NO_3^- to be enriched in ^{15}N, as ^{14}N would preferentially be lost to gaseous intermediates, although other loss mechanisms are conceivable. However, *Robinson et al.* [2004] concluded that this was unlikely, and for the current discussion it is assumed that their conclusion was correct, and $\delta^{15}N$ measurements by PD will be assumed to be accurate; if this should prove to be incorrect, the reasoning here should be revisited. The second possibility, embraced here, is that a contaminant pool of adsorbed N is included in the Cmb measurement.

Analyses by combustion (Cmb) and persulphate-denitrifier (PD) on numerous samples from Gulf of Alaska core ODP 887 show the same general trends and a ~1:1 relationship vs. $\delta^{15}N_{bulk}$, with a discrepancy between the two methods of ~ 2 ‰ (Figure A1.5). If this discrepancy were due to the inclusion of an isotopically invariant contaminant in the Cmb measurement, it should be resolvable by mass balance, as

$$\delta^{15}N\ (cmb) * N\ (cmb) = \delta^{15}N\ (fru) * N\ (fru) + \delta^{15}N\ (contam) * N\ (contam) \qquad (1)$$

where N (cmb), N (fru) and N (contam) are the masses of N measured by combustion, N intrinsic to the frustule, and N adsorbed as a contaminant, respectively. If the PD method provides an accurate representation of $\delta^{15}N$ (fru) and N (fru), and N (contam) = N (cmb) – N (fru), $\delta^{15}N$ (contam) can be easily solved for. Unfortunately, reliable N contents are not

available for the ODP 887 samples as measured by Cmb, as the accuracy of N content determination using the EA-IRMS system is inadequate (K. Gordon, University of British Columbia, pers. comm. 2003). However, N contents of the Peroxide samples (section A1.3) were determined by CNS, which should show the same contaminant pool. When the contaminant pool is calculated using the CNS data, the results vary dramatically between different cleaning methods, though they seem consistent for samples cleaned by the same (Table A1.2). These suggest that the surface environment of the diatom frustule is modified differently by the different cleaning protocols, leading to different adsorption-desorption kinetics and, as a result, differing $\delta^{15}N$ of the contaminant pools for different samples.

The extremely low $\delta^{15}N$ calculated for the 'contaminant' of LF samples is particularly surprising, and is difficult to reconcile with simple N_2 adsorption on the Cmb samples. The LF samples also showed the smallest mass difference between Cmb and PD measurements, despite the large surface area of these samples measured by BET (above). It seems probable, therefore, that there is an additional problem with the PD measurements for these samples. It is proposed that adsorption of NO_3 produced during the oxidation of these relatively organic-rich samples has contributed a high-$\delta^{15}N$ contaminant to the PD samples, causing them to be slightly higher, and more N-rich. Although such a NO_3 contamination should also be present in the samples measured by Cmb, it may be incompletely represented in the combustion products and may therefore have a lesser effect.

When all ODP 887 samples are taken together, the range of variability for $\delta^{15}N_{frustule}$ (Cmb) is 4.3‰ (31 samples, 80 analyses), similar to that of $\delta^{15}N_{frustule}$ (PD) of 3.9 ‰ over the same depth interval (24 samples, 28 analyses). The difference between the $\delta^{15}N$ of frustules and corresponding bulk measurements ($\delta^{15}N_{fru\text{-}bulk}$) is smaller with both methods, 2.7‰ for PD and 3.0‰ for Cmb. We can conclude that, although the adsorption problem certainly introduces an offset in the absolute values, the general trends and variability in $\delta^{15}N_{frustule}$ is not completely compromised in these samples.

A1.6 Summary

The measurement of $\delta^{15}N_{frustule}$ is not trivial. First, the 'frustule-bound' component is an operationally-defined fraction of the total sedimentary N, the identity of which is difficult to verify. As shown in the oxidation tests, the use of different oxidation methods (which did

Table A1.2: Comparison of OG analyses by Combustion and Persulphate-denitrifier

Sample	Oxidation method	$\delta^{15}N$ Cmb (‰)	N Cmb (μmol/g)	$\delta^{15}N$ PD (‰)	N PD (μmol/g)	Mass difference (μmol/g)	$\delta^{15}N$ of contaminant (‰)
OG-9	LF	5.8	12.5	6.9	11.6	0.9	-8.0
OG-10	LF	6.0	12.4	9.1	10.0	2.4	-7.2
OG-15	PyP	9.5	22.1	11.5	16.4	5.7	3.8
OG-16	PyP	9.4	24.3	11.3	18.2	6.1	3.7
OG-17	PyP-a	8.1	14.3	11.8	10.4	3.9	1.8
OG-18	PyP-a	8.8	15.0	12.5	11.0	4.0	1.4

not even address the full range of methods present in the literature, as HNO_3 was not included) can lead to very different results. The operational definition is, therefore, not completely satisfactory, and the published $\delta^{15}N_{frustule}$ measurements, obtained via a range of methods, should be viewed with caution.

Peroxide appeared to destroy a fraction of the opal, which may be a particular problem for very recent sediments and fresh diatoms that are not protected by a diagenetic aluminosilicate overcoat. The discrepancies between $\delta^{15}N$ measurements made by Cmb and PD are consistent with a general adsorption of N_2, though it appears that the $\delta^{15}N$ of this adsorbed component varies according to the oxidation method used. There is also circumstantial evidence for an additional contaminant on the frustules detected by the PD method, tentatively ascribed to NO_3^- and/or nitrate salts formed in significant quantities when oxidizing large quantities of organic matter in a single oxidation step.

A1.7 References

Braman, R. S., and S. A. Hendrix, Nanogram Nitrite and Nitrate Determination in Environmental and Biological-Materials by Vanadium(Iii) Reduction with Chemi-Luminescence Detection, *Analytical Chemistry*, 61, 2715-2718, 1989.

Brunauer, S., P. H. Emmett, and E. Teller, Adsorption of gases in multimolecular layers, *Journal of the American Chemical Society*, 60, 309-319, 1938.

Crosta, X., and A. Shemesh, Reconciling down core anticorrelation of diatom carbon and nitrogen isotopic ratios from the Southern Ocean, *Paleoceanography*, 17, 2002.

Crosta, X., A. Shemesh, J. Etourneau, R. Yam, I. Billy, and J. J. Pichon, Nutrient cycling in the Indian sector of the Southern Ocean over the last 50,000 years, *Global Biogeochemical Cycles*, 19, 10, 2005.

Fowler, C. E., Y. Hoog, L. Vidal, and B. Lebeau, Mesoporosity in diatoms via surfactant induced silica rearrangement, *Chemical Physics Letters*, 398, 414-417, 2004.

Ganeshram, R. S., T. F. Pedersen, S. E. Calvert, G. W. McNeill, and M. R. Fontugne, Glacial-interglacial variability in denitrification in the world's oceans: Causes and consequences, *Paleoceanography*, 15, 361-376, 2000.

Guyer, E. P., and R. H. Dauskardt, Fracture of nanoporous thin-film glasses, *Nature Materials*, 3, 53-57, 2004.

Kuroda, Y., K. Yagi, N. Horiguchi, Y. Yoshikawa, R. Kumashiro, and M. Nagao, New light on the state of active sites in CuZSM-5 for the NO decomposition reaction and N-2 adsorption, *Physical Chemistry Chemical Physics*, 5, 3318-3327, 2003.

Mortlock, R. A., and P. N. Froelich, A Simple Method for the Rapid-Determination of Biogenic Opal in Pelagic Marine-Sediments, *Deep-Sea Research Part a-Oceanographic Research Papers*, 36, 1415-1426, 1989.

Robinson, R. S., B. G. Brunelle, and D. M. Sigman, Revisiting nutrient utilization in the glacial Antarctic: Evidence from a new method for diatom-bound N isotopic analysis, *Paleoceanography*, 19, 2004.

Sequi, P., and R. Aringhieri, Destruction of Organic Matter by Hydrogen Peroxide in the Presence of Pyrophosphate and its Effect on Soil Specific Surface Area, *Soil Sci. Soc. Am. J.*, 41, 340-342, 1977.

Shemesh, A., S. A. Macko, C. D. Charles, and G. H. Rau, Isotopic Evidence for Reduced Productivity in the Glacial Southern-Ocean, *Science*, 262, 407-410, 1993.

Sigman, D. M., The Role of Biological Production in Pleistocene Atmospheric Carbon Dioxide Variations and the Nitrogen Isotope Dynamics of the Southern Ocean, Doctoral, MIT/WHOI, Cambridge, Massachusetts, 1997.

Sigman, D. M., K. L. Casciotti, M. Andreani, C. Barford, M. Galanter, and J. K. Bohlke, A bacterial method for the nitrogen isotopic analysis of nitrate in seawater and freshwater, *Analytical Chemistry*, 73, 4145-4153, 2001.

Smith, G. F., and H. Diehl, A new general procedure in the low-temperature wet oxidation of organic compositions, *Talanta*, 4, 185-193, 1960.

Sumper, M., A phase separation model for the nanopatterning of diatom biosilica, *Science*, 295, 2430-2433, 2002.

Vrieling, E. G., T. P. M. Beelen, R. A. van Santen, and W. W. C. Gieskes, Diatom silicon biomineralization as an inspirational source of new approaches to silica production, *Journal of Biotechnology*, 70, 39-51, 1999.

Appendix 2

Frustule-bound nitrogen in diatom cultures: detailed methodology and inconclusive results

This appendix describes the protocol used for growing diatom cultures, and the attempts made to measure $\delta^{15}N_{frustule}$. The manifold problems encountered resulted in a dearth of clear conclusions, however there are some tendencies apparent in the data that may help direct future research, in particular, the consistent observation of ^{15}N-enrichment within the diatom frustule when compared to the bulk diatom biomass.

A2.1 Methods

Batch cultures were grown under standard nutrient-replete conditions and continuous light (~140 μmol photons m^{-2} s^{-1}), following the protocols of *Needoba and Harrison* [2004]. Cultures were isolates of *Thalassiosira weissflogii* (aquila), a small (5 – 10 μm diameter) centric diatom, with the exception of one culture of *Coscinodiscus wailesii*, a much larger (> 150 μm) centric diatom acquired from the Bigelow Laboratory for Ocean Sciences (http://ccmp.bigelow.org). Culture medium was prepared from natural coastal seawater of Burrard Inlet, collected at the West Vancouver Laboratory (Department of Fisheries and Oceans), and filtered through a 0.45 μm membrane. Nutrients were added as per *Needoba and Harrison* [2004], including $NaNO_3$ with $\delta^{15}N$ of 1.6 ± 0.1 ‰ at starting concentrations between 400 and 700 μM and NO_3^- : $Si(OH)_4$: PO_4^{3-} of 10 : 8 : 1. Nutrients were always available in excess and never limited growth, ensuring large fractionation factors. The pH was adjusted to 8.1 with 1 - 5 mL HCl, and the medium was 'sterilized' by passing it through a 0.2 μm membrane. Cultures of 20 L were inoculated from ~ 0.5 L starting batches, and grown in glass carbuoys stirred with a magnetic teflon-coated stirbar. Sodium bicarbonate

was added midway in order to maintain a sufficient carbon source under peak growth conditions. Ripe cultures typically contained 1 - 5 x 10^6 cells L^{-1}.

Cultures were 'harvested' either by sudden death (addition of 5 mL 5.25 % NaOCl per L of culture, followed by immediate pH neutralization using HCl) or were placed in complete darkness and allowed to die and settle. Cultures allowed to settle slowly were amended with 1.422 g sodium silicate and 3.22 ml 25 % HCl to discourage frustule dissolution. Diatom biomass was collected by filtration of 20-40 mL of culture onto pre-combusted glass fibre filters (GFF, 25 mm), typically in triplicate. The filters were then dried, halved with a stainless scalpel, rolled in silver foil, pelletized and analyzed for $\delta^{15}N$ by combustion (Cmb, see Appendix 1 for details). Meanwhile, the dead culture was allowed to settle for 3 to 24 h, after which the supernatant was siphoned off. The remaining 4 to 8 L of diatom-rich slurry was then concentrated by centrifuging in 250 mL polycarbonate bottles, decanting the supernatant, and adding more slurry. The final product was then filtered onto a 47 mm polycarbonate membrane (0.45 μm pore size) and dried in an oven at 50 °C. One 20 L culture yielded approximately 200 - 800 mg dry weight diatom biomass, sufficient for one measurement of $\delta^{15}N_{frustule}$ by combustion.

The diatom slurry was 'shampooed' by placing it in 250 mL of a 0.5% sodium dodecyl sulphate (SDS) solution, which was agitated with an ultrasonic probe for 20 minutes, centrifuged and decanted, twice. The clean slurry was then poured onto a polycarbonate membrane (5 μm pore size) and washed thoroughly with distilled, deionized water. This was dried, and then the samples were oxidized by one of two methods: the Liquid Fire reaction as described in Appendix 1, referred to as LF, during which abundant fumes and fuschia condensate were noted during oxidation given the large amount of labile organic matter; alternatively, a single H_2O_2 cleaning, followed by a reductive cleaning with a dithionite-citric acid solution, followed by $HClO_4$ at 100 °C (Robinson, 2005), referred to here as Perox-chl. The $\delta^{15}N$ of cleaned frustules was variously analyzed by Combustion (Cmb) and the persulphate-denitrifier method (PD) as described in Appendix 1.

In total, 276 L of diatom culture were grown and harvested, though most of the results were compromised by, variously, a mysterious flagellate invader, accidental spillage, and the problem of atmospheric contamination during measurement by Cmb (Appendix 1). Here, only selected results are shown.

A2.2 Results

The $\delta^{15}N$ of "fresh" and "bulk-dry" fractions agreed well with each other (within 1 ‰) for a given culture, including some measurements by both Cmb and PD. This shows the good fundamental intercomparability between the methods. As discussed in Appendix 1, however, the Cmb measurement for $\delta^{15}N_{frustule}$ is compromised by atmospheric N_2 adsorption. Once recognized, an attempt was made to circumvent this problem by using the PD method – unfortunately, it resulted in reproducibility that was far worse. Replicate measurements by PD gave standard deviations (1σ) of up to 25 ‰ (n=3). This compares to typical standard deviation for the method of 0.3 ‰ [*Robinson et al.*, 2004]. The problem is unlikely to lie with the effectiveness of persulphate at converting organic N to NO_3^-, as PD measurements of bulk-dry samples with up to 1964 μmol N/g agreed so well with Cmb measurements, indicating quantitative conversion of organic N (Table A2.1). Instead, the poor reproduciblity of *T. w.* culture samples may reside, unexpectedly, with the cleaning method.

When *T. w.* samples were cleaned by LF, Scanning Electron Microscope (SEM) images revealed small, shattered fragments with very few intact valves (Figure A2.1). Nonetheless, when $\delta^{15}N_{frustule}$ was measured by Cmb and, for the single sample JD-5, by both Cmb and PD, the N contents were similar to those typically observed in sedimentary diatom frustules. In contrast, when *T. w.* cultures were cleaned by Perox-PerCl, the frustules were converted to a gel-like substance, and the N contents were much higher than measured in any other oxidized frustules by Cmb or PD. Given the demonstrated tendency for H_2O_2 to weaken Si-O bonds in glass ([*Guyer and Dauskardt*, 2004], see Appendix 1), and the fragility of *T. w.* frustules, this suggests that the *T. w.* frustules were obliterated by the H_2O_2 cleaning, but not dissolved due to the low solubility of $Si(OH)_4$ in the acidic H_2O_2 solution. Rather, the frustule mass persisted as a hydrated silica gel. This gel may have protected some of the organic matter from oxidation, including organic N not intrinsic to the frustule, explaining the high N content of the H_2O_2 cleaned analytes when compared to other samples and also when compared to *T. w.* cleaned by LF (Table A2.1). Sedimentary diatoms are pre-selected for heavy silicifaction by dissolution of fragile frustules in the water column, and are further 'armoured' by diagenetic aluminosilicate overgrowths [*Ragueneau et al.*, 2000], hence they are likely much more resistant to destruction by H_2O_2 than are delicate, cultured *T. w.*

Table A2.1: Culture results

Culture	Size (L)	Species	Fresh $\delta^{15}N$	Bulk dry $\delta^{15}N$ (‰)		Oxidation	Oxidized $\delta^{15}N$ (‰)		STD (1σ)		Ox mass ($\mu mol\ g^{-1}$)
			Cmb	Cmb	**PD**		Cmb	**PD**	Cmb	**PD**	
JD-2	20	*T. w.*	-3.1	-2.27		Liquid fire	-0.61		0.34 (2)		16.0
JD-4	20	*T. w.*	-1.4	-0.45		Liquid fire	0.47				50.5*
JD-5	20	*T. w.*	-5.6			Liquid fire	-1.21	**-0.60**			**11.4**
TW-1	40	*T. w.*	-9.1	-8.1	**-8.1**	POx-Pchl		**31.0**		**25.2**	**30.1**
Feb04 1	4	*T. w.*	-5.5			POx-Pchl		**4.1**			**42.1**
Feb04 2	4	*T. w.*	-5.0			POx-Pchl		**18.75**		**6.7 (2)**	**28.9**
Feb04 3	4	*T. w.*	-5.3			POx-Pchl		**16.5**			**57.9**
Feb04 4	4	*T. w.*	-4.4			POx-Pchl		**28.2**			**26.6**
DC-1	20	*C. wailesii*	**	-11.5	**-10.5**	POx-Pchl		**16.4**		**4.1 (4)**	**13.7**

* Oxidation likely incomplete, no SDS pre-oxidation shampoo

**Culture died unexpectedly, no fresh sample collected

Table caption: Results of diatom cultures. "Cmb" N isotopic measurements, shown in regular typeface, were made by combustion, while "PD" measurements, shown in boldface, were made by the Persulphate-Denitrifier method as described in Appendix 1. The standard deviation (STD) is shown for replicates where available, with the number of replicates shown in parentheses.

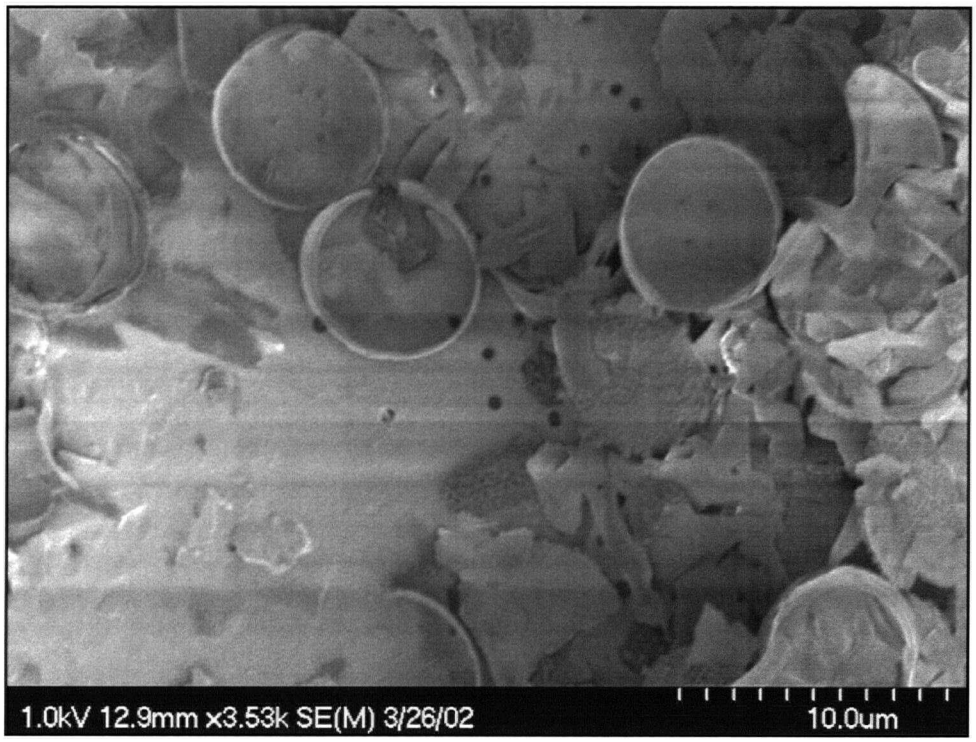

A2.1: Cultured diatom sample following oxidative cleaning. This SEM image shows the culture sample JD-5 following oxidative cleaning by the Liquid Fire reaction. Most of the fragile *Thalassiosira weissflogii* frustules were heavily fragmented during the cleaning process. However, the fragments are definitely solid silica, and some intact valves and girdle bands are visible. The fragments are resting on a Nuclepore membrane; black circles are 0.45 μm holes in the membrane.

frustules. In accord with this, the heavier frustules of *Coscinodiscus wailesii* appear to have been more resistant to the H_2O_2 cleaning, with no observation of a gel-like phase, N contents more typical of oxidized diatoms, and better (though still poor) reproducibility.

These results indicate that frustules can be partially consumed by unexpected chemical interactions, and cleaning methods must be selected with great care. They also suggest that common, easily cultured diatom species like *T. w.*, including *T. oceanica* and *T. pseudonana*, may not be optimal for studying frustule-bound organic components. Cultures of heavily silicified diatoms may be far more appropriate to this task, particularly when their predominance in the sedimentary archive is considered.

A2.3 Discussion

Given the problem with the Perox-PerCl cleaning method, only *T. w.* samples cleaned by LF are discussed here. As shown in Table A2.1, the $\delta^{15}N_{frustule}$ of these samples was consistently higher than $\delta^{15}N_{diatom}$, by 1.0 to 4.7 ‰. It is difficult to assess the degree of error inherent in these values; there is certainly some measurement error associated with the Cmb measurements due to N_2 contamination (Appendix 1). Most culture material was completely combusted prior to recognition of the contaminant, thus it was only possible to make additional measurements by the PD method on the single sample JD-5. Encouragingly, however, the methods agreed within analytical error for this single available sample and the N content measured by PD was indistinguishable from that typically observed in sedimentary frustules (11 μmol N g^{-1}). Regardless, all measurements showed that $\delta^{15}N_{frustule}$ was greater than $\delta^{15}N_{diatom}$, and strongly suggest a ^{15}N-enrichment of the frustule N of 1 – 5 ‰.

The existence of such an offset can be rationalized as follows. Isotopic fractionation of N during NO_3^- uptake in diatoms is dominated by fractionation during the reduction of NO_3^- to NO_2^-, a reaction catalyzed by the enzyme *nitrate reductase*, which has an intrinsic isotope effect of 16 - 25 ‰ [*Ledgard et al.*, 1985; *Needoba et al.*, 2003; *Granger et al.*, 2004; *Needoba et al.*, 2004]. The expression of a net fractionation in the N_{org} of diatom biomass can only occur via the loss of the residual, ^{15}N-enriched NO_3^- from the cell interior, shown to occur by passive efflux [*Needoba et al.*, 2004]. The $\delta^{15}N$-NO_3^- of residual nitrate in the internal pool of *T. w.*, grown under similar conditions to those shown, here can be as high as 36 ‰ [*Needoba et al.*, 2004]. Large fractionation between the nitrate substrate and diatom

biomass may result from slow growth under NO_3^--rich conditions, lack of active pumping of NO_3^- into cell, or strong efflux of residual NO_3^- [*Needoba et al.*, 2004]. In contrast, rapid growth of frustule may cause heavy, residual NO_3^- in the cell to be reduced rapidly to N_{org}. It follows that, if NO_3^- reduction is sufficiently rapid during the brief interval of frustule formation, and the ^{15}N-enriched NO_3^- within the cell is mostly consumed, the N_{org} within the frustule would be enriched in ^{15}N relative to the rest of the diatom. If true, the $\delta^{15}N_{diatom}$ - $\delta^{15}N_{frustule}$ difference may depend on a complex interplay between NO_3^- efflux and growth rate. A second, alternative possibility is evoked by the fact that the $\delta^{15}N_{frustule}$ of the *T. w.* cultures shown here is closer to the initial $\delta^{15}N$-NO_3^- of the culture medium (1.6 ‰). This suggests the possibility that fractionation between substrate and frustule N is reduced during rapid uptake of NO_3^- from outside the cell during frustule formation. The resolution of these possibilities will require further investigation.

As a final note, the single heavily silicified diatom culture presented here appears to be markedly different from the *T. w.* cultures. Given the uncertainties with the Perox-Perchl cleaning method used, this cannot be relied upon as a robust result and requires confirmation. However, assuming for the moment that it is a real result, the high $\delta^{15}N$ would require it to result from the reduction of residual intracellular nitrate. This would suggest that the large difference between $\delta^{15}N$-NO_3^- and $\delta^{15}N_{diatom}$ (~12 ‰) of this large, slowly-growing diatom, equated to a strongly ^{15}N-enriched intracellular nitrate pool that was largely consumed during rapid frustule formation.

Again, the analytical problems prevent a satisfying conclusion to this Appendix. However, the indication that significant and potentially variable $\delta^{15}N_{diatom}$ - $\delta^{15}N_{frustule}$ differences can occur demands that more research be made into this parameter, in order to better understand the growing number of sedimentary $\delta^{15}N_{frustule}$ records.

A2.4 References

Granger, J., D. M. Sigman, J. A. Needoba, and P. J. Harrison, Coupled nitrogen and oxygen isotope fractionation of nitrate during assimilation by cultures of marine phytoplankton, *Limnology and Oceanography*, 49, 1763-1773, 2004.

Guyer, E. P., and R. H. Dauskardt, Fracture of nanoporous thin-film glasses, *Nature Materials*, 3, 53-57, 2004.

Ledgard, S. F., K. C. Woo, and F. J. Bergersen, Isotopic Fractionation During Reduction of Nitrate and Nitrite by Extracts of Spinach Leaves, *Australian Journal of Plant Physiology*, 12, 631-640, 1985.

Needoba, J. A., and P. J. Harrison, Influence of low light and a light: Dark cycle on NO3- uptake, intracellular NO3-, and nitrogen isotope fractionation by marine phytoplankton, *Journal of Phycology*, 40, 505-516, 2004.

Needoba, J. A., D. M. Sigman, and P. J. Harrison, The mechanism of isotope fractionation during algal nitrate assimilation as illuminated by the N-15/N-14 of intracellular nitrate, *Journal of Phycology*, 40, 517-522, 2004.

Needoba, J. A., N. A. Waser, P. J. Harrison, and S. E. Calvert, Nitrogen isotope fractionation in 12 species of marine phytoplankton during growth on nitrate, *Marine Ecology-Progress Series*, 255, 81-91, 2003.

Ragueneau, O., P. Treguer, A. Leynaert, R. F. Anderson, M. A. Brzezinski, D. J. DeMaster, R. C. Dugdale, J. Dymond, G. Fischer, R. Francois, C. Heinze, E. Maier-Reimer, V. Martin-Jezequel, D. M. Nelson, and B. Queguiner, A review of the Si cycle in the modern ocean: recent progress and missing gaps in the application of biogenic opal as a paleoproductivity proxy, *Global and Planetary Change*, 26, 317-365, 2000.

Robinson, R. S., B. G. Brunelle, and D. M. Sigman, Revisiting nutrient utilization in the glacial Antarctic: Evidence from a new method for diatom-bound N isotopic analysis, *Paleoceanography*, 19, 2004.

Appendix 3

Opal determinations for diatom-rich horizons of ODP 887B

ODP 887 has an unusually large range of variability in opal content, from <10% to almost pure opal. In order to better understand the opal measurements, a series of tests was conducted to investigate the upper limit of the measurement technique [*Mortlock and Froelich*, 1989], and a comparison was made to the Si/Al to allow an approximate conversion between the two in the absence of opal measurements.

A part of the core was chosen in which there is a broad range of opal concentrations, including the highest Si/Al of *McDonald* [1997]. They were measured first into aliquots of the weight typically used, 20 mg of dry sediment (run #1). Next, the samples with < 45 % opal were remeasured in 10 mg aliquots and the > 45 % opal samples were remeasured in 5 mg aliquots (run #2). Third, similar 10 and 5 mg aliquots were remeasured again, but each sample was sonicated with an ultrasonic probe during the alkaline dissolution step (run #3).

The use of smaller masses decreased accuracy at low opal concentrations, but clearly increased the sensitivity of the method to high opal concentrations (Fig A3.1). In addition, sonication enhanced the solubility of opal in the very opal-rich samples, leading to values up to 18% higher than in run #1. Sonication did not affect the value of low-opal samples, as shown by repeat measurements of standards Saanich Inlet bulk (SN) and Jervis Inlet bulk (JV-5), that are identical with and without sonication. Because these low-opal samples contain relatively more clay minerals, yet showed less of an increase with sonication, it is highly unlikely that dissolution of clay minerals contributed to the higher measured opal.

Despite the increase in Si measured in the sonicated opal-rich samples, no measurements exceeded 32 wt % Si. The silicate concentrations of these samples were well within the calibrated range of the spectrophotometer (< 3 mM Si, calibration range 0 - 12

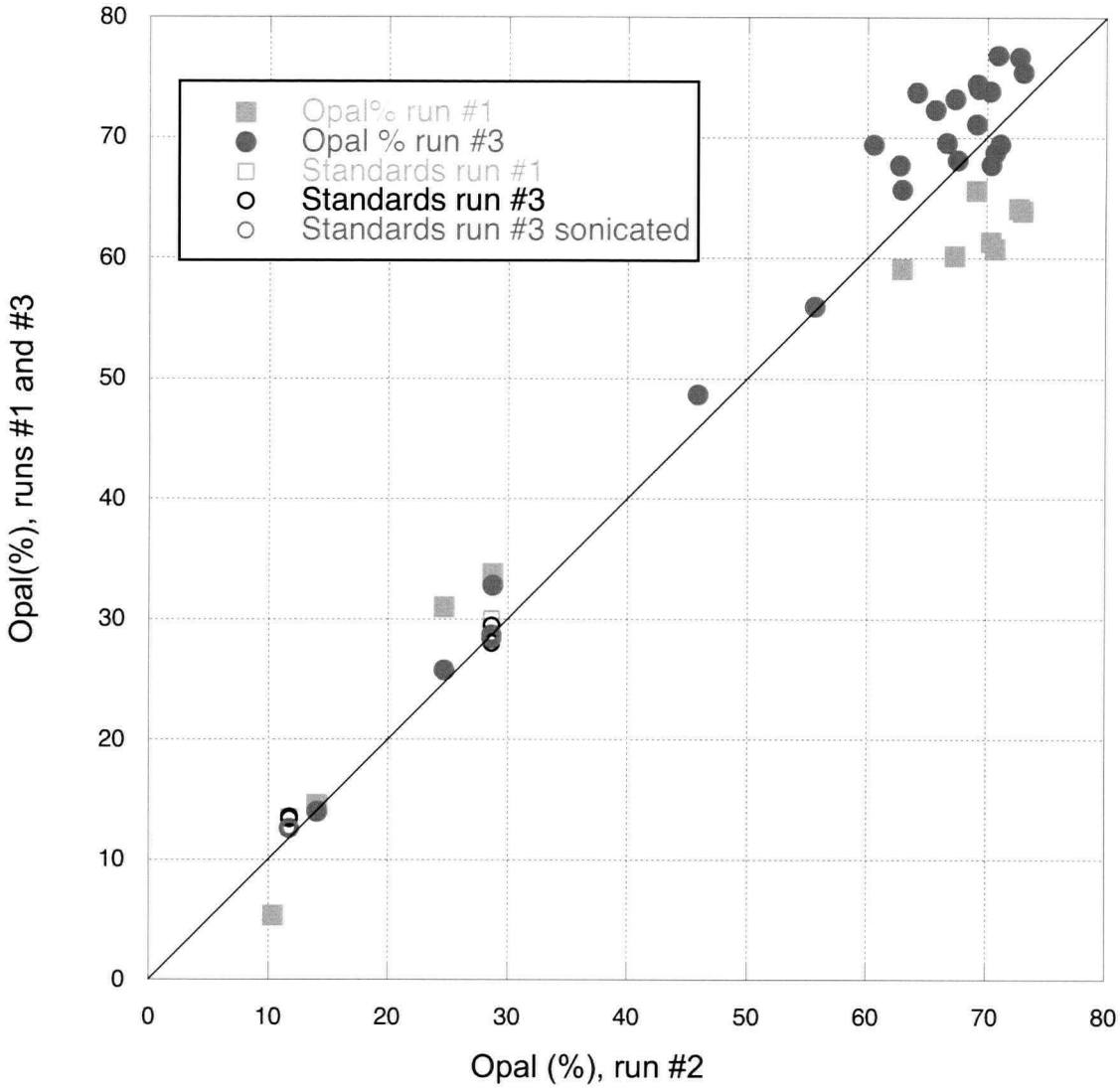

A3.1: Sensitivity of opal measurements to aliquot size and sonication. Replicate measurements of samples from ODP 887 are shown using three different methods as described in the text. The x-axis shows wt. % opal for measurements with small aliquots. On the y-axis are shown the corresponding wt. % opal measurements with larger aliquots (run #1) and with small aliquots, sonicated (run #3). Standards are also shown as open squares and circles. Smaller aliquots increased the sensitivity of the method at high opal concentrations, as did sonication, making a combined increase in measured opal of up to 17 %.

mM), thus it seems likely that this represents a true upper limit of biogenic Si in these most opal-rich samples. The maximum Si/Al measured by XRF [1997] was 30.45 and corresponds to the maximum measured Si concentration of 32.0 wt % Si in sample 2H1-135; a rudimentary calculation can be performed to estimate the Si : opal ratio for this sample, as follows.

The $CaCO_3$ concentration in 2H1-135 is 3.86 wt %, while C_{org} is 0.44 wt %, equivalent to about 1 wt% total organic matter. Ice-rafted detritus is negligible in this sample and thus, approximately 95% of the sample by weight should be accounted for by opal, clay and salt. Assuming 70 ± 10 % porosity for this sample, salt accounts for 4.1 ± 1.5 wt %. Thus, opal and clay together account for ~ 90 ± 2 wt % of the sediment. If we assume an average clay Si/Al of 2.7 ± 0.5, and a Si/Al of 99 in opal, the Si/Al of 30.45 requires a concentration of 82.4 % opal, ± 2%. This is slightly higher than the value of 76.8 % opal calculated from the measured Si of 32.0 wt% using the nominal Si : opal ratio of 2.4, as suggested by Mortlock and Froelich [1989]. This may indicate that dissolution of opal remained incomplete despite sonication, or alternatively that the *Mortlock and Froelich* [1989] ratio underestimates the water content of the opal under consideration here. In this case, a Si : opal ratio of ~ 2.55 may be more appropriate for these samples. However, the difference is minor, so all opal values presented elsewhere in the thesis are calculated using the *Mortlock and Froelich* [1989] ratio of 2.4, with the caveat that true opal concentrations may be up to ~ 8 % higher.

More than 200 samples from the upper part of 887B were analyzed for opal concentration. When plotted against the Si/Al of *McDonald* [1997] a relatively consistent, though non-linear, relationship is apparent (Figure A3.2). In order to make the best use of existing measurements, a 3rd order polynomial regression vs. Si/Al was made, giving an r^2 of 0.95 as shown in Figure A3.2. As apparent from the figure, the regression is most reliable at high and low opal, where it is generally accurate within +/- 6 wt% opal, with a larger degree of scatter between ~30 and 65 wt% opal.

A3.1 References

McDonald, D., The Late Quaternary History of Primary Productivity in the Subarctic East Pacific, M.Sc., University of British Columbia, Vancouver, 1997.

Mortlock, R. A., and P. N. Froelich, A Simple Method for the Rapid-Determination of Biogenic Opal in Pelagic Marine-Sediments, *Deep-Sea Research Part a-Oceanographic Research Papers*, 36, 1415-1426, 1989.

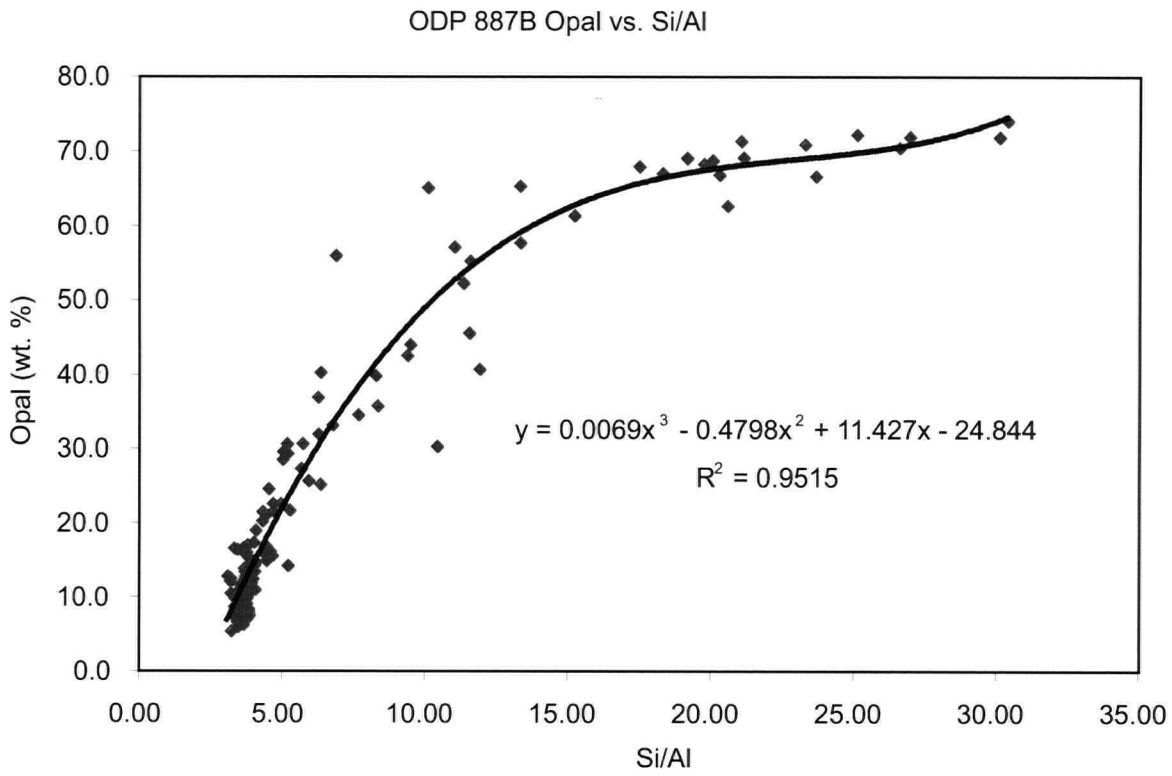

A3.2: Relationship of Si/Al to wt. % opal. Si/Al was determined by X-Ray Fluorescence [McDonald, 1997] while wt. % opal was measured here. The black line shows the third order polynomial regression fit to the data, using the equation shown. The regression is least reliable for intermediate Si/Al (7 - 15). This regression is used for "calculated opal" shown elsewhere in this thesis.

Appendix 4

Age model for Gulf of Alaska Hole ODP 887B

The age model previously developed by *McDonald* [1997] (Here McD97) was altered to include new constraints. First, five radiocarbon ages on mixed planktonic foraminifera (dominated by *Globigerina bulloides* and *Neogloboquadrina pachyderma*), separated directly from the core, were measured by J. Southon at the University of California, Irvine. Radiocarbon ages were calibrated using the CALIB program, HTML version 5.0.2 [*Stuiver and Reimer*, 1993] with the ^{14}C curves of Hughen *et al.* [2004] and Reimer *et al.* [2004]. Calibrated ages (in years before present) are shown in Table A4.1 with the 2 sigma maximum and minimum age estimates, and a "selected mean" that is the midpoint of the most likely 1 sigma range. These were corrected for surface ocean ^{14}C disequilibrium by adding a reservoir effect of 750 years (i.e. a ΔR of 350 years in addition to the standard marine reservoir effect of 400 years) [*Southon et al.*, 1990; *Kiefer and Kienast*, 2005].

Second, the composite benthic $\delta^{18}O$ record of *McDonald* [1997], including measurements on *Gyroidinoides*, *Uvigerina* and *Cibicidoides* spp. (*Cibicidoides* measurements were adjused by +0.64 ‰ following [*Shackleton and Opdyke*, 1973; *Zahn et al.*, 1991]), was tied visually to the global benthic $\delta^{18}O$ stack of *Lisiecki and Raymo* ([2005], herein referred to as LR05). The LR05 stack improves on previous stacks by greatly increasing the number of records, with much better representation of the Pacific, and maximizes the preservation of signal amplitudes while minimizing temporal distortions by employing only a minimal tuning to obliquity. The age of the core bottom is well constrained by the Brunhes-Matuyama magnetic reversal, recovered in the longer cores 887 A and C, and found at 45.86 m in the composite depth model. The 887 B age model was developed on an ash-free depth scale by removing a total of 1.29 m from the record as identified by visual

Table A4.1
Radiocarbon ages, raw and calibrated, for ODP 887B

Core section	Interval	Comp. depth	UCIAMS	^{14}C age	±	Calibrated 2-sigma range			Selected mean
	cm	(m)	#	(BP)		oldest	youngest	range	Age ka
887B 1H1	32.5 - 35	0.34	13045	7950	35	8300	7857	443	8.060
887B 1H1	51.0 - 53.0	0.52	13046	11810	30	13159	12849	310	12.985
887B 1H1	64.0 - 67.0	0.65	13048	12995	30	14652	13834	818	14.108
887B 1H1	111.0 - 113.0	1.12	13050	16405	45	19067	18727	340	18.899
887B 1H2	10.0 - 13.0	1.62	13058	21470	70	25396	24474	922	24.811

Calibrated ages, in years BP, use reservoir age of deltaR = 350, for a total of 750.
Ranges include 100 y reservoir age error.

logging, and suspicious minor element chemistry, typified by low concentrations of Ni, Cr, Sr and Mg. The age-depth relationship was transferred back to the composite depth model for reporting (mcd).

The large changes in opal concentration throughout 887 were shown to be linked to large changes in sedimentation rate by *McDonald et al.* [1999]. Using measured ^{230}Th fluxes, these authors showed that the sedimentation rate during the accumulation of opal-rich layers between 50 and 100 ka more than five times the rate in adjacent, low-opal sediments. The radiocarbon data from the uppermost part of the core also clearly show a large change in sedimentation rate near 15 ka. Sedimentation rate changes present a problem when constructing an age model, especially given the low resolution of the δ^{18}O benthic record (Figure A4.1), itself an unavoidable consequence of the frequent lack of carbonate preservation at this site. The sedimentation rate is unlikely to be linear between recognizable tie points. In light of this, tie points were chosen with an eye to the opal concentrations, aiming primarily to find a tight fit to the δ^{18}O stack, but doing so in such a way that the sedimentation rates are increased during high opal intervals as much as possible. Although there is a fair degree of subjectivity in this approach, it seems likely to be closer to the truth than the assumption of constant sedimentation rate. Indeed, the resulting age model has a higher correlation factor to LR05 than the McD97 age model (0.96 over the last glacial cycle). The excellent fit to the global LR05 benthic stack, apparently matching amplitude to within < 0.1 ‰ for most measurements, provides confidence in the robustness of this correlation. The record has a less obvious correlation to LR05 below 33 mcd, perhaps indicating hiatuses or slumps. The lower glacial cycles should therefore be viewed with caution, and further benthic δ^{18}O measurements are warranted.

The age model was resampled between tie points using linear integration [*Paillard et al.*, 1996]. The resulting age model is compared with that of McD97 in Figure A4.2. The fact that age differences between the McD97 are usually less than 5 ka, despite being generated by different investigators using different assumptions, is encouraging.

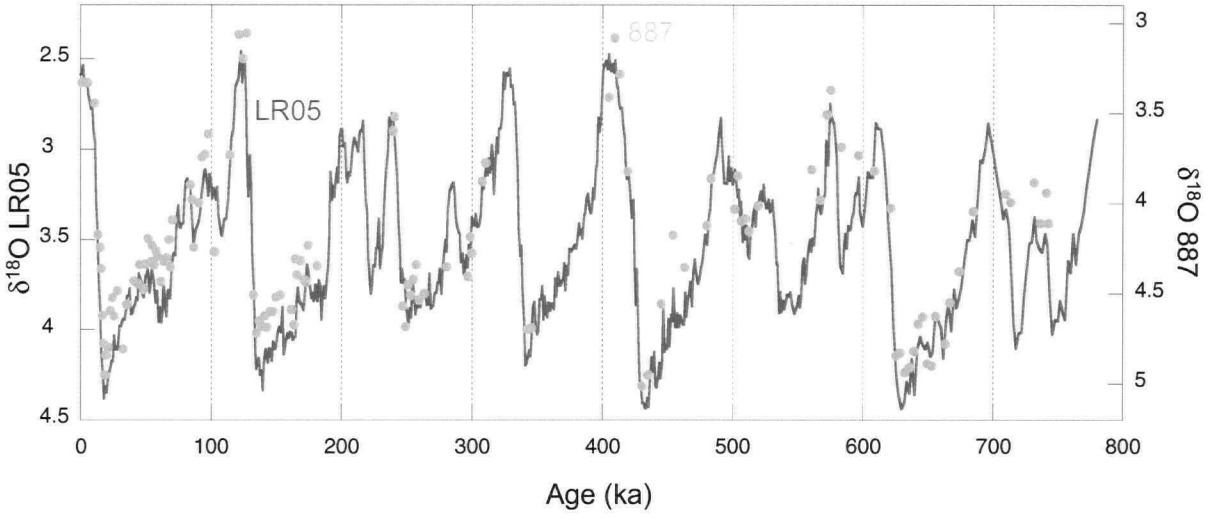

A4.1: Benthic $\delta^{18}O$ age constraint for ODP 887. The benthic LR05 stack is shown in grey. All benthic composite $\delta^{18}O$ measurements for 887 are shown as filled orange circles.

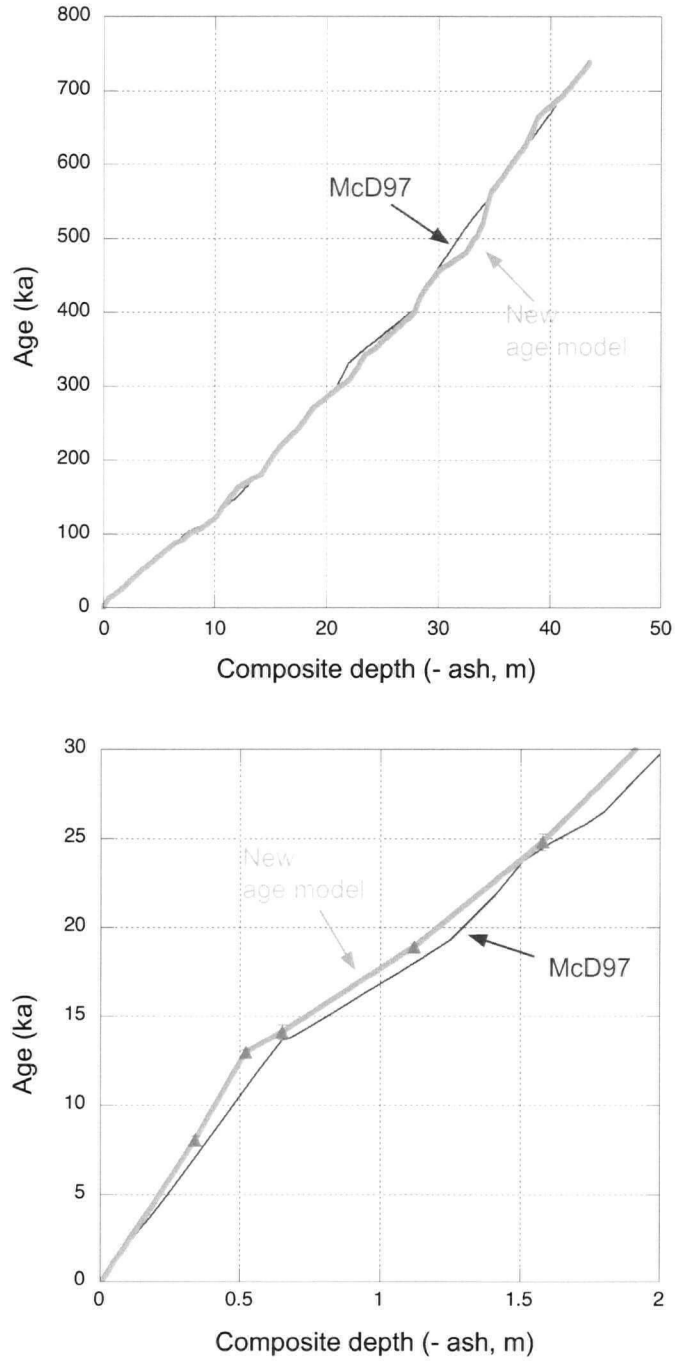

A4.2: Comparison of new 887 age model with previous age model. The new age model presented here is shown as an orange line, while the age model of McD97 is shown as a thin blue line. The upper panel shows the full age model vs. the ash-free depth scale. The lower panel shows the age model over the period of radiocarbon dating, with radiocarbon ages from Table A4.1 shown as orange triangles.

A4.1 References

Hughen, K. A., J. R. Southon, C. J. H. Bertrand, B. Frantz, and P. Zermeno, Cariaco basin calibration update: Revisions to calendar and C-14 chronologies for core PL07-58PC, *Radiocarbon*, 46, 1161-1187, 2004.

Kiefer, T., and M. Kienast, Patterns of deglacial warming in the Pacific Ocean: a review with emphasis on the time interval of Heinrich event 1, *Quaternary Science Reviews*, 24, 1063-1081, 2005.

Lisiecki, L. E., and M. E. Raymo, A Pliocene-Pleistocene stack of 57 globally distributed benthic delta O-18 records, *Paleoceanography*, 20, 2005.

McDonald, D., The Late Quaternary History of Primary Productivity in the Subarctic East Pacific, M.Sc., University of British Columbia, Vancouver, 1997.

McDonald, D., T. F. Pedersen, and J. Crusius, Multiple late Quaternary episodes of exceptional diatom production in the Gulf of Alaska, *Deep-Sea Research II*, 46, 2993-3017, 1999.

Paillard, D., L. Labeyrie, and P. Yiou, Macintosh program performs time-series analysis, *EOS Trans. AGU*, 77, 379, 1996.

Reimer, P. J., M. G. L. Baillie, E. Bard, A. Bayliss, J. W. Beck, C. J. H. Bertrand, P. G. Blackwell, C. E. Buck, G. S. Burr, K. B. Cutler, P. E. Damon, R. L. Edwards, R. G. Fairbanks, M. Friedrich, T. P. Guilderson, A. G. Hogg, K. A. Hughen, B. Kromer, G. McCormac, S. Manning, C. B. Ramsey, R. W. Reimer, S. Remmele, J. R. Southon, M. Stuiver, S. Talamo, F. W. Taylor, J. van der Plicht, and C. E. Weyhenmeyer, IntCal04 terrestrial radiocarbon age calibration, 0-26 cal kyr BP, *Radiocarbon*, 46, 1029-1058, 2004.

Shackleton, N. J., and N. Opdyke, Oxygen isotope and paleomagnetic stratigraphy of equatorial Pacific core V28-238: oxygen isotope temperatures and ice volume on a 10e5 and 10e6 year scale, *Quaternary Research*, 3, 39-55, 1973.

Southon, J. R., D. E. Nelson, and J. S. Vogel, A record of past ocean-atmosphere radiocarbon differences from the northeast Pacific, *Paleoceanography*, 5, 197-206, 1990.

Stuiver, M., and P. J. Reimer, Extended C-14 Data-Base and Revised Calib 3.0 C-14 Age Calibration Program, *Radiocarbon*, 35, 215-230, 1993.

Zahn, R., T. F. Pedersen, B. D. Bornhold, and A. C. Mix, Water mass conversion in the glacial subarctic Pacific (54 N, 148 W): Physical constraints and the benthic-planktonic stable isotope record, *Paleoceanography*, 6, 543-560, 1991.